Investigating the role of AMPK in adipogenesis

Sophia Bustraan

A thesis submitted for the degree of Doctor of Philosophy

Imperial College London

London Institute of Medical Sciences

December 2022

STATEMENT OF ORIGINALITY

I, Sophia Bustraan, declare that the work presented in this thesis is my own, and that any work undertaken with the assistance or collaboration of others has been clearly stated. Where information has been derived from the published or unpublished work of others it has been acknowledged in the text and in the list of references.

COPYRIGHT DECLARATION

The copyright of this thesis rests with the author. Unless otherwise indicated, its contents are licensed under a Creative Commons Attribution-Non Commercial 4.0 International Licence (CC BY-NC).

Under this licence, you may copy and redistribute the material in any medium or format. You may also create and distribute modified versions of the work. This is on the condition that: you credit the author and do not use it, or any derivative works, for a commercial purpose.

When reusing or sharing this work, ensure you make the licence terms clear to others by naming the licence and linking to the licence text. Where a work has been adapted, you should indicate that the work has been changed and describe those changes.

Please seek permission from the copyright holder for uses of this work that are not included in this licence or permitted under UK Copyright Law.

ABSTRACT

AMP-activated protein kinase (AMPK), a master regulator of metabolism, is activated by cellular energy stress. It restores the cellular energy balance by upregulating catabolic, ATP producing pathways and by downregulating anabolic, ATP utilising pathways. It is a therapeutic target in diabetes due to its ability to increase glucose uptake and in non-alcoholic fatty liver disease, due to inhibition of hepatic de novo lipogenesis. Both diseases are strongly correlated with obesity, but as yet AMPK has not been targeted in obesity. Obesity is the excessive accumulation of fat, which is mostly stored in adipose tissue. To determine whether adipose tissue AMPK could be targeted in the treatment of obesity it is important to increase our understanding of the effects of activation of AMPK in adipose tissue. Previous work from the Carling lab has shown that a mouse with genetic, global constitutive activation of AMPK, called the AMPKγ1^{D316A} mouse, is protected from diet induced obesity due to increased ATP uncoupling in the white adipose tissue (WAT) through skeletal muscle associated mechanisms of thermogenesis.

In this work, AMPKγ1^{D316A} adipose tissue or adipocytes were unable to retain the AMPKγ1^{D316A} characteristics when removed from the environment of the AMPKγ1^{D316A} mouse, suggesting that the phenotype is not tissue autonomous. Meanwhile, pharmacological activation of AMPK in a skeletal muscle myocyte led to an increase in adipogenesis, strengthening the link between AMPK activation and the adipocyte-myocyte relationship. Pharmacological activation of AMPK during adipose tissue derived stem cell differentiation suppressed adipogenesis, which was found to be independent of AMPK's inhibition of lipogenesis. Instead, AMPK acted in the initial phases of adipogenesis whilst slowing proliferation. AMPK activation in embryonic stem cell adipogenesis also suppressed differentiation, and maintained higher levels of stem cell markers. Pharmacological AMPK activation also led to a dose dependent reduction in adipocyte lipid droplet size which may be due to its inhibition of lipogenesis, or reflect the disruption of terminal differentiation, preventing the formation of a mature adipocyte with large lipid droplets. However, the suppression of adipogenesis and reduction in lipid droplet size with AMPK activation were accompanied by a decrease in leptin gene expression, indicating that AMPK activation may lead to lipodystrophy in adipose tissue. This work furthers our knowledge of the AMPKγ1^{D316A} mouse and the effect of pharmacological AMPK activation in adipogenesis, and leaves more to be explored.

ACKNOWLEDGEMENTS

I have been privileged to have undertaken my PhD in a truly wonderful research group. I would like to thank my supervisor David Carling for his approachable supervision style, constructive feedback and support throughout my PhD. I would also like to thank Alice Pollard for her guidance, friendship, and inspirational enthusiasm for science and adipose tissue. I am also grateful to Nav Navaratnam, Angela Woods, Rebeca Fiadeiro, Lucy Penfold, Eneko Pascual, Yang Chen, Laura Wilson, Lida Kabir and past members of the Cell Stress group for their assistance and friendship throughout my PhD and for making the lab a fun and enriching place to be.

I would also like to thank Alex Sardini for his help with the adipose tissue allograft experiments, Phill Mucket for his assistance with mouse breeding and genotyping, the Genomics facility and Marian Dore for their help with the RNA sequencing and analysis, Chad Whilding for the analysis of liver lipid droplet size, Alexis Barr for help with using the Operetta microscope and Aditi Prahdan and Sam Peel for help with using the Yokogawa microscope and for assisting my work at AstraZeneca.

I am grateful to the BBSRC and AstraZeneca for funding this work, as well as Jon Read for supporting me during my time at AstraZeneca.

Finally, I am fortunate to be surrounded by supportive friends and family who have helped me to maintain a healthy work-life balance throughout my PhD. Thank you to Max for making me delicious dinners to fuel my thesis writing. And thank you to my wonderful parents who have always enthusiastically cheered me on whilst I pursued my academic endeavours, and who have instilled in me the drive necessary to undertake a PhD.

TABLE OF CONTENTS

STATEMENT OF ORIGINALITY 2
COPYRIGHT DECLARATION 3
ABSTRACT 4
ACKNOWLEDGEMENTS 5
TABLE OF CONTENTS 6
LIST OF FIGURES 10
LIST OF TABLES 15
LIST OF ABBREVIATIONS 16
1. INTRODUCTION 20
1.1 OBESITY 20
1.1.1 Drivers of Obesity 20
1.1.2 Consequences of Obesity 25
1.1.3 Intervention in Obesity 27
1.2 Adipose tissue 29
1.2.1 Adipogenesis 32
1.2.2 Adipose tissue lineage 34
1.2.3 Adipose tissue function 42
1.2.4 Non-shivering thermogenesis 49
1.2.5 Adipose tissue in disease 51
1.2.6 Brown and beige adipocytes for cell therapy 55
1.3 AMPK 56
1.3.1 Structure of AMPK 57
1.3.2 AMPK Function 60
1.3.3 Pharmacological activation 66
1.3.4 AMPK in adipose tissue and obesity 69

1.4 D316A MOUSE 71
1.5 PROJECT AIMS 75
2. MATERIALS AND METHODS 77
2.1 MATERIALS 77
2.1.1 General reagents 77
2.1.2 Buffers 78
2.1.3 Cell culture media 79
2.1.4 Antibodies 81
2.1.5 Primers 83
2.2 ANIMAL STUDIES 84
2.2.1 Declaration 84
2.2.2 Animal models 84
2.2.3 Animal husbandry and diet administration 84
2.2.4 Genotyping 85
2.2.5 Transplant surgery 85
2.2.6 Comprehensive Laboratory Animal Monitoring System 86
2.2.7 Tissue dissection 86
2.3 GENERAL METHODS 87
2.3.1 Histology 87
2.3.2 Cell culture 87
2.3.3 Live proliferation and apoptosis 88
2.3.4 Fluorescence Activated Cell Sorting 88
2.3.5 Protein isolation 88
2.3.6 Bradford assay 89
2.3.7 Western blotting 89
2.3.8 TGFβ-1 ELISA 90

2.3.9 Immunofluorescence and image analysis 90
2.3.10 EdU labelling 91
2.3.11 RNA isolation 91
2.3.12 cDNA synthesis and qPCR 91
2.3.13 RNA sequencing 92
2.3.14 Oil Red O quantification 92
2.3.15 Senescence associated β-galactosidase assay 93
2.3.16 AMPK activity assay 93
2.4 ILLUSTRATIONS 93
2.5 STATISTICAL ANALYSIS 93
3. ADIPOSE ALLOGRAFT TRANSPLANT 95
3.1 INTRODUCTION 95
3.2 D316A ALLOGRAFT TRANSPLANT 97
3.3 DISCUSSION 104
4. PHARMACOLOGICAL ACTIVATION OF AMPK IN ADIPOCYTES 107
4.1 INTRODUCTION 107
4.2 PHARMACOLOGICAL ACTIVATION OF AMPK IN ADIPOGENESIS 109
4.2.1 991 and BI-9774 in adipogenesis 109
4.2.2 AMPK activation in other models of adipogenesis 122
4.2.3 Comparison of pharmacological and genetic activation of AMPK in adipocytes 133
4.2.4 Transcriptomic differences with pharmacological and genetic activation of AMPK in adipocytes 136
4.2.4 Further investigation of AMPK activation by BI-9774 in adipogenesis 143
4.2.5 Importance of timing of AMPK activation in adipogenesis 151
4.3 INVESTIGATING THE MECHANISM OF AMPK REDUCTION OF ADIPOGENESIS 161
4.3.1 TGFβ and WNT signalling pathways 161

4.3.2 Inhibition of lipogenesis 169
4.4 EFFECT OF AMPK ACTIVATION ON PROLIFERATION 175
4.5 EFFECT OF AMPK ACTIVATION ON LIPID DROPLET SIZE 183
4.5.1 AMPK activation reduces lipid droplet size 183
4.5.2 Lipid droplet size as a measure of adipocyte maturity 192
4.6 EFFECT OF AMPK ACTIVATION IN MATURE ADIPOCYTES 194
4.7 DISCUSSION 200
4.7.1 Pharmacological activation of AMPK does not suppress adipogenesis through inhibition of lipogenesis 201
4.7.2 Activation of AMPK slows proliferation in adipogenesis 204
4.7.3 Activation of AMPK in adipogenesis effects adipocyte morphology 206
4.7.4 Conclusion 208
5. GENETIC ACTIVATION OF AMPK AND THE ADIPOSE-MUSCLE LINK 210
5.1 INTRODUCTION 210
5.2 D316A SVF ADIPOCYTES 212
5.2.1 Adipogenesis of D316A SVF 212
5.2.2 Muscle gene expression with AMPK activation 224
5.3 MYOBLAST ADIPOGENIC DIFFERENTIATION WITH AMPK ACTIVATION 228
5.3.1 C2C12 adipogenic differentiation with AMPK 229
5.3.2 Human skeletal muscle myoblast adipogenic differentiation with AMPK 234
5.4 DISCUSSION 238
6. SUMMARY AND FUTURE PERSPECTIVES 244
REFERENCES 248

LIST OF FIGURES

FIGURE 1.1 SUMMARY OF THE CAUSES AND CONSEQUENCES OF OBESITY 21
FIGURE 1.2 GUT-BRAIN SIGNALLING AND HYPOTHALAMIC CONTROL OF ENERGY INTAKE AND EXPENDITURE..... 22
FIGURE 1.3 LOCATION OF ADIPOSE TISSUE DEPOTS IN HUMANS AND MICE..... 31
FIGURE 1.4 STAGES OF ADIPOGENESIS 32
FIGURE 1.5 LINEAGE OF ADIPOCYTES 36
FIGURE 1.6 LIPID DROPLET BIOGENESIS 43
FIGURE 1.7 STIMULATION OF LIPOLYSIS IN ADIPOCYTES 46
FIGURE 1.8 UCP1-DEPENDENT AND INDEPENDENT MECHANISMS 49
FIGURE 1.9 ACTIVATION OF AMPK 57
FIGURE 1.10 STRUCTURE OF THE AMPK SUBUNITS..... 58
FIGURE 1.11 AMPK DOWNSTREAM TARGETS..... 61
FIGURE 1.12 AMPK INHIBITION OF LIPOGENESIS..... 62
FIGURE 1.13 D316A TRANSGENE..... 72
FIGURE 3.1 IWAT ALLOGRAFT TRANSPLANT PILOT EXPERIMENT 97
FIGURE 3.2 BODY WEIGHT AND BODY WEIGHT GAIN IN ALLOGRAFT RECIPIENT MICE ON A HIGH FAT DIET..... 98
FIGURE 3.3 EMRI MEASUREMENTS OF MASS..... 99
FIGURE 3.4 CLAMS ANALYSIS OF ALLOGRAFT RECIPIENT MICE ON A HIGH FAT DIET 100
FIGURE 3.5 POST-MORTEM TISSUE WEIGHTS OF TRANSPLANT RECIPIENT MICE 101
FIGURE 3.6 THE MORPHOLOGY OF LIVERS OF TRANSPLANT MICE 102
FIGURE 3.7 IMAGES OF THE ALLOGRAFT TRANSPLANT 103
FIGURE 3.8 THE MORPHOLOGY OF NATIVE AND ALLOGRAFT IWAT..... 104
FIGURE 4.1 SVF ISOLATION FROM IWAT 108
FIGURE 4.2 TIMELINE OF ADIPOGENIC DIFFERENTIATION FROM THE SVF WITH AN AMPK ACTIVATOR..... 109
FIGURE 4.3 METHOD FOR QUANTIFYING NUCLEI COUNTS AND LIPID STAINING FROM WHOLE WELL SCANS IN IMAGEJ 110
FIGURE 4.4 TITRATION OF BI-9774 IN SVF ADIPOGENESIS. 112
FIGURE 4.5 TITRATION OF 991 IN SVF ADIPOGENESIS. 114

FIGURE 4.6 CHARACTERISATION OF AMPK ACTIVATION BY BI-9774 IN ADIPOCYTES 116
FIGURE 4.7 CHARACTERISATION OF AMPK ACTIVATION BY 991 IN ADIPOCYTES . 117
FIGURE 4.8 CHARACTERISATION OF AMPK ACTIVATION BY BI-9774 IN THE UNDIFFERENTIATED SVF 119
FIGURE 4.9 ASSESSING THE PRESENCE OF BI-9774 IN MEDIA AFTER 2 DAYS..... 121
FIGURE 4.10 TIMELINE OF ADIPOGENESIS OF E14 CELLS WITH AMPK ACTIVATION 122
FIGURE 4.11 CHARACTERISATION OF AMPK ACTIVATION IN E14 CELLS BY 991 DURING ADIPOGENESIS 123
FIGURE 4.12 LIPID DROPLET STAINING TO ASSESS AMOUNT OF ADIPOCYTES FORMED FROM E14 CELLS 124
FIGURE 4.13 EFFECT OF AMPK ACTIVATION ON E14 ADIPOGENESIS 127
FIGURE 4.14 EFFECT OF AMPK ACTIVATION IN E14 ADIPOGENESIS ON STEMNESS MARKERS 129
FIGURE 4.15 BI-9774 IN ADIPOGENESIS OF SVF ADIPOCYTES FROM HIGH FAT DIET MICE 130
FIGURE 4.16 BI-9774 IN ADIPOGENESIS OF PDGFRA SELECTED PROGENITORS... 132
FIGURE 4.17 COMPARISON OF AMPK ACTIVATION FROM THE D316A MUTATION AND WITH BI-9774 BY SAMS ASSAY 134
FIGURE 4.18 COMPARISON OF AMPK ACTIVATION FROM THE D316A MUTATION AND WITH BI-9774 BY WESTERN BLOTTING..... 135
FIGURE 4.19 RNA SEQUENCING EXPERIMENT 137
FIGURE 4.20 CELLS FOR RNA SEQUENCING EXPERIMENT BEFORE RNA ISOLATION 138
FIGURE 4.21 SAMPLE CLUSTERING OF D316A, WT AND BI-9774 SVF ADIPOCYTES139
FIGURE 4.22 VOLCANO PLOTS OF DIFFERENTIALLY EXPRESSED GENES 140
FIGURE 4.23 BUBBLEGUM PLOT OF THE HALLMARK GENE SETS FOR BI-9774 AND D316A COMPARED TO WT 141
FIGURE 4.24 MOST SIGNIFICANTLY CHANGED GO TERMS 142
FIGURE 4.25 GSEA PLOTS FOR ADIPOGENESIS IN BI-9774 VS DMSO 143
FIGURE 4.26 CHARACTERISATION OF AMPK ACTIVATION ON ADIPOCYTE MARKER GENE EXPRESSION. 145

FIGURE 4.27 CHARACTERISATION OF AMPK ACTIVATION ON ADIPOCYTE ASSOCIATED PROTEIN EXPRESSION. 146
FIGURE 4.28 EFFECT OF AMPK ACTIVATION ON AN INDIRECT READOUT OF LIPOLYSIS IN ADIPOCYTES..... 148
FIGURE 4.29 CHARACTERISATION OF AMPK ACTIVATION IN ADIPOGENESIS ON ADIPOCYTE THERMOGENESIS 150
FIGURE 4.30 TIMELINE OF ADIPOGENESIS WITH AMPK ACTIVATED AT DIFFERENT TIME POINTS 151
FIGURE 4.31 PROGRESSION OF ADIPOGENESIS WHEN AMPK IS ADDED AT DIFFERENT TIME POINTS 152
FIGURE 4.32 CHARACTERISATION OF AMPK ACTIVATION AND ADIPOGENESIS WHEN BI-9774 IS ADDED AT DIFFERENT TIME POINTS IN ADIPOGENESIS 153
FIGURE 4.33 EFFECT OF AMPK ACTIVATION FROM DIFFERENT TIME POINTS ON ADIPOCYTE MARKER GENE EXPRESSION 155
FIGURE 4.34 EFFECT OF AMPK ACTIVATION FROM DIFFERENT TIME POINTS IN ADIPOGENESIS ON ADIPOCYTE LIPID ACCUMULATION 156
FIGURE 4.35 TIMELINE OF ADIPOGENESIS WITH CHRONIC AND PULSE ACTIVATION OF AMPK 157
FIGURE 4.36 EFFECT OF PULSE AMPK ACTIVATION IN ADIPOGENESIS ON AMPK ACTIVATION AND ADIPOCYTE ASSOCIATED PROTEINS 158
FIGURE 4.37 EFFECT OF PULSE AMPK ACTIVATION IN ADIPOGENESIS ON ADIPOCYTE MARKER GENE EXPRESSION 159
FIGURE 4.38 EFFECT OF PULSE AMPK ACTIVATION IN ADIPOGENESIS ON ADIPOCYTE FORMATION 160
FIGURE 4.39 GSEA PLOT FOR TGFB SIGNALLING IN BI-9774 VS WT 161
FIGURE 4.40 CHARACTERISATION OF THE EFFECT OF AMPK ACTIVATION ON TGFB IN SVF ADIPOCYTES..... 164
FIGURE 4.41 ASSESSING THE EFFECT OF BI-9774 ON THE DOWNSTREAM TARGETS OF TFGB 166
FIGURE 4.42 CHARACTERISING THE SUBCELLULAR LOCALISATION OF TGFB AND WNT DOWNSTREAM SIGNALLING PROTEINS AFTER AMPK ACTIVATION 168
FIGURE 4.43 COMPARATIVE EFFECT OF AMPK ACTIVATION WITH ACC INHIBITION IN ADIPOGENESIS 170

FIGURE 4.44 TITRATION OF PF-05175157 IN SVF ADIPOGENESIS..... 171
FIGURE 4.45 COMPARATIVE EFFECT OF PULSE AMPK ACTIVATION TP PULSE ACC INHIBITION IN ADIPOGENESIS ON ADIPOCYTE MARKER GENE EXPRESSION 173
FIGURE 4.46 EFFECT OF PULSE ACC INHIBITION IN ADIPOGENESIS ON ADIPOCYTE FORMATION..... 174
FIGURE 4.47 GSEA PLOTS FOR PROLIFERATION IN BI-9774 VS WT 175
FIGURE 4.48 CELL CYCLE PHASES IN SVF ADIPOCYTES 176
FIGURE 4.49 CHANGE IN NUCLEI COUNTS THROUGHOUT ADIPOGENESIS WITH AMPK ACTIVATION..... 178
FIGURE 4.50 EFFECT OF AMPK ACTIVATION ON PROLIFERATION THROUGHOUT DIFFERENTIATION. 179
FIGURE 4.51 LIVE MEASUREMENT OF APOPTOSIS THROUGHOUT ADIPOGENESIS WITH AMPK ACTIVATION..... 180
FIGURE 4.52 EFFECT OF AMPK ACTIVATION ON SENESCENCE IN ADIPOGENESIS181
FIGURE 4.53 EFFECT OF AMPK ACTIVATION ON PROPORTION OF PROLIFERATING CELLS..... 182
FIGURE 4.54 EFFECT OF AMPK ACTIVATION ON ADIPOCYTE LIPID DROPLET SIZE184
FIGURE 4.55 CHARACTERISATION OF AMPK ACTIVATION ON LIPID CONTENT IN SVF ADIPOCYTES 185
FIGURE 4.56 METHOD FOR MEASURING LIPID DROPLET PARAMETERS..... 186
FIGURE 4.57 QUANTIFICATION OF EFFECT OF BI-9774 ON LIPID DROPLET SIZE ... 187
FIGURE 4.58 EFFECT OF AMPK ACTIVATION ON CIDEC IN ADIPOCYTES 188
FIGURE 4.59 EFFECT OF AMPK ACTIVATION ON CIDEC IN ADIPOCYTES 190
FIGURE 4.60 EFFECT OF INHIBITION OF ACC ON LIPID DROPLET SIZE 191
FIGURE 4.61 COMPARISON OF CHRONIC AND PULSE BI-9774 TREATMENTS..... 193
FIGURE 4.62 AMPK ACTIVATION IN MATURE ADIPOCYTES 195
FIGURE 4.63 EFFECT OF AMPK ON ADIPOGENESIS IN MATURE ADIPOCYTES..... 196
FIGURE 4.64 EFFECT OF AMPK ACTIVATION IN MATURE ADIPOCYTES ON ADIPOCYTE MARKER GENES 198
FIGURE 4.65 EFFECT OF AMPK ON LIPID DROPLET SIZE IN MATURE ADIPOCYTES 199
FIGURE 4.66 EFFECT OF AMPK IN MATURE ADIPOCYTES..... 200
TO FIGURE 5.1 ANALYSIS OF D316A AND WT SVF ADIPOCYTE RNA SEQUENCING 212

FIGURE 5.2 GSEA PLOT FOR ADIPOGENESIS IN D316A VS WT 213
FIGURE 5.3 EFFECT OF D316A MUTATION ON ADIPOCYTE MARKER GENES 214
FIGURE 5.4 THE EFFECT OF THE D316A MUTATION ON ADIPOGENESIS 215
FIGURE 5.5 MORPHOLOGY OF WT AND D316A SVF ADIPOCYTES 216
FIGURE 5.6 CHARACTERISING THE EFFECT OF THE D316A MUTATION ON MITOCHONDRIA IN SVF ADIPOCYTES 217
FIGURE 5.7 STIMULATION OF ADRENERGIC RECEPTORS IN WT AND D316A SVF ADIPOCYTES 219
FIGURE 5.8 EFFECT OF BI-9774 IN THE D316A SVF ADIPOCYTES 220
FIGURE 5.9 THE EFFECT OF PHARMACOLOGICAL ACTIVATION OF AMPK IN D316A SVF ADIPOCYTES 222
FIGURE 5.10 EFFECT OF AMPK ACTIVATION ON ADIPOCYTE MORPHOLOGY IN D316A SVF ADIPOCYTES 223
FIGURE 5.11 GSEA PLOTS FOR MYOGENESIS 225
FIGURE 5.12 NUMBER OF OVERLAPPING DIFFERENTIALLY EXPRESSED GENES BETWEEN TISSUE AND CELL RNA SEQUENCING DATA 226
FIGURE 5.13 MUSCLE ASSOCIATION OF OVERLAPPING DIFFERENTIALLY EXPRESSED GENES BETWEEN TISSUE AND CELL RNA SEQUENCING DATA . 228
FIGURE 5.14 CHARACTERISING AMPK ACTIVATION IN C2C12 CELL ADIPOGENESIS 230
FIGURE 5.15 THE EFFECT OF ACTIVATING AMPK IN C2C12 ADIPOGENESIS 231
FIGURE 5.16 C2C12 DERIVED ADIPOCYTES 232
FIGURE 5.17 EFFECT OF AMPK ACTIVATION DURING C2C12 ADIPOGENESIS ON ADIPOCYTE MARKER GENES 234
FIGURE 5.18 EFFECT OF AMPK ACTIVATION IN HUMAN SKELETAL MUSCLE MYOBLAST ADIPOGENIC DIFFERENTIATION 236
FIGURE 5.19 EFFECT OF AMPK ACTIVATION IN HUMAN SKELETAL MUSCLE MYOBLAST ADIPOGENIC DIFFERENTIATION WITH ROSIGLITAZONE 237
FIGURE 6.1 ACTIVATION OF AMPK IN ADIPOGENESIS 247

LIST OF TABLES

TABLE 1.1 PROPOSED ADIPOCYTE LINEAGES 38
TABLE 1.2 SUBTYPES OF PDGFRA EXPRESSING ADIPOCYTE PROGENITORS 40
TABLE 2.1 CELL CULTURE MEDIA 79
TABLE 2.2 PRIMARY ANTIBODIES 81
TABLE 2.3 FACS ANTIBODIES 82
TABLE 2.4 SECONDARY ANTIBODIES 83
TABLE 2.5 GENOTYPING PRIMERS 83
TABLE 2.6 QPCR PRIMERS 83
TABLE 4.1 PPARΓ EXPRESSION THROUGH E14 ADIPOGENESIS 128
TABLE 4.2 CEBPA EXPRESSION THROUGHOUT E14 ADIPOGENESIS 129
TABLE 4.3 LIST OF GENES IN THE CORE ENRICHMENT OF THE HALLMARK TGFB SIGNALLING GENE SET ENRICHED IN THE BI-9774 TREATED SVF ADIPOCYTES 162
TABLE 4.4 WHITFIELD GENE SET FOR CELL CYCLE STAGES 177
TABLE 4.5 BURTON ADIPOGENESIS GENE SETS FOR STAGES OF ADIPOGENESIS 192
TABLE 5.1 LIST OF OVERLAPPING SIGNIFICANT DIFFERENTIALLY EXPRESSED GENES BETWEEN D316A VS WT IWAT AND D316A VS WT SVF ADIPOCYTES . 227

LIST OF ABBREVIATIONS

α-MSH	α-melanocyte stimulating hormone
β-AR	β-adrenergic receptor
ACC	acetyl-CoA Carboxylase
Adipoq	adiponectin (gene)
AgRP	Agouti-related protein
AICAR	5-aminoimidazole-4-carboxamide ribonucleoside
AID	autoinhibitory domain
AMPK	AMP activated protein kinase
ANOVA	analysis of variance
ARC	hypothalamic arcuate nucleus
ATGL	adipose triglyceride lipase
BAT	brown adipose tissue
BMI	body mass index
BMP	bone morphogenetic protein
BSA	bovine serum albumin
CAG	CMV early enhancer element/chicken β-actin promoter
CAMKK2	calcium/calmodulin dependent protein kinase kinase 2
cAMP	cyclic AMP
CBM	carbohydrate binding motif
CBS	cystathionine-β-synthase
CEBP	CCAAT enhancer binding protein
ChREBP	carbohydrate response element binding protein
CIDE	cell death inducing DFFA like effector
CKB	creatine kinase B
CKMT2	creatine kinase, mitochondrial 2
CLAMS	laboratory animal monitoring system
Cre	Cre recombinase
CREBP	cyclic AMP response element binding protein
CVD	cardiovascular disease

DAG	diacylglycerol
DMEM	Dulbecco’s modified eagle medium
DMSO	dimethyl sulfoxide
DPP4	dipeptidyl-peptidase 4
Ebf2	early B cell factor 2
ECM	extracellular matrix
EdU	5-ethynyl-2’-deoxyuridine
ELISA	enzyme-linked immunosorbent assay
EMRI	echo magnetic resonance imaging
ER	endoplasmic reticulum
ERK	extracellular signal-regulated kinase
ES	embryonic stem
eWAT	epididymal white adipose tissue
FACS	fluorescence activated cell sorting
FAS	fatty acid synthase
FBS	foetal bovine serum
FGF21	fibroblast growth factor 21
GABPα	GA binding protein α
GAPDH	glyceraldehyde 3-phosphate dehydrogenase
GLP-1	glucagon-like peptide-1
GLUT1/4	glucose transporter type 1/4
GSEA	gene set enrichment analysis
HEPES	4-(2-hydroxyethyl)-1-piperazineethanesulfonic acid
HIF	hypoxia inducible factor
HRP	horseradish peroxidase
HSL	hormone sensitive lipase
IBMX	3-isobutyl-1-methylxanthine
ICAM1	intracellular adhesion molecule 1
Il-6	interleukin 6
iWAT	inguinal white adipose tissue

KLF	Krüppel-like factors
LKB1	liver kinase B1
Lpl	lipoprotein lipase (gene)
MAG	monoacylglycerol
MAPK	mitogen-activated protein kinase
MC4R	melanocortin-4 receptor
MHO	metabolic healthy obese
mTOR	mammalian target of rapamycin
mTORC1	mammalian target of rapamycin complex 1
MYF5	myogenic factor 5
MYOD	myoblast determination protein 1
NAFLD	non-alcoholic fatty liver disease
NES	normalised enrichment score
NPY	neuropeptide Y
NST	non-shivering thermogenesis
PBS	phosphate buffered saline
PCR	polymerase chain reaction
PDGFR	platelet derived growth factor receptor
PGC1α	peroxisome proliferator-activated receptor gamma coactivator 1-α
PKA	protein kinase A
POMC	pro-opiomelanocortin
PPAR	peroxisome proliferator activated receptor
PRDM16	PR domain containing 16
PREF-1	preadipocyte factor-1
PVN	paraventricular nucleus
qPCR	quantitative polymerase chain reaction
RER	respiratory exchange ratio
RFP	red fluorescent protein
Rpl13a	ribosomal protein L13a (gene)
RYR	ryanodine receptor

scRNA-seq	single-cell RNA sequencing
SERCA	sarco/endoplasmic reticulum calcium ATPase
SMAD	suppressor of mothers against decapentaplegic
SMART	skeletal muscle-like AMPK reprogrammed thermogenic
SNS	sympathetic nervous system
SOX2	sex determining region Y-box 2
SREBP	sterol regulatory element binding protein
SVF	stromal vascular fraction
T2D	type 2 diabetes
T_3	triiodothyronine
TAG	triacylglycerol
TBC1D1/4	TBC1 domain family member 1/4
TBS-T	Tris buffered saline Tween 20
TGFβ	transforming growth factor β
TNFα	tumour necrosis factor α
TOMM20	translocase of the outer mitochondrial membrane complex subunit 20
TSC2	tuber sclerosis complex 2
UCP1	uncoupling protein 1
ULK1	unc-51 like autophagy activating kinase
WAT	white adipose tissue
WGA	wheat germ agglutinin
WNT	wingless/integrated
WT	wild-type
WT1	Wilms' tumour protein 1
ZFP423	zinc finger protein 423

1. INTRODUCTION

1.1 OBESITY

Obesity is a global epidemic, defined by the World Health Organisation as “abnormal or excessive fat accumulation that may impair health”. It is primarily diagnosed using an individual’s body mass index (BMI), which is calculated by dividing one’s weight by the square of their height. A BMI of 25 - 30kg/m^2 designates that a person is overweight and a BMI above 30kg/m^2 classifies that person as obese. Obesity can be subdivided into 3 classes, class I being BMI 30 - 35kg/m^2, class II being 35 - 40kg/m^2 and a BMI of 40kg/m^2 being class III. In addition to BMI, waist circumference, waist to hip ratio and the proportion of body mass that is fat mass and ethnicity should be taken into consideration to give a diagnosis of obesity (Misra et al., 2006). Levels of obesity have increased globally, tripling since 1975 so that in 2016 13% of the adult population worldwide was considered obese, whilst childhood and adolescent obesity has increased over 8-fold (NCD-RisC, 2017). This has led to a shift in deaths related to being overweight being greater than those related to being underweight. The health complications that arise from obesity are the metabolic syndrome and predisposition for metabolic disease, increased risk of certain cancers, joint problems leading to disability and decreased mobility, fertility complications and psychiatric disorders such as depression.

1.1.1 Drivers of Obesity

The drivers of obesity are numerous and multifactorial, although ultimately come down to a chronic positive energy imbalance, meaning that the long term level of energy intake from calorie consumption is higher than the level of energy expenditure (Figure 1.1). The rapid rise in obesity is thought to have occurred when an energy flipping point was reached. Around the turn of the century, energy expenditure for daily life decreased due to technological advances in transport and home life, but this was not associated with weight gain in the population. The greater availability of low cost, energy-dense foods and increased portion sizes from the 1970s onwards led to the energy flipping point, where more energy was being taken in than expended, and so obesity became more prevalent (Blüher, 2019; Kral and Rolls, 2004; Rippin et al., 2019; Swinburn et al., 2011; Young and Nestle, 2002). Obesity has been associated with wealth, as levels of obesity are greater in high income countries and amongst the wealthy where food is more attainable than in low income countries (Monteiro et al., 2004; NCD-RisC, 2016). However, amongst high-income

countries where access to food is no longer rate limiting, there is a shift towards obesity levels being higher in those with lower socioeconomic opportunities and less access to health education, healthy food options and gyms, sports clubs or past times involving physical activity (Monteiro et al., 2004).

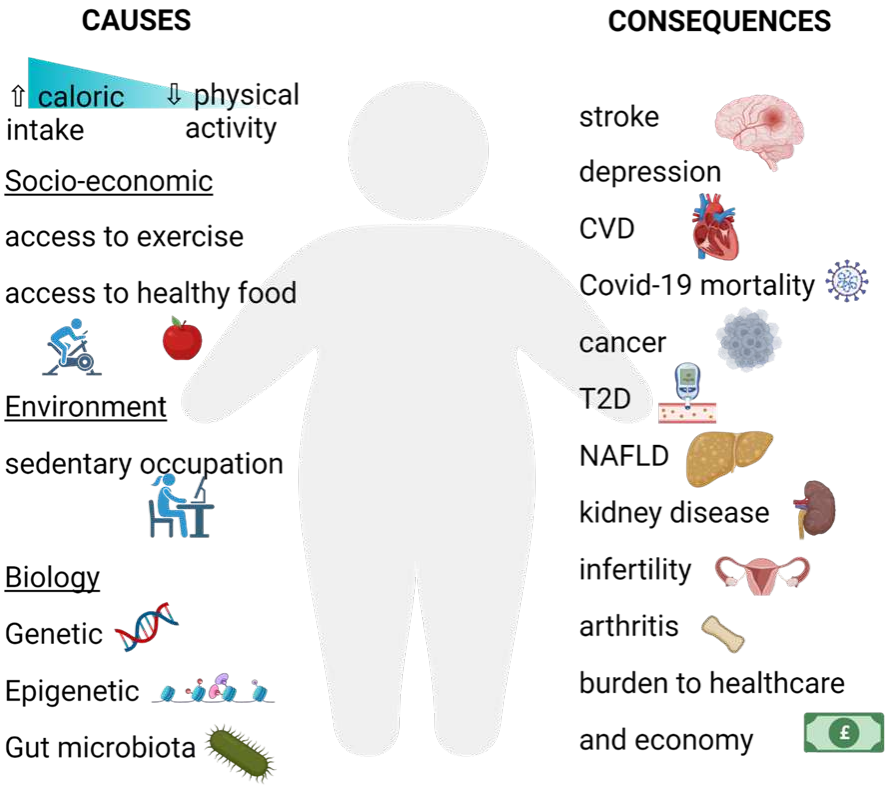


Figure 1.1 Summary of the causes and consequences of obesity

Non-exhaustive examples of the causes of energy imbalance leading to obesity and the consequences of obesity. (CVD, cardiovascular disease; T2D, type 2 diabetes; NAFLD, non-alcoholic fatty liver disease).

When food is consumed, complex gut-brain cross talk occurs to determine satiation or hunger (Figure 1.2) (Clemmensen et al., 2017). Enteroendocrine cells in the gastrointestinal tract contain G-coupled protein receptors to sense nutrients and in response release either hunger inducing orexigenic hormones or satiating anorexigenic hormones. These nutrient responsive hormones act on the caudal brainstem to give information about feeding and nutrient content either directly by entering circulation, or by acting locally on Vagal Afferent neurons that signal to the caudal brainstem (Clemmensen et al., 2017). The caudal

brainstem then relays these signals to the hypothalamus, which regulates energy homeostasis and initiates a response. There are distinct regions within the hypothalamus with different neuronal subpopulations expressing neuropeptides including the arcuate nucleus (ARC) and the paraventricular nucleus (PVN). In the ARC the orexigenic agouti-related protein (AgRP)/ neuropeptide Y (NPY) expressing neurons regulate neurons expressing anorexigenic pro-opiomelanocortin (POMC), which can be cleaved to produce α-melanocyte stimulating hormone (α-MSH), and together these regulate melanocortin-4 receptor (MC4R) expressing neurons in the PVN to modulate hunger and satiation (Clemmensen et al., 2017; Pigeyre et al., 2016; Wolfgang and Lane, 2006).

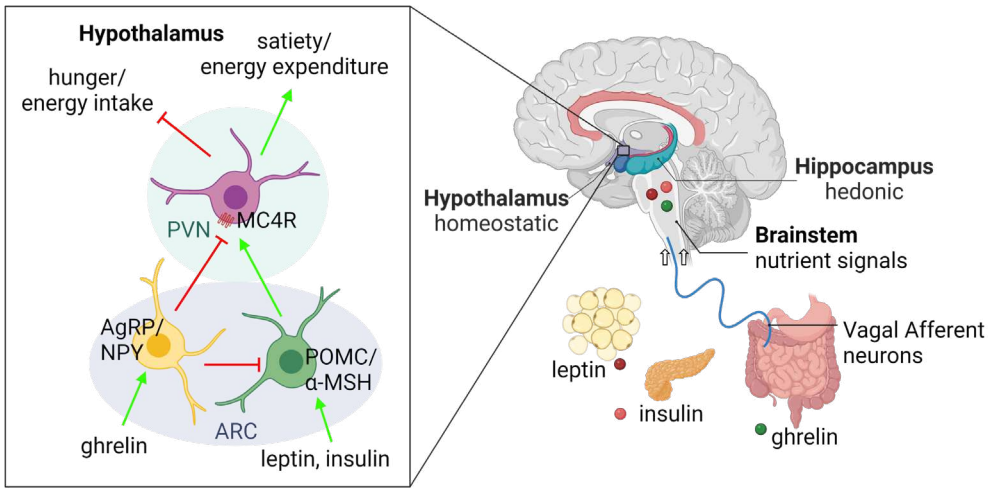


Figure 1.2 Gut-brain signalling and hypothalamic control of energy intake and expenditure

Nutritional status is signalled to the caudal brainstem through the vagal afferent neurons and orexigenic (such as ghrelin) or anorexigenic (such as leptin or insulin) hormones from the body. The brainstem relays this to the hippocampus to coordinate the hedonic response to food, and to the hypothalamus which coordinates the homeostatic response. In the hypothalamus anorexigenic signals such as leptin and insulin lead to stimulation of (pro-opiomelanocortin) POMC/ α-melanocyte stimulating hormone (α-MSH) expressing neurons in the arcuate nucleus (ARC) which stimulate melanocortin 4 receptor (MC4R) expressing neurons in the paraventricular nucleus (PVN). Meanwhile, orexigenic hormones such as ghrelin stimulate agouti-related peptide (AgRP)/ neuropeptide Y (NPY) expressing neurons which inhibit POMC/ α-MSH expressing neurons as well as MC4R neurons. MC4R

expressing neurons then regulate energy intake in response to hunger and energy expenditure in response to satiety. Adapted from (Nasrallah and Horvath, 2014).

Response to eating is not simply regulated by energy homeostasis. The hedonic value of food, influenced by its palatability, induces reward responses in the mesolimbic system in the brain that can cause an addiction to eating (Clemmensen et al., 2017; Murray et al., 2014). Receptors for nutrient responsive hormones are found on dopaminergic neurons, and functional magnetic resonance imaging studies show that the reward signalling in response to food is the same as in the response to addictive drugs. This can cause individuals to overeat, and to choose more palatable foods over nutritious foods.

A multitude of nutrient responsive hormones have been identified and these include insulin, ghrelin and leptin. The only orexigenic hormone identified is ghrelin. It is released from the stomach and acts primarily on the orexigenic AgRP/NPY neurons to increase hunger, and its signalling is supressed postprandial, although there is less suppression in obesity (Murray et al., 2014; Oussaada et al., 2019). Leptin and insulin are examples of anorexigenic hormones. Insulin is known for regulating the postprandial metabolic response to food to reduce blood glucose levels. Leptin is produced in adipose tissue, so an increase in adipose tissue means an increase in leptin levels. Both insulin and leptin stimulate anorexigenic neurons in the hypothalamus and dopaminergic neurons to promote the hedonic response to food (Murray et al., 2014; Oussaada et al., 2019). Obesity is associated with leptin resistance and insulin insensitivity in the brain (Oussaada et al., 2019).

On top of the changes in energy balance there are genetic, physiological, psychological and societal factors that will contribute to whether an individual becomes obese. Genetics cannot fully account for the rise in obesity, given the rapid rate of increase. However, some individuals are more predisposed to obesity, and heritability has been shown in twin and adoption studies (Pigeyre et al., 2016). There are three types of genetic obesity- monogenic, syndromic and polygenetic. In polygenic obesity, there is an accumulation of mutations which contribute to an increased risk of obesity. A genome wide association study identified 97 loci that are associated with high BMI (Locke et al., 2015). These loci were mostly associated with the central nervous system in the hypothalamus supervising the homeostatic response and also the hippocampus supervising the hedonic response. This reinforces the importance of the role of gut-brain signalling in eating and obesity. In addition, energy

metabolism and adipocyte differentiation pathways were identified. The 97 loci identified were only responsible for a 2.7% variation in BMI. Each loci acts additively, with each SNP leading to an increase of 0.1kg/m^2. For most cases, the genetic factors contributing to obesity are complex and intertwined with other factors. In addition, polygenetic predisposition to obesity is modulated by non-genetic factors such as diet and exercise (Rohde et al., 2019; Vimaleswaran et al., 2009). As the majority of genome wide studies on obesity are carried out on people of European ancestry, some significant associated alleles may be undiscovered, as there is heterogeneity between different ethnic groups (Locke et al., 2015; Stryjecki et al., 2018).

Monogenic obesity is caused by a single gene mutation and is relatively rare accounting for around 3% of obesity (Kleinendorst et al., 2018), but leads to childhood-onset of obesity. Leptin (*LEP*) and leptin receptor (*LEPR*) mutations, mutations in *POMC* and in *MC4R* are the most common monogenic pathogenesis, with *MC4R* mutations being overall the most common leading to insatiable hunger (Kleinendorst et al., 2018).

Syndromic obesity is also relatively rare and obesity phenotypes are accompanied by neurological defects and dysmorphia. One well characterised example of syndromic monogenic obesity is Prader-Willi syndrome which occurs in 1 in 15,000 to 30,000 births (Stryjecki et al., 2018). It is caused by maternal imprinting and in addition to severe obesity patients also suffer from neurological developmental disorders and short stature (Pigeyre et al., 2016). Obesity in Prader-Willi syndrome is caused by insatiable hunger creating increased food intake.

Epigenetic status has a cause and effect relationship with obesity. An association has been shown between increased BMI and DNA methylation at the hypoxia inducible factor (HIF) 3α locus in blood and in adipose tissue, and also methylation of *LEP* in blood and adiponectin gene *ADIPOQ* in adipose tissue (Houde et al., 2015; Pigeyre et al., 2016; Rohde et al., 2019). Some of these epigenetic effects may be transgenerational, and evidence points to exercise leading to methylation changes in spermatozoa and maternal and paternal diet being a risk factor for childhood obesity (Huypens et al., 2016; Lawlor et al., 2012; Rohde et al., 2019; Woo Baidal et al., 2016).

Reduced energy expenditure is a contributor to obesity. There are three forms of physiological energy expenditure- resting metabolic rate, physical activity and

thermogenesis. The resting metabolic rate encompasses all of the energy required for basal cellular processes. Energy metabolism in humans is hardwired for energy storage to help survive prolonged periods of fasting, and so weight loss creates a counteractive slowing of resting metabolic rate, which makes it difficult to maintain weight loss long term (Rosenbaum et al., 2008; Thivel et al., 2013; Wadden et al., 1996). Physical activity is energy expenditure by skeletal muscle for movement. Modern life and has led to decreased physical activity. Also, disability or immobility can limit access to physical exercise. Thermogenesis is the energy expended as heat. In humans this mostly compromises of diet induced thermogenesis, the postprandial energy expended during the absorption and metabolism of food. The macronutrient composition of a meal will effect energy expended for diet induced thermogenesis, with more energy required to metabolise proteins and fats than carbohydrates (Oussaada et al., 2019). Thermogenesis, also occurs in response to cold exposure, although it is more prominent in rodents and human infants.

Other factors that can increase predisposition to obesity are gut microbiota diversity, perturbed sleep patterns and prescribed medications (Bray et al., 2016; Hebebrand et al., 2017). The gut microbiota increase efficiency of nutrient harvest from food through the fermentation of macromolecules. Release of nutrient responsive signalling metabolites by gut microbiota can modulate the homeostatic and hedonic responses to food, and also can effect insulin response, lipid storage and inflammation (Torres-Fuentes et al., 2017). High fat and sugar diets are associated with decreased gut microbiota diversity, which is associated with increased ghrelin levels (Clemmensen et al., 2017; Torres-Fuentes et al., 2017). Sleep duration and quality is negatively correlated with BMI. Sleep duration studies are limited, and may need to be more longitudinal to see a relationship, but short-term studies have shown that reduced sleep duration leads to decreased satiety and therefore increased food intake and a net gain in energy intake (St-Onge, 2017).

The etiology of obesity is incredibly complex and varies between individuals. The population wide increase stems from individual's physiological responses to the modern day, counter-evolutionary obesogenic environment.

1.1.2 Consequences of Obesity

Obesity has physical, mental and societal impacts for an individual, and impacts on the individual in turn effect society and the economy (Figure 1.1). It was calculated that in 2015, 4 million deaths and 120 million life adjusted years could be attributed to high BMI

(Collaborators, 2017). Obesity is one of the components of the metabolic syndrome, a cluster of symptoms that increase the risk of developing cardiovascular disease (CVD) and type 2 diabetes (T2D), and it increases the risk of having other components of the metabolic syndrome. The other components of the metabolic syndrome are hypertension, high levels of serum triglycerides, high fasting blood glucose levels and low levels of circulating high density lipoprotein-cholesterol.

The most common cause of obesity related death is CVD which causes almost 70% of obesity related deaths (Collaborators, 2017). Men are more at risk for CVD than pre-menopausal women, due to increased visceral type adipose tissue associated with inflammation. This inflammatory profile combined with the increase in fatty acids in circulation can lead to mitochondrial dysfunction and apoptosis in cardiomyocytes. In addition, obesity is related to alterations in cardiac function and structure and is associated with other CVD risk factors such as hypertension that compose the metabolic syndrome (Piché et al., 2018).

The global increase in obesity has been followed by a global increase in T2D incidence, which has risen since the 1980s, and 61.3% of T2D patients in the USA are also obese (Prevention, 2017; Zhou et al., 2016). Diabetes is defined as chronic hyperglycaemia and reduced insulin sensitivity, measured by elevated 8 hour fasting or 2 hour postprandial blood glucose levels. It is thought that increased nutrients lead to increased levels of free fatty acids which cause oxidative damage and impair the function of the glucose cellular uptake transporter glucose transport type (GLUT) 4. Therefore cells are unable to import glucose for energy, leading to use of alternative fuel sources and altered metabolism. This causes increased blood glucose levels and impaired insulin response, eventually leading to insulin producing pancreatic β-cells being unable to produce sufficient levels of insulin (Abdelaal et al., 2017; Chatterjee et al., 2017; Malone and Hansen, 2019). Weight loss is able to reverse the progression to T2D.

Obesity increases the risk of an abundance of diseases in addition to CVD and T2D, including non-alcoholic fatty liver disease (NAFLD) and also non-metabolic diseases such as certain types of breast and colon cancers, reproductive and fertility disorders and can lead to joint problems affecting mobility (Abdelaal et al., 2017). Obesity has also been highlighted as a major risk factor after age for complications from Covid-19 including increased length of hospital stay, increased risk of intensive care unit admission, and increased risk of death (Yu

et al., 2021). In addition it leads to a higher risk of all-cause mortality and early death. In addition to physiological effects obesity is associated with psychiatric disorders such as depression which can stem from body dissatisfaction as well as stigma, prejudice and discrimination from society (Hardin et al., 2018; Phelan et al., 2015). Finally, obesity puts strain on healthcare systems and is a burden on the economy. Obese people are more likely to have higher absenteeism from work or an inability to work due to disability, which leads to reduced productivity (Lehnert et al., 2013). Healthcare spending on obese patients is also higher, with spending increasing with BMI. Given the far reaching and detrimental consequences of obesity, focus on treatment is important.

1.1.3 Intervention in Obesity

Targeting obesity is beneficial for the health and mortality of the individual and also the wider economy. Obesity intervention focuses on weight reduction, with loss of greater than 5% of body weight being considered clinically meaningful for reducing obesity comorbidities and improving mortality (Bray et al., 2016).

Lifestyle interventions to tackle obesity involve diet changes to reduce energy intake and exercise to increase energy expenditure, with a goal of shifting towards a negative energy imbalance. Low calorie diets prescribe an intake of 1200-1500kcal/day for women and 1500-1800kcal/day for men. When rapid intervention is needed very low calorie diets can be employed with a daily intake of 200-800kcal. Very low calorie diets have shown a rapid return to normal blood glucose levels but are difficult to adhere to (Bray et al., 2016). It is recommended to have at least 150 minutes per week of aerobic exercise, and this should be increased for those who are obese or trying to maintain weight loss (Bray et al., 2016). However, increasing physical activity without diet intervention will not achieve weight loss (Fock and Khoo, 2013). Cognitive behavioural therapies and motivational interviewing can be used to support lifestyle interventions (Barrett et al., 2018). Whilst lifestyle interventions are important for weight loss, relying on them alone have proved unsuccessful for long term weight loss due to issues with adherence, which are influenced by will power, lack of accessibility and other factors.

The most successful long-term treatment for obesity is bariatric surgery which gives post-surgery weight reduction, reduced risk of obesity comorbidities and increased mortality (Izquierdo and Crujeiras, 2019; Sjöström et al., 2007). Three types of bariatric surgery are available, Roux-en-Y gastric bypass, sleeve gastrectomy and adjustable gastric banding

which all reduce the size of the stomach. Roux-en-Y gastric bypass gives the greatest weight loss and remission of T2D (Bray et al., 2016). Bariatric surgery changes levels of gut-derived nutrient responsive hormones and therefore modified homeostatic and hedonic responses to food. After surgery, patients show shifts in food choice to low energy foods, and lowered responses to high caloric foods, in addition to lower feelings of hunger and higher satiety from meals (Clemmensen et al., 2017; Münzberg et al., 2015). Patients who had bariatric surgery showed a shift in DNA methylation to a non-obese state, and there have been reported differences between the epigenomes of children who were born to mothers before bariatric surgery to those who were born after (Izquierdo and Crujeiras, 2019; Lawlor et al., 2012). Currently bariatric surgery is reserved for those with a BMI greater than 40kg/m^2 in the absence of comorbidities, or greater then 35kg/m^2 with comorbidities (Fock and Khoo, 2013). However, given its high success rate, and increased ease with the use of laparoscopy, the candidate requirements may change. Unfortunately, given the high rate of obesity amongst the population this is not a feasible option to tackle a global epidemic of obesity.

Attempts have been made to pharmacologically mimic of the effects of bariatric surgery. Glucagon-like peptide-1 (GLP-1) is one of the anorexigenic gut derived hormones whose levels are modified post-surgery. The GLP-1 receptor agonist Ligraglutide is one of the current pharmacological therapeutics offered to treat obesity, although nausea is a frequently reported side effect (Bray et al., 2016). A more effective GLP-1 analogue Semaglutide is soon to be available in the UK (Phillips and Clements, 2022). It is thought that they work through a combination of mechanisms including simultaneously stimulating insulin production and increasing insulin sensitivity, as well as increasing satiety. Whilst GLP-1 analogues focus on the homeostatic response, Contrave, a dual dopamine/norepinephrine uptake inhibitor and opioid agonist, targets the hedonic mesolimbic reward system to reduce food cravings and enhances the anorexigenic effects of α-MSH in the hypothalamus (Bray et al., 2016). Another pharmacological target for weight loss is fat absorption. Orlistat inhibits gastrointestinal and pancreatic lipase to reduce absorption of dietary fat by 30% (Angelidi et al., 2022). Although this is a well-tolerated drug, mostly because it is not absorbed, it does lead to gastrointestinal side effects such as steatorrhea. With all current pharmacological therapeutics offered for obesity side effects remain an issue, particularly cardiovascular, nausea and depressive effects, and not all of them deliver sufficient weight loss.

In summary, obesity is an increasing global epidemic with a complex network of physiological, psychological and environmental causes that leads to increased risk of morbidity and mortality for the individual as well as social stigmatisation and societal economic burden. Calls to update the definition of obesity to reflect its complexity have been made in hope that it can improve selection of therapy for patients (Hebebrand et al., 2017). In order to reduce the global rate of non-communicable diseases obesity would need to be halted (Assembly, 2013; Kontis et al., 2014). However, so far there is a lack of population-wide accessible treatment with guaranteed success. One area of interest it to increase energy expenditure by enhancing non-shivering thermogenesis (NST), an energy expending mechanism that is used for protection from hypothermia in rodents and infants. As obesity is caused by positive energy imbalance, adipose tissue is a key player as the regulator of energy utilisation and storage.

1.2 Adipose tissue

Adipose is an endocrine organ found distributed throughout the bodies of vertebrates that regulates energy storage and metabolism. The distinguishing cell type of adipose tissue are adipocytes, of which three main types exist, white, brown and beige. Whilst white adipocytes are primarily described as energy storage cells, brown and beige adipocytes utilise energy to generate heat by NST. In obesity there is unhealthy expansion of adipose tissue leading to cell death, inflammation, fibrosis and insensitivity to insulin within the tissue, which has whole body metabolic consequences. Given its role in energy regulation, adipose tissue is seen as a key therapeutic target in treating obesity. This has led to much interest in its origins and to the discovery of the heterogeneity that exists within adipose tissue.

White adipose tissue (WAT) is the most abundant adipose tissue in both mice and humans, containing large white adipocytes. A major role of the white adipocyte is to store excess energy in the form of triglycerides inside a large, unilocular lipid droplet which can be accessed during times of fasting through lipolysis to release free fatty acids. In addition it performs an endocrine function through the release of a wide range of signalling molecules called adipokines to relay information on nutritional status to peripheral tissues. Brown adipose tissue (BAT) is seen as having an opposing role to WAT due to its energy utilising properties. Brown adipocytes are morphologically distinct from white adipocytes and are smaller, with smaller, multilocular lipid droplets used to fuel NST. They also have increased expression of the master regulator of mitochondrial biogenesis, peroxisome proliferator

activated receptor (PPAR) gamma coactivator 1α (PGC1α). Therefore increased mitochondrial content with rounder mitochondria which express uncoupling protein 1 (UCP1) to uncouple the mitochondrial proton gradient from ATP synthesis in order to generate heat during NST. NST in brown adipocytes is stimulated by adrenergic signalling, typically in response to cold stimuli. Cold and other stimuli can also lead to browning of WAT, creating beige adipocytes. Beige adipocytes were first described as brown adipocytes that occurred in rodent WAT depots upon cold exposure (Cousin et al., 1992; Young et al., 1984). These cells appeared close to the vasculature and showed BAT-like morphology with multilocular lipid droplets and increased mitochondrial density with brown adipocyte-like mitochondria. They are also capable of NST in response to adrenergic signalling and may be able to compensate for loss of functional BAT (Schulz et al., 2013). Adipose tissue is innervated and vascularised. In addition to adipocytes other cell types such as fibroblasts, preadipocytes, neuronal, endothelial and immune cells exist in the tissue.

Adipose tissue is distributed throughout the body in depots which differ slightly between humans and mice (Figure 1.3). These depots can be grouped into subcutaneous and visceral depots. Subcutaneous depots include anterior, retroperitoneal and inguinal (iWAT) in mice, or femoral, abdominal, upper and cranial subcutaneous in humans (Pollard and Carling, 2020). Visceral WAT depots include mesenteric and epididymal (eWAT) in mice, in humans there is also cardiac and omental WAT. BAT in mice is found at interscapular, subscapular, perirenal, auxillary and cranial locations, with the interscapular region being the most abundant and well-studied. In humans, BAT in the neck and supraclavicular regions are the most investigated, but it also exists in pericardial, paravertebral and suprarenal locations.

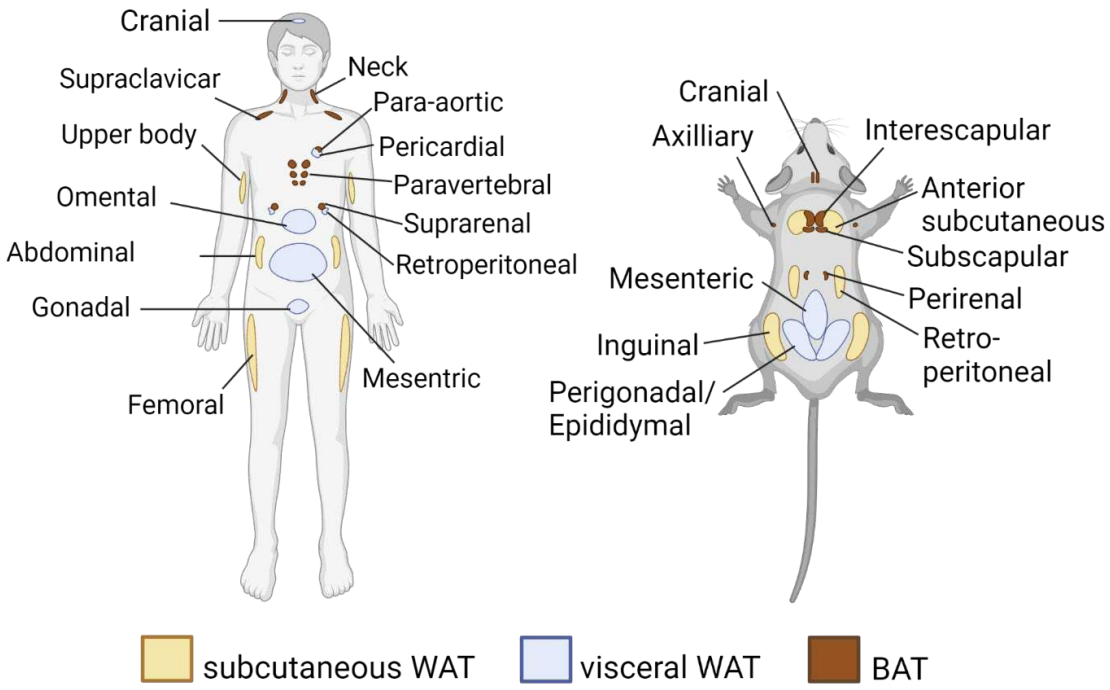


Figure 1.3 Location of adipose tissue depots in humans and mice

The distribution of subcutaneous white adipose tissue (WAT), visceral WAT and brown adipose tissue (BAT) depots in humans and mice. Adapted from (Pollard and Carling, 2020) and (Schoettl et al., 2018).

For years the accepted dogma on BAT in humans was that it was present at birth to cope with cold exposure upon leaving the uterus, and that it was gradually lost over the first years of development. This was disputed when flurodeoxyglucose [F^{18}] positron emission tomography studies showed a metabolically active tissue in the neck and shoulder regions with the same density as fat tissue (Nedergaard et al., 2007). This region was further resolved with computerised tomography scanning and biopsies showing a fat tissue with multilocular lipid droplets and UCP1 expression, substantiating the existence of BAT in adults. Human BAT is activated in response to cold, and is less likely to show up in scans of warm individuals (van Marken Lichtenbelt et al., 2009). In adults it is thought to be more prevalent in women and younger adults, and its activity is negatively correlated with BMI (Cypess et al., 2009; van Marken Lichtenbelt et al., 2009). Human BAT expresses *UCP1*, *DIO2*, *PRDM16*, *PGC1α* and mitochondrial marker cytochrome c at higher levels than in WAT (Virtanen et al., 2009) and bears some resemblance to mouse BAT (Cypess et al.,

2013). Nonetheless, adult human BAT is distinct from mouse BAT, and more closely resembles mouse beige adipocytes when gene expression signatures are assessed (Sharp et al., 2012; Shinoda et al., 2015; Wu et al., 2012). Infant interscapular BAT more closely resembles classical rodent BAT (Lidell et al., 2013).

1.2.1 Adipogenesis

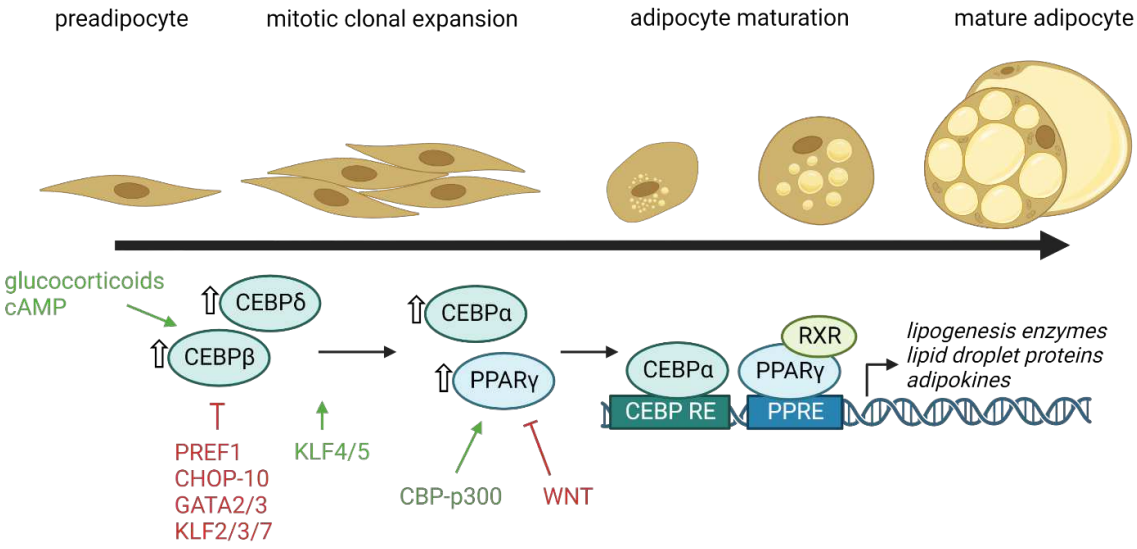


Figure 1.4 Stages of adipogenesis

The differentiation of preadipocytes to a mature adipocytes begins with mitotic clonal expansion and increased levels of CCAAT/enhancer-binding protein (CEBP) β and CEBPδ. These lead to an increase in CEBPα and peroxisome proliferator activated receptor γ (PPARγ) which bind to response elements (RE) to coordinate the expression of adipocyte genes, promoting the maturation of adipocytes with growth of lipid droplets. Adipogenesis is controlled by a range of pro- and anti-adipogenic factors. (cAMP, cyclic AMP; PREF1, preadipocyte factor 1; CHOP-10, CEBP homologous protein-10; GATA, GATA binding factor; KLF, Krüppel-like factors; CBP, CREB binding protein; WNT, wingless-related integration site; RXR, retinoid X receptor; CEBP RE, CEBP response element; PPRE, PPARγ response element).

Adipocytes differentiate from preadipocytes which are derived from progenitor cells originating from mesenchymal stem cells. The regulatory control of the differentiation of preadipocytes to mature adipocytes has been well characterised *in vitro* mostly using the preadipocyte cell line 3T3-L1 (Figure 1.4). Whilst some of this regulation is proven to exist *in*

vivo, translating all elements of 3T3-L1 differentiation into human adipogenesis has not been possible due to limitations in studying adipogenesis in humans *in situ*. *In vitro* differentiation of 3T3-L1 cells begins two days after the cells have reached confluence, allowing for growth arrest and synching of the cell cycle to G1 (Tang et al., 2003b). Adipogenesis is then induced with an adipogenic cocktail typically composed of insulin, glucocorticoid receptor agonists and cyclic AMP (cAMP) agonists. After induction, 3T3-L1 cells re-enter the cell cycle and go through one to two rounds of division increasing their cell number in a process called mitotic clonal expansion. It is not clear whether this is a prerequisite for *in vivo* differentiation. Differentiation begins with a rise in the levels of CCAAT enhancer binding protein (CEBP) β and δ (Tang and Lane, 1999). CEBPβ binding to DNA is required for mitotic clonal expansion to occur (Tang et al., 2003a; Zhang et al., 2004). Without CEBPβ and CEBPδ, it is not possible to form healthy adipose tissue *in vivo*. However, once formed, CEBPβ and CEBPδ are not required for maintenance of the depot (Lee et al., 2019). Glucocorticoids and cAMP signalling can initiate the action of CEBPβ, but the glucocorticoid receptor is not essential for adipogenesis *in vivo* (Lee et al., 2019; Park et al., 2012). Rising levels of CEBPβ and CEBPδ cause an increase in PPARγ and then CEBPα. PPARγ and CEBPα are the master regulators of adipogenesis. However, PPARγ is the only essential transcription factor and adipogenesis can still occur in the absence of CEBPα, although it generates insulin resistant cells (Farmer, 2006; Lefterova et al., 2008; Rosen et al., 2002; Wu et al., 1999). There are two isoforms of PPARγ, PPARγ1 which is constitutively expressed and PPARγ2 which is more adipose tissue specific although there is likely compensation for each other *in vivo* (Farmer, 2006). A bimodal switch model has been proposed for adipogenesis, whereby PPARγ and CEBPα, alongside PPARγ and CEBPβ form positive feedback loops, reaching a threshold to commit a preadipocyte to differentiation (Park et al., 2012). After mitotic clonal expansion and withdrawal from the cell cycle, preadipocytes are committed to terminal differentiation. PPARγ binds to a host of adipocyte related genes all containing PPAR response elements and there is a lot of overlap between PPARγ and CEBPα binding sites (Lefterova et al., 2008). Genes upregulated in adipogenesis include those involved in glucose and lipid uptake and metabolism and genes encoding adipokines allowing for lipid droplet formation and adipocyte maturation (Ahmadian et al., 2013). Adipogenesis is also accompanied by cytoskeletal reorganisation as the cell transforms from a flat fibroblast with a central nucleus to a spherical cell with a more oval shaped nucleus located at the periphery (Verstraeten et al., 2011).

A host of additional transcription factors play a part in commitment to adipogenesis with either pro- or anti-adipogenic roles. The anti-adipogenic transcription factors are expressed in preadipocytes and include the common preadipocyte marker preadipocyte factor-1 (PREF-1), CEBP homologous protein-10 which binds to CEBPβ and antagonises its DNA binding activity and GATA2 and 3 who are also thought to disrupt CEBPβ DNA binding (de Sá et al., 2017; Hudak and Sul, 2013; Tang and Lane, 2000). Some transcription factor family isoforms have opposing roles, such as members of the Krüppel-like factors (KLF), where KLF2, 3 and 7 are anti-adipogenic whilst KLF4 and 5 are pro-adipogenic in early differentiation (García-Niño and Zazueta, 2021). Epigenetic modifiers have been implicated in adipogenesis both *in vitro* and *in vivo*. These include cAMP response element binding protein binding protein-p300, which leads to H3K27 acetylation at the PPARγ enhancer to promote expression, and wingless/integrated (WT1), which leads to H3K27me3 repression to inhibit adipogenesis (Lee et al., 2019).

Several transcription factors regulate the differentiation of brown adipocytes over other cell types. Early B cell factor 2 (EBF2) is enriched in BAT compared to WAT and enhances the binding of PPARγ to thermogenic and mitochondrial genes to promote brown adipogenesis (Rajakumari et al., 2013). Without EBF2 embryos are unable to form functional BAT. The transcriptional coregulatory PR domain containing 16 (PRDM16) protein can form a repressor complex with C-terminal binding protein to reduce the expression of white adipocyte relevant genes (Kajimura et al., 2008; Seale et al., 2009). Bone morphogenetic protein (BMP) 7 promotes brown adipogenesis in both mouse and human cell lines and BMP7 deficient mice lack functional, UCP1 expressing BAT (Okla et al., 2015; Tseng et al., 2008). Differentiation of white adipocytes is promoted by BMP2 and BMP4. BMP2 in humans is a depot-specific paracrine adipogenic factor (Denton et al., 2019). Zinc finger protein 423 (ZFP423) is a transcriptional regulator that maintains the white adipocyte phenotype through the disruption of brown adipocyte transcriptional regulation by EBF2 and PRDM16 (Shao et al., 2016; Shao et al., 2021b). When there is loss of ZFP423 there is browning of white adipose tissue depots.

1.2.2 Adipose tissue lineage

In humans, adipose tissue first appears in the 14th week of gestation and has finished maturing by the 23rd week (Berry et al., 2014; Rosen and Spiegelman, 2014). In rodents most adipose tissue is present by E16.5 (Han et al., 2011). The developmental origins of

adipose tissue is mostly attributed to the mesoderm with the exception of the craniofacial and salivary gland depots which derive from an ectodermal precursor from the neuronal crest (Billon et al., 2007; Sebo and Rodeheffer, 2019). No adipocytes have been shown to come from the endoderm.

Adipocytes share a mesenchymal stem cell precursor with myocytes, osteocytes and chondrocytes. Whilst white and beige adipocytes are closely related and reside in the WAT depots, brown adipocytes share a closer lineage with skeletal muscle myocytes, another thermogenic tissue cell type (Figure 1.5). Both brown adipocytes and myocytes share a myogenic factor 5 (MYF5) expressing precursor and originate from a paired box 3 and paired box 7 lineage (Seale et al., 2008; Timmons et al., 2007). EBF2 or myoblast determination protein 1 (MYOD) expression in the MYF5 population of the developing mesoderm distinguish the development of brown adipocyte or skeletal muscle precursors respectively (Wang et al., 2014). A transcriptional regulation complex consisting of PRDM16 and euchromatic histone lysine methyltransferase 1 promote the differentiation of brown adipocytes over myocytes by inducing the expression of brown adipocyte specific genes both *in vitro* and *in vivo* (Ohno et al., 2013; Seale et al., 2008; Seale et al., 2007). CEBPβ can form a transcriptional complex with PRDM16 to promote brown adipogenesis over myogenesis (Kajimura et al., 2009).

Whilst beige adipocytes are phenotypically very similar to brown adipocytes, and their thermogenic gene expression is driven by PRDM16, they are a distinct cell type that do not typically arise from a MYF5 lineage (Seale et al., 2008; Seale et al., 2011; Wu et al., 2012). Interestingly, $MYF5^{+}$ precursors were shown to be able to give rise to some white and beige adipocytes in WAT when the deletion of phosphatase tensin homologue through a MYF5 Cre recombinase (Cre) lead to differential expansion of WAT depots and WAT lipodystrophy (Sanchez-Gurmaches et al., 2012). The contribution of $MYF5^{+}$ precursors was greater in retroperitoneal WAT and interscapular WAT and very low in iWAT and eWAT. Because of the low presence of $MYF5^{+}$ precursors in WAT depots, MYF5 is not a marker for white or beige adipocytes in WAT, but this demonstrates the complexity of defining adipocyte lineage. Beige adipocytes come from either transdifferentiation of mature white adipocytes or de novo differentiation from precursor populations (Barbatelli et al., 2010; Min et al., 2019; Rosenwald et al., 2013; Wang et al., 2013; Wu et al., 2012). Although not completely resolved, it is likely that upon initial recruitment there is de novo differentiation from

precursors, of which several unique precursors have been identified, and then upon subsequent recruitment there is transdifferentiation, possibly from previously beige adipocytes that retain epigenetic memory of the beige phenotype (Roh et al., 2018; Sanchez-Gurmaches and Guertin, 2014a; Shao et al., 2019).

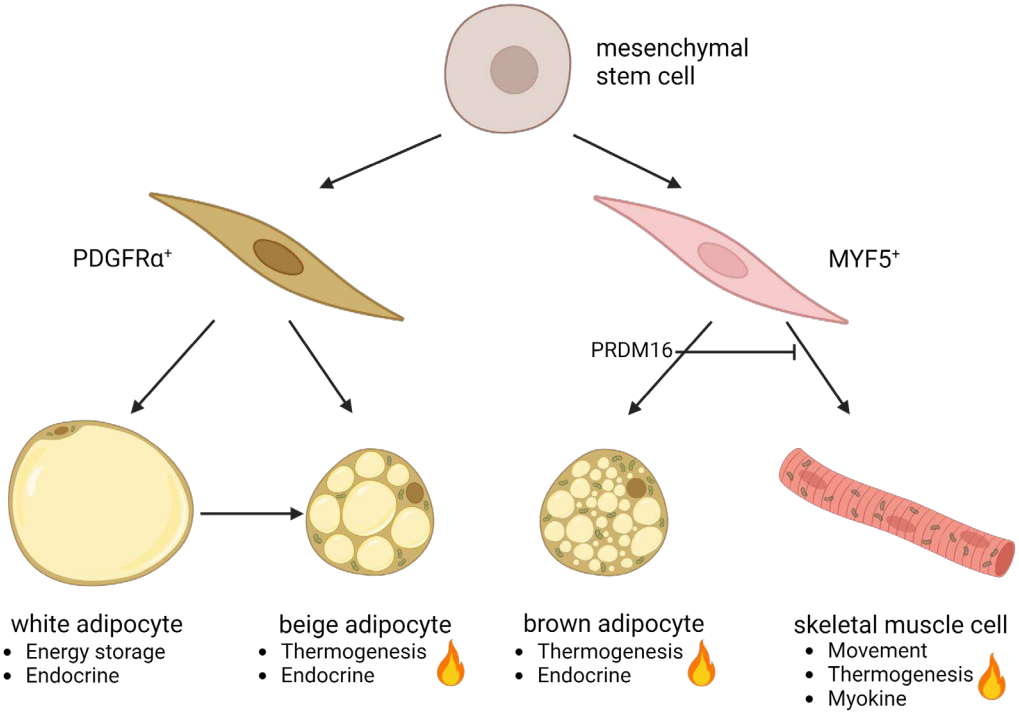


Figure 1.5 Lineage of adipocytes

A simplified overview of adipocyte lineages. All adipocytes share a mesenchymal stem cell precursor. White and beige adipocytes come from a platelet-derived growth factor receptor α (PDGFRα) expressing precursor. The primary functions of white adipocytes are for energy storage in large unilocular lipid droplets and endocrine signalling. Beige adipocytes may arise from their own precursor or from the transdifferentiation of white adipocytes. They have smaller, multilocular lipid droplets and increased mitochondrial content and are capable of thermogenesis. Brown adipocytes share a myogenic factor 5 (MYF5) expressing precursor with skeletal muscle, and the expression of PR domain containing 16 (PRDM16) promotes the differentiation of brown adipocytes over skeletal muscle. Both brown adipocytes and skeletal muscle are thermogenic, and skeletal muscle is important for movement. Brown adipocytes have small, multilocular lipid droplets and high mitochondrial content.

The adipose tissue vasculature is a source of progenitor cells (Berry et al., 2014; Gupta et al., 2012; Min et al., 2016; Sanchez-Gurmaches and Guertin, 2014a; Tang et al., 2008; Tran et al., 2012). Much work has been done to determine the progenitor cells that are recruited upon adipose tissue expansion to generate preadipocytes and give rise to new mature adipocytes. Lineage tracing studies, the identification of population specific cell surface markers for fluorescence activated cell sorting (FACS) and single-cell RNA sequencing (scRNA-seq) has enabled the discovery of candidate progenitor populations and differentiation hierarchies. Adipose tissue can be divided into mature adipocytes and stromal vascular fraction (SVF), which includes all the other cell types residing in adipose tissue such as endothelial, smooth muscle, fibroblast and immune cells. Upon dissection and enzymatic digestion of adipose tissue, these two fractions can be physically separated by density, as mature adipocytes are lipid laden and float above the SVF which can be pelleted by centrifugation. The initial FACS strategy to select adipose tissue progenitor cells from WAT was to isolate based on Lin^- $CD29^+$ $CD34^+$ $Sca\text{-}1^+$ $CD24^+$ expression (Rodeheffer et al., 2008). Lin^- removed $CD31^+$ endothelial cells and $CD45^+$ hematopoietic cells, the other markers selected a more stem cell-like population. When transplanted into mice these progenitors were able to make adipocytes. This study opened up the investigation into adipocyte progenitor cells.

There are several lineages proposed for adipocytes, summarised in Table 1.1. Endothelial, hematopoietic and mesothelial origins are generally ruled out as contributing to adipogenesis *in vivo* (Kanda et al., 2009; Sanchez-Gurmaches and Guertin, 2014a; Westcott et al., 2021). Lineage tracing shows that surface protein platelet derived growth factor receptor (PDGFR) α is a marker for the precursor fibroblasts which give rise to all mature adipocytes in a range of depots (Berry and Rodeheffer, 2013; Cattaneo et al., 2020). PDGFRα expression is lost upon differentiation and not expressed in mature adipocytes, therefore it is a good progenitor specific marker in adipose tissue (Lee et al., 2012b). PDGFRα progenitors in WAT can be split into subpopulations with unique cell surface markers that have unique functions, with examples shown in ScRNA-seq studies have also identified a differentiation hierarchy between adipose tissue derived stem cell subpopulations. These tend to fall into three categories- a more stem-like adipocyte progenitor which can be marked by surface marker dipeptidyl-peptidase 4 (DPP4), a committed adipocyte precursor with surface marker intracellular adhesion molecule 1 (ICAM1), and a population with surface marker CD142, which has been described as either an adipogenic regulatory population, or an alternative

adipocyte precursor (Hepler et al., 2018; Merrick et al., 2019; Rennert et al., 2016; Rondini and Granneman, 2020; Schwalie et al., 2018b). The stem-like adipocyte progenitors marked by DPP4 are more proliferative, more multipotent with osteogenic differentiation potential and are less responsive to adipogenic stimuli than committed adipocyte precursor populations (Merrick et al., 2019; Rennert et al., 2016; Schwalie et al., 2018b). These progenitors can be found residing in the reticular interstitium surrounding adipose tissue, introducing a novel location for adipocyte progenitors, and are the beginning of a differentiation hierarchy, forming ICAM1+ and CD142+ cells that then mature to adipocytes *in vivo* (Stefkovich et al., 2021). The committed ICAM1+ adipocyte precursors are the most adipogenic population, readily forming adipocytes either spontaneously or with minimal stimulation (Burl et al., 2018; Hepler et al., 2018; Merrick et al., 2019). The population marked by CD142 has been described as an anti-adipogenic, adipocyte regulatory population (Schwalie et al., 2018a). CD142 has also been described to mark an alternative adipocyte progenitor that is formed from DPP4+ progenitors (Merrick et al., 2019).

Table 1.2. White adipocyte differentiation factor ZFP423 is expressed in adipose tissue mural cells, the pericytes and smooth muscle cells that surround the endothelial vasculature, indicating that mural cells are a source of adipocyte progenitors (Gupta et al., 2012). Mural cells and other smooth muscle cell progenitors are thought to give rise to brown and beige adipocytes (Berry et al., 2016; Gupta et al., 2012; Long et al., 2014; Shamsi et al., 2021; Shao et al., 2019; Tang et al., 2008).

Table 1.1 Proposed adipocyte lineages

Origin	**Surface markers**	**Description**	**References**
Endothelial	CD31	VE-Cadherin tracing showed endothelial cells form adipocytes *in vitro* and *in vivo*. Deletion of PPARγ in endothelial cells doesn't affect fat mass.	(Kanda et al., 2009; Sanchez-Gurmaches and Guertin, 2014b; Tran et al., 2012)

Hematopoietic	CD45	Hematopoietic stem cells were able to form adipocytes when transplanted into mice. Deletion of PPARγ in hematopoietic cells does not prevent adipose tissue depot formation.	(Kanda et al., 2009; Sera et al., 2009)
Mesothelial	WT1 KRT19	Lineage tracing showed WT1 marked visceral adipocytes. WT1 is not a specific mesothelial cell marker, cells with more specific markers such as KRT19 don't form adipocytes.	(Chau et al., 2014; Westcott et al., 2021)
Fibroblast	PDGFRα	Marks all adipocyte precursors, subpopulations exist.	(Berry et al., 2014; Cattaneo et al., 2020)
Mural	PDGFRβ	Source of beige adipocytes, recruited in eWAT expansion in response to high fat diet and can lead to an 'insulin-tolerant' obese phenotype.	(Berry et al., 2016; Gupta et al., 2012; Long et al., 2014; Shao et al., 2016; Tang et al., 2008; Vishvanath et al., 2016)
Other smooth muscle	Myosin heavy chain 11, Transient receptor potential vanilloid 1	Source of beige adipocytes in iWAT. Source of highly thermogenic adipocytes in BAT recruited upon cold exposure. Source of adipocytes in mouse and human perivascular WAT, which more closely resembles BAT.	(Angueira et al., 2021; Long et al., 2014; Shamsi et al., 2021)

ScRNA-seq studies have also identified a differentiation hierarchy between adipose tissue derived stem cell subpopulations. These tend to fall into three categories- a more stem-like adipocyte progenitor which can be marked by surface marker dipeptidyl-peptidase 4 (DPP4), a committed adipocyte precursor with surface marker intracellular adhesion molecule 1 (ICAM1), and a population with surface marker CD142, which has been described as either an adipogenic regulatory population, or an alternative adipocyte precursor (Hepler et al., 2018; Merrick et al., 2019; Rennert et al., 2016; Rondini and Granneman, 2020; Schwalie et al., 2018b). The stem-like adipocyte progenitors marked by DPP4 are more proliferative, more multipotent with osteogenic differentiation potential and are less responsive to adipogenic stimuli than committed adipocyte precursor populations (Merrick et al., 2019; Rennert et al., 2016; Schwalie et al., 2018b). These progenitors can be found residing in the reticular interstitium surrounding adipose tissue, introducing a novel location for adipocyte progenitors, and are the beginning of a differentiation hierarchy, forming $ICAM1^+$ and $CD142^+$ cells that then mature to adipocytes *in vivo* (Stefkovich et al., 2021). The committed $ICAM1^+$ adipocyte precursors are the most adipogenic population, readily forming adipocytes either spontaneously or with minimal stimulation (Burl et al., 2018; Hepler et al., 2018; Merrick et al., 2019). The population marked by CD142 has been described as an anti-adipogenic, adipocyte regulatory population (Schwalie et al., 2018a). CD142 has also been described to mark an alternative adipocyte progenitor that is formed from $DPP4^+$ progenitors (Merrick et al., 2019).

Table 1.2 Subtypes of PDGFRα expressing adipocyte progenitors

Surface marker	**Outcome**	**References**
$PDGFR\alpha^+$ CD24	$CD24^+$ are stem-like adipocyte progenitors with greater potential for adipogenesis *in vivo.* $CD24^-$ are more committed preadipocytes.	(Berry et al., 2014; Rodeheffer et al., 2008)
$PDGFR\alpha^+$ CD9	$CD9^{high}$ are associated with myofibrotic transformation, increased fibrosis and	(Marcelin et al., 2017)

	inflammation, and pathological adipose tissue expansion in obesity. $CD9^{low}$ are more adipogenic.	
$PDGFR\alpha^{+}$ CD34	$CD34^{-}$ cells express the lowest levels of PDGFRα and generate a more beige-like cell. $CD34^{high}$ cells have greater lipid turnover and are more abundant in the adipose tissue of patients with T2D than in those who don't have T2D. $CD34^{-}$ cells are less abundant in T2D patients	(Raajendiran et al., 2019)
$PDGFR\alpha^{+}$ $SCA\text{-}1^{+}$ CD81	CD81 marks a highly proliferative beige adipocyte progenitor. Loss of CD81 in mice lead to diet induced obesity, and in humans CD81 levels correlated with metabolic health.	(Oguri et al., 2020)

Within a depot it has been shown that there are adipocytes originating from different lineages and with different functions residing alongside each other (Kahn et al., 2019). This mosaicism has been demonstrated with lineage tracing, such as tracing the MYF5 in different depots, which shows different proportions of cells originating from a MYF5 lineage depending on the adipose tissue depot. In the retroperitoneal adipose tissue depot, there are adipocytes occurring from the MF5 lineage next to adipocytes that did not arise from a MYF5 lineage (Sanchez-Gurmaches and Guertin, 2014b). Spatial transcriptomic and spatial mapping studies have also revealed functional mosaicism within the adipose tissue depot (Bäckdahl et al., 2021). Within human abdominal subcutaneous adipose tissue it was observed that there were three prominent adipocyte subtypes dispersed throughout the depot. One subtype marked by expression of leptin and correlated with obesity. Another was marked by perilipin and was more insulin sensitive and carried out more glucose and lipid metabolism. The third subpopulation was marked by serum amyloid A1/2 and played a role in retinol metabolism. Clonal expansion and differentiation of mesenchymal stem cell

progenitors also gave functionally heterogeneous adipocytes that clustered into specific subtypes, with one cluster showing a preference for adiponectin production and another showing a preference for leptin production (Min et al., 2019). Therefore, there is vast heterogeneity within adipose tissue.

1.2.3 Adipose tissue function

Adipocytes are morphologically distinct from other cell types due to the presence of their large lipid droplets. The lipid droplet is central to the function of the adipocyte, allowing for accessible energy storage in the form of triacylglycerol (TAG) that can be rapidly released by lipolysis. In addition, lipid droplets can protect the cell from lipotoxicity by preventing exposure to free fatty acids which can trigger the unfolded protein response by the endoplasmic reticulum (ER), or disrupt the mitochondrial membrane potential (Olzmann and Carvalho, 2019; Wang et al., 2011). Adipocyte lipid droplets are composed of a neutral lipid core primarily consisting of TAG and a phospholipid monolayer. Lipid droplets form from the ER which is the site of lipid synthesis enzymes (Olzmann and Carvalho, 2019; Wilfling et al., 2014). Although the exact mechanism of lipid droplet biogenesis is unknown, the current opinion is that synthesis of TAGs and other lipids occurs in the ER and leads to their accumulation between the inner and outer leaflets of the phospholipid membrane (Figure 1.6).

TAG synthesis occurs through a multistep pathway where fatty acids donated by acyl-CoA are esterified onto a glycerol back bone. The first step is the acylation of the TAG backbone glycerol-3-phosphate to lypophosphatidic acid, and this reaction is catalysed by glycerol-3-phosphate acetyl transferase with acyl-CoA. The second step is the acetylation of lypophosphatidic acid to phosphatidic acid by acylglycerophosphate acyltransferase and acyl-CoA. Phosphatidic acid phosphohydrolases enzymes then convert phosphatidic acid to diacylglycerol (DAG) by removing the phosphate group. Finally, DAG can be converted to TAG by the final acylation with acyl-CoA and this is catalysed by diacylglycerol acyltransferase (Qi et al., 2017).

The accumulation of lipids causes a lipid lens to form from the cytosolic lipid envelope, eventually reaching a size threshold where it begins to bud off and form a small nascent lipid droplet. In adipocytes these can grow and mature to form very large lipid droplets. Initial growth occurs by increased lipid accumulation, either through ER acquired lipids or through locally synthesised lipids. Maturation occurs through lipid droplet fusion and transfer of lipids

from a smaller lipid droplet to a larger lipid droplet (Olzmann and Carvalho, 2019; Qi et al., 2017; Wilfling et al., 2014).

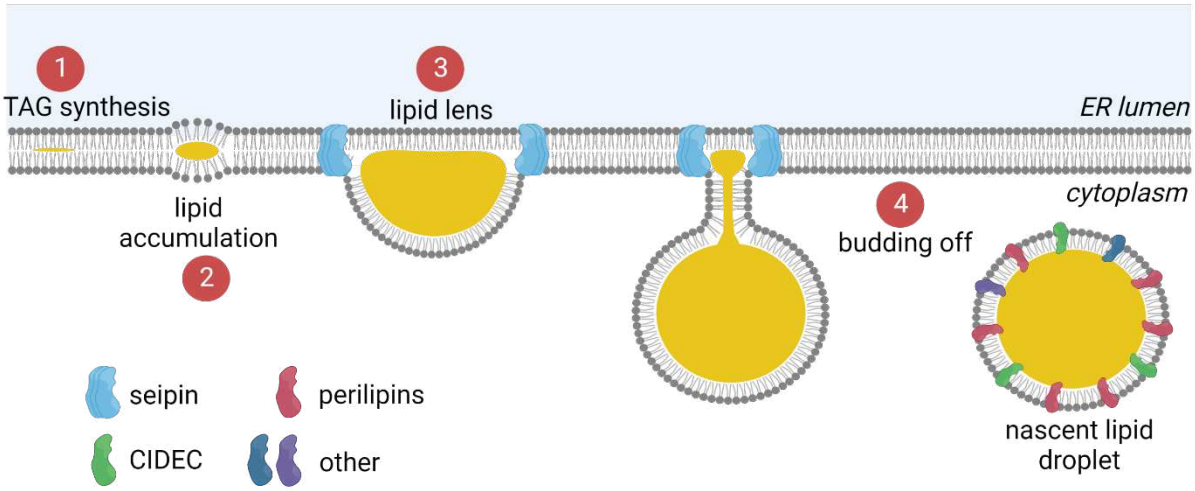


Figure 1.6 Lipid droplet biogenesis

The current opinion on lipid droplet biogenesis is that triacylglycerols (TAG) are synthesised and accumulate in the endoplasmic reticulum (ER) membrane. As TAGs accumulate, a lipid lens develops that bulges into the cytoplasm. Once a size threshold has been reached, the lipid droplet buds off from the ER membrane. Seipin is important for lipid droplet biogenesis, and proteins such as CIDEC and perilipins are localised to the lipid droplet membrane.

A study in monkey fibroblasts showed that 85% of lipid droplets are in contact with the ER, although it is not known whether this is equivalent in the case of adipocytes which have much larger lipid droplets (Valm et al., 2017). These contacts are thought to be essential for the transfer of lipids and some of the lipid droplet associated proteins such as enzymes for lipid synthesis from the ER to the lipid droplet. In addition to the ER, lipid droplets are able to form dynamic contacts with other organelles to allow for transfer of lipids and proteins (Valm et al., 2017). This can occur during times of nutrient stress, for example to fuel fatty acid β-oxidation in the mitochondria, or for recycling of lipids in the lysosome by a specialised autophagy called lipophagy (Schuldiner and Bohnert, 2017; Varghese et al., 2019).

Proteomic studies have revealed hundreds of lipid droplet associated proteins (Qi et al., 2017). Some of these proteins are acquired through transfer from the ER, whilst some are directly targeted to the lipid droplet. The ER protein seipin is critical for nascent lipid droplet formation and growth (Wang et al., 2016). It is found at the ER-lipid droplet contact points

and may be responsible for determining where these points will form (Salo et al., 2019). It also regulates the transfer of protein and lipids from the ER to the lipid droplet (Salo et al., 2016; Zoni et al., 2021). The cell death inducing DFFA like effector (CIDE) proteins, of which there are three isoforms A, B and C, are important in lipid droplet growth (Konige et al., 2014; Qi et al., 2017). CIDEC, also called fat-specific protein 27, is found distributed around the lipid droplet and is enriched at lipid droplet to lipid droplet contact points (Gong et al., 2011). It is necessary for the maturation of lipid droplets by coalescence and the formation of large, mature lipid droplets in adipocytes (Jambunathan et al., 2011). CIDEC mediates pore formation for the unidirectional transfer of neutral lipids from smaller lipid droplets to larger lipid droplets driven by the higher internal pressure in the smaller lipid droplet (Gong et al., 2011). Because it relies on these biophysical differences, CIDEC mediated lipid transfer does not occur between lipid droplets of the same size, even if CIDEC is present at lipid droplet to lipid droplet contact points. CIDEA is also involved in lipid droplet fusion, although it mediates a slower rate of lipid transfer than CIDEC. In BAT CIDEA translocates to the nucleus where it acts as a coactivator to promote thermogenesis and so it is a marker of brown and beige adipocytes (Gong et al., 2011; Konige et al., 2014). CIDEB is mostly expressed in the liver (Konige et al., 2014). The most abundant lipid droplet associated proteins are the perilipins (Sztalryd and Brasaemle, 2017). Whilst perilipin 2 and 3 are ubiquitously expressed across tissues, perilipin 1 and 4 are specific to adipocytes, and perilipin 5 is found in oxidative tissues including BAT (Sztalryd and Brasaemle, 2017; Wang et al., 2011). Perilipin1 interacts with CIDEC to enhance lipid droplet size (Sun et al., 2013b). Perilipins coat the lipid droplet and can regulate access to lipids by acting as a scaffold for lipid droplet-protein interactions.

The energy stored in lipid droplets can be accessed through lipolysis and subsequent oxidation of the released fatty acids. TAGs in the lipid droplet are broken down in a stepwise process catalysed by lipases to generate free fatty acids and glycerol (Figure 1.7) (Zechner et al., 2017). In the first step, adipose tissue triglyceride lipase (ATGL) breaks down TAG to DAG, releasing one fatty acid. Hormone sensitive lipase (HSL) then catalyses the breakdown of DAG to monoacylglycerol (MAG), releasing a second fatty acid. Finally, MAG lipase breaks down MAG to release the final fatty acid and one glycerol molecule. In WAT the released non-esterified fatty acids are transported into circulation with fatty acid binding protein 4 and glycerol is exported through aquaporin 7 to be used for energy in peripheral tissues (Duncan et al., 2007; Maeda et al., 2004). Perilipin 1 prevents lipolysis by blocking

access to HSL and binding the ATGL coactivator cgi-58 to prevent ATGL activation (Sztalryd and Brasaemle, 2017). Perilipin 5 prevents lipolysis by binding and sequestering HSL, and through mutually exclusive binding to either ATGL or to cgi-58, preventing them from being in proximity with each other.

Adipose tissue is highly innervated which allows for relaying of nutritional information from the hypothalamus via norepinephrine released from the sympathetic nervous system (SNS). Lipolysis occurs at a basal rate, but in response to fasting or cold exposure norepinephrine is released by the SNS to stimulate lipolysis at a much greater rate. In BAT stimulated lipolysis releases free fatty acids to fuel UCP1 mediated NST in the mitochondria. Denervation of BAT leads to loss of thermogenesis, and denervation of WAT can lead to increased WAT mass through reduced lipolysis and increased adipocyte size (Blaszkiewicz et al., 2019). Norepinephrine stimulates lipolysis through β-adrenergic receptor (β-AR) signalling (Duncan et al., 2007). β-ARs are G-coupled protein receptors of which three isoforms exist- β1, β2 and β3. The β1 isoform is expressed in preadipocytes, and expression is switched to β3 during differentiation. Meanwhile in human adipocytes, β2 is the predominant isoform (Blondin et al., 2020; Lee et al., 2015). The development of small molecules for isoform specific stimulation, such as CL-316,243 which specifically targets β3-AR, has aided research into β-AR biology (Himms-Hagen et al., 1994). β-AR activation recruits G_s which activates adenylate cyclase, increasing the intracellular cAMP concentration, leading to activation of protein kinase A (PKA) (Figure 1.7). Activation of PKA then leads to lipolysis by its phosphorylation and activation of HSL and ATGL, which translocate to the lipid droplet surface, and also PKA phosphorylation of perilipins to allow lipases to access the lipid droplet (Braun et al., 2018).

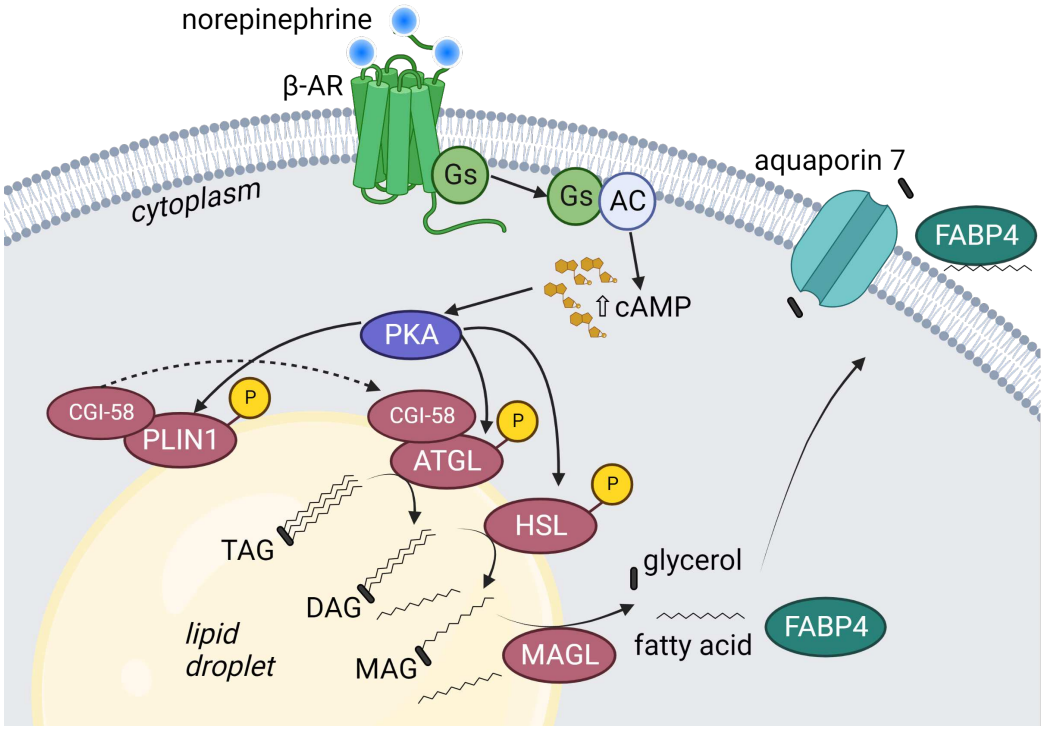


Figure 1.7 Stimulation of lipolysis in adipocytes

Norepinephrine binds to β-adrenergic receptors (β-AR) causing G_s to bind to adenylate cyclase (AC), increasing the intracellular cyclic AMP (cAMP) concentration. This activates protein kinase A (PKA) which phosphorylates perilipin 1 (PLIN1) and prevents it from sequestering ATGL coactivator CGI-58. PKS also phosphorylates adipose tissue triglyceride lipase (ATGL) and hormone sensitive lipase (HSL). These translocate to the lipid droplet surface and catalyse the first and second steps of lipolysis respectively, breaking down triacylglycerol (TAG) to diacylglycerol (DAG) and monoacylglycerol (MAG), releasing fatty acids. MAG lipase (MAGL) catalyses the breakdown of MAG to glycerol and a fatty acid. Glycerol is transported out of the cell through aquaporin 7 and fatty acids are transported out of the cell with fatty acid binding protein 4 (FABP4). Adapted from (Li et al., 2022).

In addition to stimulating lipolysis, β-AR stimulation can also increase thermogenic gene expression in BAT and WAT, leading to browning of WAT (Guilherme et al., 2020; Tabuchi and Sul, 2021). This occurs through PKA phosphorylation of mitogen-activated protein kinase (MAPK) which increases the expression of PGC1α (Cao et al., 2004). Alongside this, p38 MAPK increases the binding of transcriptional regulators to the UCP1 gene promoter,

whilst cAMP stimulates cAMP response element binding protein (CREB) binding to the UCP1 promoter to increase UCP1 expression.

Adipose tissue is highly vascularised. The vasculature is important for adipose tissue function, for receiving and sending of hormone and nutrient signals, and for transport of non-esterified fatty acids and glycerol generated by WAT and heat generated by BAT to the rest of the body. The vasculature is also an important source of adipocyte progenitors, and adipogenesis and angiogenesis are linked processes with adipocytes in culture able to form vascular networks (Fukumura et al., 2003; Han et al., 2011; Min et al., 2016; Muller et al., 2019). Blocking angiogenesis during eWAT development can prevent healthy depot formation (Han et al., 2011). Increasing angiogenesis may lead to metabolic improvement in obesity as more insulin can be delivered to adipose tissue (Robciuc et al., 2016).

Insulin works in conjunction with the SNS to deliver information on nutritional status to adipose tissue. Binding of insulin to the insulin receptor leads to a multitude of changes in the adipocyte phosphoproteome and the full effect of insulin signalling is yet to be understood (Humphrey et al., 2013). The key effects of insulin signalling in adipocytes are the translocation of GLUT4 and fatty acid transporter proteins to the plasma membrane and increased glucose and long chain fatty acid uptake (Stahl et al., 2002). Imported glucose and long chain fatty acids are directed towards lipid synthesis and storage pathways (Calejman et al., 2022). Unlike β-AR signalling which occurs in the fasted state, insulin is released post-prandially and is anti-lipolytic in adipose tissue (Jönsson et al., 2019).

Central to its endocrinal role adipose tissue secretes a large array of peptide and non-peptide factors referred to as adipokines into the vasculature. Adipokines communicate nutritional status to a range of peripheral tissues and modulates their insulin sensitivity and metabolism. There are over 600 adipocyte secreted factors (Fasshauer and Blüher, 2015). The major adipokines discussed in the literature are leptin and adiponectin. As discussed previously, leptin is released postprandially and acts as an anorexigenic hormone in the hypothalamus and in the hindbrain, increasing insulin sensitivity, lowering blood glucose levels and stimulating the hedonic response to food, as well as increasing energy expenditure (Murray et al., 2014; Oussaada et al., 2019). Circulating leptin levels correlate with obesity, and it can also act in an autocrine manner to promote adipogenesis (Karastergiou and Mohamed-Ali, 2010). *ADIPOQ* is the most highly expressed gene in adipose tissue and encodes for adiponectin (Fasshauer and Blüher, 2015). In the circulation,

adiponectin can exist as a trimer, hexamer and even larger 18-mer and 36-mer complexes. Adiponectin improves peripheral insulin sensitivity and secretion, increases energy expenditure, decreases hepatic glucose production whilst promoting hepatic fatty acid oxidation and is negatively correlated with insulin resistance (Fasshauer and Blüher, 2015; Rosen and Spiegelman, 2014). In addition it acts locally to increase adipose tissue mass (Karastergiou and Mohamed-Ali, 2010). Other adipokines such as tumour necrosis factor α (TNFα) and interleukin 6 (IL-6) are secretory peptides that are not adipose tissue specific, but in adipose tissue they promote inflammation (Karastergiou and Mohamed-Ali, 2010). Proteomic studies have revealed several BAT-related adipokines termed batokines that are secreted in response to thermogenic stimuli (Villarroya et al., 2019). These include fibroblast growth factor 21 (FGF21), which increases browning of WAT, several anti-inflammatory factors targeting macrophages, myostatin for cross-talk with skeletal muscle and BMP8b, which can indirectly increase innervation and vascularisation of BAT. Metabolites secreted by browning adipocytes were also able to act as signalling factors, inducing browning in other white adipocytes and increasing glucose and mitochondrial metabolism in skeletal muscle (Whitehead et al., 2021).

Some adipocyte function is depot or location specific. Subcutaneous adipose tissue depots such as the iWAT are thought to have a higher propensity for browning and thermogenic protein expression than visceral adipose tissue depots such as eWAT (de Jong et al., 2015). Differences between the sex distribution and role in disease of subcutaneous and visceral adipose tissue depots is discussed in the next section. The adipose tissue surrounding the vasculature is called perivascular adipose tissue. It has been found to regulate vasoconstriction by secreting an adipokine called adipocyte derived relaxing factor, which prevents blood vessel constriction in response to the vasoconstrictor norepinephrine (Britton and Fox, 2011). It has also been found to secrete pro-inflammatory cytokines in the context of obesity, eventually leading to vascular endothelial cell stress which causes vascular stiffness and vascular dysfunction. Another distinct type of adipose tissue is bone marrow adipose tissue, located either in low haematopoietic bone marrow where it is called constitutive bone marrow adipose tissue, or in bone marrow with active haematopoiesis where it is called regulated bone marrow (Pachón-Peña and Bredella, 2022). Bone marrow adipose tissue expands with ageing or in patients with anorexia nervosa or T2D, and secretes adipokines that regulate osteogenesis and lead to reduced bone density and increased risk of fracture.

1.2.4 Non-shivering thermogenesis

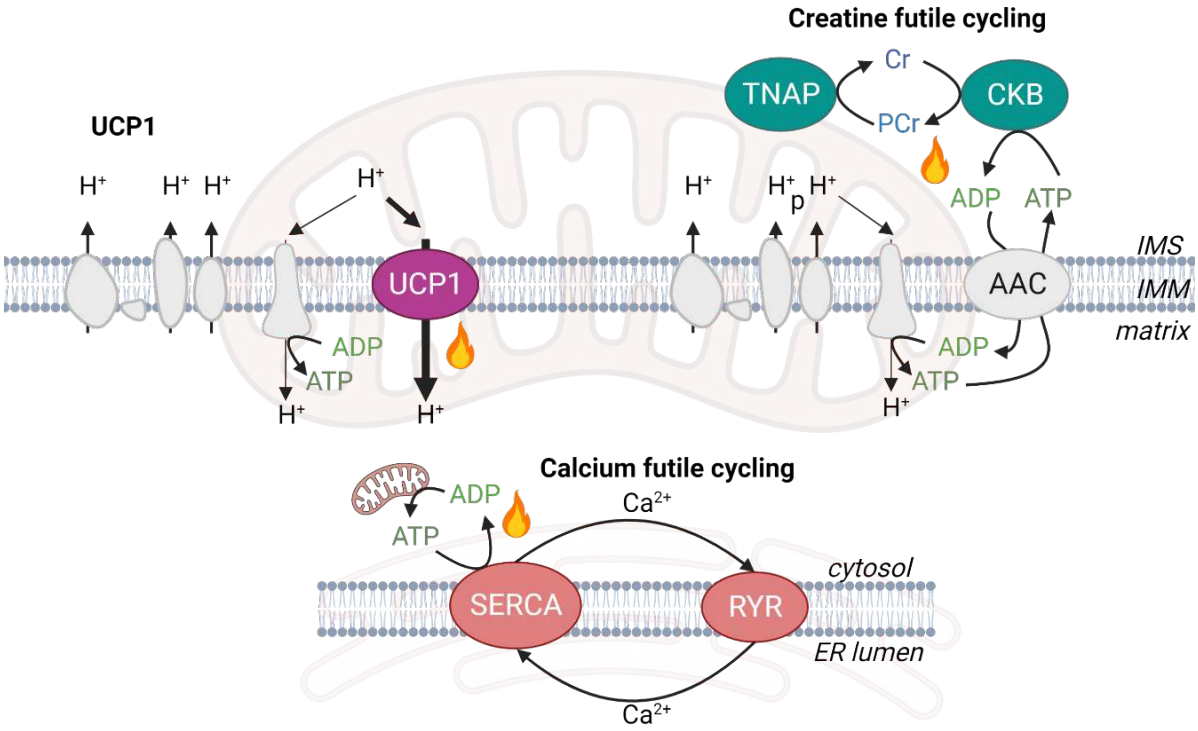


Figure 1.8 UCP1-dependent and independent mechanisms

Uncoupling protein 1 (UCP1) mediates non-shivering thermogenesis (NST) by uncoupling the mitochondrial electron transport chain generated proton gradient from ATP synthase, generating heat instead of ATP. The main mechanisms of UCP1-independent NST are creatine and calcium futile cycling. Creatine futile cycling occurs in the mitochondria and is mediated by creatine kinase B (CKB) and tissue-nonspecific alkaline phosphatase (TNAP) which shuttle phosphate between ATP and phosphocreatine (PCr), generating heat. In calcium futile cycling, calcium is pumped out of the sarcoplasmic reticulum in muscle cells, or the endoplasmic reticulum (ER) in adipocytes into the cytosol by sarco/endoplasmic reticulum calcium-ATPase (SERCA), consuming ATP generated by the mitochondria and producing heat. The calcium is then brought back into the ER by the ryanodine receptor (RYR) to complete the cycle. Adapted from (Roesler and Kazak, 2020), (Rahbani et al., 2021) and (Brownstein et al., 2022). (AAC, adenine nucleotide translocator; IMS, inner membrane space; IMM, inner mitochondrial membrane).

Thermogenesis to maintain body temperature homeostasis occurs by either shivering or non-shivering mechanisms. In shivering thermogenesis there is rapid contraction of skeletal muscle, which requires large amounts of ATP hydrolysis and leads to heat production, but this cannot be maintained long term due to its interference with movement. NST occurs to maintain body temperature in response to cold stimulus, or to expend energy in response to excess calorie intake. There are several NST mechanisms reported in animals that can be split into UCP1-dependent and UCP1-independent mechanisms. Rodents and human infants primarily utilise UCP1-dependent NST and so this is a well-studied mechanism.

UCP1 is a proton and long chain fatty acid symporter that is found at the inner mitochondrial membrane. Upon long chain fatty acid anion binding it uncouples the mitochondrial proton gradient generated by the electron transport chain in respiration from ATP synthesis (Figure 1.8), generating heat and also reducing metabolic efficiency which can protect from diet induced obesity (Fedorenko et al., 2012). BAT is optimised for UCP1 mediated NST as it is extremely rich in mitochondria, has high UCP1 content, is highly innervated for rapid induction of NST and highly vascularised for transport of heat through the circulation (Kozak and Anunciado-Koza, 2008). The mitochondria of beige adipocytes in cold exposed mice iWAT was found to be similar to BAT mitochondria in terms of UCP1 function, although it is not as thermogenic as BAT, as uncoupled respiration was slightly lower (Bertholet et al., 2017; Shabalina et al., 2013). Human BAT expresses higher levels of UCP1 than human WAT, but lower levels in comparison to mouse BAT (Porter et al., 2016; Vijgen et al., 2013). Additionally, with human BAT being a relatively small tissue, the significance of its contribution to energy expenditure in humans is questionable. Interestingly, mathematical modelling has predicted that human beige adipocytes can carry out UCP1-independent NST, and studies in the UCP1 knock out mouse show that UCP1-independent NST also occurs in rodents (Granneman et al., 2003; Liu et al., 2003; Nyman et al., 2017; Ukropec et al., 2006). The two alternative NST mechanisms with demonstrated contributions to thermogenesis are futile creatine cycling and futile calcium cycling (Figure 1.8).

Creatine can be phosphorylated to phosphocreatine, which is used as a phosphate donor for ADP when ATP levels are low in skeletal muscle during exercise. Whilst in skeletal muscle levels of ATP to creating are stoichiometric, in beige adipocytes they are substoichiometric, indicating futile cycling (Kazak et al., 2015). In the mitochondria of cold exposed BAT, creatine kinase B (CKB) regulates the shuttling of P_i from ATP to creatine to create ADP and

phosphocreatine, and tissue nonspecific alkaline phosphatase regenerates creatine through the dephosphorylation of phosphocreatine (Rahbani et al., 2021; Sun et al., 2021). *In vivo* disruption of creatine synthesis or uptake in adipocytes renders mice more cold sensitive and more susceptible to diet induced obesity at thermoneutrality (Kazak et al., 2017; Kazak et al., 2019). In addition to this, CL-316,243 induced browning showed that the majority of beige adipocytes in eWAT did not express UCP1, but are able to carry out creatine cycling (Bertholet et al., 2017). Proteomic studies of human BAT has shown expression of creatine kinase enzymes in mitochondria and evidence of both coupled and uncoupled respiration (Müller et al., 2016).

Calcium cycling is typically used in the skeletal muscle for contraction. Calcium is released from the sarcoplasmic reticulum by the ryanodine receptor (RYR) to initiate contraction, and brought back into the sarcoplasmic reticulum by the sarco/endoplasmic reticulum calcium ATPase (SERCA). The first studies on calcium futile cycling for thermogenesis took place in the skeletal muscle (Bal et al., 2012; Maurya et al., 2015; Rowland et al., 2015). However, it is now known that calcium futile cycling can increase energy expenditure in adipose tissue and that adipose tissue browning in the absence of UCP1 is accompanied by upregulation of genes involved in calcium cycling (Ikeda et al., 2017; Pollard et al., 2019). This mechanism is thoroughly investigated in a mouse model where PRDM16 is overexpressed the adipose tissue of UCP1 knock out mice driving the formation of beige adipocytes lacking UCP1 in iWAT. Mice showed increased SERCA2B mediated futile cycling upon α1-AR and β3-AR stimulation, and were protected from cold exposure and diet induced obesity (Ikeda et al., 2017). Interestingly this pattern follows through in PRDM16 driven browning in pig adipocytes *in vitro*, which naturally lack UCP1 expression (Nowack et al., 2017). Further support for futile calcium cycling NST comes from work in our lab, where a mouse with constitutively activated AMPK was protected from diet induced obesity through increased NST in the absence of UCP1 or creatine futile cycling, but with an increase in expression of SERCA1 and RYR1 (Pollard et al., 2019).

1.2.5 Adipose tissue in disease

High caloric intake triggers expansion of adipose tissue which can occur either by hypertrophy where there is an increase in adipocyte cell volume, or by hyperplasia whereby there is an increase in the number of adipocytes (Tchoukalova et al., 2010). Pathological expansion of adipose tissue in leads to increased hypoxia, inflammation, fibrosis, impaired

angiogenesis and ultimately dysregulated adipokine secretion, insulin resistance, ectopic fat accumulation and metabolic perturbations in peripheral tissues associated with obesity. These processes are intertwined and determining the initiating event is difficult.

Hypoxia is well characterised in mouse models of obesity and can induce inflammation and fibrosis (Trayhurn, 2014). Hypoxia is associated with increased HIF1α and Ten-eleven translocase expression leading hypomethylation and increased expression of pro-inflamatory adipokines in obese patients (Ali, 2021). The extracellular matrix (ECM) is rich in collagen and is important for cell communication, signalling and to act as a tissue scaffold. ECM remodelling is important for healthy adipose tissue expansion, but in obesity there is excessive ECM accumulation which leads to fibrosis (Crewe et al., 2017; Marques et al., 2018; Sun et al., 2013a). Fibrosis leads to adipose tissue rigidity and mechanical inflexibility impairing adipocyte growth, adipose tissue remodelling and angiogenesis. It also is associated with increased inflammation and insulin resistance (Li et al., 2021b). Fibrosis can be triggered by hypoxia induced HIF1α signalling. In adipocyte precursors, HIF1α can effect cell fate switching to a more fibrotic and less adipogenic cell type (Shao et al., 2021a).

Inflammation appears to be important for healthy adipose tissue expansion with a balance between pro- and anti-inflammatory immune responses required for adipogenesis and ECM remodelling. However, in obesity inflammation becomes chronic and pathological and begins in adipose tissue before occurring in other metabolic tissues (Crewe et al., 2017; Unamuno et al., 2018; Zatterale et al., 2020). Pathological inflammation can be triggered by lipid accumulation, hypoxia induced HIF1α signalling, fibrosis, adipocyte hypertrophy and cell death (Zatterale et al., 2020). Another contributing factor is a reduction in glutamine levels which occur in obesity leading to increased glycolysis in adipocytes which indirectly increases the production of pro-inflammatory adipokines (Petrus et al., 2020). Pro-inflammatory cytokines such as IL-6 and TNFα recruit immune cells to infiltrate adipose tissue. Macrophages are the most abundant immune cell in adipose tissue and form crown-like structures around dead adipocytes to clear away toxic lipid species from the lipid droplet (Cinti et al., 2005). Whilst macrophage clearing is beneficial in healthy adipose tissue, crown-like structures become more prevalent in obese adipose tissue as there is an increase in apoptosis and necrosis of hypertrophic adipocytes (Cinti et al., 2005; Crewe et al., 2017; Murano et al., 2008). In obesity there is increased polarisation towards pro-inflammatory M1

macrophages and a decrease in anti-inflammatory M2 macrophages (Unamuno et al., 2018; Zatterale et al., 2020).

Pro-inflammatory cytokines lead to adipokine dysregulation causing peripheral insulin resistance (Crewe et al., 2017). Adipokine levels correlate with BMI and can serve as biomarkers of metabolic status, with many being upregulated in obesity but some, such as adiponectin which exerts metabolic benefits, being downregulated (Arita et al., 1999; Dahlman et al., 2012). Subpopulations of adipocytes that are associated with higher adiponectin levels are lower in obese patients (Bäckdahl et al., 2021). IL-6 or TNFα are upregulated in obesity and can directly inhibit peripheral insulin signalling through downregulation of glucose transporter GLUT4 and disruption of insulin receptor-insulin receptor substrate 1 interactions (Ali, 2021; Crewe et al., 2017). Insulin resistance also occurs through excess lipolysis and release of free fatty acids in obesity which degrade the insulin receptor (Capurso and Capurso, 2012; Gao et al., 2004). BMI correlates with adipocyte insulin resistance, and the proportion of adipocyte subpopulations with higher insulin sensitivity decrease in obesity (Bäckdahl et al., 2021; Roberts et al., 2009; Rydén et al., 2019).

There are differences in the structure and function of different adipose tissue depots which means they have different implications in disease. Generally speaking, the subcutaneous depots are seen as being protective in CVD and metabolic disease whilst visceral depots are harmful and this has caused subcutaneous adipose tissue to be nicknamed ‘good fat’ whilst visceral is called ‘bad fat’. Some of the differences may be due to location, as subcutaneous adipose tissue is located at the periphery whilst visceral adipose tissue is closer to organs. Although debated, it is likely that visceral depots expand through hypertrophy leading to hypoxia, inflammation with more M1 macrophages and fewer regulatory T cells and eventually ectopic lipid deposition (Bilal et al., 2021; Liu et al., 2021a; Palmer and Clegg, 2015). On the contrary subcutaneous depots first expand by hyperplasia coupled with more functional adipocyte heterogeneity, which improves insulin sensitivity and adipose tissue function. Proteomic studies of human adipose tissue depots show a tendency towards lipogenic and glycolytic pathways in visceral adipose tissue, making it a good glucose sink for peripheral tissues, but there is also an increase in proteins related to oxidative stress and mitochondrial dysfunction (Raajendiran et al., 2021). There is sexual dimorphism in the depot distribution between males and females which is thought to be regulated by oestrogen

as ovariectomy removes male-female differences (Palmer and Clegg, 2015). Males and post-menopausal females accumulate more visceral adipose tissue, giving an ‘android’ body shape whilst pre-menopausal females accumulate subcutaneous adipose tissue giving a more ‘gynoid’ body shape. These sex-specific differences explain why pre-menopausal women are better protected from cardiac disease than men and post-menopausal women.

Dysfunction of adipose tissue is fundamental to lipodystrophy, a family of diseases classified by loss of adipose tissue. Whilst lipodystrophy is opposite to obesity in terms of effect on adipose tissue mass, both lead to a domino effect of expended adipose tissue storage capacity causing ectopic lipid accumulation resulting in metabolic syndrome and other co-morbidities such as NAFLD, T2D and CVD. (Danforth, 2000; Gonzaga-Jauregui et al., 2019; Lotta et al., 2017). Therefore the whole body metabolic and disease outcomes are similar in obesity and lipodystrophy. In particular lipodystrophies are accompanied by high prevalence of insulin resistance and T2D (Gonzaga-Jauregui et al., 2019). This is due to lipid spill over into liver and muscle, leading to lipid toxic events such as impaired insulin signalling, decreased glucose uptake and low grade inflammation, which contribute to insulin resistance as well as dyslipidaemia (Borén et al., 2013; Shulman, 2014). In lipodystrophy there is also a loss of leptin due to the loss of adipose tissue, and loss of or insensitivity to leptin is sometimes seen in monogenic obesity (Farooqi et al., 1999; Lim et al., 2021). Many of the therapies that are used to tackle obesity can also alleviate the metabolic effects of lipodystrophy. Diet and exercise intervention, leptin administration, drugs such as metformin and statins and even Roux-en-Y bypass surgery have been employed to improve the health of patients with lipodystrophy (Lim et al., 2021; Petersen et al., 2002; Simha et al., 2003).

Loss of adipose tissue in lipodystrophies can either be localised, occurring at a specific location after incident, partial, or generalised, where there is complete loss of adipose tissue. Localised lipodystrophies can be acquired for example at a vaccination injection site. Meanwhile partial or generalised lipodystrophies can be either acquired or genetic, with genetic lipodystrophies being congenital and/or familial. Whilst is has traditionally been considered an ultra-rare disease with prevalence estimates of 1.3-4.7 diagnosed cases per million, it is possible that some ‘apple’ shaped adipose tissue distributions are actually partial lipodystrophies, and genetic studies have shown that up to 1 in 7000 carry a lipodystrophy associated mutation (Mann and Savage, 2019). Often, those that carry lipodystrophy associated mutations have components of the metabolic syndrome but undiagnosed

lipodystrophy (Chiquette et al., 2017; Gonzaga-Jauregui et al., 2019). The etiology of acquired lipodystrophies is varied and often rooted in autoimmune or other immune system disorders, and tend to progress with time (Lim et al., 2021). Familial and congenital lipodystrophies can be poly or monogenic (Rochford, 2022). Of the monogenic lipodystrophies, key players in adipogenesis and lipid droplet formation and function are commonly mutated. These include PPARγ which causes familial partial lipodystrophy type 3, perilipin 1 which causes familial partial lipodystrophy type 4, CIDEC causing familial atrial lipodystrophy type 5, HSL causing familial partial lipodystrophy type 6 and seipin causing Berardinelli–Seip congenital lipodystrophy type 2 (Magré et al., 2001; Rochford, 2022).

1.2.6 Brown and beige adipocytes for cell therapy

Since the discovery of BAT in adult humans there has been much anticipation over the possibility of utilising adipose tissue NST for obesity and T2D therapy. This could occur through activation of existing BAT or through recruitment of beige adipocytes. Studies in humans have observed that acute or chronic exposure to low temperatures was able to increase BAT activity and energy expenditure, but only in subjects who already had detectable BAT (Chondronikola et al., 2014; Yoneshiro et al., 2013). Up to 6 weeks of chronic cold exposure also lead to weight loss. However, weight loss was mild, and long term studies have not yet been carried out (Luze et al., 2022; Yoneshiro et al., 2013). Activation of BAT in humans was investigated using the β3-AR specific agonist mirabegron at maximal concentrations that caused off-target effects on the β1- and β2-AR. In this study, mirabegron increased energy expenditure. However, no effects on body weight were reported (Blondin et al., 2020; Cypess et al., 2015).

Instead of activating BAT, the induction of beige adipocytes in WAT is another potential avenue to target obesity. FGF21 is predominantly synthesised by the liver but upon cold exposure synthesis in BAT and WAT is increased, and adipose tissue expresses FGF21 receptors (Fisher et al., 2012; Kharitonenkov et al., 2005). In pre-clinical studies FGF21 has been shown to improve insulin sensitivity, body weight, adiponectin levels and stimulate browning and thermogenesis in disease models (Geng et al., 2020; Kharitonenkov et al., 2005). However, in humans the effects have been more modest, and there are indications that FGF21 leads to bone loss as it promotes adipogenesis over osteogenesis (Geng et al., 2020). Thiazolidinediones such as rosiglitazone and pioglitazone are PPARγ ligands that were used to treat T2D as they improved insulin sensitivity. However, due to their adverse

cardiovascular effects they are no longer in use in the clinic (Xu et al., 2022). Part of their improved insulin sensitivity may have come through stimulation of adipogenesis and increased WAT mass, which ultimately lead to weight gain. Thiazolidinediones also have also been shown to induce browning *in vitro*. However, in humans pioglitazone was unable to induce BAT activity or induce metabolic benefits associated with BAT (Loh et al., 2018). Other browning agents in mice which could be investigated in the context of obesity include thyroid hormones, retinoic acid and AMP activated protein kinase (AMPK) activators (Cuevas-Ramos et al., 2019).

Cell therapy is an alternative method to introduce brown or beige adipocytes into humans. Several studies have shown that transplantation of brown adipocytes derived from human inducible pluripotent stem cells, adipose tissue derived stem cells or MSCs are able to improve the metabolic status of mice, with improved glucose tolerance and reduced body weight gain (Kishida et al., 2015; Lee et al., 2017; Min et al., 2016; Singh et al., 2020; Su et al., 2018). Allogenic transplantation of $DPP4^{+}$ adipose-derived stem cells to diabetic wound sites were able to induce healing in mice (Rennert et al., 2016). Interestingly, a T2D patient with non-functional beige adipose tissue was able to have functional beige adipocytes reprogrammed from their preadipocytes. These reprogrammed beige adipocytes secreted adipokines that induced insulin sensitivity in primary adipocytes from the same T2D patient (Su et al., 2018). Taking advantage of advances in cellular reprogramming and cell therapy technology could be a new therapeutic approach.

1.3 AMPK

AMPK is a master regulator of energy metabolism. ATP is the cellular energy currency, generating energy for enzymatic reactions through the hydrolysis of its phosphate bonds to form ADP and AMP. AMPK is activated by cellular energy stress whereby there are increases in the levels AMP and ADP which indicate a fall in ATP. Activation can occur by phosphorylation from its upstream kinases liver kinase B1 (LKB1) and calcium/calmodulin dependent protein kinase kinase 2 (CAMKK2) and is sustained by protection from dephosphorylation through direct binding of nucleotides or small molecule activators (Figure 1.9). In response, AMPK works to restore cellular ATP levels and phosphorylates a myriad of downstream targets to downregulate anabolic, ATP diminishing pathways and to upregulate catabolic, ATP producing pathways.

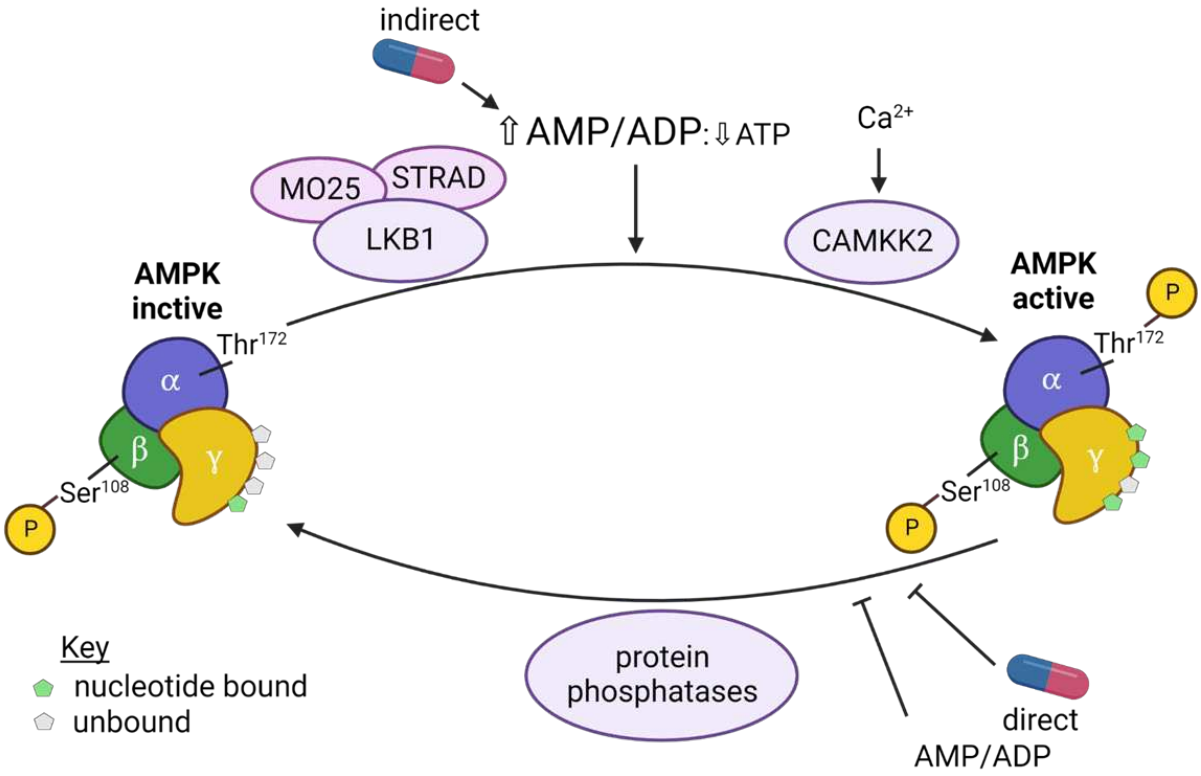


Figure 1.9 Activation of AMPK

AMPK is activated by increased AMP/ADP: ATP levels and upstream kinases liver kinase B1 (LKB1) and calcium/calmodulin-dependent protein kinase kinase 2 (CAMKK2) in response to increased intracellular calcium levels. AMPK can be activated directly by pharmacological activators, or indirectly by drugs that effect the AMP/ADP: ATP levels. The binding of AMP/ADP or of pharmacological activators to AMPK protect it from dephosphorylation by protein phosphatases.

1.3.1 Structure of AMPK

AMPK is a heterotrimer composed of a catalytic α subunit and regulatory β and γ subunits, with nucleotides binding directly to the AMPKγ subunit. There exist two α, two β and three γ isoforms, meaning there is a possibility for 12 different formations of AMPK. Different isoforms exhibit differential tissue specificities that vary amongst species.

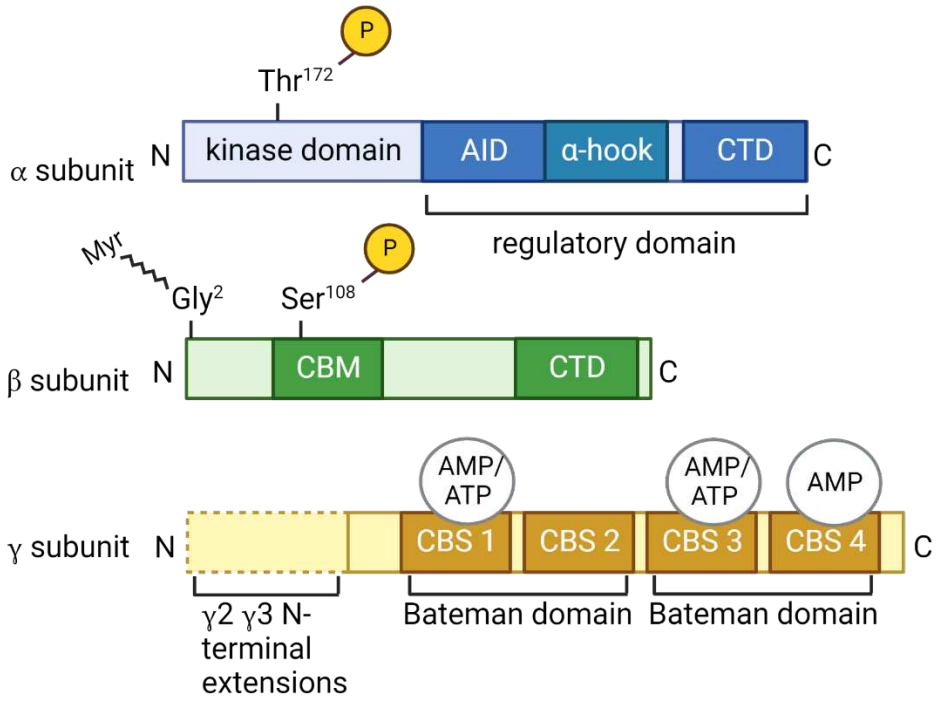


Figure 1.10 Structure of the AMPK subunits

The structure of the AMPK subunits. The AMPKα subunit contains an N-terminal kinase domain with the Thr^{172} phosphorylation site for upstream kinases. The autoinhibitory domain (AID) prevents the phosphorylation of Thr^{172}, but AMP/ADP binding leads to conformational changes in the α-hook so that the AID can no longer prevent phosphorylation. The AMPKα subunit contains a C-terminal domain (CTD) for binding to the AMPKβ subunit. The AMPKβ subunit contains the Gly^{2} myristoylation (Myr) site, a carbohydrate binding motif (CBM) containing the Ser^{108} autophosphorylation site and another CTD for binding to the other subunits. The N-terminus of the AMPKγ2 and γ3 subunits contain N-terminal extensions of various lengths. All of the AMPKγ subunits contain 4 AMP/ADP/ATP binding cystathionine-β-synthase (CBS) motifs which together make up 2 Bateman domains. Adapted from (Gowans and Hardie 2014).

The catalytic AMPKα subunit contains the N-terminal kinase domain and C-terminal regulatory fragment. Phosphorylation of Thr^{172} located in the activation loop within the kinase domain leads to activation of AMPK (Figure 1.10) (Hawley et al., 1996; Willows et al., 2017b). Before the upstream kinases that phosphorylated Thr^{127} were known they were referred to as AMPK kinases. Studies of the yeast AMPK orthologue, sucrose non-

fermenting 1 protein kinase, revealed that its upstream kinases Pak1p, Tos3p and Elm1p shared sequence homology with the mammalian proteins LKB1 and CAMKK2 (Hong et al., 2003; Sutherland et al., 2003). LKB1 works in complex with Ste20-related adaptor protein and mouse protein-25 to phosphorylate AMPKα at Thr^{172} (Hawley et al., 2003; Shaw et al., 2004; Woods et al., 2003a). Germ line LKB1 mutations cause Peutz-Jeghers syndrome, a rare hereditary polyp disorder that predisposes to cancer (Hemminki et al., 1998). The Peutz-Jeghers syndrome mutations in LKB1 lead to inactivation, thereby reducing AMPK activity, although the impact of reduced AMPK activity in disease progression, and tumour formation is unclear (Forcet et al., 2005). CAMKK2 was initially ruled out as the upstream kinase of AMPK (Hawley et al., 1995) until studies in LKB1 deficient cell lines showed that it is capable of activating AMPK (Hawley et al., 2005; Hurley et al., 2005; Woods et al., 2005). CAMKK2 activates AMPK when there are increased intracellular calcium levels, thereby integrating calcium signalling with cellular energy levels.

The AMPKγ regulatory subunit can detect small fluctuations in nucleotide levels (Oakhill et al., 2011). It contains four nucleotide binding sites called cystathionine-β-synthase (CBS) motifs (Figure 1.10). CBS 1 pairs with CBS 2, and CBS 3 with CBS 4 to make two Bateman domains. CBS 1,3 and 4 bind nucleotides, with CBS 4 being permanently bound to AMP under physiological conditions, and CBS 1 and 3 being exchangeable nucleotide binding sites (Xiao et al., 2007). The AMPKγ exchangeable nucleotide binding sites bind AMP leading to conformational changes in the structure that protect AMPKα Thr^{172} from dephosphorylation by protein phosphatases. AMPKγ CBS 3 can bind to AMP or ADP, forming interactions with the α-hook in the regulatory fragment of the AMPKα subunit to protect Thr^{172} from dephosphorylation and sustain AMPK activation (Figure 1.9) (Xiao et al., 2013; Xiao et al., 2011). It is thought that when ATP is bound to CBS 3 in AMPKγ there is steric clash with the α-hook region in AMPKα preventing interaction. The α-hook may convey nucleotide binding information to the autoinhibitory domain (AID) in the AMPKα subunit, and when AMP is bound the AID is released from the kinase domain which allows for AMPKα Thr^{172} phosphorylation (Chen et al., 2013; Xiao et al., 2013). AMPKγ can bind to ADP and AMP tighter than to ATP, facilitating regulation by AMP and ADP under physiological conditions where the concentration of ATP is significantly higher (Gowans et al., 2013; Xiao et al., 2011). AMPKγ2 and γ3 isoforms contain N-terminal extensions not present in AMPKγ1, and each isoform displays differences in level of nucleotide regulated allosteric regulation and protection from dephosphorylation (Ross et al., 2016). Isoform expression

varies between tissues and between species and AMPKγ1 is the predominant isoform in human and rodent tissues (Cheung et al., 2000; Mahlapuu et al., 2004). AMPKγ3 is expressed only in glycolytic skeletal muscle fibres (Mahlapuu et al., 2004). In humans, AMPKγ2 is highly expressed in the heart, and specific mutations are associated with Wolf-Parkinson-White syndrome where patients exhibit cardiac abnormalities with sinus bradycardia. However, mouse models with the AMPγ2 Wolf-Parkinson-White syndrome mutations do not recapitulate the human phenotype unless expressed specifically in the heart, perhaps because AMPKγ1 is the predominant endogenous isoform in the mouse heart (Carling, 2017; Yang et al., 2016b).

The AMPKβ subunit is a scaffold for heterotrimer formation with a C-terminal domain that binds to the AMPKα and AMPKγ subunits (Gowans and Hardie, 2014; Xiao et al., 2007). It undergoes myristoylation at Gly^{2}, which has been suggested to be essential for phosphorylation of AMPKα Thr^{172} and membrane associated response to cellular stress (Figure 1.10) (Oakhill et al., 2010). The AMPKβ subunit contains a carbohydrate binding motif (CBM)- sometimes called the glycogen binding domain- which allows for AMPK to bind to glycogen, and overexpression of AMPK is associated with glycogen accumulation (Hudson et al., 2003; Polekhina et al., 2005). Within the AMPKβ CBM is the autophosphorylation site Ser^{108}, which is phosphorylated *in vivo* (Woods et al., 2003b). Phosphorylated Ser^{108} along with other residues in the CBM in AMPKβ form electrostatic interactions with residues in the N-terminal lobe of the AMPKα subunit kinase domain to create a binding pocket referred to as the ADaM site. (Xiao et al., 2013) The ADaM site allows for allosteric activation of AMPK by direct, small molecule activators which stimulate conformational changes that further protect AMPK from dephosphorylation. The existence of the ADaM site suggests that there may be a natural ligand for activating AMPK, but as of yet the identity of this ligand has not been determined.

1.3.2 AMPK Function

AMPK plays an important role in regulating energy metabolism. It was initially discovered as the AMP sensitive kinase that reduced the activity of the fatty acid synthesis regulator acetyl-CoA carboxylase (ACC) and the cholesterol synthesis regulator 3-hydroxy-3-methylglutaryl-CoA reductase (Carling et al., 1989; Carling et al., 1987; Munday et al., 1988). In order to restore the AMP/ADP to ATP ratio, AMPK prevents cell growth and the synthesis of cholesterol, lipid, amino acids and carbohydrates, and promotes fatty acid oxidation,

glycolysis, autophagy and mitophagy (Figure 1.11). AMPK substrates share a consensus phosphorylation motif summarised φX(B,X)XX(Ser/Thr)XXXφ where φ represents hydrophobic residues, B represents basic residues and Ser/Thr is the site of phosphorylation (Steinberg and Carling, 2019). Discovery of this motif has facilitated substrate identification (Marin et al., 2015).

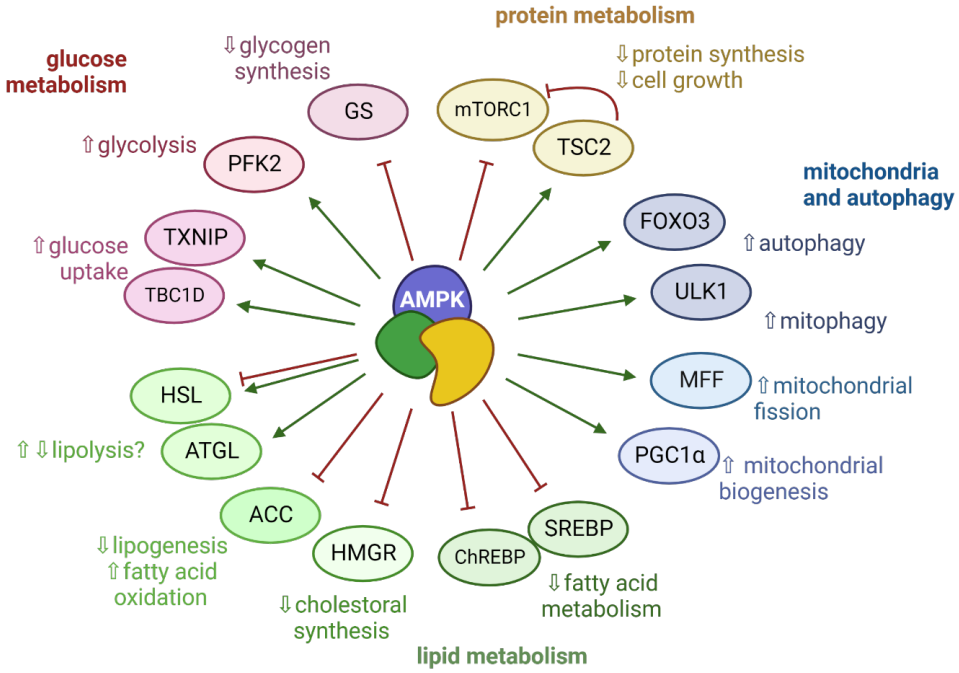


Figure 1.11 AMPK downstream targets

Some of the direct downstream targets of AMPK. The pathways these proteins are involved in are adjacent and the effect of AMPK activation is indicated by arrows. These fall into 4 main categories, regulation of protein metabolism, glucose metabolism, lipid metabolism, and regulation of mitochondria and autophagy. (HSL, hormone sensitive lipase; ATGL, adipose tissue triglyceride lipase; ACC, acetyl Co-A carboxylase; HMGR, 3-hydroxy-3-methylglutaryl-CoA reductase; ChREBP, carbohydrate response element binding protein; SREBP, sterol regulator element binding protein; PGC1α, peroxisome proliferator-activated receptor gamma coactivator 1α; MFF, mitochondrial fission factor; ULK1, Unc-51 like autophagy activating kinase; FOXO3, forkhead box protein O3; TSC2, tuberous sclerosis complex 2; mTORC1, mammalian target of rapamycin complex 1; GS, glycogen synthase; PFK2, phosphofructokinase 2; TXNIP, thioredoxin-interacting protein; TBC1 domain family member).

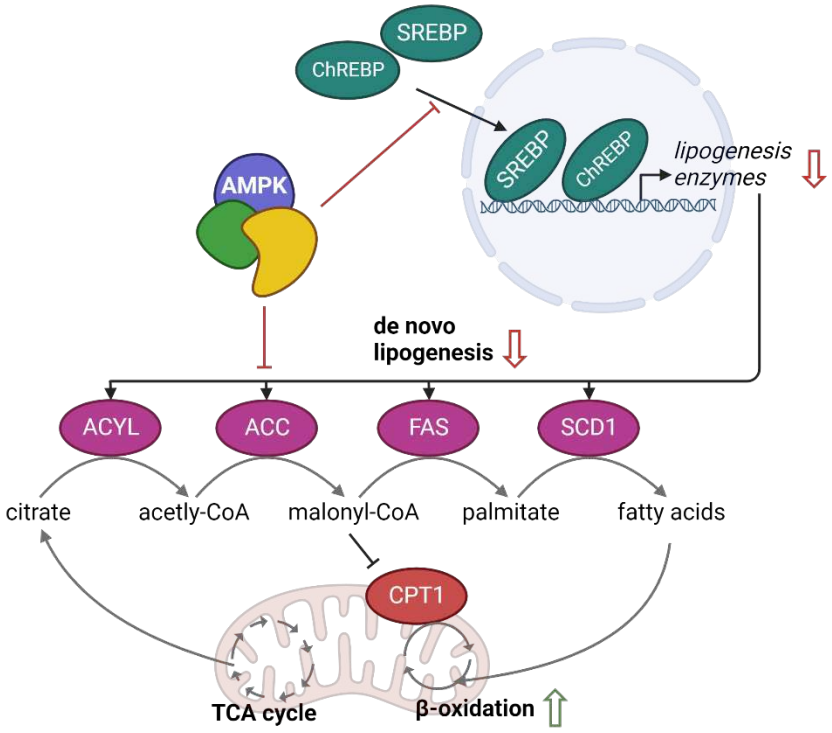


Figure 1.12 AMPK inhibition of lipogenesis

AMPK regulates lipogenesis by preventing the nuclear translocation of carbohydrate response element binding protein (ChREBP) and sterol regulator element binding protein (SREBP) so they cannot activate the transcription of lipogenic enzymes. It also inhibits acetyl-CoA carboxylase (ACC), blocking the conversion of acetyl-CoA to malonyl-CoA, the irreversible step in lipogenesis. Malonyl-CoA inhibits carnitine palmitoyltransferase 1 (CPT1) which is involved in fatty acid β-oxidation, so activation of AMPK also increases β-oxidation. (ACYL, ATP citrate lyase; FAS, fatty acid synthase; stearoyl-CoA desaturase 1).

One of AMPK's most definitive roles is in the inhibition of lipogenesis through the phosphorylation and inhibition of ACC which catalyses the initial and irreversible step in fatty acid synthesis of acetyl-CoA conversion to malonyl-CoA (Figure 1.12) (Garcia and Shaw, 2017; O'Neill et al., 2013). Malonyl-CoA inhibits carnitine palmitoyltransferase I, a mitochondrial protein located on the outer mitochondrial membrane that is essential for transfer of long chain fatty acids into the mitochondria for fatty acid oxidation (Garcia and Shaw, 2017; Herzig and Shaw, 2018; O'Neill et al., 2013). Therefore, in addition to suppressing lipid synthesis, AMPK phosphorylation of ACC also promotes fatty acid

oxidation through a reduction in malonyl-CoA. AMPK can also modulate lipid synthesis through the phosphorylation of transcription factor sterol regulatory element binding protein (SREBP) and carbohydrate response element binding protein (ChREBP) which regulates the transcription of genes involved in fatty acid synthesis such as ACC and fatty acid synthase (FAS) (Figure 1.12) (Kawaguchi et al., 2002; Li et al., 2011).

The role of AMPK in lipolysis to access energy stored in lipids is controversial and there is evidence showing that AMPK activates lipolysis in adipocytes in response to β-AR stimulation, and on the contrary that lipolysis is suppressed in response to AMPK activation (Ahmadian et al., 2011; Chuang et al., 2021; Dagon et al., 2006; Daval et al., 2005; Yin et al., 2003). Although lipolysis releases free fatty acids that can fuel fatty acid oxidation, the subsequent re-esterification of free fatty acids is energetically expensive, muddying predictions as to what role AMPK would play (Day et al., 2017). Events such as fasting and exercise that stimulate cAMP also stimulate AMPK activation, and AMPK can phosphorylate ATGL at Ser^{406} which promotes lipolysis (Ahmadian et al., 2011; Daval et al., 2005). On the other hand, AMPK can also phosphorylate HSL at Ser^{565} which prevents cAMP stimulated phosphorylation and activation of HSL at Ser^{563} by PKA (Chuang et al., 2021; Watt and Steinberg, 2008). To add further complication, adipose tissue specific AMPKα knock out studies show that AMPK stimulates basal levels of lipolysis but is inhibitory to β-AR stimulated lipolysis, whilst adipose tissue specific AMPKβ knock out studies show no effect on basal or stimulated lipolysis (Kim et al., 2016; Mottillo et al., 2016).

AMPK regulates glucose metabolism. It promotes glucose uptake by increasing translocation of GLUT4 to the plasma membrane through phosphorylation of TBC1 domain family member (TBC1D) 1 and 4 and reducing GLUT1 endocytosis through phosphorylation of thioredoxin-interacting protein (Kjøbsted et al., 2015; Wu et al., 2013). AMPK can increase glycolysis in some tissues by phosphorylation and activation of 6-phosphofructo-2-kinase, increasing the production of fructose 2,6-bisphosphate, the metabolite that regulates glycolysis by activating the rate determining enzyme 6-phosphofructo-1-kinase (Marsin et al., 2000). Meanwhile, AMPK represses glycogen synthesis for glucose storage by inhibition of glycogen synthase, which is important for restoring cellular energy levels as glycolysis is an important source of ATP whilst synthesis of glycogen utilises ATP (Bultot et al., 2012).

Mitochondria is an important organelle for cellular energy regulation as it is the location of oxidative phosphorylation and fatty acid oxidation. AMPK mainly regulates mitochondrial

biogenesis through the phosphorylation of PGC1α (Jäger et al., 2007). AMPK can also promote PGC1α activation indirectly by increasing NAD^+ biosynthesis which activate NAD^+ dependent sirtuin 1, which deacetylates PCG1α (Cantó et al., 2009; Marin et al., 2015). AMPK is important for mitochondrial health as it regulates mitochondrial biogenesis and turnover. Damaged mitochondria are cleared by fragmentation in a process called mitochondrial fission, and then the damaged fragments are degraded by mitophagy in specialised lysosomes. AMPK phosphorylation of mitochondrial fission factor allows for dynamin-related protein 1 mediated mitochondrial fission (Toyama et al., 2016).

Mitophagy and autophagy are closely related processes, both requiring the formation of lysosomes and allowing for recycling of nutrients and increasing ATP levels during nutrient stress. AMPK can regulate autophagy through inhibition of negative regulators and activation of positive regulators. AMPK inhibits mammalian target of rapamycin complex 1 (mTORC1) by inhibition of its subunit raptor and the activation of its suppressor tuber sclerosis complex 2 (TSC2) (Gwinn et al., 2008; Inoki et al., 2003; Steinberg and Carling, 2019). Inhibition of mTORC1 allows for the translocation of transcription factor EB to the nucleus to coordinate the expression of lysosomal biogenesis genes (Young et al., 2016). Meanwhile mTORC1 phosphorylates Forkhead box O3, increasing its transcriptional activity, directing the transcription of autophagic genes (Greer et al., 2007; Mammucari et al., 2007; Steinberg and Carling, 2019; Zhao et al., 2007). In addition, AMPK phosphorylation of Unc-51 like autophagy activating kinase (ULK1) is important for orchestrating lysosome biogenesis and mitophagy through its regulation of lysosome formation proteins such as vacuolar protein sorting 34, beclin-1 and parkin (Garcia and Shaw, 2017; Herzig and Shaw, 2018; Hung et al., 2021; Kim et al., 2011; Steinberg and Carling, 2019). Loss or inhibition of AMPK prevents the formation and maturation of autophagosomes (Jang et al., 2018).

AMPK activation leads to a reduction in cell growth and proliferation (Motoshima et al., 2006; Zang et al., 2009). Activation of AMPK is accompanied by increased phosphorylation and activation of tumour suppressor p53 and increased phosphorylation and stabilisation of cell cycle inhibitor p27, although it is not clear whether it directly phosphorylates either (Jones et al., 2005; Lee et al., 2012a; Liang et al., 2007). Cell cycle progression involves biosynthesis of cellular contents in preparation for mitosis. It is thought that most of AMPK's regulation of cell cycle comes from the inhibition of mammalian target of rapamycin (mTOR) through TSC2, and also through increased phosphorylation of the mTOR inhibitory site Thr^{2446}

(Cheng et al., 2004; Inoki et al., 2003). mTOR is responsible for integrating growth factor and nutrient status signals to promote protein synthesis through regulation of protein translation and elongation, and inhibition of these processes leads to a reduction in cell cycle progression (Fingar Diane et al., 2004; Horman et al., 2002). Lipogenesis is also important for cell growth, and so disruption of fatty acid synthesis by AMPK will also suppress proliferation (Motoshima et al., 2006).

The role of AMPK in cancer is heavily disputed. Some studies show that it is pro-tumorigenic as it increases glucose uptake to enhance the Warburg effect and it promotes cell survival (Kjøbsted et al., 2015; Vara-Ciruelos et al.; Wu et al., 2013). However, it also slows proliferation and lipid synthesis which is essential for cancer cell growth (Hadad et al., 2014; Penfold et al., 2018).

AMPK mediates whole-body homeostatic responses to caloric restriction and exercise which deplete ATP levels, and also regulates adipokine signalling (Minokoshi et al., 2002; Steinberg and Carling, 2019; Winder and Hardie, 1996; Yamauchi et al., 2002). In skeletal muscle, AMPK mediates the response to exercise by causing a switch from glycolytic, fast-twitch type IIb fibres to oxidative, slow-twitch type I fibres. (O'Neill et al., 2011; O'Neill et al., 2013). This increases mitochondrial content and fatty acid oxidation which in turn increases exercise capacity. Contraction of skeletal muscle leads to an AMPK dependent phosphorylation of TBC1D1 and TBC1D4 to increase glucose uptake through GLUT4 translocation, improving whole body insulin sensitivity as skeletal muscle acts as a glucose sink (Kjøbsted et al., 2017). The effect of AMPK activation in adipocyte glucose uptake is disputed, with evidence for it being involved in increasing basal and insulin stimulated glucose uptake upon treatment with adiponectin (Wu et al., 2003). Other evidence shows that activation of AMPK can reduce insulin stimulated glucose uptake (Chuang et al., 2021). However, the effect of AMPK activation on glucose uptake may be due to off target effects of the small molecules used in studies, and so it is likely that AMPK activation does not play a role in glucose uptake in adipocytes (Chuang et al., 2021; Kopietz et al., 2021; Sakoda et al., 2002). Despite its characteristic inhibition of glycogen synthase, activation of AMPK in the muscle leads to accumulation of glycogen (Aschenbach et al., 2002; Bultot et al., 2012). It is thought that this is a side effect of the increase in glucose uptake (Aschenbach et al., 2002).

Activation of AMPK in the liver inhibits de novo lipogenesis- the production of lipids from carbohydrates- and also increases fatty acid oxidation, through phosphorylation of ACC and

SREBP (Foretz et al., 2018; Garcia et al., 2019; Li et al., 2011; Woods et al., 2017). This prevents triglyceride accumulation in the liver and protects from NAFLD. AMPK appears to play an indirect role in suppressing liver gluconeogenesis, the synthesis of glucose from non-carbohydrate substrates in response to starvation that when perturbed can lead to hyperglycaemia (Zhang et al., 2019b). AMPK may suppress gluconeogenesis through inhibition of coactivators of transcription factors for gluconeogenesis genes and by improving insulin sensitivity, as insulin signalling inhibits gluconeogenesis.

Skeletal muscle AMPK is activated in response to leptin signalling, and adiponectin signalling increases AMPK activity in skeletal muscle and liver, which leads to increased fatty acid oxidation and glycolysis (Minokoshi et al., 2002; Yamauchi et al., 2002). Hypothalamic AMPK responds to gut and adipose tissue signalling hormones to regulate food intake (Andersson et al., 2004; López et al., 2016). Activation of hypothalamic AMPK by adiponectin or ghrelin promotes expression of orexigenic AgRP, causing increased food intake and body weight gain (Andersson et al., 2004; Wen et al., 2010). Meanwhile, anorexigenic hormones such as leptin and insulin inhibit hypothalamic ARC and PVN AMPK activity, which is contradictory to their effect on AMPK in other tissues (Andersson et al., 2004; López et al., 2016; Minokoshi et al., 2004). This leads to reductions in food intake which is proposed to occur as a result of unrestricted ACC activity and therefore increased levels of malonyl-CoA in the ARC or palmitoyl-CoA in the PVN, which downregulates orexigenic neuropeptides NPY and AgRP and upregulates anorexigenic neuropeptide α-MSH (Gao et al., 2007; Wolfgang and Lane, 2006).

1.3.3 Pharmacological activation

Due to its broad role in metabolism, AMPK is a popular candidate for the development of pharmacological activators. AMPK can be activated indirectly by small molecules that affect the cellular AMP to ATP ratio, mostly through disruption of mitochondrial oxidative phosphorylation, with several indirect small molecule activators existing in nature (Steinberg and Carling, 2019). Metformin has been used as an anti-diabetic since the 1950s and was found to indirectly activate AMPK through inhibition of mitochondrial complex I which increased the AMP to ATP ratio, with AMPK activation required for some of metformin's beneficial metabolic effects (Zhou et al., 2001). The AMPK-dependent metabolic benefits of metformin are mediated by the reduction of liver lipogenesis and subsequent increased insulin sensitivity (Fullerton et al., 2013). Resveratrol, a natural plant metabolite, has been

shown to mimic the metabolic benefits and anti-cancer effects of caloric restriction (Kulkarni and Cantó, 2015). In lower eukaryotes it increases lifespan, and in higher eukaryotes it improves high fat diet perturbed cardiovascular health, insulin sensitivity and exercise capacity (Baur et al., 2006; Kulkarni and Cantó, 2015). The two key targets of resveratrol are AMPK and sirtuin 1, which upregulate mitochondrial biogenesis through PGC1α (Baur et al., 2006). Resveratrol indirectly activates AMPK through the inhibition of ATP synthase, which increases the AMP to ATP ratio (Kulkarni and Cantó, 2015). Although resveratrol has a host of possible targets, AMPK activation is required for its *in vivo* metabolic benefits (Um et al., 2010). In addition to metformin and resveratrol, a range of other small molecules have been shown to indirectly activate AMPK, but due to their indirect nature, their mechanisms of action are difficult to ascertain, and they may not be suitable for use in humans.

AMPK can also be activated directly by small molecules that can either be a nucleotide mimetic which bind to the AMPKγ subunit, or they can bind to the ADaM site (Steinberg and Carling, 2019). 5-Aminoimidazole-4-Carboxamide Ribonucleoside (AICAR) was the first described small molecule activator of AMPK (Corton et al., 1995). AICAR is the precursor for ZMP, a less potent allosteric activator of AMPK than AMP. AICAR was shown to have beneficial effects in obese rodents *in vivo*, lowering plasma triglyceride and free fatty acid levels whilst reversing insulin resistance (Buhl et al., 2002). In addition, it improved insulin stimulated glucose uptake in skeletal muscle (Kjøbsted et al., 2015). Whilst the use of AICAR has aided in the study of AMPK, it also shows off target effects on other AMP regulated enzymes such as fructose 1,6-bisphosphatase and glycogen phosphorylase and so not all effects from AICAR can be attributed to AMPK (Steinberg and Carling, 2019). This was shown to be the case *in vivo*, where some of AICAR's effects on glucose metabolism are due to the AMPK independent effects from changes in hepatic nucleotide levels (Choi et al., 2019; Hasenour et al., 2014).

A-769662 is a direct small molecule activator of AMPK that does not bind to the AMPKγ subunit to mimic AMP activation, and therefore doesn't have the off target effects of an AMP mimetic (Cool et al., 2006). Instead, A-769662 binds to the ADaM site within AMPK. Like other AMPK activators, A-769662 had beneficial metabolic effects on obese mice, reducing hepatic and plasma triglyceride levels and lowering body weight gain. However, it has poor uptake in non-hepatic tissues and has poor bioavailability *in vivo* (Steinberg and Carling,

2019). In addition, the specificity of A-769662 has been questioned as it is able to inhibit Na^+/K^+-ATPase in skeletal muscle cells *in vitro* (Benziane et al., 2009).

Other direct small molecule activators of AMPK have been identified and share a similar structure to A-769662 (Myers et al., 2017; Xiao et al., 2013; Zadra et al., 2014). Studies revealed that these compounds are ligands for the ADaM binding site (Giordanetto and Karis, 2012; Xiao et al., 2013). ADaM ligands can work synergistically with AMP or AMP mimetics for dual activation of AMPK (Bultot et al., 2016; Scott et al., 2014). Other ADaM ligands showed beneficial effects in diabetic animal models and improved skeletal muscle glucose uptake, but showed side effects such as enlarged hearts (Cokorinos et al., 2017; Myers et al., 2017). Small molecule activators show selectivity for different AMPK complex subunit isoforms with ADaM ligands tending to activate AMPKβ1 complexes more than AMPKβ2 complexes, providing a potential mechanism for selective targeting of AMPK in different tissues (Cokorinos et al., 2017; Rajamohan et al., 2016; Willows et al., 2017a). 991 is a more potent activator of AMPK than A-769662. However, so far there are no published examples of its use *in vivo* (Xiao et al., 2013). Salicylate, a naturally occurring molecule derived from willow bark, and the break down product of aspirin can also bind to the ADaM site to activate AMPK. Mice treated with salicylic acid show improved metabolic effects, although the concentration required to activate AMPK *in vivo* is higher than what is generally used in humans. At these high concentrations, salicylic acid is also able to act independently of AMPK activation, improving NAFLD through its mitochondrial uncoupling action (Hawley et al., 2012; Smith et al., 2016). A wealth of natural and synthetic AMPK activators have been identified, and more potent, specific and direct *in vivo* activators are becoming available. Boehringer's BI-9774 is one promising compound that shows successful target engagement at low doses in rodent studies (Grempler et al., 2018).

Recently, a small molecule activator of AMPK O304 was found to have beneficial effects on glucose uptake in mice and so was entered into a proof-of-concept phase IIa clinical trial for patients with T2D who were on metformin (Steneberg et al., 2018). In patients, treatment with O304 improved glucose metabolism and in addition reduced blood pressure and improved microvascular perfusion which is important considering the microvascular complications that are associated with diabetes. The mechanism of action of O304 is unknown but is thought to work by preventing AMPK dephosphorylation. Another direct activator to reach clinical trials is PXL770, an ADaM site ligand that showed metabolic

improvements in *ob/ob* mice which are hyperphagic obese due to a leptin mutation. PXL770 improved NAFLD, with reversal of hepatic triglyceride accumulation, fibrosis and inflammation (Gluais-Dagorn et al., 2022). In clinical trials it reduced hepatic de novo lipogenesis and improved insulin response in patients with NAFLD, and it reduced liver fat content in a subgroup of patients that also had diabetes (Cusi et al., 2021; Fouqueray et al., 2021). These studies highlight the clinical relevance of targeting AMPK activation.

1.3.4 AMPK in adipose tissue and obesity

Currently AMPK activators are being trialled and used for the treatment of T2D and NAFLD and they demonstrate clear improvements in glucose uptake and reduction of hepatic de novo lipogenesis. Targeting AMPK in obesity is interesting to explore given that obesity is caused by a chronic positive energy imbalance, and AMPK is a key regulator of energy metabolism.

Inhibition of hypothalamic AMPK in obesity could reduce hyperphagia. Animal studies have shown how adenovirus activation of hypothalamic AMPK promotes feeding whilst inhibition of hypothalamic AMPK reduces body weight (López et al., 2016). Moreover, AMPK located in the ventromedial hypothalamus can suppress BAT thermogenesis through the SNS and can contribute to regulation of body weight (López et al., 2016; Whittle et al., 2012). Reducing hypothalamic AMPK activity could increase NST in BAT, increasing energy expenditure and reducing body weight (Whittle et al., 2012). However, as of yet, specific inhibition of hypothalamic AMPK in humans is not possible, and whole body inhibition of AMPK would be predicted to lead to a number of deleterious metabolic effects.

AMPK activity in adipose tissue is negatively correlated with obesity in humans (Mortensen et al., 2009). Consuming a high fat diet is associated with decreased AMPK activity whilst weight-loss induced by diet or surgery is associated with increased AMPK activity (Albers et al., 2015; Fritzen et al., 2015; Lindholm et al., 2013; Xu et al., 2015). Increased subcutaneous adipose tissue AMPK activity may play a role in the improvement in metabolic syndrome and insulin sensitivity following weight loss in humans (Albers et al., 2015; Gauthier et al., 2011; Martínez-Agustin et al., 2010; Xu et al., 2015; Xu et al., 2012). AMPK activity is higher in subcutaneous adipose tissue, which is associated with protective effects from metabolic syndrome, compared to visceral adipose tissue, which is associated with inflammation (Gauthier et al., 2011; Martínez-Agustin et al., 2010).

AMPK in rodent BAT and WAT can be activated through β-AR stimulation and can play a role in SNS or small molecule stimulated browning (Hutchinson et al., 2005; Koh et al., 2007; Mulligan et al., 2007). When WAT is lacking AMPK there is a blunted induction of beige gene expression including reduced expression of UCP1, and lack of elevation of oxygen consumption in response to cold or CL-316,243 (Mottillo et al., 2016; Wu et al., 2018). AMPK modulates brown adipogenesis and loss of adipose tissue AMPK can induce BAT fibrosis instead of brown adipocyte formation (Perdikari et al., 2017; Zhao et al., 2017). During brown adipogenesis, AMPK increases the activity of TCA cycle enzyme isocitrate dehydrogenase 2 which catalyses the conversion of isocitrate to α-ketoglutarate (Yang et al., 2016a). α-ketoglutarate is the metabolite for the Ten-eleven translocase mediated demethylation of the PRDM16 promoter. So increased AMPK activity means higher levels of α-ketoglutarate for increased PRDM16 expression and brown adipogenesis.

Mitochondrial turnover is essential for optimal BAT function, and AMPK activity is higher in BAT than in any other tissue (Mulligan et al., 2007). When adipose tissue AMPK is ablated, BAT displays abnormal mitochondrial morphology with disrupted cristae (Mottillo et al., 2016; Wu et al., 2018). This is thought to be due to the lack of AMPK-ULK1 mediated mitophagy to clear damaged mitochondria (Mottillo et al., 2016). Mice that have adipocyte AMPK ablated with an adiponectin Cre are less tolerant to cold exposure and have lower core and surface temperatures, due to impaired NST (Mottillo et al., 2016; Wu et al., 2018). They are more susceptible to weight gain on a high fat diet and display metabolic syndrome, with reduced glucose and insulin tolerance, and greater susceptibility to liver triglyceride accumulation, fibrosis and steatosis.

Pharmacological or genetic activation of adipose tissue AMPK protects from diet-induced obesity by promoting browning of WAT and increasing mitochondrial content in BAT, thereby increasing energy expenditure through NST (Pollard et al., 2019; Wang et al., 2015; Wu et al., 2018; Yan et al., 2016; Zhao et al., 2017). Resveratrol induces the expression of beige adipocyte genes and increases *in vitro* oxygen consumption in iWAT SVF derived adipocytes in an AMPK dependent manner (Wang et al., 2015). *In vivo* treatment with resveratrol caused a beige morphology with multilocular lipid droplets and increased UCP1 expression in the iWAT of high fat diet fed mice. Chronic activation of AMPK with A-769662 is protective to mice on a high fat diet leading to reduced body weight gain and improved glucose and insulin tolerance (Wu et al., 2018). In addition, there is increased whole body

oxygen consumption and energy expenditure and increased tolerance to cold exposure. This is due to browning of iWAT which has smaller, multilocular lipid droplets, increased mitochondrial content and increased expression of beige genes including UCP1. The essential role of AMPK was demonstrated in differentiated iWAT SVF when the A-769662 stimulated expression of beige genes and increased respiration rate was not seen when AMPK was ablated. Several other small molecules have also been shown to both induce adipose tissue browning and increase AMPK activation, although not directly, protecting mice from diet induced obesity (Chen et al., 2021; Jeon et al., 2021; Liu et al., 2021b). In addition, metformin reduces obesity associated fibrosis in mice, particularly in visceral adipose tissue, which is modulated through AMPK activation *in vitro* (Luo et al., 2016). The clinical trial candidate PXL770 was able to activate AMPK in adipose tissue, reducing levels of inflammation both *in vivo* and when used to treat *ob/ob* eWAT explants (Gluais-Dagorn et al., 2022).

A model for chronic AMPK activation was achieved through loss of the tumour suppressor folliculin, which forms an AMPK repressor complex with folliculin-interacting protein (Yan et al., 2016). Mice with adipose tissue specific ablation of folliculin also showed browning of iWAT, increased UCP1 expression and energy expenditure, and protection from high fat diet induced obesity. This occurred through AMPK regulation of PGC1α and oestrogen related receptor α which increased mitochondrial content. Finally, our lab investigated the effect of global constitutive activation of AMPK in mice and found that it protected from high fat diet induced obesity through an Ucp1-independent NST mechanism in iWAT (Pollard et al., 2019). This mouse model has formed the basis of this thesis and is described in detail below.

1.4 D316A MOUSE

Mutation of AMPKγ1 Asp^{316} to Ala (D316A) eliminates the tight binding of AMP to CBS 4 and decreases the susceptibility of AMPK to dephosphorylation of Thr^{172} (Woods et al., 2017; Xiao et al., 2007). This conferred constitutive activation with approximately three fold increase in AMPK activity. The first published mouse model with D316A constitutive activation was under the control of an albumin promoter for liver specific expression (Woods et al., 2017). When the liver-specific D316A mice were placed on a high fructose diet they were protected from liver steatosis, with reduced de novo lipogenesis and no accumulation of liver triglycerides associated with high fructose diets (Woods et al., 2017). There was no

change in the rate of fatty acid oxidation in the livers of D316A mice, likely due to the low increase in AMPK activity compared to other models of AMPK activation (Foretz et al., 2018; Garcia et al., 2019), which may help to circumvent some of the negative effects of chronic AMPK activation (Yavari et al., 2016).

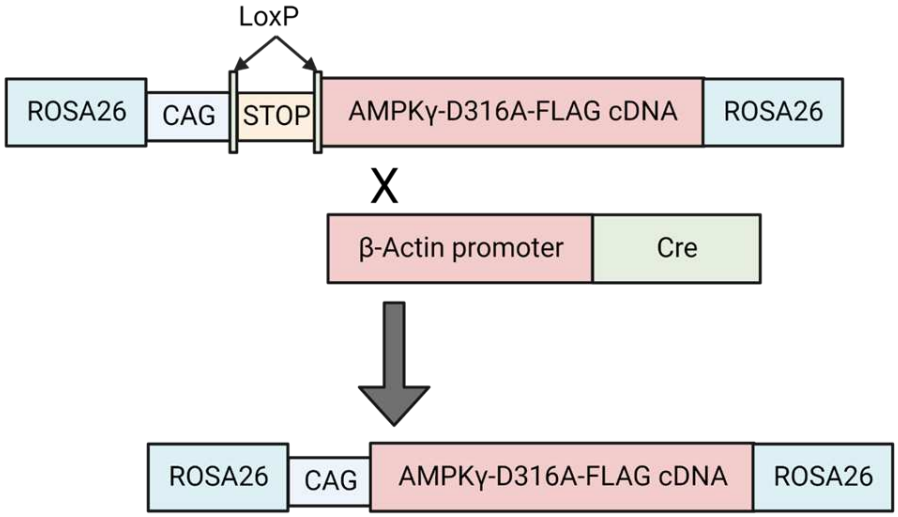


Figure 1.13 D316A transgene

To generate a mouse model with global constitutive activation of AMPK, a mouse with the AMPKγ1 D316A mutation inserted in the ROSA26 locus is crossed with a β-actin Cre mouse to generate a mouse with AMPKγ1 D316A expression driven by a CMV early enhancer element/chicken β-actin (CAG) promoter in every cell in the body from embryonic day 1.

To generate a whole body AMPKγ1-D316A or AMPKγ1- wild-type (WT) mouse, mice harbouring a construct with the D316A transgene (D316A-Tg) or WT transgene (WT-Tg) with a STOP cassette flanked by LoxP sites, inserted within the ROSA26 locus and behind the CMV early enhancer element/chicken β-actin promoter (CAG), were crossed with a mouse with a Cre under the control of a β-actin promoter (Figure 1.13). This led to removal of the STOP cassette so the transgene is expressed. The D316A-Tg contains a 3' FLAG tag so that expression of D316A can be confirmed by Western blotting. The β-actin Cre AMPKγ1-D316A mouse will be referred to as the D316A mouse for the remainder of this work. Expression of the D316A-Tg in the D316A mouse was confirmed in 12 tissues including liver, muscle, WAT and brain (Pollard, 2017). The use of the CAG promoter should drive strong enough expression of the transgene so that it can compete with the endogenous AMPKγ1 in complex formation. The WT-Tg was able to replace 100% of endogenous

AMPKγ1, and the D316A-Tg replaced 50% of endogenous AMPKγ1. Of note, although there was a small increase in heart weight in the D316A mouse, they displayed no cardiac abnormalities (Pollard et al., 2019). Interestingly, activation of AMPK in mice with a Bl6/129 background led to increased accumulation of glycogen in cysts in the kidney collecting ducts (Wilson et al., 2021).

The most striking phenotype of the D316A mouse was that it was protected from high fat diet induced obesity. Compared to WT mice, there was a significant reduction in body weight gain, lower fat mass as measured by echo MRI (eMRI), protection from liver triglyceride accumulation with lower liver weights and improved insulin sensitivity as measured by homeostatic model assessment of insulin resistance (Pollard, 2017; Pollard et al., 2019). Although there was no significant decrease in rate of glucose clearance, there was a reduction in fasting serum insulin levels in the D316A mouse. There were no differences in food intake between the D316A and WT mice on a chow or high fat diet and so protection from obesity cannot be attributed to differences in energy intake. Instead, there was an increase in energy expenditure in the D316A mouse on a high fat diet, with an increase in oxygen consumption but no difference in movement, ruling out increased exercise as the mechanism for increased energy expenditure. The D316A mice showed an increased respiratory exchange ratio (RER) on a high fat diet, indicative of more carbohydrate than fat substrate utilisation. The surface temperature, but not core temperature, of the D316A mouse was higher than the WT mouse which combined with increased oxygen consumption, points towards a NST mediated mechanism for obesity protection. However, there were no differences in response to high fat diet in the BAT of WT or D316A mice and so it was determined that BAT was not responsible for the increased energy expenditure.

Instead, browning of iWAT was shown to be responsible for the increase in energy expenditure. On a chow diet, the D316A mouse iWAT displays a more brown morphology with smaller, multilocular lipid droplets compared to the large unilocular lipid droplets in the WT mouse. These differences remain when on a high fat diet, and iWAT tissue weight was lower in D316A mice. In addition, D316A mice have a higher mitochondrial content in iWAT on both a chow and a high fat diet as is seen by staining for mitochondrial membrane protein translocase of the outer mitochondrial membrane 20 (TOMM20) and by Western blotting for oxidative phosphorylation proteins. D316A mice also had more PGC1α protein expression. However, unlike in classical WAT browning, UCP1 protein expression was not detectable.

This indicated that the D316A mouse has a novel adipocyte using UCP1-independent thermogenesis which is responsible for increasing energy expenditure and providing protection from high fat diet induced obesity.

RNA sequencing was carried out on the iWAT, BAT, liver and skeletal muscle of the D316A and WT mice on both chow and high fat diets. Principal component analysis showed that the gene expression signature of the D316A iWAT bore some resemblance to BAT. Surprisingly, on a high fat diet, there was upregulation of genes associated with skeletal muscle in the D316A mouse iWAT, including skeletal muscle lineage markers such as *Myod1* and *Myogenin 6*. Furthermore, there was an upregulation in genes involved in skeletal muscle-associated NST- *Atp2a1* encoding SERCA1, *Ryr1* and *Ckmt1* encoding creatine kinase, genes for Ucp1-independent NST mechanisms in beige adipocytes (Bertholet et al., 2017; Kazak et al., 2015). To investigate whether futile creatine cycling was involved in D316A NST, mice on a high fat diet were treated with creatine kinase inhibitor β-guanidinopropionic acid, but this did not affect body weight in D316A or WT mice and so is unlikely to be the mechanism for UCP1-independent NST. Therefore, it has been hypothesised that futile calcium cycling with SERCA1 and RYR1 are responsible for the increased energy expenditure and protection from high fat diet body weight gain. Interestingly, SERCA2, the isoform previously described in beige adipocyte UCP1-independent futile calcium cycling, was not detected in D316A mouse iWAT (Ikeda et al., 2017). AMPK has been shown to regulate SERCA in the context of vascular endothelial and smooth muscle cells. In cardiac and vascular endothelial cells ablation of AMPK leads to increased oxidation of SERCA which inhibits its activity and leads to ER stress (Dong et al., 2010). In arterial smooth muscle cells AMPK can phosphorylate phospholamban at its inhibitory site Thr^{17} which prevents it from inhibiting SERCA (Schneider et al., 2015). Because of the upregulation in skeletal muscle associated genes in the high fat diet D316A mouse, the novel adipocytes were called skeletal muscle-like AMPK reprogrammed thermogenic (SMART) cells.

RNA sequencing of iWAT from mice on a chow diet showed upregulation of genes involved in AMPK associated pathways such as fatty acid metabolism, TCA cycle, glycolysis, mitochondrial translation and brown fat differentiation, consistent with their morphology. Therefore it would appear that AMPK reprograms WAT to a more beige like state, and high fat diet activates UCP1-independent NST.

One bonus of the D316A model is that increased non-canonical NST did not rely on genetic deletion of UCP1 as was required in another study where SERCA2B mediated NST was observed, and may be more translatable to humans with pharmacological activation of AMPK (Ikeda et al., 2017). A tamoxifen inducible β-actin CRE D316A mouse model was used to see whether activation of AMPK could reverse high fat diet induced obesity, to assess the translatability of AMPK activation in obesity. After four weeks on a high fat diet, mice were injected with tamoxifen to induce expression of WT AMPK or D316A AMPK with continued high fat diet feeding (Pollard et al., 2019). Induction of the D316A transgene lead to moderately reduced bodyweight gain compared to the WT mouse. There were clear genotype differences in the morphology of iWAT, with D316A mice showing smaller, multilocular lipid droplets accompanied by increased ATP synthase and succinate dehydrogenase protein. Interestingly there was vascularisation of D316A iWAT that was not present in WT mice. In addition, there was a significant reduction in serum insulin levels and liver triglyceride levels. This suggests that activation of AMPK in obesity may have beneficial effects in patients.

At the same time as the discovery of SMART cells, another novel beige adipocyte was described called the glycolytic beige cell (Chen et al., 2019b). Glycolytic beige cells arise from a MYOD progenitor in iWAT and their differentiation to a highly glycolytic beige adipocyte is driven by GA binding protein α (GABPα). Glycolytic beige cells are formed in cold exposed mice lacking β-AR. They express UCP1 and are capable of carrying out thermogenesis to protect mice from hypothermia in cold exposure. In addition, single-nuclei RNA sequencing studies have allowed for transcriptome analysis of mature adipocytes which are too bulky and fragile for single-cell sorting for scRNA-seq, and have identified adipocyte subpopulations and novel thermogenic regulating adipocytes (Emont et al., 2022; Hagberg et al., 2018; Sun et al., 2020). This adds to a growing body of literature showing the rich heterogeneity of adipocytes within adipose tissue (Min et al., 2019; Pollard and Carling, 2020).

1.5 PROJECT AIMS

The D316A mouse demonstrates how AMPK can play a role in lineage determination in adipose tissue, generating metabolic benefits to a mouse in the context of obesity. However, exactly how AMPK is able to influence adipocyte lineage, and whether the effect on adipocytes is fully cell autonomous is still unclear. In addition, the generation of the D316A

mutation in humans is not clinically possible, and so it is important to see whether the use of pharmacological activators of AMPK is able to mimic the effects of the D316A mouse. The aim of this thesis is to further explore the role of AMPK in adipocytes, particularly in adipogenesis.

Aim 1. To determine the autonomy of the D316A adipocytes, and their therapeutic potential in adipose tissue allograft transplantation. Adipose tissue from the D316A mouse will be transplanted into WT recipient mice which will subsequently undergo high fat diet feeding to see whether the allograft is able to confer protection from diet induced obesity. This will give clues as to whether the changes observed in the D316A adipose tissue are due to effects from adipose tissue. This work will be discussed in Chapter 3.

Aim 2. To determine the effects of AMPK activation in adipogenesis. Whilst AMPK activation in adipogenesis has been previously explored, most studies make use of preadipocyte fibroblast cell lines which may not as accurately recapitulate adipogenesis as primary cell lines. In addition, most studies do not use direct or potent activators of AMPK. To address this aim, primary adipocyte progenitors will be obtained from WT mouse SVF for *in vitro* differentiation, and the potent, AMPK ADaM site ligand BI-9774 will be used for pharmacological activation of AMPK. This work will be discussed in Chapter 4.

Aim 3. Exploring the role of AMPK in adipose tissue and muscle cell fate determination. Adipocytes and skeletal muscle cells share a mesenchymal stem cell progenitor, and the D316A mouse as well as the glycolytic beige adipocyte demonstrate a close link between the two. Primary SVF derived adipocytes from the D316A mouse will be obtained to explore this link further. Then, the effect of AMPK on the adipogenic differentiation of C2C12 mouse myoblasts will be investigated. This work will be discussed in Chapter 5.

2. MATERIALS AND METHODS

2.1 MATERIALS

2.1.1 General reagents

Ethanol, β-mercaptoethanol, 4-(2-hydroxyethyl)-1-piperazineethanesulfonic acid (HEPES), $MgCl_2$, sucrose, ATP, AMP, SAMS peptide, $CaCl_2$, 2-ethanesulfonic acid, K_2HPO_4, Na_2HPO_4, ortho-phosphoric acid, NaCl, NaPP, phenylmethylsulphonyl fluoride, trypsin inhibitor, benzamidine, DTT, collagenase I, collagenase II, dispase II, dNTP mix, dimethyl sulfoxide (DMSO), insulin, triiodothyronine (T_3), dexamethasone, 3-isobutyl-1-methylxanthine (IBMX), indomethacin, retinoic acid, rosiglitazone, foetal bovine serum (FBS), 2% gelatine solution, fatty acid free bovine serum albumin (BSA), neutral goat serum, DAPI, cold fish skin gelatine, Oil Red O, paraformaldehyde, Triton X-100, polyvinylidene fluoride membrane, Ponceau S solution, horse radish peroxidase (HRP) substrate, isoprenaline hydrochloride were obtained from Merck (Dorset, UK).

Gibco™ Dulbecco's Modified Eagle Medium (DMEM) GlutaMAX, Gibco™ DMEM/F12, Gibco™ phenol red free DMEM/F12, Gibco™ Glasgow Minimal Essential Medium, Gibco™ L-glutamine, Gibco™ sodium pyruvate, Gibco™ penicillin-streptomycin, Gibco™ non-essential amino acids solution, Gibco™ TrypLE express enzyme, Invitrogen™ protein A, Invitrogen™ 3-(N-morpholino)-propanesulfonic acid SDS running buffer, Invitrogen™ 4-12% Bis-Tris gels, Invitrogen™ First-strand buffer, Invitrogen™ SuperScript II Reverse Transcriptase, Invitrogen™ TRIzol, Invitrogen™ LipidTOX green neutral lipid stain, Invitrogen™, DNAse I, Oxoid™ skimmed milk powder, Pierce™ BSA protein standard, Invitrogen™ TGF beta-1 enzyme-linked immunosorbent assay (ELISA) Kit, Invitrogen™ Click-iT (5-ethynyl-2'-deoxyuridine) EdU Alexa Fluor 488 HCS Assay, Invitrogen™ SYBR Safe DNA Gel Stain, Invitrogen™ Wheat Germ Agglutinin (WGA) Alexa Fluor 594 Conjugate, BSA Powder, methanol and prestained protein ladder were obtained from ThermoFisher Scientific (Loughborough, UK).

Tris-base, acetate, chloroform, EDTA, glycerol, KCl, NaOH, Tris-HCl and Tween-20 were obtained from VWR (West Sussex, UK).

Agarose, BioMix Red and SensiMix SYBR Hi-ROX were obtained from Bioline (London, UK).

Hank's balanced salt solutions (HyClone) was obtained from Cytiva (Sheffield, UK).

Embryonic stem (ES) cell FBS was obtained from the Welcome Trust MRC Stem Cell Institute (Cambridge, UK).

Random primers were obtained from Roche (Hertfordshire, UK).

Protein assay dye reagent was obtained from Bio-Rad (Hertfordshire, UK).

PageRuler Plus HCl was obtained from Honeywell Fluka (Berkshire, UK)

RNeasy kit was obtained from Qaigen (Crawley, UK).

Red blood cell lysis buffer was obtained from BioLegend (London, UK).

NucLight rapid red dye and Caspase-3/7 dye were obtained from Sartorius (Goettingen, Germany).

Vectashield mounting medium was obtained from Vector Laboratories (Peterborough, UK).

Glycine was obtained from Melford (Ipswich, UK).

SkGM-2 Skeletal Muscle Cell Growth Medium-2 BulletKit was obtained from Lonza (Slough, UK).

Senescence detection kit (BioVision) was obtained from Abcam (Cambridge, UK).

Leukaemia inhibitory factor was a gift from Dr Tristan Rodriguez (Imperial College London).

BI-9774 (Boehringer) was provided by AstraZeneca (Cambridge, UK).

991 was synthesised as described previously (Xiao et al., 2013).

2.1.2 Buffers

Phosphate buffered saline (PBS)- 137mM NaCl, 2.7mM KCl, 4.3mM Na_2HPO_4, 1.4mM K_2HPO_4, pH7.4.

Tris buffered saline Tween 20 (TBS-T)- 150mM NaCl, 50mM Tris-HCl, 0.1% Tween20 (v/v) pH 7.6.

Tris-acetate EDTA- 40mM Tris-acetate, 1mM EDTA in distilled water.

HEPES buffer A- 50mM HEPES pH7.5 at 4°C, 50mM NaFl, 5mM NaPP, 1mM EDTA, 10% Glycerol (v/v), 1mM DTT, 4µg/ml trypsin inhibitor, 0.1mM phenylmethylsulphonyl fluoride, 175µg/ml benzamidine.

HEPES buffer G- 50mM HEPES pH7.5 at 4°C, 1mM EDTA, 10% Glycerol (v/v), 1mM DTT, 4µg/ml trypsin inhibitor, 0.1mM phenylmethylsulphonyl fluoride, 175µg/ml benzamidine.

Cytosolic protein extraction buffer- 10mM MES pH 6.5, 5mM $MgCl_2$, 1mM $CaCl_2$, 15mM NaCl, 60mM KCl, 0.25M sucrose, 0.5% Triton X-100, 0.5mM sodium metabisulfite, 1mM DTT, 4µg/ml trypsin inhibitor, 0.1mM phenylmethylsulphonyl fluoride, 175µg/ml benzamidine.

Nuclear protein extraction buffer- 20mM Tris-HCl pH 7.9, 10mM EDTA, 300mM NaCl.

Sample buffer- 50mM Tris-HCl, pH 7.4, 2.5% (w/v) SDS, 1% (v/v) β-mercaptoethanol, 10% glycerol, 0.05% (w/v) bromophenol blue.

Tris-glycine transfer buffer- 25mM Tris-HCl, 192mM glycine, 10% (v/v) methanol.

4% paraformaldehyde- 4% (w/v) paraformaldehyde, NaOH, PBS, pH 7.4.

4% BSA- 4% BSA (w/v), TBS-T.

4% Milk- 4% skimmed milk powder (w/v), TBS-T.

Immunofluorescence blocking buffer- 1.1% (v/v) BSA, 0.1% Triton X-100.

AMPK assay mix- per reaction, 0.5ml 1mM AMP, 0.5ml 1mM SAMS, 0.5ml HEPES buffer G, 1% Triton X-100.

SVF digest media- 2mg/ml dispase II, 1ml/ml collagenase I, 1ml/ml collagenase II, 25U/ml dnase I in DMEM/F12.

FACS buffer- 0.5% BSA (w/v), 5mM EDTA in PBS.

2.1.3 Cell culture media

Mammalian cell culture medium used in this work are detailed below.

Table 2.1 Cell culture media

Media	Base	Additives
SVF medium	DMEM/F12	10% (v/v) FBS, 1mM sodium pyruvate, 2mM L-glutamine, 1% (v/v) penicillin-streptomycin

Adipogenic induction medium	DMEM/F12	10% (v/v) FBS, 1mM sodium pyruvate, 2mM L-glutamine, 1% (v/v) penicillin-streptomycin, 1µg/ml Insulin, 3nM T_3, 0.25µM dexamethasone, 0.5mM IBMX, 0.2mM indomethacin
Adipogenic maintenance medium	DMEM/F12	10% (v/v) FBS, 1mM sodium pyruvate, 2mM L-glutamine, 1% (v/v) penicillin-streptomycin, 1µg/ml insulin, 3nM T_3
ES cell base medium	Glasgow Minimal Essential Medium	10% (v/v) ES cell serum, 1% (v/v) non-essential amino acids, 1mM sodium pyruvate, 1mM L-glutamine, 50µM β-mercaptoethanol
ES cell adipogenic maintenance medium	Glasgow Minimal Essential Medium	10% (v/v) ES cell serum, 1% (v/v) non-essential amino acids, 1mM sodium pyruvate, 1mM L-glutamine, 50µM β-mercaptoethanol, 1µg/ml insulin, 3nM T_3, 10mM rosiglitazone
ES cell adipogenic induction medium	Glasgow Minimal Essential Medium	10% (v/v) ES cell serum, 1% (v/v) non-essential amino acids, 1mM sodium pyruvate, 1mM L-glutamine, 50µM β-mercaptoethanol, 1µg/ml insulin, 3nM T_3, 0.25µM dexamethasone,

		0.5mM IBMX, 0.2mM indomethacin, 10mM rosiglitazone
C2C12 growth medium	DMEM	10% (v/v) FBS, 1% (v/v) penicillin-streptomycin
Human muscle cell growth medium	SkBMTM-2 Skeletal Muscle Myoblasts Basal Medium	Gentamicin sulphate, human epidermal growth factor, dexamethasone, FBS, L-glutamine

2.1.4 Antibodies

Table 2.2 Primary antibodies

Primary antibodies are all used at 1/1000 and are listed below. Abbreviations; Western Blot (WB), Immunofluorescence (IF), Cell Signalling Technology (CST), creatine kinase B (CKB), creatine kinase, mitochondrial 2 (CKMT2), extracellular signal-regulated kinases (ERK), glyceraldehyde 3-phosphate dehydrogenase (GAPDH), suppressor of mothers against decapentaplegic (SMAD), translocase of the outer mitochondrial membrane complex subunit 20 (TOMM20).

Target	**Species raised in**	**Supplier**	**Catalogue number**	**Application**
ACC	Mouse	Milipore	05-1098	WB
p-ACC^{Ser79}	Rabbit	CST	3661	WB
AMPKα	Mouse	CST	2793	WB
p-AMPKα^{Thr172}	Rabbit	CST	2535	WB
β-Catenin	Rabbit	CST	8480	WB
CIDEC	Rabbit	Novus Biologicals	NB100-430	WB
CKB	Rabbit	Abclonal	A12631	WB
CMKT2	Rabbit	Abcam	55963	WB
ERK	Mouse	CST	4696	WB
p-ERK$^{Thr202/Tyr204}$	Rabbit	CST	9101	WB
FAS	Rabbit	CST	3180	WB

GAPDH	Rabbit	Abcam	9485	WB
HSL	Rabbit	CST	4107	WB
p-HSL^{Ser563}	Rabbit	CST	4139	WB
Lamin B	Rabbit	Abcam	16048	WB
Total OXPHOS	Mouse	Abcam	110413	WB
PGC1α	Rabbit	Novus Biologicals	NBP1-04676	WB
Perilipin1	Rabbit	Abcam	3526	WB
PPARγ	Rabbit	CST	2435	WB, IF
SERCA1	Rabbit	Abcam	2819	WB
SERCA2	Mouse	Invitrogen	MA3-919	WB
SIP2	Mouse	In house		WB
SMAD2/3	Rabbit	CST	8685	WB
p-SMAD2$^{Ser465/467}$	Rabbit	CST	3108	WB
p-SMAD3$^{Ser423/425}$	Rabbit	CST	9520	WB
TOMM20	Rabbit	Santa-Cruz	11415	WB
UCP1	Rabbit	Abcam	10983	WB
ULK1	Rabbit	Sigma	A7481	WB
p-ULK1^{Ser555}	Rabbit	CST	5869	WB
vinculin	Rabbit	Sigma	V9131	WB

Table 2.3 FACS antibodies

FACS antibodies are all used at a 1/50 dilution.

Target	**Conjugated fluorophore**	**Supplier**	**Catalogue number**
CD31	Fluorescein isothiocyanate	BioLegend	102405
CD45	Allophycocyanin/Cyanine 7	BioLegend	103115
CD140a	Phycoerythrin	BioLegend	135905

Table 2.4 Secondary antibodies

Antibody	Species raised in	Dilution	Supplier	Catalogue number	Application
Anti-Mouse IRDye® 800CW	goat	1/20000	LiCore Biosciences	926-32210	WB
Anti-Rabbit IRDye® 680RD	goat	1/20000	LiCore Biosciences	926-68071	WB
Anti-Rabbit HRP-linked	goat	1/1000	CST	7074	WB
Anti-Rabbit Alexa Fluor 647	goat	1/1000	Invitrogen	A-31573	IF
Anti-Mouse Alexa Fluor 647	goat	1/1000	Invitrogen	A-31571	IF

2.1.5 Primers

Table 2.5 Genotyping primers

Gene	Sequence	Product size (base pairs)
AMPKγ1	F1- GGACGACGATGACAAGTGAG F2- CACGTTTCCGACTTGAGTTG R- TAAGCCTGCCCAGAAGACTC	WT- 365 Transgene (containing FLAG)- 498
β-Actin Cre	F- CGTACTGACGGTGGGAGAAT R- CCCGGCAAAACAGGTAGTTA	178
IL2	F- CTAGGCCACAGAATTGAAAGATCT R- GTAGGTGGAAATTCTAGCATCATCC	324

Table 2.6 qPCR primers

Abbreviations; Adiponectin (Adipoq), Leptin (Lep), Lipoprotein lipase (Lpl), Preadipocyte factor-1 (Pref-1), ribosomal protein L13a (Rpl13a), (sex determining region Y)-box 2 (Sox2).

Name	Forward sequence	Reverse sequence
36B4	AGATTCGGGATATGCTGTTGGC	TCGGGTCCTAGACCAGTGTTC
Adipoq	AGGCCGTTCTCTTCACCTAC	CTGGTGTATGGGCTATGGGT

Cebpα	GCGGGAACGCAACAACATC	GTCACTGGTCAACTCCAGCAC
Cidec	GCCACGCGGTATTGCCAGGA	GGGTCTCCCGGCTGGGCTTA
Fas	TGCTCCCAGCTGCAGGC	GCCCGGTAGCTCTGGGTGTA
Lep	GAGACCCCTGTGTCGGTTC	CTGCGTGTGTGAAATGTCATTG
Lpl	ATCGGGCCCAGCAACATTAT	ACTCCTCCTCCATCCAGTTG
Nanog	TCTTCCTGGTCCCCACAGTTT	GCAAGAATAGTTCTCGGGATGAA
Oct-4	CGGAAGAGAAAGCGAACTAGC	ATTGGCGATGTGAGTGATCTG
Pparγ	TGAAAGAAGCGGTGAACCAC	AGCTGATTCCGAAGTTGGTG
Pref-1	CCCAGGTGAGCTTCGAGTG	GGAGAGGGGTACTCTTGTTGAG
Rpl13a	CTGTGAAGGCATCAACATTTCTG	GACCACCATCCGCTTTTTCTT
Sox2	GATCAGCATGTACCTCCCCG	CTGGGCCATGTGCAGTCTAC
Ucp1	AGGCTTCCAGTACCATTAGGT	CTGAGTGAGGCAAGCTGATTT

2.2 ANIMAL STUDIES

2.2.1 Declaration

All experiments involved in the generation of transgenic animals were approved by the Gothenburg Ethics Committee. All in vivo studies were performed in accordance with the UK Animals (Scientific Procedures) Act (1986) and approved by the Animal Welfare and Ethical Review Board at Imperial College London.

2.2.2 Animal models

The two animal models used in this work were the β-actin Cre AMPKγ1^{WT} (WT) and the β-actin Cre AMPKγ1^{D316A} (D316A) mutants generated from a C57BL/6J strain as described previously (Woods et al., 2017). Both mutants contain a transgene of AMPKγ1 that is either WT or expresses the D316A point mutation, and both constructs contain a FLAG (DYKDDDDK) tag.

2.2.3 Animal husbandry and diet administration

Animals were housed in individually ventilated cages at 21°C, with *ad libitum* access to food and water and 12 hour light/ dark cycles. Mice were maintained on an RM3 chow diet (Special Diet Services, Essex UK), with a nutrient profile of 11.48% energy from oil, 27.28% from protein and 61.24% from carbohydrate. For high fat diet studies mice were provided a

45% high fat diet (SNIFF, Soest Germany) with a nutrient profile of 45% energy from fat, 20% from protein and 35% from carbohydrates.

2.2.4 Genotyping

To determine mouse genotypes, ear biopsies were taken at 3 weeks of age and digested in 0.5M NaOH by heating twice for 10 minutes at 100°C with vortexing in between. Digests were neutralised with an equal volume of 0.5M Tris pH 8. To assess the presence of the β-actin Cre gene, digests were polymerase chain reaction (PCR) amplified on a thermal cycler (G-STORM) with 5 minutes at 95°C, then a 40 times cycle of 95°C for 30 seconds, 60°C for 40 seconds, 72°C for 60 seconds, followed by 72°C for 5 minutes. Primers for the Cre recombinase and an IL2 house keeper control (Table 2.5) and 1x Biomix Red DNA polymerase mix were used. PCR products were separated by gel electrophoresis on a 1% agarose gel made in tris-acetate EDTA at 120V for 30 minutes with 1x SYBR safe DNA gel stain and visualised with a gel imaging system (Bio Rad). To assess the status of AMPKγ1, primer sets were used to allow determination of a WT or an AMPKγ1 homozygote or heterozygote mutation (Table 2.5) and a thermal cycler program of 94°C for 5 minutes followed by 35 cycles of 94°C for 1 minute, 60°C for 1 minute, 72°C for 2 minutes, followed by 72°C for 5 minutes.

2.2.5 Transplant surgery

Study design: One month old C57BL/6J male mice were used for adipose tissue allograft transplantation surgeries. Adipose tissue donor mice that were either AMPKγ1 WT or AMPKγ1 D316A were littermates of phenotypic AMPKγ1 WT recipient mice. Allograft transplantation of adipose tissue was performed with surgical aseptic technique. The donor mouse was culled and the left iWAT depot was removed and placed into cold, sterile saline solution. The recipient mouse was anesthetised with isoflurane and hair was removed from around the surgery area. An incision was made in the lower left flank so that the native fat pad was just visible and a pocket was made for the allograft to be placed into. The pocket was washed with sterile saline solution and then the donor tissue was placed on top of the native tissue. The incision was closed with suturing and the animal was placed into a 30°C warming chamber for recovery. Once it had recovered from the anaesthesia it was placed in a clean cage with a wet diet, daily checks and pain killer administration for the following three days. After surgery mice were singly housed for the rest of the study. 4 weeks after surgery mice were placed on a 45% high fat diet for 16 to 20 weeks. Body weights were

taken every 7 days with fat and lean mass assessed by eMRI at the end of the study, and mouse metabolic parameters were measured using a Comprehensive Laboratory Animal Monitoring System in the final 7 days of the study.

Sample size and inclusion criteria: Because of the large difference in body weight observed previously in D316A mice compared to WT mice on a high fat diet (Pollard et al., 2019), in total there were 9 transplant recipient mice included in the study. 4 mice received a WT adipose tissue and 5 of which received a D316A WT adipose tissue. Animals were included in the study if the adipose tissue graft was successfully transplanted and there were no signs of transplant rejection and the animal did not remove the graft. A small sample size was used as this was an information gathering pilot study and power calculations were not used to determine sample size.

Randomisation and blinding: Due to this being a small pilot study and as littermates were used, there was no randomisation strategy was used to designate the allograft donors to recipients. Due to the nature and size of the study, it was not possible for researchers to be blinded as to the genotype of the donor tissue.

2.2.6 Comprehensive Laboratory Animal Monitoring System

Animals were weighed and then singly housed at room temperature (21°C) in a comprehensive laboratory animal monitoring system (CLAMS) and fed *ad libitum*, with random allocation of cages to racks so that each genotype was dispersed amongst different racks. After 24 hours of acclimatisation, mice were assessed for one week from Friday to Friday and were checked twice daily. Recordings were taken at 22 minute intervals with VO_2, VCO_2, horizontal movement and vertical movement and food and drink intake data collected. CalR (Mina et al., 2018) version 1.3 was used to analyse data and do statistical analysis.

2.2.7 Tissue dissection

For all studies male WT or D316A mice aged between 3 to 5 months were culled using carbon dioxide euthanasia followed by cervical dislocation. Tissues were dissected and either placed in 4% paraformaldehyde for histology, or in sterile Hank’s balanced salt solutions for cell isolation.

2.3 GENERAL METHODS

2.3.1 Histology

After dissection tissues were placed in 4% paraformaldehyde for 24 hours whilst rocking, then transferred to 50% then 70% ethanol. Tissues were wax embedded, cut to 4μm thick sections and haematoxylin and eosin stained by Lorraine Lawrence (Imperial College London Histology). Scans of sections were acquired on the ZEISS Axio Scan.Z1 slide scanner using ZEN software. Quantification of lipid droplet size was done by Chad Whilding (LMS Microscopy Facility) on annotated regions of scanned sections using ImageJ software.

2.3.2 Cell culture

To isolate mouse iWAT SVF for cell culture, both iWAT fat pads were dissected from mice, minced into a slurry with scissors and placed into SVF digest medium. Minced fat pads were rotated for 40 minutes at 37°C with pipetting up and down every 10 minutes until disaggregated. Digests were passed through a 100μm filter and centrifuged at 250xg for 5 minutes to pellet the SVF and floating adipocytes were removed with a wide mouth pipette. The SVF pellet was resuspended in 1x red blood cell lysis buffer and incubated at room temperature for 4 minutes. Red blood cell lysis buffer was quenched in PBS and the SVF was pelleted by centrifugation at 250xg for 5 minutes. The SVF was resuspended in SVF medium (Table 2.1), counted and seeded at appropriate densities. For adipogenic differentiation of primary mouse SVF, cells at 80% confluence were placed into adipogenic induction medium (Table 2.1) for 2 days, after which media was exchanged for adipogenic maintenance medium (Table 2.1). Media was refreshed every 2 to 3 days and with mature adipocytes present from day 7 onwards.

The mouse ES cell line E14 was a gift from Dr Tristian Rodriguez. They were cultured on 0.1% gelatine coated tissue culture dishes in ES cell base medium with LIF (Table 2.1). The C2C12 mouse myoblast cell line (ATCC) was cultured in C2C12 growth medium (Table 2.1). Human skeletal muscle cells CC2580 (Lonza) are obtained from upper arm or leg biopsies and were cultured in human muscle cell growth medium (Table 2.1) according to the manufacturer's directions. For adipogenic differentiation of E14 cells, cells were dissociated into a single cell suspension with trypLE and then seeded as hanging drops on the lid of a 10cm petri dish with 1000 cells per 20μl drop in ES cell base medium (Table 2.1). At day 2, embryoid bodies had formed and were collected and grown on 10cm dishes pre-coated with 0.1% gelatine in ES cell base medium plus 100μM retinoic acid, allowing the embryoid

bodies to adhere to the dish. From day 5 to 7 cells were grown in ES cell base medium. From day 7 to 15 cells were grown in ES cell adipogenic maintenance medium (Table 2.1). On day 11 embryoid bodies were dissociated into a monolayer with trypLE. From days 16 to 20 cells were grown in an ES cell adipogenic induction medium (Table 2.1). From day 21 till the end point at day 24 cells were grown in ES cell adipogenic maintenance medium. For adipogenic differentiation of C2C12 cells, human skeletal muscle cells, primary SVF or primary PDGFRα cells, cells were grown to 80% confluence and then media was exchanged for adipogenic induction medium (Table 2.1). Cells were grown in adipogenic induction medium from day 0 to 2, and then media was exchanged for adipogenic maintenance medium (Table 2.1) with media changes every 2 to 3 days, with mature adipocytes present from day 8 onwards. All cells were grown in a 37°C humidified incubator with 5% CO2.

2.3.3 Live proliferation and apoptosis

Cells were seeded in tissue culture 96 well plates and put through adipogenic differentiation in the IncuCyte S3 (Sartorius) with the addition of a NucLight Rapid Red (Sartorius 4717) and a green caspase-3/7 dye (Sartorius 4440). Phenol red free DMEM/F12 was used as the base medium. Bright field and fluorescence scans were taken every 2 hours for 4 areas per well at 10x magnification and the IncuCyte S3 software was used to count live and apoptotic nuclei.

2.3.4 Fluorescence Activated Cell Sorting

To isolate PDGFRα expressing cells from the SVF, the iWAT SVF was isolated and after red blood cell lysis and quenching, the SVF was resuspended in FACS buffer and incubated with conjugated FACS antibodies (Table 2.3) for 15 minutes at room temperature in the dark. Cells were centrifuged at 250xg for 5 minutes, resuspended in FACS buffer and passed through a 30µm cell strainer into FACS tubes. Cells were FACS sorted (BD FACS Aria III) with assistance from James Elliot and Bhavik Patel (LMS Flow Cytometry Facility). PDGFRα cells were selected with CD45 and CD31 stained cells discarded. Selected cells were seeded in SVF growth media at appropriate densities.

2.3.5 Protein isolation

Protein was isolated from cells by washing with ice cold PBS followed by rapid lysis and scraping in ice cold HEPES buffer A, 1% Triton X-100. Cells were centrifuged at 13,000rpm for 10 minutes at 4°C and the pellet was discarded. To separate the cytosolic and nuclear fractions, cells were washed in ice cold PBS and rapidly lysed and scraped into cytosolic

protein extraction buffer and left on ice for 15 minutes. Cells were centrifuged at 3,600rpm for 10 minutes at 4°C and the supernatant containing the cytosolic proteins was collected. To remove any excess cytosolic proteins, the remaining pellet was resuspended in cytosolic protein extraction buffer again and left on ice for 15 minutes before centrifuging at 3,600rpm for 10 minutes at 4°C, this time discarding the supernatant. The pellet was resuspended in nuclear extraction buffer and sonicated with a probe sonicator for 10 seconds to release the nuclear proteins. Then, both the cytosolic and nuclear fractions were centrifuged at 13,000rpm for 10 minutes at 4°C and the supernatants collected.

2.3.6 Bradford assay

To quantify protein concentration, protein lysates were diluted 1/20 in water and then diluted 1/20 in 1x Protein assay dye reagent in a flat bottom 96-well plate. A BSA protein standard was serially diluted to generate a reference standard curve. After 5 minutes of incubation at room temperature the absorbance was read at 595nm on a SpectroMax plate reader (Molecular Devices). Protein concentrations were calculated with reference to the standard curve and corrected for dilution factors.

2.3.7 Western blotting

1µg/µl protein lysate in sample buffer was heated to 100°C for 5 minutes, unless looking at the mitochondrial complex proteins when the samples were not heated. 10µg of protein along with a protein molecular weight ladder was loaded onto a 4-12% Bis-Tris gel with 1x 3-(N-morpholino)-propanesulfonic acid SDS running buffer for separation by SDS-PAGE. Protein was then transferred from gel to polyvinylidene fluoride membrane by electrophoresis in a tris-glycine transfer buffer. After transfer, blots were stained with Ponceau S solution to visualise protein loading and then blocked with 4% BSA for one hour. Blots were incubated with primary antibodies (Table 2.2) in 4% BSA overnight at 4°C then washed three times in TBS-T. Blots were incubated with secondary antibodies (Table 2.4) in 4% milk for one hour at room temperature and then washed three times in TBS-T. Blots were imaged with an Odyssey Imaging System (LI-COR Biosciences) and quantified using Image Studio Lite Ver 5.2. For proteins that could not be visualised with the LI-CORE, blots were incubated with HRP conjugated secondary antibodies (Table 2.4) in 4% milk for one hour at room temperature, then washed three times in TBS-T. Blots were incubated with HRP substrate for one minute and then visualised using the Gel Doc imaging system (Bio Rad).

2.3.8 TGFβ-1 ELISA

Transforming growth factor β (TGFβ) protein levels were assessed using the TGFβ-1 ELISA kit according to the manufacturer's instructions. A clear, flat bottom 96 well plate was coated overnight in capture antibody and then washed 3 times in wash buffer. The wells were then blocked with ELISA diluent for one hour at room temperature and then washed with wash buffer. 50µg/100µl protein lysate was acid activated with 1N HCl for 10 minutes at room temperature, and then neutralised with equal volume 1N NaOH. 2-fold serial dilutions of a TGFβ-1 standard were made to generate a standard curve were added to the plate along with the protein lysate and an ELISA diluent blank control. The plate was incubated overnight at 4°C. Wells were washed 5 times in wash buffer with excess liquid blotted away and then incubated with detection antibody for 1 hour at room temperature. Wells were washed 5 times in wash buffer with excess liquid blotted away and then incubated with TBM solution for 10 minutes at room temperature before the reaction was stopped with Stop solution. The absorbance at 450nm was then read on a SpectroMax plate reader.

2.3.9 Immunofluorescence and image analysis

Cells were washed with PBS and then fixed in 4% paraformaldehyde plus 2% sucrose for 10 minutes at room temperature. Cells were washed three times with PBS. Cells were blocked and permeabilised with immunofluorescence blocking buffer for one hour at room temperature. Cells were incubated with primary antibody in immunofluorescence blocking buffer overnight at 4°C. Cells were washed three times with PBS and incubated with secondary antibodies in immunofluorescence blocking buffer for one hour at room temperature followed by three PBS washes. For lipid droplet staining, cells were incubated with 1/500 LipidTOX dye for 30 minutes at room temperature in the dark. Cells were washed in PBS and then incubated with 1µg/ml DAPI for 5 minutes in the dark at room temperature and then put into fresh PBS. If cells were on coverslips these were mounted onto slides with mounting medium. Images were acquired on either the ZEISS Axio Scan.Z1 slide scanner with ZEN software, the EVOS M700, Operetta or Yokogawa microscopes. Images acquired on the EVOS M700 were analysed with ImageJ software. Images acquired on the Operetta were analysed with Harmony software. Images acquired on the Yokogawa microscope were analysed with Columbus software.

2.3.10 EdU labelling

Before fixing with paraformaldehyde, cells were labelled with 10μM EdU for 30 minutes. Fixed cells were blocked and permeabilised with immunofluorescence blocking buffer for 1 hour at room temperature. To detect EdU the Click-iT EdU Assay kit was used according to the manufacturer's instructions. The Click-iT EdU reaction cocktail containing EdU reaction buffer, CuSO4, Alexa Fluor 488 Azide and buffer additive was made immediately before use. The cells were incubated with the Click-iT EdU reaction cocktail for 30 minutes at room temperature in the dark and then washed three times in the immunofluorescence blocking buffer.

2.3.11 RNA isolation

RNA was isolated from cells using TRIzol plus 0.4 (v/v) chloroform. The mix was shaken for 15 seconds then incubated for 2 minutes at room temperature before being centrifuged at 12,000xg for 10 minutes at 4°C. The clear aqueous phase was taken and mixed with 0.53 (v/v) ethanol and RNA was purified with an RNeasy kit according to the manufacturer's instructions. The RNA was loaded onto an RNA spin column and centrifuged at 12,000xg for 1 minute. The column was then twice washed with RPE buffer plus ethanol by centrifuging at 12,000xg for 1 minute and discarding the flow through, and then dried by centrifuging with no buffer at 12,000xg for 2 minutes. RNA was eluted into RNase free water by centrifuging at 12,000xg for 1 minute. RNA concentrations were measured on the NanoDrop photospectrometer (Thermo Scientific).

2.3.12 cDNA synthesis and qPCR

1μg RNA was incubated at 65°C for 10 minutes with 5ng/μl random hexamers, 1mM dNTP mix and RNase free water to a volume of 10μl. Then, 1x first-strand buffer, 20mM DTT, 200U SuperScript™ II Reverse Transcriptase, 10mM MgCl2 and RNase free water was added to the RNA mix to make a final volume of 20μl and incubated at 25°C for 10 minutes, 50°C for 50 minutes, 85°C for 5 minutes. For quantitative PCR (qPCR), 2μl cDNA was added to 1x SensiMix SYBR Hi-ROX, 400nM forward/reverse primer mix (Table 2.6) and RNase free water to make up a total volume of 10μl. Reactions were run on a thermal cycler (Bio-Rad CFX) to measure c(t) values. qPCR primer linearity was evaluated by pooling all cDNA and serial diluting to make a standard curve. To interpret gene expression, the c(t) values were input into the linear equation y=mx+c generated from the standard curves and x

was found. This value was then transformed with 10^x to account for the logarithmic scale of the standard curve and then normalised to a housekeeping gene.

2.3.13 RNA sequencing

RNA was extracted from primary SVF derived adipocytes from 3 month old male mice, 5 D316A and 6 WT, with WT mice split into DMSO and 1.25μM BI-9774 chronic treatment through differentiation. RNA sequencing was done by Dr Laurence Game, Ivan Andrew and Max Taylor (LMS Genomics Facility). RNA quality was assessed using the Agilent 2100 RNA 6000 Nano assay and libraries were prepared using the NEBNext Ultra II Directional RNA Library Prep Kit with NEBNext Poly(A) mRNA Magnetic Isolation Module following manufacturer's instructions. Library quality was evaluated using the Agilent 2100 High-Sensitivity DNA assay, and their concentrations measured using the Qubit™ dsDNA HS Assay Kit. Libraries were pooled in equimolar quantities and sequenced on a NextSeq2000 to generate a minimum of 40 million Paired End 60bp reads per sample. For analysis, reads were aligned to UCSC mouse genome (mm10) using STAR version 2.7.7a (Dobin, Davis et al. 2013), with argument "----quantMode TranscriptomeSAM GeneCounts". Gene-based read counts were performed by STAR as well. Generated count data were then used to normalise and identify differentially expressed genes using DESeq2 (Love, Huber et al. 2014) and DEGs were defined with Benjamini-Hochberg adjusted $P < 0.05$. Gene Set Enrichment Analysis (GSEA) was performed using GSEA software (Subramanian, Tamayo et al. 2005) on pre-ranked list generated by DESeq2. A false discovery rate (q-value) cut off of 0.25 was set for enrichment. This work was done by Marian Dore (LMS Bioinformatics Facility). DAVID online GO analysis tool was used to generate GO terms associated with significantly differentially expressed genes.

2.3.14 Oil Red O quantification

To stain lipid, cells were washed with PBS and fixed with 4% paraformaldehyde for 10 minutes at room temperature. Cells were washed twice with distilled water and then incubated with filtered Oil Red O for 15 minutes at room temperature whilst shaking. Oil Red O was removed and cells were washed 4 times with distilled water. Images were acquired on the EVOS M7000. To quantify, Oil Red O was dissolved with 100% isopropanol and incubated for 10 minutes at room temperature whilst shaking. 200μl of the dissolved Oil Red O was transferred to a clear, flat bottom 96 well plate and absorbance was measured at 500nm on a spectrophotometer.

2.3.15 Senescence associated β-galactosidase assay

To measure senescence, the Senescence Detection Kit (BioVision K320) was used according to the manufacturer's instructions. Cells were washed with PBS and fixed with the provided fixative for 10 minutes at room temperature. The staining solution containing 1mg/ml X-gal was added to the cells and they were incubated overnight at 37°C. Cells were stained with Oil Red O and DAPI. Brightfield and DAPI images were collected on the EVOS M7000 and SA-β-gal positive cells were quantified using a script on ImageJ. Briefly, the DAPI was used to determine the total number of cells. To count the number of blue cells, colour deconvolution was applied with the pre-set Brilliant Blue vectors to select out only the blue in the image and the number of blue cells were counted.

2.3.16 AMPK activity assay

AMPK activity was assayed using the SAMS peptide assay as described (Davies, Helps et al. 1995). Briefly, AMPK was immunoprecipitated from cell protein lysates using a pan-AMPKβ antibody SIP2 and a protein A slurry in which were mixed for 2 hours at 4°C. The immunoprecipitates were washed twice by centrifuging at 13,000xg for 1 minute at 4°C, discarding the supernatant and resuspending in HEPES buffer A, 1% Triton X-100 for the first wash and HEPES buffer G for the second wash. After the second wash the supernatant was discarded and 10µl HEPES buffer A, 1% Triton X-100, 30µl AMPK assay mix containing the SAMS peptide for AMPK to phosphorylate, and 10µl ^{32}P was added to each sample. Reactions were mixed on the vibrax for 20 minutes at 37°C and then 10µl of reaction was spotted onto P81 paper, which was washed in 1% ortho-phosphoric acid. P81 papers were then dried and placed in scintillation tubes containing scintillant and radioactivity was measured in a scintillation counter.

2.4 ILLUSTRATIONS

Illustrative figures were created with BioRender.com.

2.5 STATISTICAL ANALYSIS

Statistics are performed when there are 3 or more biological replicates and number of biological replicates are reported as n= in each figure legend. For SVF cell experiments mouse adipose are harvested on the same day and where cells are treated with small molecules the SVF from each mouse is split into control and treatment groups. All data figures are presented as the mean ± SEM. Differences between two data sets were analysed using a Student's two-tailed t-test. F-tests were used to compare the variance's

and where there was a significant difference between the variances ($p<0.05$), Welch's correction was applied. One-Way analysis of variance (ANOVA) was used to assess differences between multiple groups with Dunnett's correction for multiple comparisons when comparing between one control group, or post-hoc Tukey's test when comparing the differences between all groups. When comparing the differences between two variables with multiple groups per variable, 2-way ANOVA was used with Šidák's correction for multiple comparisons. For all, a statistically significant difference was defined as $p<0.05$. All statistical analysis were performed using GraphPad Prism software version 9.1.

3. ADIPOSE ALLOGRAFT TRANSPLANT

3.1 INTRODUCTION

The D316A mouse is protected from diet induced obesity with lower body weight gain, reduced fat mass, reduced liver mass, lower liver triglycerides and improved insulin sensitivity (Pollard et al., 2019). It is thought that increased ATP uncoupling in the iWAT confers this protection, as there is an increase in the RER and subcutaneous temperature that is not related to BAT. The iWAT of the D316A mouse has smaller, multilocular lipid droplets, increased mitochondrial content and increased UCP1-independent thermogenesis. If the protection from diet induced obesity is solely reliant on the iWAT, then it may be possible to use transplantation of D316A iWAT to protect a WT recipient mouse from diet induced obesity.

Three main types of adipose tissue transplantation exist: autograft, allograft and xenograft. Autograft transplantation is the insertion of tissue from one location to another within the same individual. Autografting of adipose tissue has become increasingly popular in reconstructive and cosmetic procedures (Azoury et al., 2021). An allograft is the transplantation of tissues between members of the same species, and a xenograft is transplantation of tissue from one species to another. The first adipose tissue transplantation studies were allografts of BAT which were inserted under the kidney capsule to learn more about the tissue's function (Ferren, 1966; Nechad and Olson, 1983; White et al., 2019).

Because of the therapeutic potential of activating BAT in metabolic diseases, most transplantation studies in the literature are preclinical studies done to introduce BAT into a host. In mice with Type 1 diabetes, BAT allografts returned glucose levels to normal, independent of insulin, with changes in levels of adipokines and other circulating plasma hormones thought to be responsible (Gunawardana and Piston, 2012, 2015; Stanford et al., 2013). BAT transplantation can also be used as an alternative to activating cold exposure for treating obesity through the overall increase of BAT mass. It has been shown to reduce body weight gain, improve glucose uptake and lower liver triglyceride accumulation in a post-surgery high fat diet model (Liu et al., 2013; Zhu et al., 2014). Furthermore, in mice that are already obese, it leads to improvements in body weight, insulin tolerance and circulating adipokine levels, increased energy expenditure and response to β-AR signalling and improved thermogenesis in the native BAT (Liu et al., 2015). Similar improvements in obesity have been achieved with WAT allografts from healthy donors to *ob/ob* mice, where

increasing the number of donor depots in the recipient increases beneficial effects (Klebanov et al., 2005). iWAT allografts have also improved the metabolic characteristics of seipin deficient mice which are a model of lipodystrophy, including improving leptin levels, restoring insulin response, lowering blood glucose levels and reducing liver triglyceride content (Wang et al., 2018). In addition, adipose tissue allografts have been found to improve fertility in animal models of polycystic ovary syndrome or in *ob/ob* mice which are infertile, by increasing adiponectin levels (Klebanov et al., 2005; Yuan et al., 2016).

More translational studies have used xenograft transplants of human brown adipocyte cells or precursors into immunocompromised mice. Human adipocyte precursors, inducible pluripotent stem cells or fibroblasts were differentiated into beige adipocytes and transplanted into immunocompromised mice (Kishida et al., 2015; Lee et al., 2017; Min et al., 2016; Silva et al., 2014). The cells formed depots with vascularisation and circulating human adiponectin was detected in the mice. These mice had lower body weight gain, improved glucose metabolism and liver health on a high fat diet. Xenograft transplantation of adipose tissue precursors was also attempted but the metabolic benefits weren't as striking with precursor cells as with mature cells (Lee et al., 2017; Silva et al., 2014). These studies are promising for the use of transplantation and cell therapy for treating obesity and other metabolic disorders.

Adipose transplantations have also been used as a method to investigate adipocyte cell biology, in particular to discover precursor populations and refine our understanding of adipocyte differentiation. Candidate adipocyte progenitor cells expressing specific lineage markers as well as a fluorescence marker are transplanted into mice and their progression followed to see if they can generate adipose tissue in *vivo*. Some discoveries from these transplantation studies include that $CD24^+$ cells can form adipocytes, but CD24 expression is lost as cells become more committed to adipogenesis (Berry and Rodeheffer, 2013; Rodeheffer et al., 2008). Further studies have revealed the differentiation hierarchy of $DPP4^+$ progenitor cells, which form mature adipocytes *in vivo* via $ICAM1^+$ and $CD142^+$ preadipocyte intermediates (Merrick et al., 2019). Adipocyte progenitor transplantation studies have also shown the effects of the microenvironment on adipose tissue expansion, with the proliferation and differentiation of precursors in response to a high fat diet dependent more on the depot they are transplanted into than the depot they originated from (Jeffery et al., 2016).

Transplantation studies are beneficial for understanding adipocyte cell biology and for determining the translational benefit of adipose tissue. An initial pilot study was set up whereby D316A iWAT or control WT iWAT was transplanted into WT recipients which were then fed a high fat diet. It was hypothesised that if the allografts survived and were successfully incorporated into the host, the study could determine firstly whether the D316A adipose tissue alone is enough to protect from diet induced obesity and secondly whether the D316A iWAT phenotype is autonomous or whether it requires external cues.

3.2 D316A ALLOGRAFT TRANSPLANT

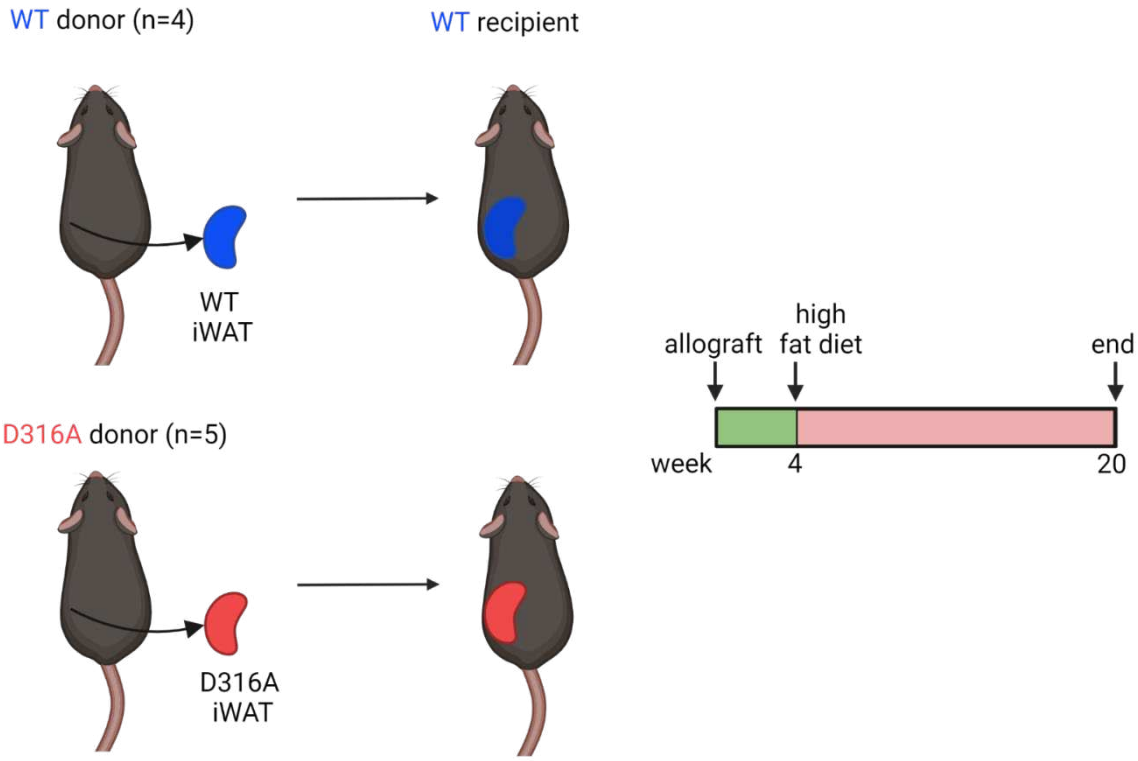


Figure 3.1 iWAT allograft transplant pilot experiment

The iWAT was removed from a freshly culled WT or D316A donor mouse and transplanted into the lower left flank above the native adipose tissue of the recipient mouse. 4 weeks after surgery the recipient mouse was placed on a high fat diet for up to 20 weeks.

The pilot study is summarised in Figure 3.1. Mice used for the study were one month old C57BL/6J males. Donor mice that had either had a β-actin Cre AMPKγ1^{D316A} AMPK mutation or were AMPKγ1^{WT} were culled and the left iWAT depot was removed, trimmed to 1cm in

length and transplanted into a pocket made on top of the left-hand side of the native iWAT depot of an AMPKγ1^{WT} recipient littermate mouse under anaesthesia. The mice were given one month to recover from surgery and for the graft to be incorporated without signs of rejection such as inflammation. There were 9 mice out of 12 in total that survived the transplant, 5 received D316A iWAT depots and 4 received WT iWAT depots. 4 mice from initial surgeries had to be culled after they chewed through their sutures and so for subsequent surgeries the incision site was made closer to the spine so that they were out of reach.

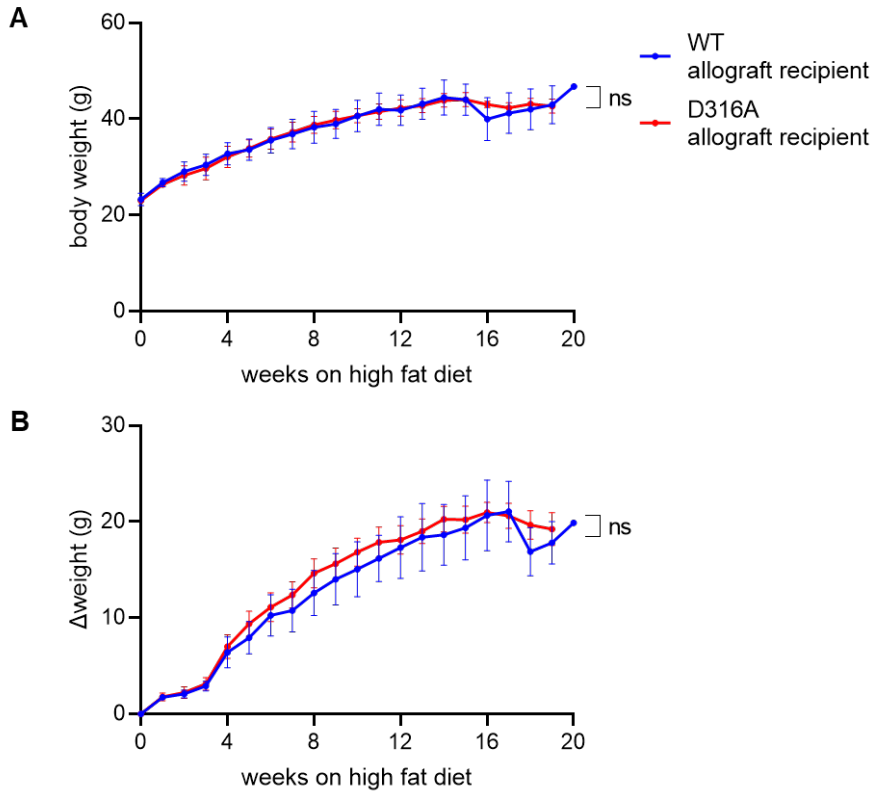


Figure 3.2 Body weight and body weight gain in allograft recipient mice on a high fat diet

Mice were weighed weekly from the initiation of high fat diet for up to 20 weeks. (A) Body weight of recipient mice with WT or D316A iWAT allografts. (B) Week to week body weight gain throughout the 20 weeks on a high fat diet. Data are shown as mean ± SEM with statistical significance determined by two-way ANOVA with Šidák's correction for multiple comparisons (WT allograft recipient n=4, D316A allograft recipient n=5).

After the one month of recovery, mice were fed a high fat diet (45% w/w) for 16 to 20 weeks. The 4-week range in time was due to the initial loss of mice because of removal of sutures and waiting for surgery room availability. Body weights were taken weekly after initiation of the high fat diet. Both groups gained weight normally throughout the experiment and there were no significant differences in body weight or body weight gain between recipients receiving WT allografts or those who received D316A allografts (Figure 3.2). This was in contrast to what was seen with the β-actin Cre D316A on a high fat diet, where there was significant protection from diet-induced obesity. As the β-actin Cre D316A mice showed reduction in fat mass accumulation on a high fat diet, recipient mice were subjected to eMRI towards the end of the study. Again, there was no difference in lean mass or fat mass between recipients of WT or D316A donor allografts (Figure 3.3).

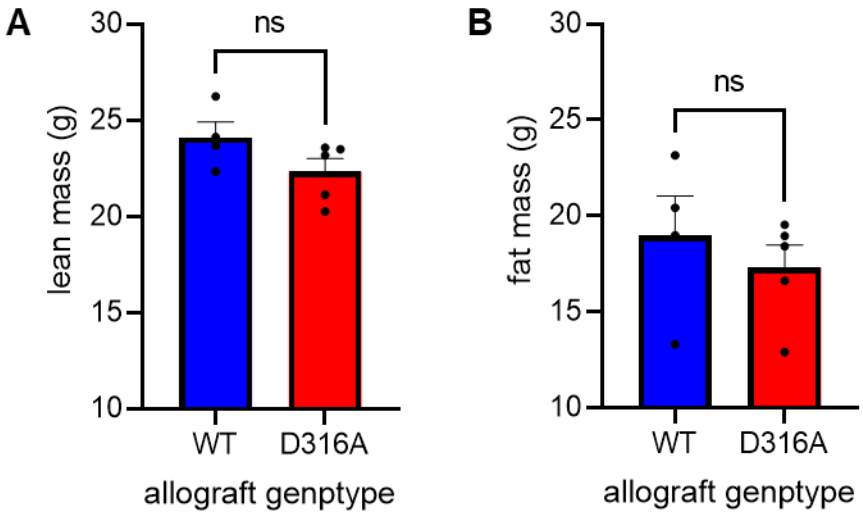


Figure 3.3 eMRI measurements of mass

Measurements of (A) lean mass and (B) fat mass in allograft recipient mice at the end of the pilot study after up to 20 weeks on a high fat diet. Data are shown as mean ± SEM with statistical significance determined by Student's t-test (WT allograft recipient n=4, D316A allograft recipient n=5).

Sometimes, experimental variables do not have an effect on body weight, but they do effect the metabolic health of the mouse, and can increase energy expenditure (White et al., 2019). For the final week of the high fat diet, mice were placed into a CLAMS to measure energy expenditure by oxygen intake and carbon dioxide output. There was no difference in oxygen

consumption (Figure 3.4A) or carbon dioxide production (Figure 3.4B), resulting in no difference in the RER (Figure 3.4C) over seven days of light and dark cycles, or when looking at the overall average values. There was also no difference in food intake (data not shown)

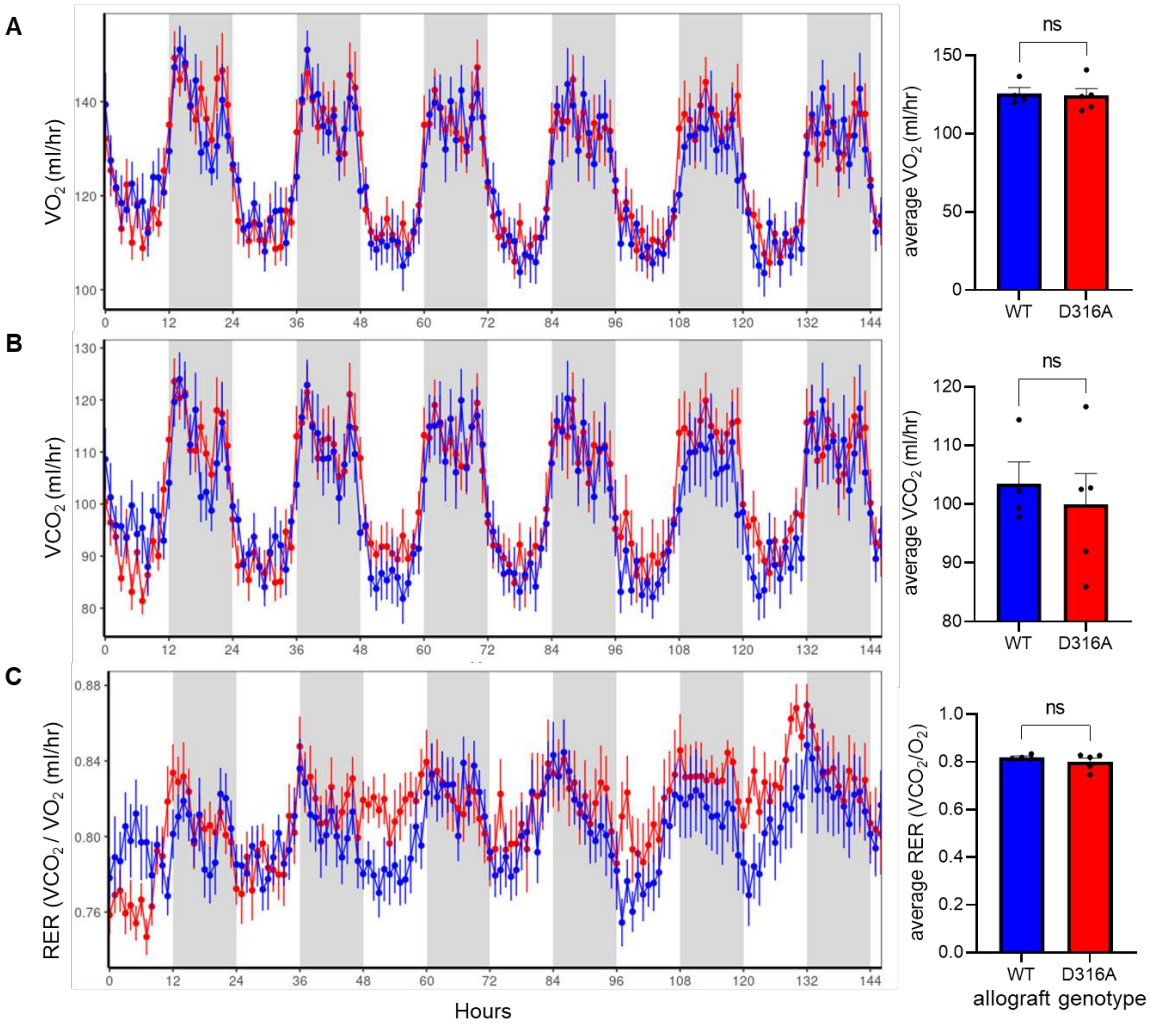


Figure 3.4 CLAMS analysis of allograft recipient mice on a high fat diet

One week CLAMS analysis of recipient mice of WT or D316A allografts after up to 20 weeks on a high fat diet to measure (A) oxygen consumption, (B) carbon dioxide production and (C) RER with the measurements over time, with light cycles in white bars and dark cycles in grey bars (left) and the full day average (right). For averages data are shown as mean ± SEM with statistical significance determined by Student's t-test (WT allograft recipient n=4, D316A allograft recipient n=5).

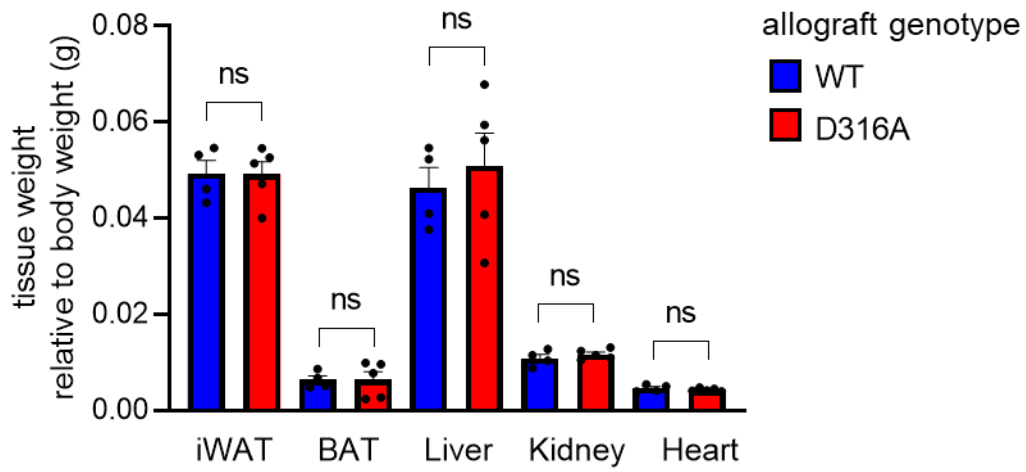


Figure 3.5 Post-mortem tissue weights of transplant recipient mice

Tissue weights relative to body weight. iWAT is the total weight of native depots and allograft. Data are shown as mean ± SEM with statistical significance determined by Student's t-test (WT allograft recipient n=4, D316A allograft recipient n=5).

After mice had been on a high fat diet for 16 to 20 weeks they were culled to assess effects of the surgery on metabolic tissues and to see how well the allograft had taken. There were no changes in the post-mortem weights of the iWAT, BAT, liver, kidney or heart when normalised to body weight (Figure 3.5). The iWAT weight was the total weight of the native and allograft depots. Haematoxylin and eosin stained liver sections show that the allograft transplantation did not confer protection from liver triglyceride accumulation as large lipid droplets were present throughout the livers of mice in receipt of either WT or D316A allografts (Figure 3.6A). Quantification of lipid droplet size in the liver showed no significant difference in average lipid droplet size between either groups (Figure 3.6B). These data together indicate that there was no protection conferred from the D316A allograft on the recipient mouse. Next it was important to determine the health of the transplant tissue and to see whether the D316A allografts retained the characteristics observed in the mouse.

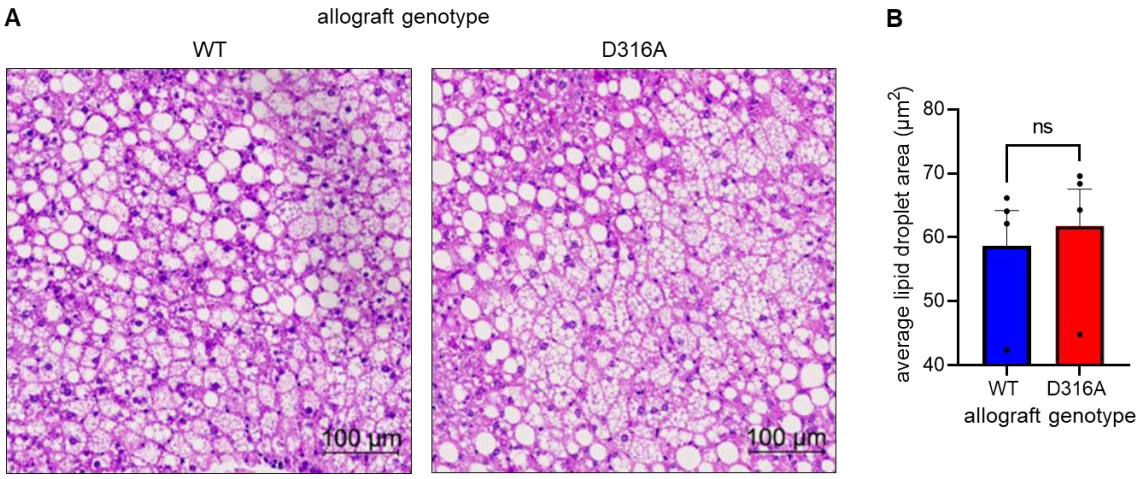


Figure 3.6 The morphology of livers of transplant mice

(A) Representative Haematoxylin and eosin stained livers from transplant mice in receipt of WT or D316A allografts. (B) Average lipid droplet area per mouse. Data are shown as mean ± SEM with statistical significance determined by Student's t-test (n=4). Scale bar represents 100µm.

After surgery the allograft was visibly positioned above the native tissue as is indicated by arrows (Figure 3.7A). Post-mortem dissection shows again that the allograft sits next to the native tissue (Figure 3.7B) and for 6 out of 9 of the mice the allograft tissue had fused onto the native tissue (Figure 3.7C). Again, haematoxylin stained WAT sections show the native and allograft transplants located next to each other (Figure 3.7D).

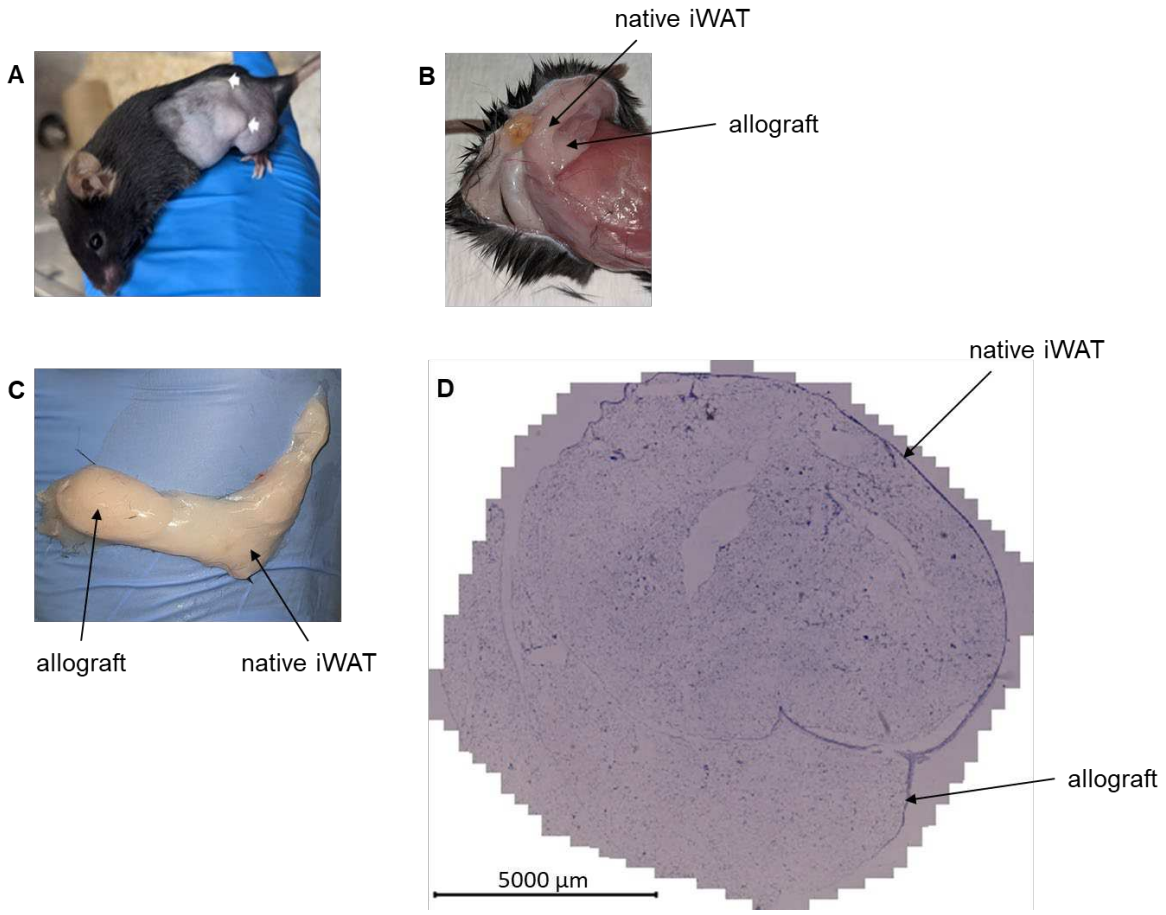


Figure 3.7 Images of the allograft transplant

(A) A recipient mouse after transplant surgery with arrows indicating where the transplanted tissue is visible through the skin. (B) A post-mortem recipient mouse at the end of the study after up to 20 weeks on a high fat diet with arrows indicating the native iWAT fat and allograft fat pads. (C) Dissected iWAT tissue from a recipient mouse with the allograft fused onto the native iWAT, with arrows indicating the native iWAT and allograft fat pads. (D) Cross section of haematoxylin stained native and allograft adipose tissue fused together. Scale bar represents 5000µm.

Representative images show no clear differences between any of the adipose tissue depots (Figure 3.8A). The native depots of the recipient mice contained large unilocular adipocytes as expected from a high fat diet WT iWAT depot. The allograft depots also generally contained large, unilocular adipocytes, showing that the D316A adipocyte morphology was mostly lost when the adipose tissue was in the environment of the WT mouse, and this was

consistent with the lack of protection from high fat diet. Interestingly, one of the D316A allografts contained a patch of smaller, multilocular adipocytes (Figure 3.8B). It may be that there were other areas of multilocular adipocytes from the other D316A allografts that haven't been captured with the sections taken. However, apart from this particular area, the rest of the D316A allografts were indistinguishable from the WT allografts.

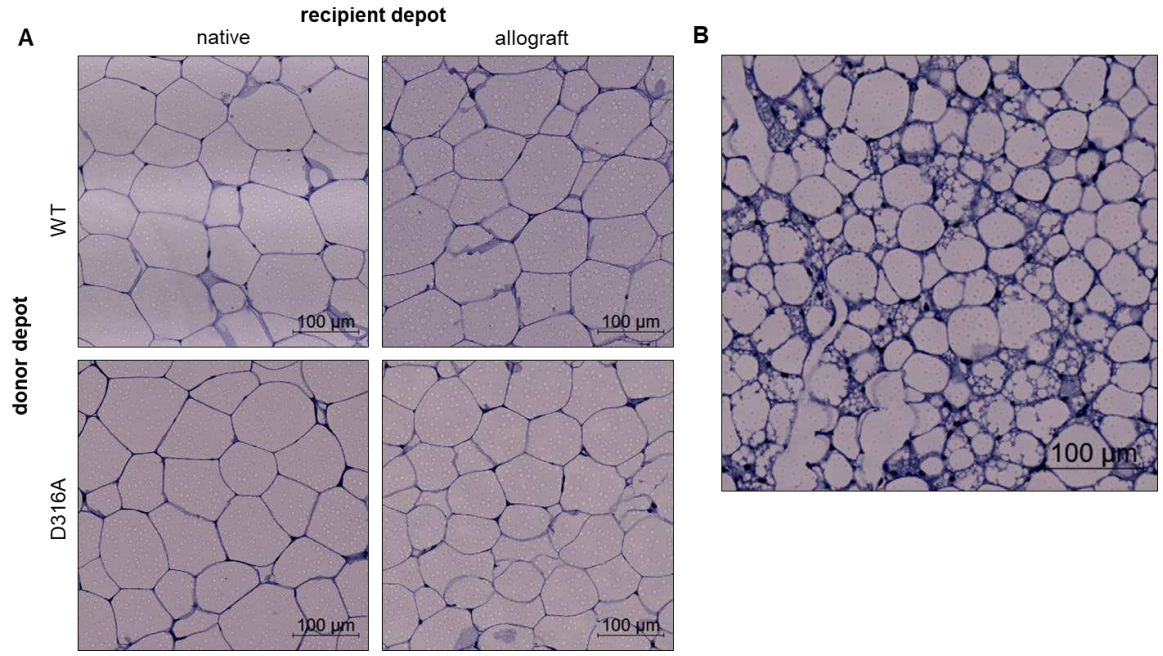


Figure 3.8 The morphology of native and allograft iWAT

(A) Representative Haematoxylin stained native iWAT and allograft iWAT from WT and D316A donors. (B) Haematoxylin stained D316A donor iWAT with multilocular lipid droplets. Scale bar represents 100µm.

3.3 DISCUSSION

Overall, this pilot study yielded no difference in recipient mouse obesity when receiving an iWAT allograft from a WT or D316A mouse. This could be for several reasons. The mice were given one month between surgery and initiation of the high fat diet for recovery and allograft incorporation into the host. However, it has been observed that over time, the transplanted tissue can gain some of the phenotypes of the host tissue (Liu et al., 2013; White et al., 2019). If this is the case, it could mean that over the study the D316A allograft gained WT adipose tissue characteristics and this led to increased lipid droplet size and

reduced energy expenditure. In addition, the transplant was carried out when the mice were one month in age and the younger cells are likely to be more plastic and influenced by external signalling from the host. If this has happened, it suggests that the phenotype of the D316A mouse iWAT is not autonomous, and external signalling through the nervous system or hormones are important for it to maintain its phenotype. This was the case when looking at cross-depot allograft transplantation, where subcutaneous or visceral adipose tissue precursors transplanted into visceral depots gained the characteristics of visceral adipose tissue (Jeffery et al., 2016). This would also suggest that the environmental cues needed to maintain the D316A phenotype are missing in the WT mouse. A single patch of D316A allograft adipocytes that retained their multilocularity was observed (Figure 3.8B), which may suggest that the D316A is able to maintain its phenotype on its own. However, it is possible that over time they too would increase in size.

Another possibility for the lack of protection from diet induced obesity with the D316A allograft is that there was not enough adipose tissue transplanted to see an effect. One study observed a correlation between improvement in metabolic health and number of donor depots transplanted into a single recipient (Klebanov et al., 2005). A 1cm long piece of adipose tissue may not be enough to protect from diet induced obesity, especially when the native adipose tissue still remains intact.

A limitation of this pilot study is that the non-transplanted right hand side iWAT from the donor mice was not taken for histology and comparison to the post-high fat diet allograft. Whilst there would have been a large difference in age between the two depots, it would have been useful to assess the changes in the allograft from its native state. It would also have been beneficial to have included a sham transplantation to have known the effects on the mouse caused by introducing a transplanted depot.

If this study were to be repeated, it may be improved by beginning the high fat diet immediately after the three day recovery from surgery, as is done in other studies. This reduces the possibility of the characteristics of the host tissue having an effect on the phenotype of the D316A tissue. To make the study more translationally relevant, it would be interesting to repeat the allograft transplantation in obese mice. This would be a better example of a clinical scenario, whereby a patient is seeking treatment for obesity, rather than a healthy person seeking preventative therapy. Healthy chow diet donors could be used, and in addition donors who have been on a high fat diet, as these were the conditions in which

the D316A mouse was demonstrating active thermogenesis (Pollard et al., 2019). Another way to investigate whether AMPK activation in a transplant could protect from diet induced obesity would be to activate AMPK in primary adipocytes obtained from differentiation of progenitors *in vitro* and transplant them into recipients as is done in other studies (Kishida et al., 2015; Lee et al., 2017; Min et al., 2016; Silva et al., 2014). This would allow for both mouse and human adipocytes to be assessed for their effectiveness. For these cell based transplants, it would be useful to have the allografts tagged with a fluorescent protein, and so using cells from a red fluorescent protein (RFP) expressing D316A donor mouse would be beneficial.

Transplantation of undifferentiated precursor cells has previously shown less effect on protection from obesity than using an adipose tissue depot (Lee et al., 2017; Silva et al., 2014). However, it could be used for the purposes of understanding more about the D316A adipocyte cell biology and development. The whole SVF or specific adipocyte precursor populations from RFP expressing D316A mice can be transplanted into recipient WT mice to see if they are able to form adipose tissue that represents the D316A adipose tissue, with smaller multilocular lipid droplets and increased mitochondrial content. If the adipocytes appear to be more like WT adipocytes, then the SVF or adipocyte precursors from an RFP WT mouse could be transplanted into a D316A mouse to see whether the environmental stimuli of the host is able to generate adipose tissue with D316A characteristics.

The reason for the lack of protection from diet induced obesity by the D316A allograft observed in this pilot study is difficult to determine, as there could be a multitude of reasons as to why this has occurred. However, use of transplantation to determine the clinical benefits of AMPK activation in cell therapy, and also to understand the cell biology of the D316A mouse and AMPK activation in a whole mouse is a handy tool which could be explored further, refined through the observations of this pilot study.

4. PHARMACOLOGICAL ACTIVATION OF AMPK IN ADIPOCYTES

4.1 INTRODUCTION

The D316A mouse showed how activation of AMPK can give rise to a unique population of adipocytes with an ability to prevent diet induced obesity (Pollard et al., 2019). Whilst this has interesting therapeutic implications, generating a D316A mutation in humans is not currently feasible. As the effects were observed with whole body constitutive activation it was not possible to determine whether the changes in the adipocytes were induced directly from cell autonomous AMPK activation or whether there was influence from the metabolic niche of the D316A mouse.

As the D316A mouse SMART cells may arise because of constitutively activating AMPK during differentiation, leading to changes in cell fate, it would be interesting to see whether pharmacological AMPK activation in differentiation alters the fate of adipose derived stem cells. There is contrasting evidence for the role of AMPK in embryonic and mesenchymal stem cell self-renewal, pluripotency and in lineage determination. Activation of AMPK in ES cells maintains levels of pluripotency markers to prevent cell differentiation. The mechanisms proposed range from β-catenin signalling (Alba, Martínez et al. 2020), MAPK signalling (Liu and Yamashita 2019), the maintenance of autophagy through phosphorylation of ULK1 (Gong, Gu et al. 2018) and through regulation of stem cell epigenetics (Shi, Wu et al. 2013). However, AMPK activation also blocks the reprograming of somatic cells to pluripotent stem cells (Vazquez-Martin, Vellon et al. 2012). It may be that AMPK pauses cells in their current state as energy intensive differentiation or reprogramming requiring protein and fatty acid synthesis are inhibited. There is also evidence that AMPK is essential for effective germ layer lineage specification, partly through its regulation of mTOR (Young, Kamireddy et al. 2016, Song, Xu et al. 2019).

In adult stem cells the interplay between mTOR and AMPK has been shown to be important in pancreatic β cell maturation, whereby mTOR is active in the immature phenotype and there is a switch to AMPK activation as the cell matures (Jaafar, Tran et al. 2019). AMPK activation can suppress adipocyte differentiation and the inhibition of mTOR regulated protein synthesis by AMPK has also been suggested as a potential mechanism (Chen, Brooks et al. 2017). In muscle stem cells it is suggested that AMPK is essential for terminal differentiation and that it prevents muscle stem cell self-renewal (Theret, Gsaier et al. 2017). AMPK is also thought to promote osteogenesis. Osteocytes and adipocytes both arise from

mesenchymal stem cells and whilst AMPK is classically inhibitory towards adipogenesis, it has been found to be activated in the early stages of osteogenesis to promote the differentiation of osteocytes from precursor cell lines and bone marrow derived stem cells (Kanazawa, Yamaguchi et al. 2008, Jang, Kim et al. 2011, Pantovic, Krstic et al. 2013, Wang, Qu et al. 2016, Abdallah and Alzahrani 2021). Again, the timing of AMPK activation, mTOR activation and autophagy is important in osteogenesis (Pantovic, Krstic et al. 2013).

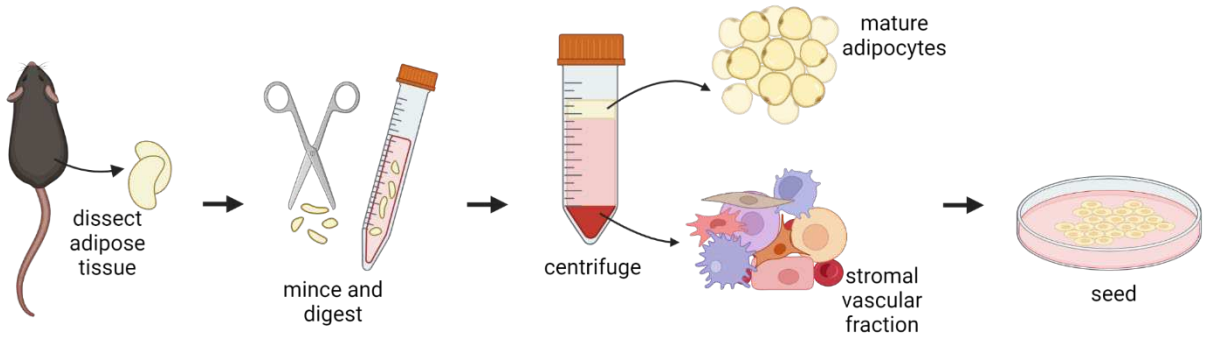


Figure 4.1 SVF isolation from iWAT

The iWAT was dissected from mice, minced and digested. Digested adipose tissue was centrifuged to separate the mature adipocytes, which were a floating fraction, and the pellet containing the heterogeneous SVF. The SVF was seeded into tissue culture dishes.

For the following experiments primary adipocytes were generated from the differentiation of the SVF and are called SVF adipocytes. Isolation of the SVF is depicted in Figure 4.1. The SVF was then put through adipogenic differentiation, depicted in Figure 4.2 to create primary SVF adipocytes. The adipogenic induction medium contained insulin, T_3, dexamethasone, IBMX and indomethacin. Dexamethasone is a synthetic glucocorticoid and IBMX increases intracellular cAMP which stimulates CREB to induce adipogenic gene expression (Lee et al., 2019; Reusch Jane et al., 2000). Indomethacin is a prostaglandin synthesis inhibitor that enhances adipogenesis although its mechanism of action is unclear (Styner et al., 2010). T_3 also displays adipogenic activity (Darimont et al., 1993). Insulin alone can stimulate adipogenesis (Merrick et al., 2019). It can increase CREB mediated expression of adipogenic genes, as well as indirectly increasing PPARγ activity which has been proposed to occur through several mechanisms that may involve phosphoinositide 3-kinase-AKT and mTOR signalling (Kim and Chen, 2004; Klemm et al., 2001; Miki et al., 2001; Zhang et al., 2009). After 2 days in induction medium cells were placed into maintenance medium

containing insulin and T_3. Between day 2 and 3 the first signs of adipogenesis were evident, with very small lipid droplets visibly forming from the ER around the nucleus. These lipid droplets grew as the adipocyte matured, and by day 8 mature adipocytes were present. Adipogenic differentiation of the SVF was never 100% efficient, and the adipocytes were always be surrounded by undifferentiated, fibroblast like cells.

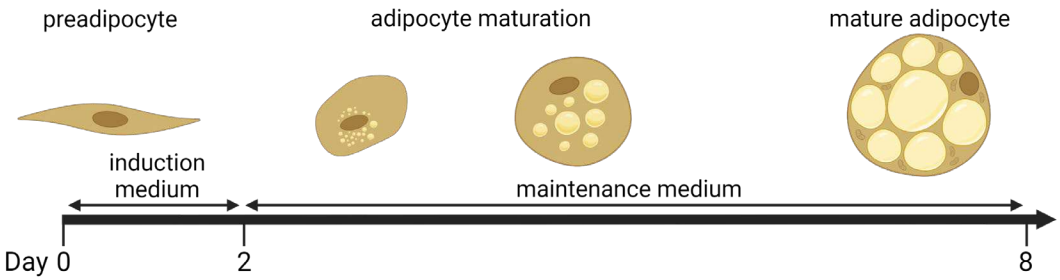


Figure 4.2 Timeline of adipogenic differentiation from the SVF with an AMPK activator
Adipogenesis was induced in the SVF with an adipogenic induction cocktail for 2 days, after which an adipogenic maintenance medium was used. The first immature adipocytes were visible by day 3, with mature adipocytes present from day 8 onwards.

Studying the pharmacological activation of AMPK in adipocyte differentiation will give more insight into its role in stem cell fate determination and whether SMART cells can be generated. It will also be interesting to see whether AMPK is potential therapeutic target in adipose tissue in the context of obesity.

4.2 PHARMACOLOGICAL ACTIVATION OF AMPK IN ADIPOGENESIS

4.2.1 991 and BI-9774 in adipogenesis

To explore the effects of AMPK activation in adipogenesis, small molecule pharmacological activators of AMPK were present throughout adipogenic differentiation of the SVF. Throughout these studies, the adipogenic index is used as an output of adipogenesis. Measurement of the adipogenic index is based on previously published methods (Merrick et al., 2019). Compared to other cell types, adipocytes contain large lipid droplets with more intense lipid neutral dye staining (Figure 4.3). To calculate the adipogenic index, whole well scans of fluorescently stained lipid droplets and nuclei were split into separate GFP and DAPI channels for individual analysis in Fiji. The Find Edges function in Fiji was used to remove any background and then a Gaussian blur was applied to fill any holes created by

the Find Edges function (Figure 4.3B). Images were converted to 8-bit to allow for a threshold to be set and then mean intensity of the whole well scan was quantified as a measurement of adipocytes. For the DAPI channel the Find Edges function was applied, images were converted to 8-bit and a threshold was applied (Figure 4.3C). The Watershed function was applied to split nuclei that may be joined together and then particles were analysed to count the number of individual nuclei. Then, the lipid droplet intensity data was divided by the number of nuclei to give the adipogenic index. For each mouse a minimum of 2 wells were used to account for any well-to-well variation, and in bar plots generated there was a data point for each well, with biological replicates distinguished by different shaped symbols. The adipogenic index gives a quick and high throughput way to measure adipogenesis.

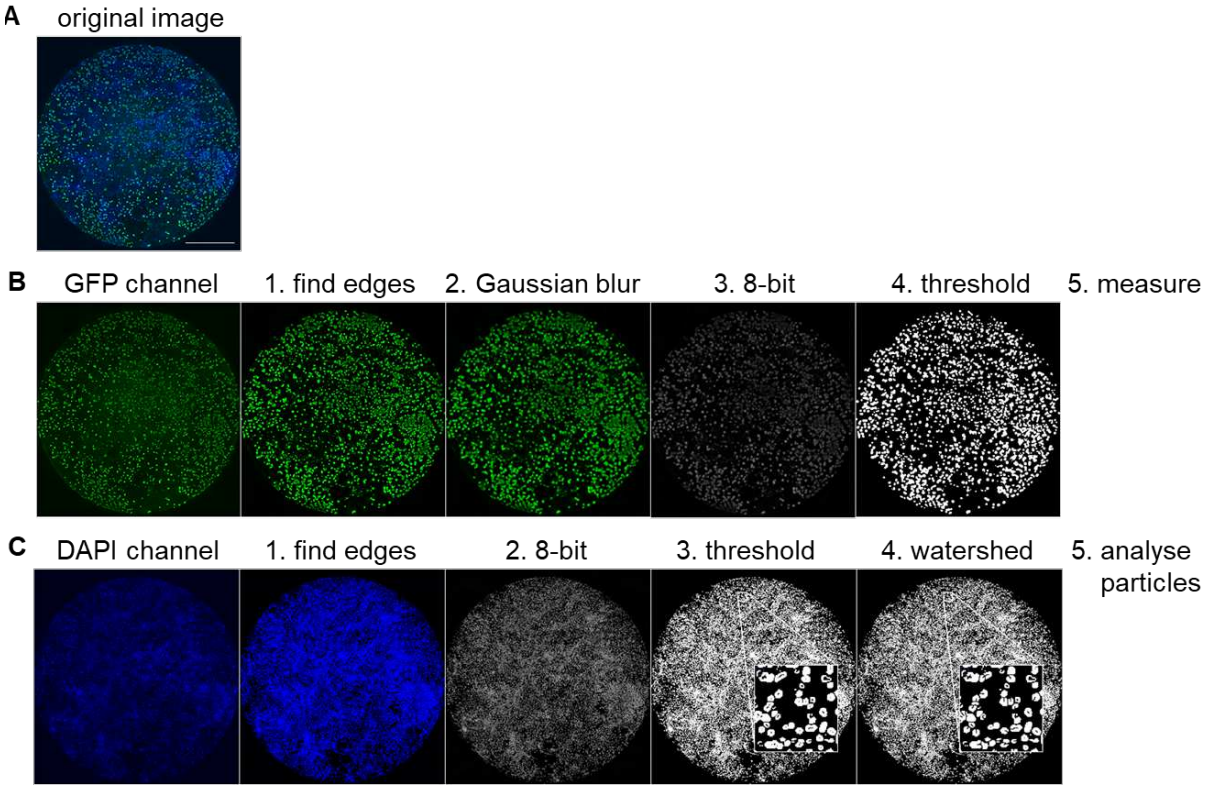


Figure 4.3 Method for quantifying nuclei counts and lipid staining from whole well scans in ImageJ

10x magnification whole well scans are captured after DAPI and LipidTox lipid droplet staining. (A) Representative original image. (B) Quantification of lipid staining in the GFP channel. (C) Counting nuclei in the DAPI channel. Scale bar represents 1500μm.

Two ADaM site binding activators of AMPK were assessed, 991, a potent activator of AMPK was used as well as BI-9774, a newer activator (Grempler et al., 2018; Xiao et al., 2013). Each compound was titrated throughout adipogenesis and the adipogenic index was calculated. The titration of BI-9774 showed a dose dependent reduction in lipid droplet staining (Figure 4.4A, B), nuclei counts (Figure 4.4C) and adipogenic index (Figure 4.4D), with a reduction in all parameters present at 1.25μM, the lowest concentration of BI-9774 used. 991 appeared to be less potent, with a minimum concentration of 2.5μM required to see a significant reduction in lipid droplet staining (Figure 4.5A, B), nuclei counts (Figure 4.5C) and the highest concentration tested of 10μM was needed to see a significant reduction in adipogenic index (Figure 4.5D). It was encouraging to see that two separate compounds gave the same effects on adipogenesis and nuclei counts, albeit at different potencies.

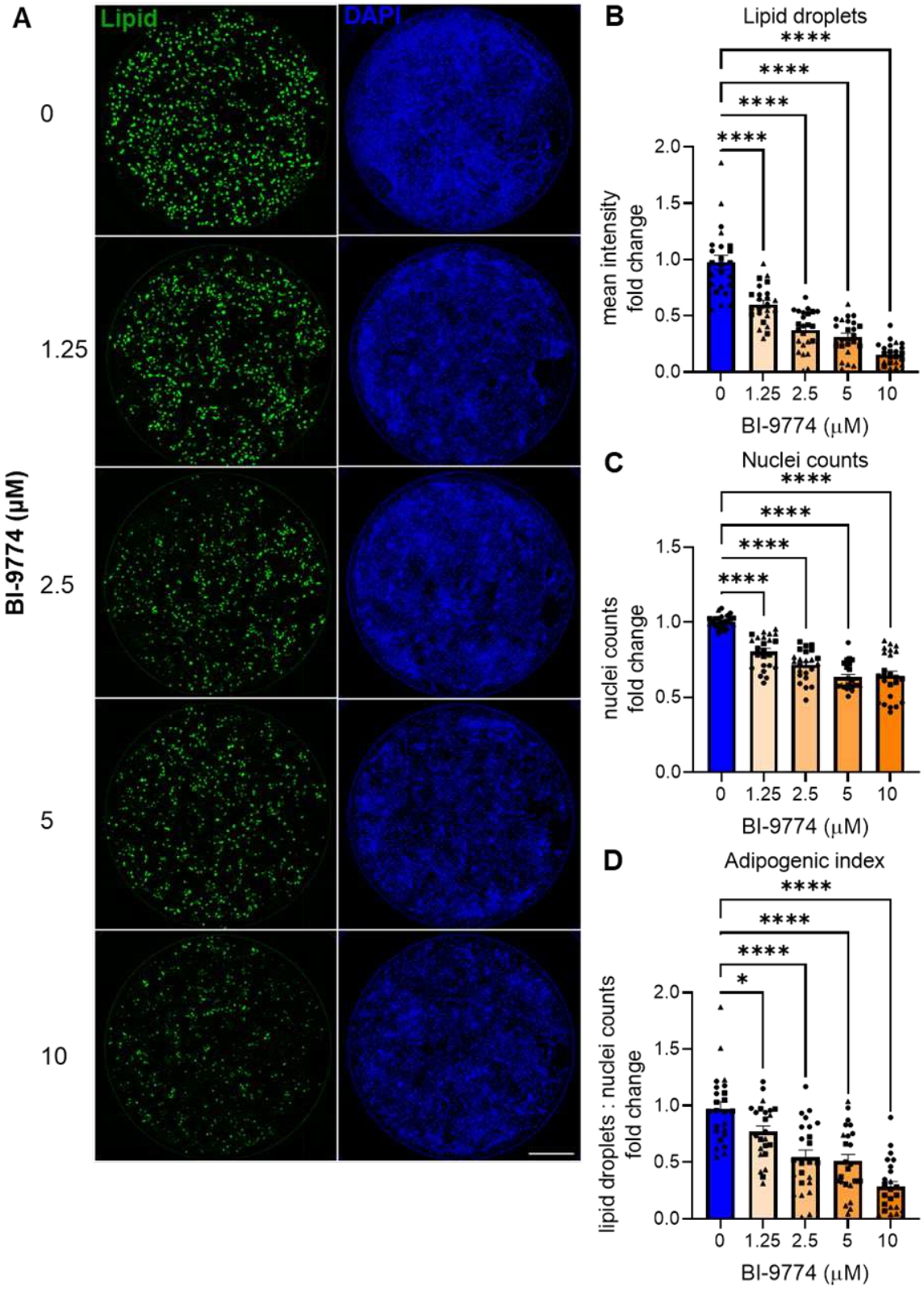


Figure 4.4 Titration of BI-9774 in SVF adipogenesis.

*BI-9774 was added from 1.25 to 10μM in adipogenesis. (A) Representative images of whole well scans with lipid droplet and DAPI staining. Quantification of (B) lipid droplet staining (C) nuclei counts and (D) adipogenic index. Data are shown as mean ± SEM, with biological replicates represented by different shaped symbols. Statistical significance is determined by one-way ANOVA with Dunnett's correction for multiple comparisons, *p<0.05, ****p<0.0001 (n=3 mice, each represented by a different shaped symbol, SVF isolated on the same day, 8 technical replicates per mouse). Scale bar represents 1500μm.*

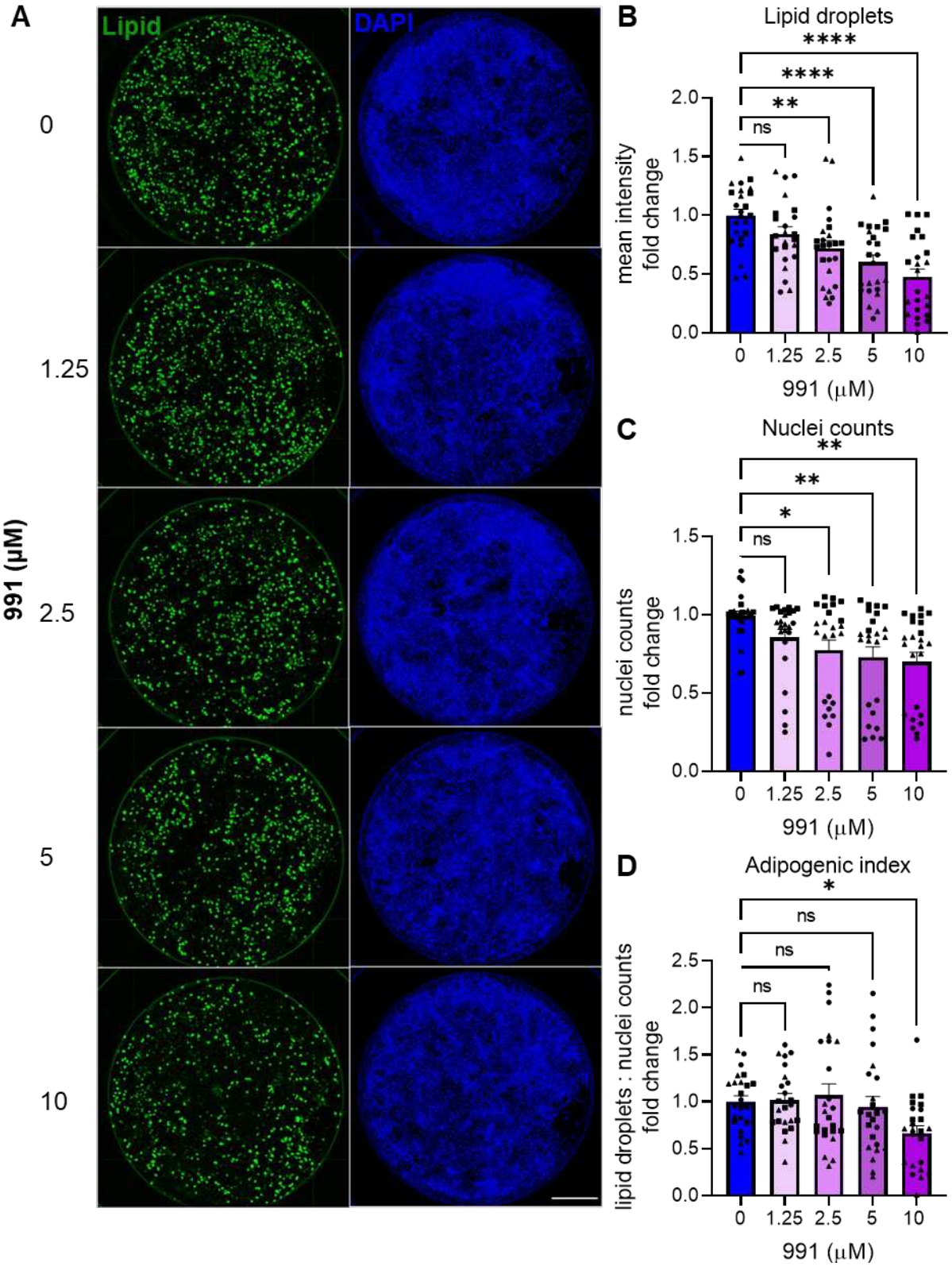


Figure 4.5 Titration of 991 in SVF adipogenesis.

*991 was added from 1.25 to 10μM in adipogenesis. (A) Representative images of whole well scans with lipid droplet and DAPI staining. Quantification of (B) lipid droplet staining (C) nuclei counts and (D) adipogenic index. Data are shown as mean ± SEM, with biological replicates represented by different shaped symbols. Statistical significance is determined by one-way ANOVA with Dunnett's correction for multiple comparisons, *p<0.05, **p<0.01, ****p<0.0001 (n=3 mice, each represented by a different shaped symbol, SVF isolated on the same day, 8 technical replicates per mouse). Scale bar represents 1500μm.*

To assess the level of AMPK activation attained with 991 and BI-9774, phosphorylation of AMPKα, as well as its downstream targets ACC and ULK1 were measured at the end of differentiation. In this data set there was much variation between the biological replicates and so each one is represented by different shaped symbols. BI-9774 increased the phosphorylation of ACC, ULK1 and AMPKα (Figure 4.6). However, only p-AMPKα reaches statistical significance at 5 and 10μM in this instance (Figure 4.6D). It appears as though the levels of AMPKα are decreasing in the Western blot, as the concentration of BI-9774 is increasing, which may explain why p-AMPKα only increases significantly at the higher concentrations. It could be that in this instance, chronic activation of AMPK throughout adipogenesis lead to a compensatory reduction in AMPKα expression. Levels of ACC decrease in the Western blot as the concentration of BI-9774 increases. This is likely because fatty acid synthesis is an important process which is upregulated in adipocytes, so if there is a decrease in the amount of adipocytes there will be a decrease in the level of ACC. Meanwhile, AMPK can phosphorylate and inhibit a greater proportion of ACC leading to even less fatty acid synthesis. With 991 there was an increase in p-ACC with all concentrations, although none of the increases were significant (Figure 4.7A, B). There was an increase in p-ULK1 for all concentrations except 2.5μM. However, again none are significant (Figure 4.7A, C). Then there was only an increase in p-AMPKα with 10μM which is significant (Figure 4.7A, D). Again, like with BI-9774, 991 appears to reduce the levels of ACC and AMPKα. With both compounds there was a dose dependent decrease in total ACC, reflective of the reduction in adipogenesis (Figure 4.6A, Figure 4.7A). Altogether, the adipogenic index data and AMPK activation data show that BI-9774 is a more potent activator than 991, and so BI-9774 was used in most of the following experiments.

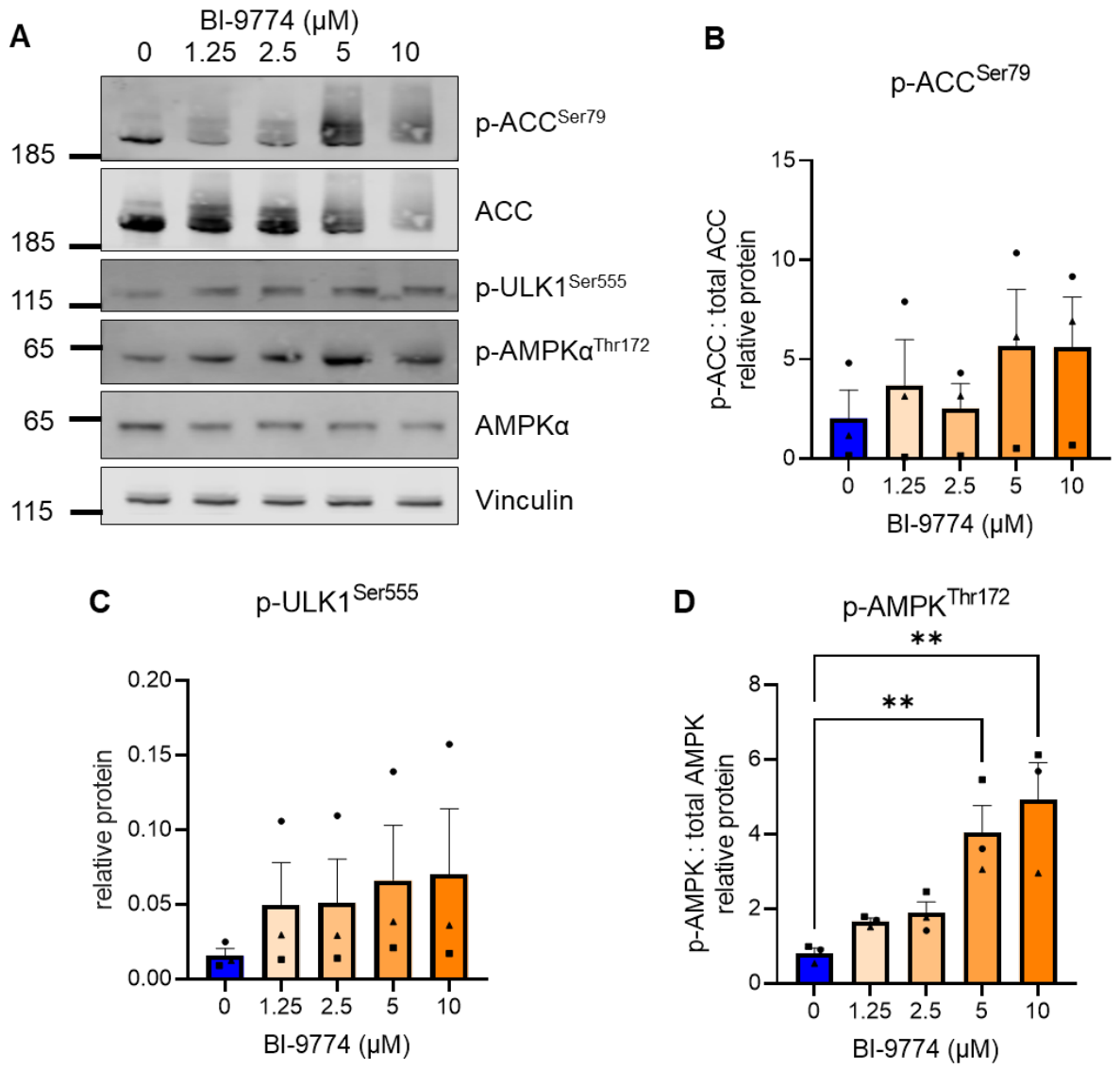


Figure 4.6 Characterisation of AMPK activation by BI-9774 in adipocytes

*SVF was differentiated to adipocytes with 1.25 to 10μM BI-9774 and activation of AMPK in the mature adipocytes was assessed. (A) Representative Western blot showing phosphorylation of AMPK targets. Quantification of (B) p-ACC relative to ACC, (C) p-ULK1 and (D) p-AMPK relative to AMPK, all normalised to vinculin. Data are shown as mean ± SEM, with biological replicates represented by different shaped symbols. Statistical significance is determined by one-way ANOVA with Dunnett's correction for multiple comparisons, **p<0.01 (n=3).*

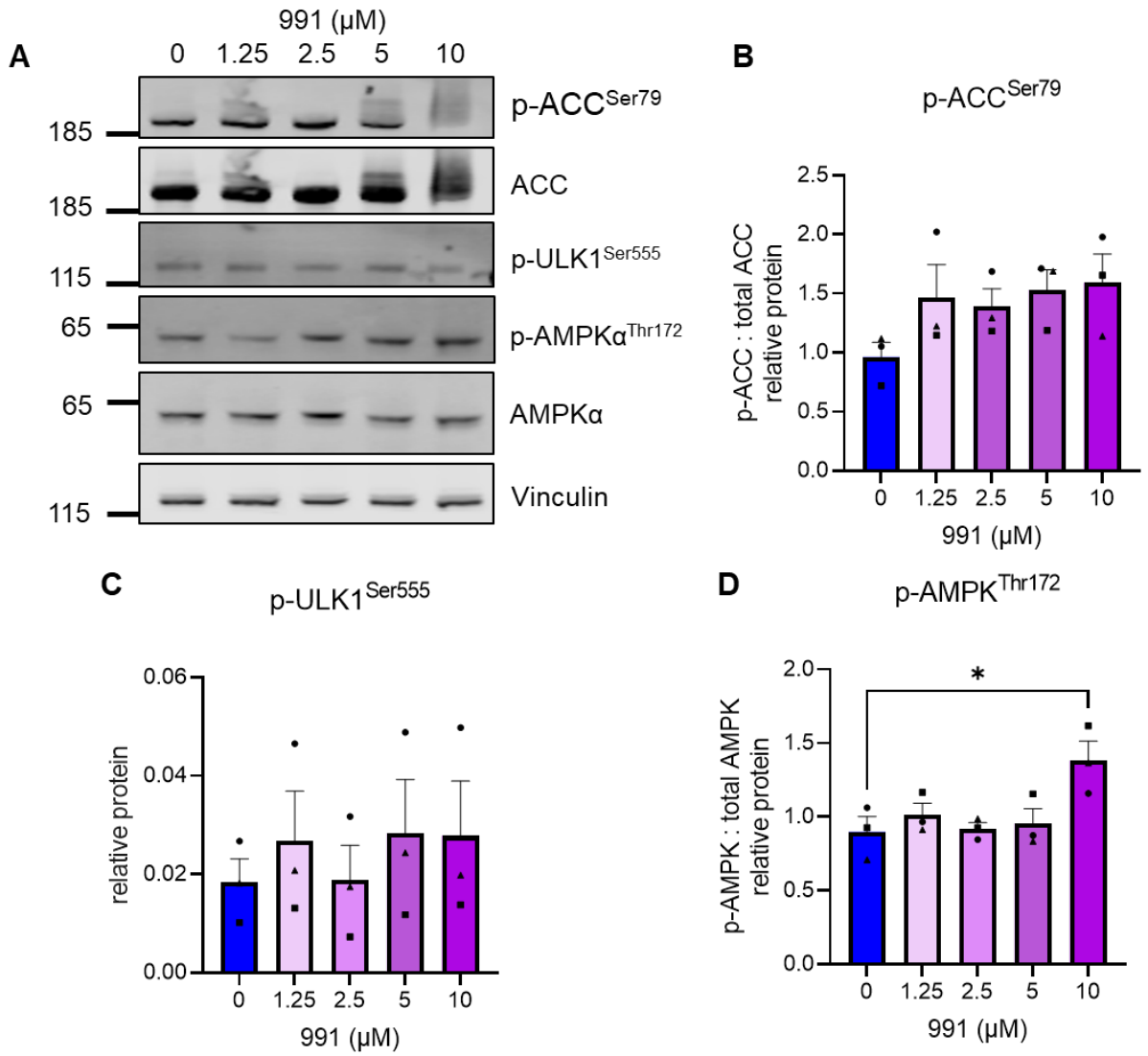


Figure 4.7 Characterisation of AMPK activation by 991 in adipocytes

*SVF was differentiated to adipocytes with 1.25 to 10μM 991 and activation of AMPK in the mature adipocytes was assessed. (A) Representative Western blot showing phosphorylation of AMPK targets. Quantification of (B) p-ACC relative to ACC, (C) p-ULK1 and (D) p-AMPK relative to AMPK, all normalised to vinculin. Data are shown as mean ± SEM, with biological replicates represented by different shaped symbols. Statistical significance is determined by one-way ANOVA with Dunnett's correction for multiple comparisons, *p<0.05 (n=3).*

The high variability in AMPK activation may be due to the variation in levels of adipogenesis between mice. To circumvent this, phosphorylation of ACC, ULK1 and AMPKα was

assessed in the undifferentiated SVF after 2 hours of treatment with BI-9774. This also gives the opportunity to look at the level of AMPK activation at the initiation of adipogenesis. In the SVF there was a significant increase in phosphorylation of ACC, ULK1 and AMPKα at 1.25 and 10μM BI-9774 (Figure 4.8). When looking at the effect on phosphorylation of downstream targets, both 1.25 and 10μM BI-9774 achieved similar levels of activation. Of note, ACC is undetectable by Western blotting in the SVF as its expression level is so low, but increases markedly during adipogenesis since fatty acid synthesis is important for adipocyte function (Figure 4.8A). This is why the levels of ACC are much higher when assessed at the end of adipogenesis (Figure 4.6A, Figure 4.7A). Because of this, levels of phosphorylated ACC are assessed relative to vinculin instead of total ACC (Figure 4.8B).

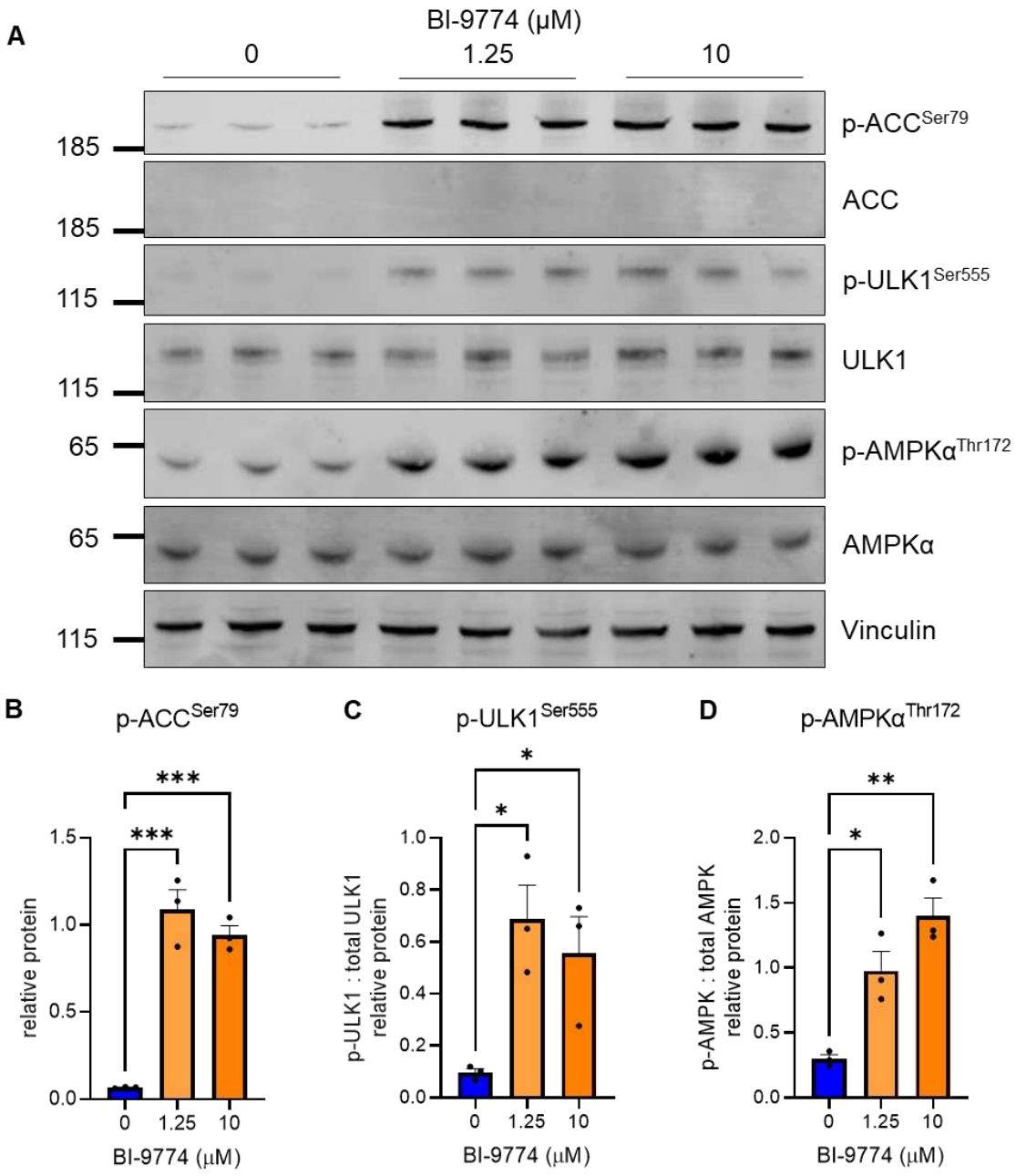


Figure 4.8 Characterisation of AMPK activation by BI-9774 in the undifferentiated SVF *Undifferentiated SVF was treated with BI-9774 for 2 hours. (A) Western blot showing phosphorylation of AMPK targets. Quantification of (B) p-ACC, (C) p-ULK1 relative to ULK1 and (D) p-AMPK relative to AMPK, all normalised to vinculin. Data are shown as mean ± SEM, with biological replicates represented by different shaped symbols. Statistical significance is determined by one-way ANOVA with Dunnett's correction for multiple comparisons, *p<0.05, **p<0.01, ***p<0.001 (n=3).*

During adipogenesis, media was refreshed every 2 to 3 days. To test the presence of BI-9774 in the media after 2 days, conditioned induction media with DMSO or BI-9774 at 1.25 and 10μM was collected from differentiating SVF and used to treat undifferentiated SVF for 2 hours, with Western blotting for phosphorylation of AMPKα and downstream targets (Figure 4.9A). There were significant increases in p-ACC (Figure 4.9B) and p-ULK1 (Figure 4.9C) in cells given the conditioned media with BI-9774. Again, ACC expression is not visible by Western blotting in the SVF where it's expression is low, although levels of p-ACC are detectable. For p-AMPKα there were increases with both concentrations. However, they only reached significance with 10μM (Figure 4.9D). This confirms that BI-9774 was maintained at a concentration sufficient to activate AMPK differentiation. All of this data together shows that 1.25μM BI-9774 is sufficient to activate AMPK and to see an effect on adipogenesis.

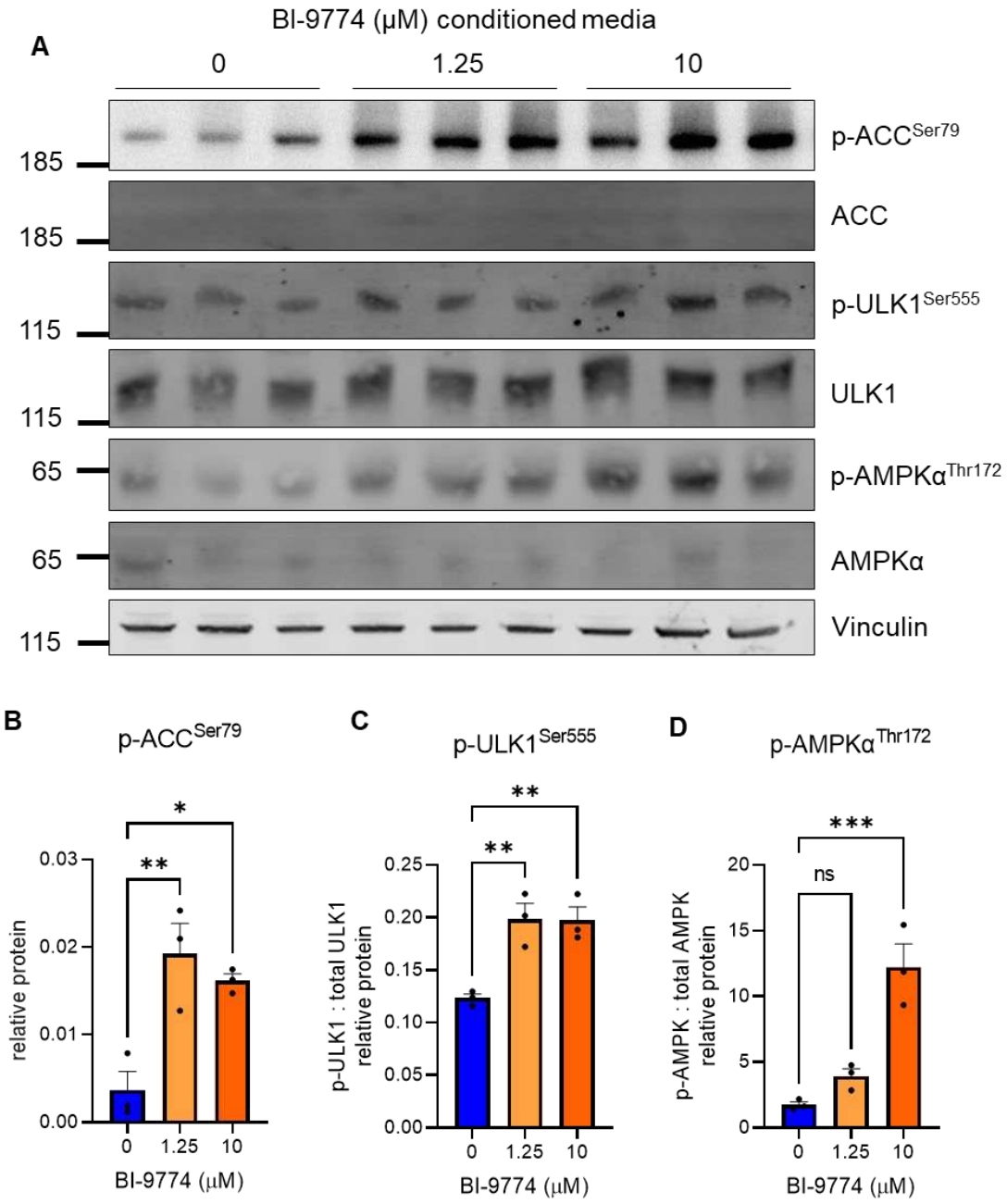


Figure 4.9 Assessing the presence of BI-9774 in media after 2 days

Adipocytes were cultured with BI-9774 in the media for 2 days and then the conditioned media was given to undifferentiated SVF for 2 hours to assess the presence of BI-9774 in the media. (A) Western blot showing phosphorylation of AMPK targets. Quantification of (B) p-ACC, (C) p-ULK1 relative to ULK1 and (D) p-AMPK relative to AMPK, all normalised to vinculin. Data are shown as mean ± SEM, statistical significance is determined by one-way

*ANOVA with Dunnett's correction for multiple comparisons, *p<0.05, **p<0.01, ***p<0.001 (n=3).*

4.2.2 AMPK activation in other models of adipogenesis

As AMPK activation reduces adipogenesis in the SVF, the effect of AMPK activation in the adipogenesis of E14 mouse ES cells, the SVF of high fat diet fed mice and of PDGFRα^{+} precursor cells were investigated. E14 cells have established adipogenic protocols (Cuaranta-Monroy et al., 2014; Dani et al., 1997). This is a more intricate and time consuming system compared to using primary SVF, illustrated in Figure 4.10. They were a model of interest as in the D316A mouse, AMPK is activated from embryogenesis (Pollard, 2017). E14 cells were dissociated and seeded as hanging drops which aggregated as embryoid bodies that have the potential to form any of the three developmental germ layers. After 2 days the embryoid bodies were collected and put into tissue culture dishes with retinoic acid to encourage them towards mesodermal differentiation. From days 7 to 16 the embryoid bodies were treated with insulin and T_3. During this time, the embryoid bodies were dissociated and seeded as a monolayer. Between days 16 to 21 there was a push for adipogenesis with an adipogenic cocktail similar to the SVF induction media used, and after day 21 adipocytes were present and cells were placed back into adipogenic maintenance media. For these experiments 991 was used instead of BI-9774, simply because at the time they were carried out 991 was the main AMPK activator in use.

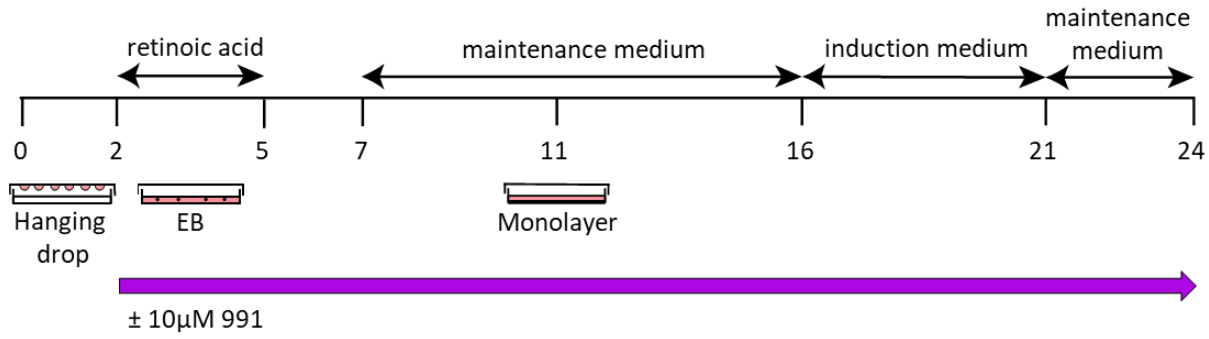


Figure 4.10 Timeline of adipogenesis of E14 cells with AMPK activation

Embryoid bodies (EB) are formed by the hanging drop method over 2 days, after which they are collected and grown in media with retinoic acid. After 5 days retinoic acid is removed. From day 7 to 16 cells are grown in ES cell adipogenic maintenance medium, during day 11 the EBs are dissociated and grown as a monolayer. ES cell adipogenic induction medium is

added between days 16 to 21, after which it is switched back to maintenance medium. To activate AMPK, 10μM 991 is used from day 2 onwards.

991 was added from day 2 of adipogenic differentiation and Western blotting showed an increase in phosphorylation of ACC, ULK1 and AMPKα (Figure 4.11A). p-ACC was close to significant (Figure 4.11B), p-ULK1 was significantly increased (Figure 4.11C) and although AMPKα showed an increase in phosphorylation, it was not significant (Figure 4.11D). As was seen with the SVF, there was high variation when AMPK activation was assessed at the end of differentiation. Overall, there was enough evidence to show that AMPK was active in this system.

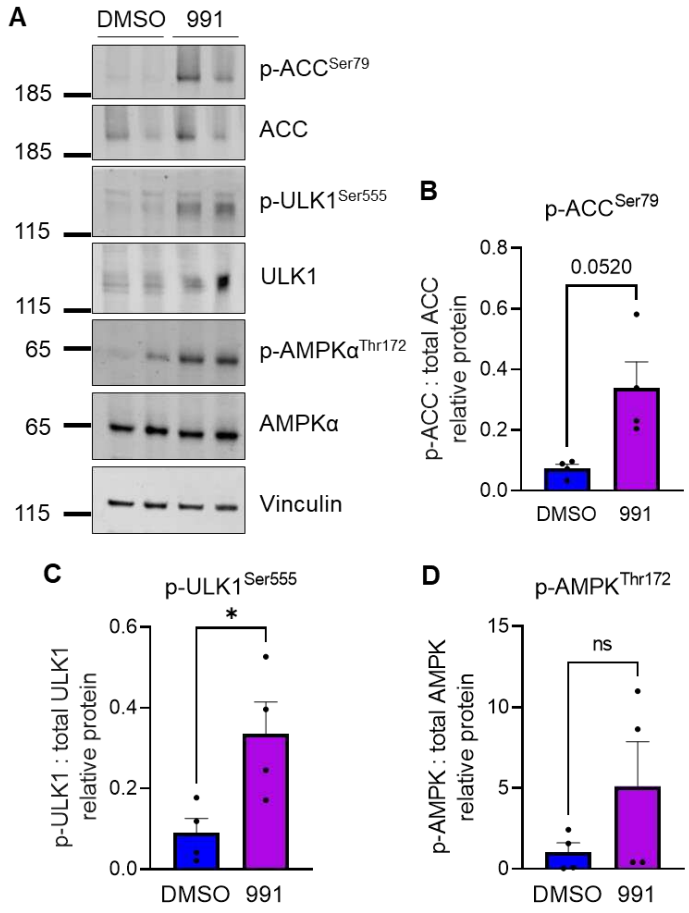


Figure 4.11 Characterisation of AMPK activation in E14 cells by 991 during adipogenesis

E14 cells were treated with 10μM 991 throughout adipogenic differentiation and its effect on AMPK was assessed at the end of differentiation. (A) A representative Western blot of the

*targets of AMPK activation. Quantification of (B) p-ACC relative to ACC, (C) p-Ulk1 relative to ULK1 and (D) p-AMPK relative to AMPK, all normalised to vinculin. Data are shown as mean ± SEM with statistical significance determined by Student's t-test with Welch's correction for (B) and (D), *p<0.05, (n=4).*

To assess adipogenesis, cells were grown on coverslips and then lipid droplets and nuclei were stained. Because of the length of the protocol the coverslips were densely populated with cells causing them to grow in 3D clumps in some areas of the coverslip, skewing the nuclear staining. Because of this, accurate quantification was not possible. Nevertheless, there was a visible reduction in lipid droplet staining when AMPK was activated during adipogenesis (Figure 4.12).

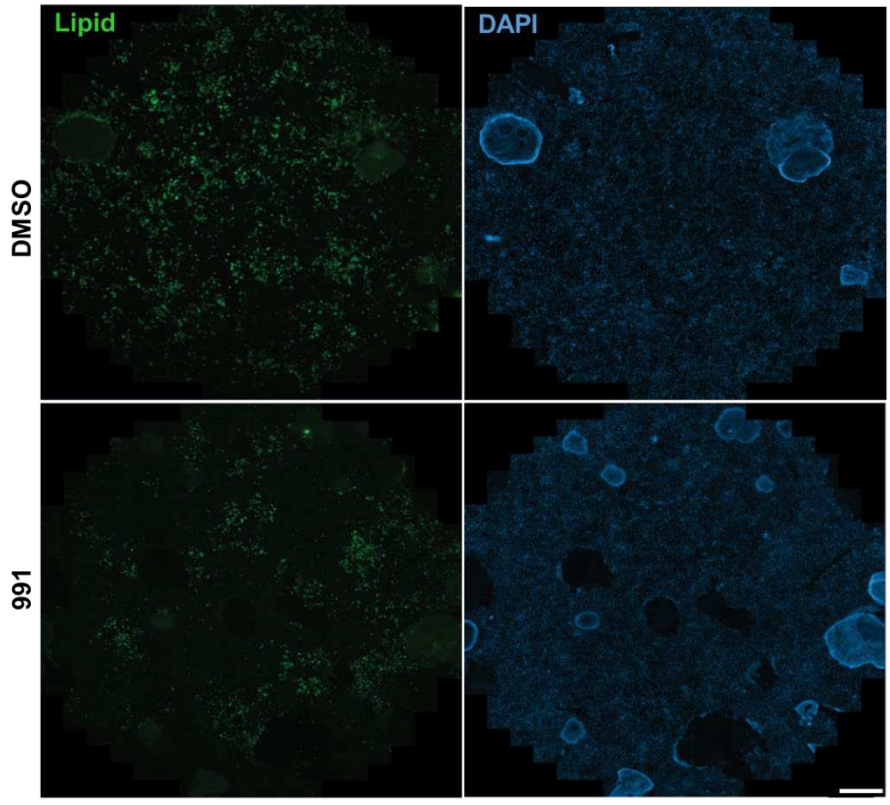


Figure 4.12 Lipid droplet staining to assess amount of adipocytes formed from E14 cells

Whole coverslip scans of E14 derived adipocytes differentiated with or without 991, stained for lipid droplets and nuclei. Scale bar represents 1000μm.

E14 cells were treated with 991 from day 2 of differentiation as shown previously, from day 16 when the adipogenic cocktail was added, and day 21 after commitment to adipogenesis (Figure 4.13A). The adipogenesis cocktail stimulated a large increase in the expression levels of the master regulators of adipogenesis *Pparγ* and *Cebpα* (Figure 4.13B, C). Addition of 991 from day 2 significantly suppresses the levels of *Pparγ* and *Cebpα* by day 16 before adipogenesis was induced, and further suppressed the increase seen after induction (Figure 4.13B, C, Table 4.1,

Table 4.2). Addition of 991 from day 16 led to an initial insignificant reduction of *Pparγ* and *Cebpα*, but the expression levels recovered by the end of adipogenesis. Assessment of mature markers *Adipoq* and *Fas* at the end of adipogenesis shows that there was only a significant decrease when 991 was added from the beginning of adipogenesis (Figure 4.13D, E). There was an increase in stem cell markers *Oct4* and *Nanog* at the end of differentiation when 991 was added from day 2 of adipogenesis, indicating that activation of AMPK maintains a more pluripotent state and reduces adipogenesis (Figure 4.14). There was no difference in the levels of sex determining region Y-box 2 (*Sox2*), although regulation of SOX2 in differentiation has been shown to be different to that of OCT4 and NANOG (Kallas et al., 2014). There was also a reduction in *Pref1*, a pre-adipocyte marker which must be downregulated for adipogenesis to progress. Given the higher levels of stem cell markers and lower levels of terminal adipocyte markers, preadipocyte markers and of master regulators of adipogenesis before adipogenic induction, AMPK activation likely prevents differentiation in E14 cells from an early stage (Hudak and Sul, 2013).

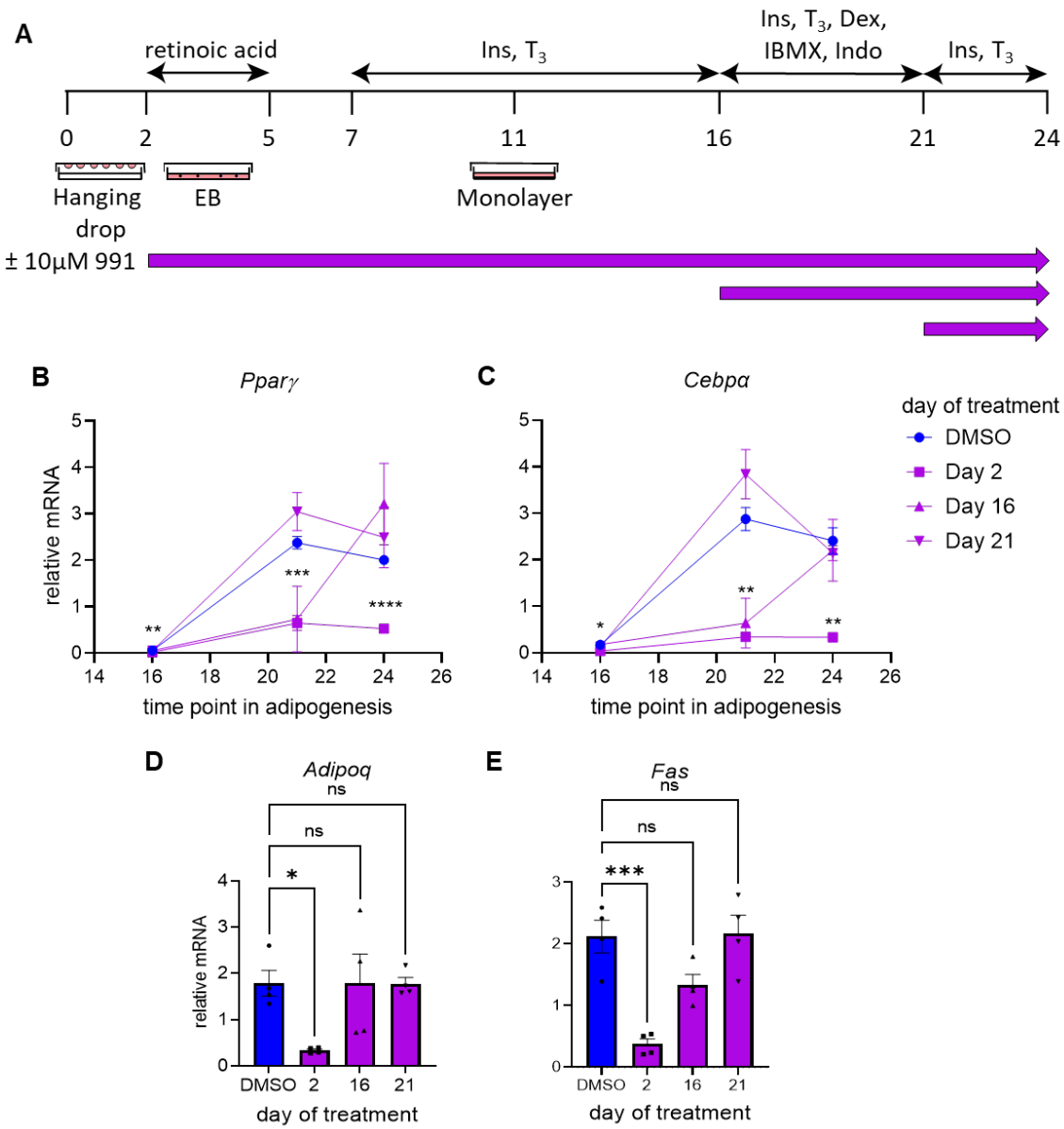


Figure 4.13 Effect of AMPK activation on E14 adipogenesis

Adipogenic differentiation of E14 cells with 991 present from days 2, 16 and 21 in adipogenesis onwards, compared to DMSO control. (A) Timeline of E14 adipogenesis with 991 added at different time points. Change in (B) Pparγ and (C) Cebpα levels throughout adipogenesis assessed at days 16, 21 and 24. Gene expression of (D) Adipoq and (E) Fas levels at the end of adipogenesis. mRNA levels relative to housekeeping gene Rpl13a. (A, B) Data are shown as mean ± SEM with statistical significance determined by two-way ANOVA with Dunnett's correction for multiple comparisons, stars are shown for day 2 vs

*DMSO with p-values shown in Table 4.1, 2. (C, D) Data are shown as mean ± SEM with statistical significance determined by one-way ANOVA with Dunnett's correction for multiple comparisons, *p<0.05, **p<0.01, ***p<0.001 ****p<0.0001 (n=3-4).*

Table 4.1 Pparγ expression through E14 adipogenesis

*Relative Pparγ mRNA levels during E14 adipogenesis when assessed on days 16, 21 and 24 with 991 added from days 2, 16 and 21 onwards. Statistical significance determined by two-way ANOVA with Dunnett's correction for multiple comparisons, **p<0.01, ***p<0.001, ****p<0.0001 (n=3-4).*

Time point	**DMSO Mean (±SD)**	**991 from day 2 Mean (±SD)**	**991 from day 16 Mean (±SD)**	**991 from day 21 Mean (±SD)**	**P-value for day 2 vs DMSO**	**P-value for day 16 vs DMSO**	**P-value for day 21 vs DMSO**
Day 16	0.056 (0.011)	0.02 (0.009)	0.054 (0.015)	0.057 (0.016)	0.0063**	0.9889	0.9992
Day 21	2.377 (0.267)	0.647 (0.329)	0.739 (1.220)	3.047 (0.821)	0.0006***	0.2630	0.3993
Day 24	2.006 (0.182)	0.528 (0.147)	3.212 (1.753)	2.459 (1.313)	<0.0001****	0.4866	0.8099

Table 4.2 Cebpα expression throughout E14 adipogenesis

*Relative Cebpα mRNA levels during E14 adipogenesis when assessed on days 16, 21 and 24 with 991 added from days 2, 16 and 21 onwards. Statistical significance determined by two-way ANOVA with Dunnett's correction for multiple comparisons, *p<0.05, **p<0.01 (n=3-4).*

Time point	DMSO Mean (±SD)	991 from day 2 Mean (±SD)	991 from day 16 Mean (±SD)	991 from day 21 Mean (±SD)	P-value for day 2 vs DMSO	P-value for day 16 vs DMSO	P-value for day 21 vs DMSO
Day 16	0.172 (0.051)	0.039 (0.012)	0.183 (0.027)	0.13 (0.033)	0.0247*	0.9602	0.4486
Day 21	2.876 (0.492)	0.343 (0.129)	0.639 (0.925)	3.838 (1.602)	0.0028**	0.0730	0.3495
Day 24	2.412 (0.564)	0.334 (0.129)	2.208 (1.325)	2.143 (0.325)	0.0087**	0.9826	0.7572

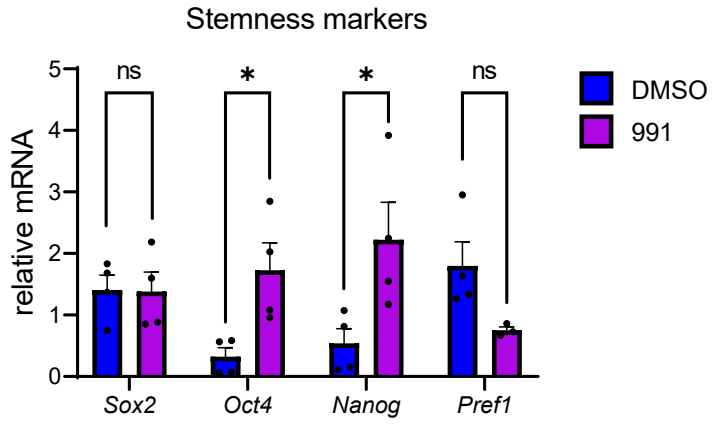


Figure 4.14 Effect of AMPK activation in E14 adipogenesis on stemness markers

*Gene expression of stemness markers were assessed at the end of E14 adipogenic differentiation with 991 added from day 2 presented as fold change to DMSO control treatment, relative to housekeeping gene Rpl13a. Data are shown as mean ± SEM with statistical significance determined by Student's t-test with Welch's correction for Pref1, *p<0.05 (n=3-4).*

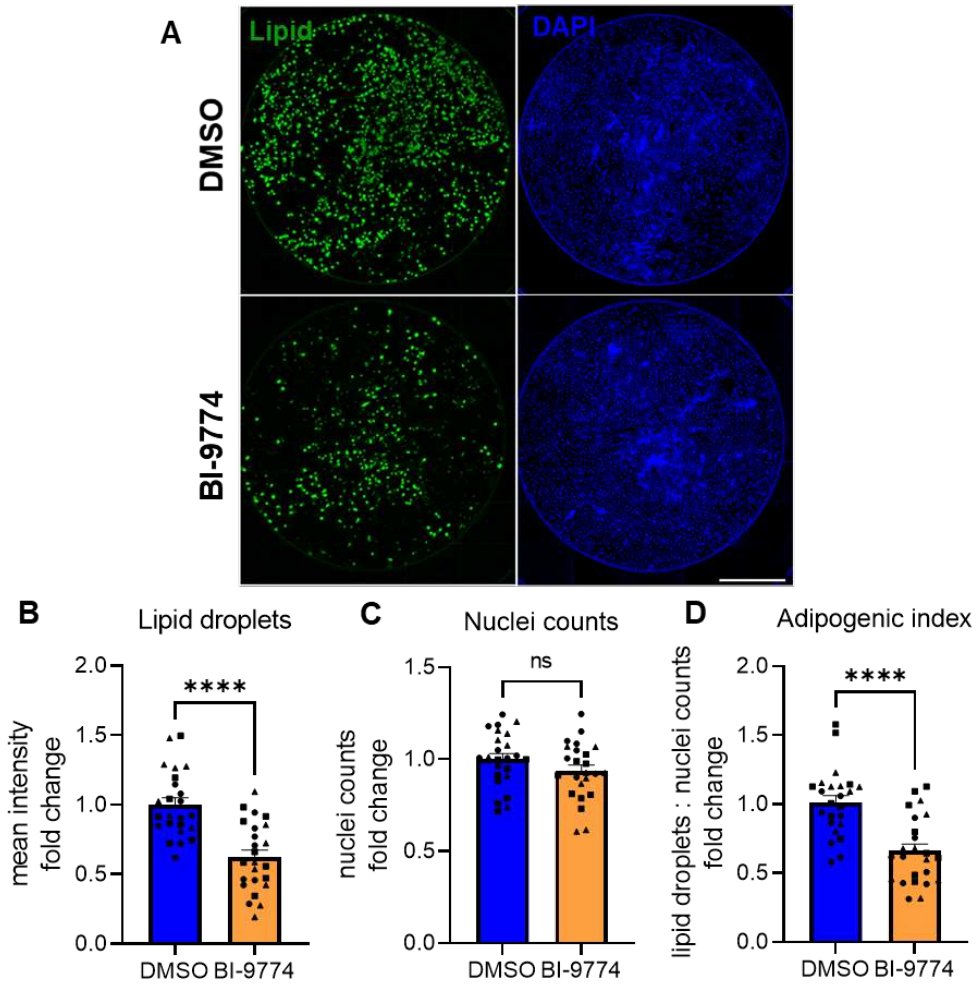


Figure 4.15 BI-9774 in adipogenesis of SVF adipocytes from high fat diet mice

*AMPK was activated with 1.25μM BI-9774 from the initiation of adipogenesis of high fat diet mouse SVF. (A) Representative images of whole well scans with lipid droplet and DAPI staining. Quantification of (B) lipid droplet staining (C) nuclei counts and (D) adipogenic index. Data are shown as mean ± SEM, with different biological replicates represented by different shaped symbols. Statistical significance is determined by Student's t-test, ****p<0.0001 (n=3 mice, each represented by a different shaped symbol, SVF isolated on the same day, 8 technical replicates per mouse). Scale bar represents 1500μm.*

The effect of AMPK activation by BI-9774 in the SVF adipogenesis of mice with diet induced obesity was assessed (Figure 4.15A). This was of interest due to the effects of the D316A

mouse in mice on a high fat diet. Quantification shows there was a significant reduction in lipid droplet staining and cell number, as well as an overall reduction in the adipogenic index in the SVF adipocytes of obese mice with BI-9774 (Figure 4.15B, C, D).

The final alternative model investigated was the PDGFRα^{+} progenitors isolated from the SVF. Isolating the PDGFRα^{+} cells from the SVF gives a purer progenitor population and may give higher efficiency of differentiation. It also removes any effects that may be coming from the non-adipocyte progenitor cells in the SVF. PDGFRα^{+} cells were FACS selected from the freshly isolated SVF, with CD31^{+} endothelial and CD45^{+} haematopoietic cells removed (Figure 4.16A). The PDGFRα and SVF populations were differentiated to adipocytes in the presence of DMSO or BI-9774. Although selecting the PDGFRα^{+} cells gave a purer progenitor population, it also reduced cell yield, and so only imaging based assays could be used. Here, x20 magnification images and Columbus software was used for quantification. Nuclei counts from x20 magnification images (Figure 4.16B) show there were fewer cells at the end of differentiation in the PDGFRα progenitor population (Figure 4.16C). This is likely because the purer population had fewer proliferative, non-adipocyte cell types in it than the SVF. There was a greater proportion of PPARγ expressing cells in the PDGFRα population. However, this increase wasn't significant (Figure 4.16D). There were fewer lipid droplets in the PDGFRα derived adipocytes compared to the SVF derived adipocytes (Figure 4.16E, F), likely a reflection of the lower total cell number (Figure 4.16G). However, there was no great difference in the adipogenic index between PDGFRα and SVF adipocytes (Figure 4.16H). Whilst there was a small reduction in the lipid droplets with BI-9774 treatment in the PDGFRα population after differentiation, the difference was not significant, and because the changes were subtle there was a negligible difference in the adipogenic index (Figure 4.16E, F, H). The small increases in differentiation efficiency that come with using a purified PDGFRα population are outweighed by the low yield of these cells.

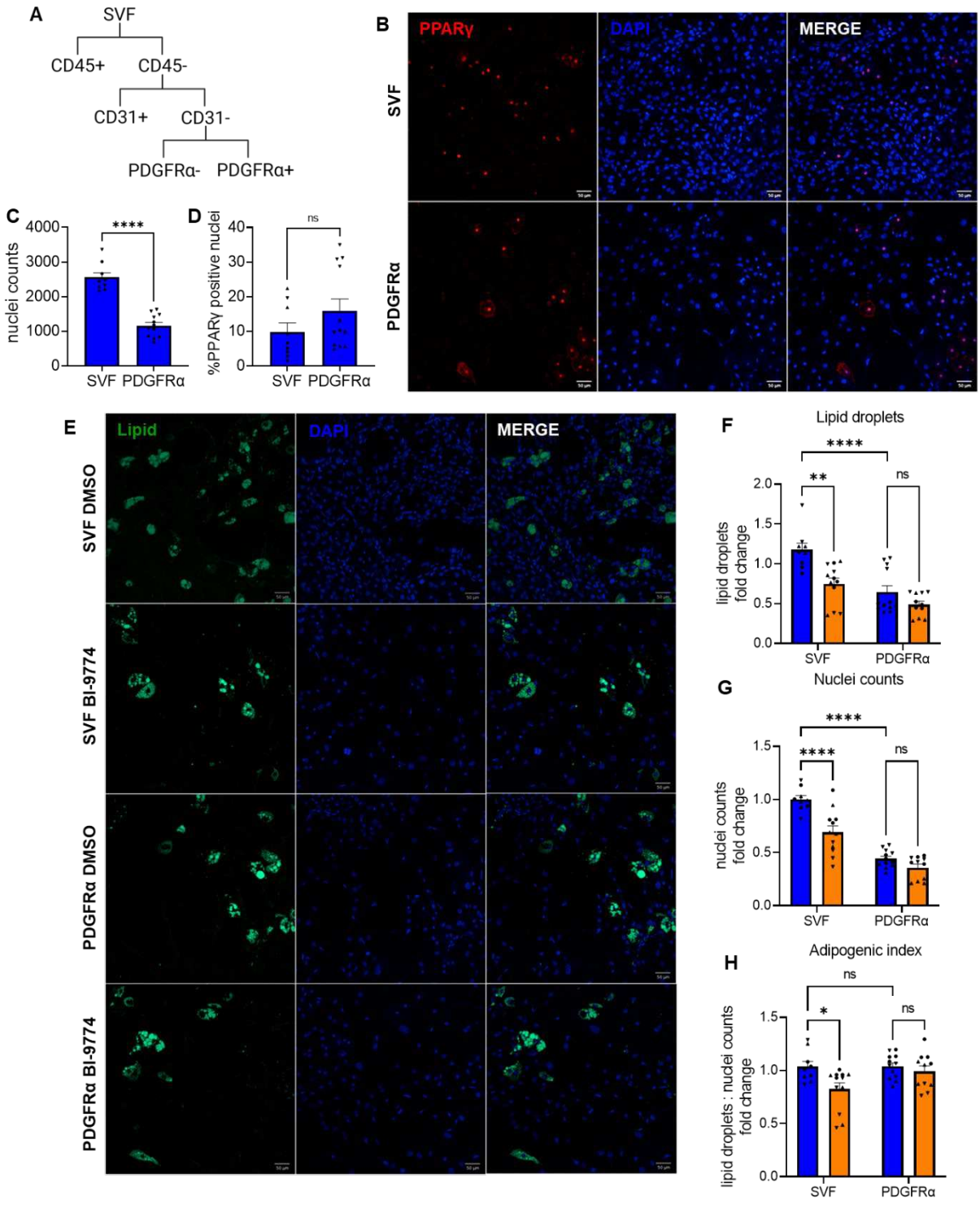


Figure 4.16 BI-9774 in adipogenesis of PDGFRα selected progenitors

PDGFRα selected progenitors were differentiated with DMSO or 1.25μM BI-9774 alongside the SVF population they were selected from. (A) FACS strategy to obtain PDGFRα

*progenitors from the SVF. (B) Representative images of PPARγ and nuclei staining in SVF and PDGFRα populations. (C) Nuclei counts from images. (D) Percentage of nuclei expressing PPARγ. (E) Representative images of lipid droplet and DAPI staining. Quantification of (F) lipid droplet staining (G) nuclei counts and (H) adipogenic index with BI-9774 treatment. Data are shown as mean ± SEM, with different biological replicates represented by different shaped symbols. Statistical significance is determined by (C, D) Student's t-test or (F, G, H) two-way ANOVA with Šidák's correction for multiple comparisons, *p<0.05, **p<0.01, ****p<0.0001 (n=3 mice, each represented by a different shaped symbol, SVF isolated on the same day, 4 technical replicates per mouse). Scale bar represents 50μm.*

E14 cells provide an interesting model to assess AMPK activation on cell pluripotency and stemness. However, it is a laborious model for adipogenesis with much heterogeneity. As PDGFRα selection greatly reduced cell yield, and there appears to be no great difference in efficiency of differentiation, the whole SVF is the best model for generating primary adipocytes to look at the effects of AMPK activation on adipogenesis.

4.2.3 Comparison of pharmacological and genetic activation of AMPK in adipocytes

The β-actin Cre D316A mouse has AMPK activated from embryonic day 1, and so may have a different effect in the SVF adipocytes than pharmacological activation. The levels of AMPK activation were compared between the D316A SVF adipocytes and WT SVF adipocytes that have had AMPK activated by 1.25μM BI-9774 (referred to as BI-9774 SVF adipocytes). Both genetic and pharmacological activation gave similar levels of kinase activity (Figure 4.17). Western blotting was used to assess levels of phosphorylation of AMPKα and of downstream targets (Figure 4.18A). Although the D316A SVF adipocytes showed small but non-significant increases in p-ACC, p-ULK1 and p-AMPKα, they were much lower than the increases in phosphorylation observed with 1.25μM BI-9774, which were all significant (Figure 4.18B, C, D). Therefore, 1.25μM BI-9774 leads to more potent activation of AMPK in SVF adipocytes than in the genetic D316A model, possibly because of the difference in mechanism of activation.

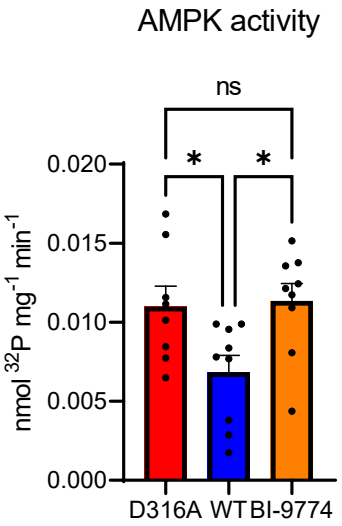


Figure 4.17 Comparison of AMPK activation from the D316A mutation and with BI-9774 by SAMS assay

*SVF obtained from D316A mice or WT mice were differentiated to adipocytes. For the WT mice these were differentiated with or without 1.25μM BI-9774. AMPK activity was assessed by SAMS assay at the end of differentiation. Data are shown as mean ± SEM with statistical significance determined by One-way ANOVA with Tukey's correction for multiple comparisons, *p<0.05, (D316A n=8, WT, BI-9774 n=9).*

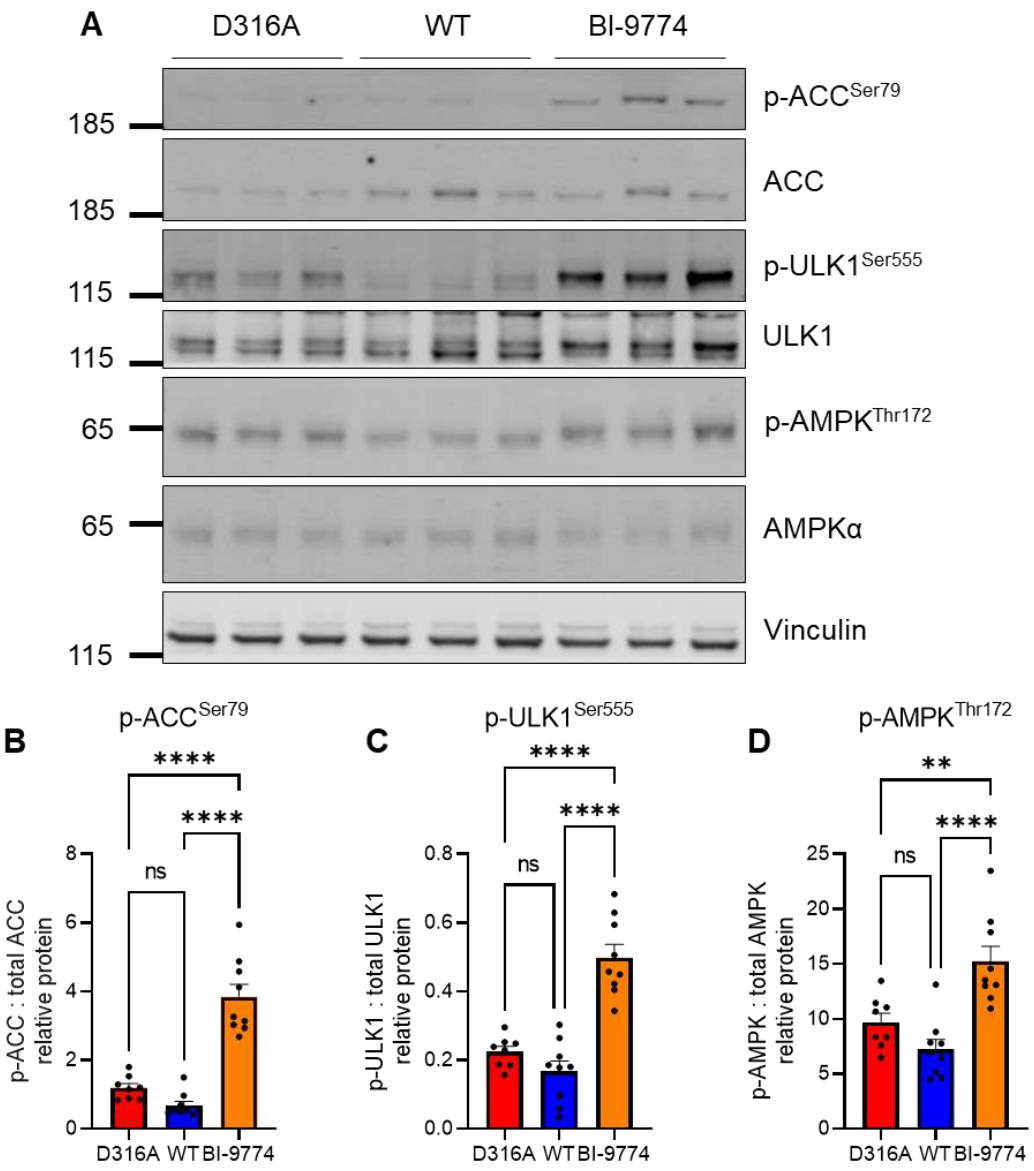


Figure 4.18 Comparison of AMPK activation from the D316A mutation and with BI-9774 by Western blotting

*SVF obtained from D316A mice or WT mice were differentiated to adipocytes. For the WT mice these were differentiated with or without BI-9774. AMPK activity was assessed at the end of differentiation. (A) Representative Western blot showing phosphorylation of AMPK targets. Quantification of (B) p-ACC relative to ACC, (C) p-ULK1 relative to ULK1 and (D) p-AMPK relative to AMPK, all normalised to vinculin. Data are shown as mean ± SEM with statistical significance determined by One-way ANOVA with Tukey's correction for multiple comparisons **p<0.01, ****p<0.0001 (D316A n=8, WT n=9).*

4.2.4 Transcriptomic differences with pharmacological and genetic activation of AMPK in adipocytes

The D316A mouse showed transcriptomic changes in adipose tissue (Pollard et al., 2019). Whilst genetic activation of AMPK reduces lipid droplet formation, it is unclear what the other effects of AMPK activation are in the population. In order to gain further understanding of AMPK activation in adipogenesis, as well as to see whether the D316A mutation has a similar effect in the SVF derived adipocytes as it does in the tissue, RNA sequencing was carried out on D316A SVF adipocytes, WT SVF adipocytes and BI-9774 SVF adipocytes. As is depicted in Figure 4.19, the iWAT SVF was isolated and plated for adipogenic differentiation from 5 D316A mice and 6 WT mice. The SVF from the WT mice were plated for differentiation with either 1.25μM BI-9774 or DMSO. At the end of adipogenesis, RNA was isolated for sequencing. Representative bright field images of the cells before RNA isolation showed a reduction in adipocytes (high contrast objects) with the addition of BI-9774 as is consistent with previous data, and also demonstrate the variation of the effect between biological replicated (Figure 4.20). There was no striking difference in adipogenesis between D316A and WT SVF.

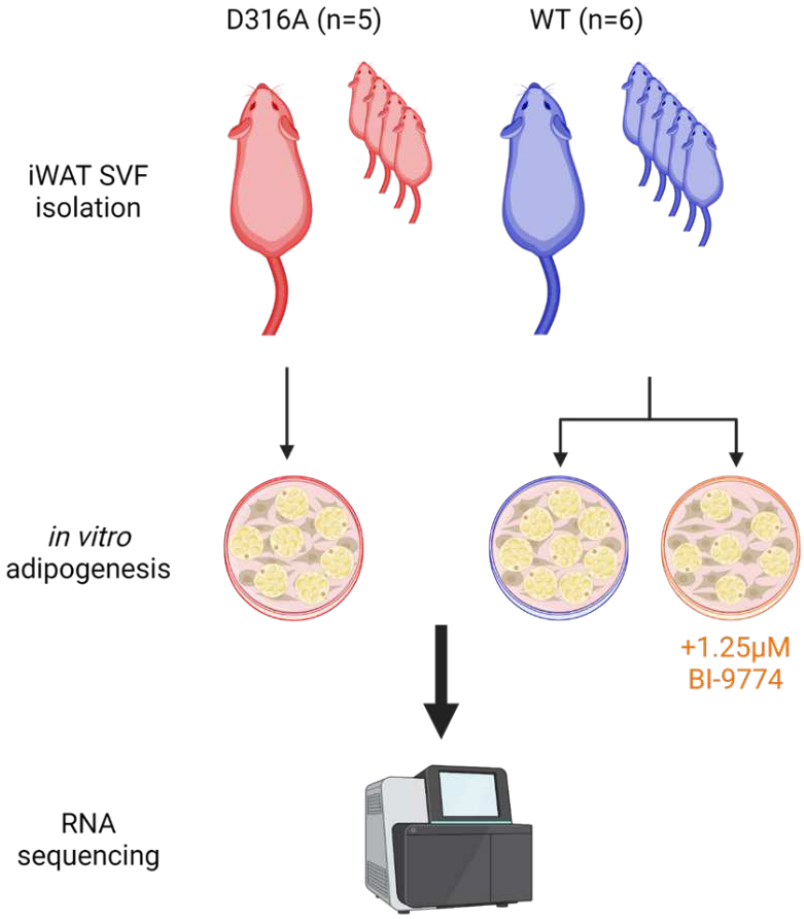


Figure 4.19 RNA sequencing experiment

The SVF was isolated from 5 D316A mice and 6 WT mice for adipogenic differentiation. The 6 WT mice were split into two groups for differentiation ± 1.25µM BI-9774. At the end of differentiation, RNA was isolated for RNA sequencing.

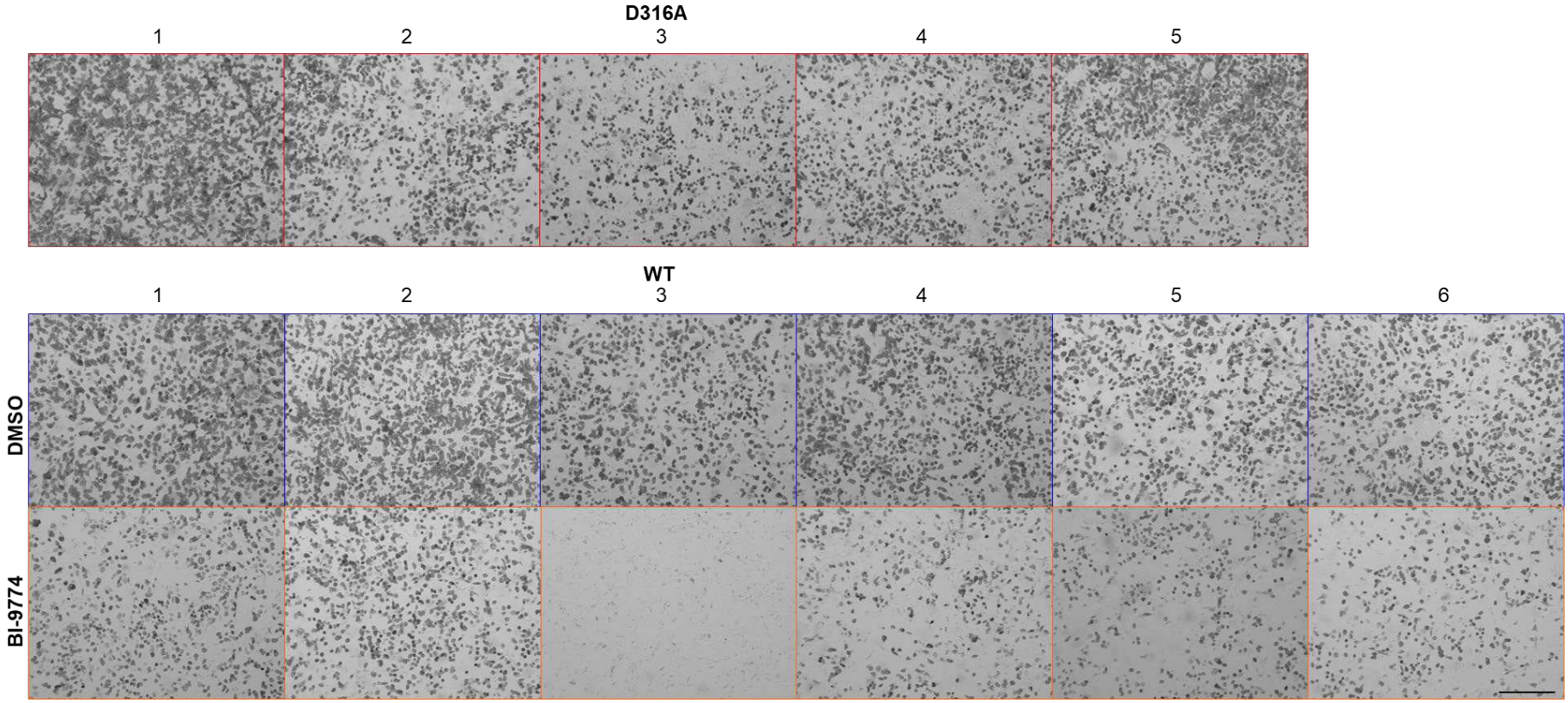


Figure 4.20 Cells for RNA sequencing experiment before RNA isolation

Representative bright field images of the cells for the RNA sequencing experiment showing levels of adipogenesis for each sample (numbered 1 to 6), with adipocytes being the darker contrast objects. Scale bar represents 275μm.

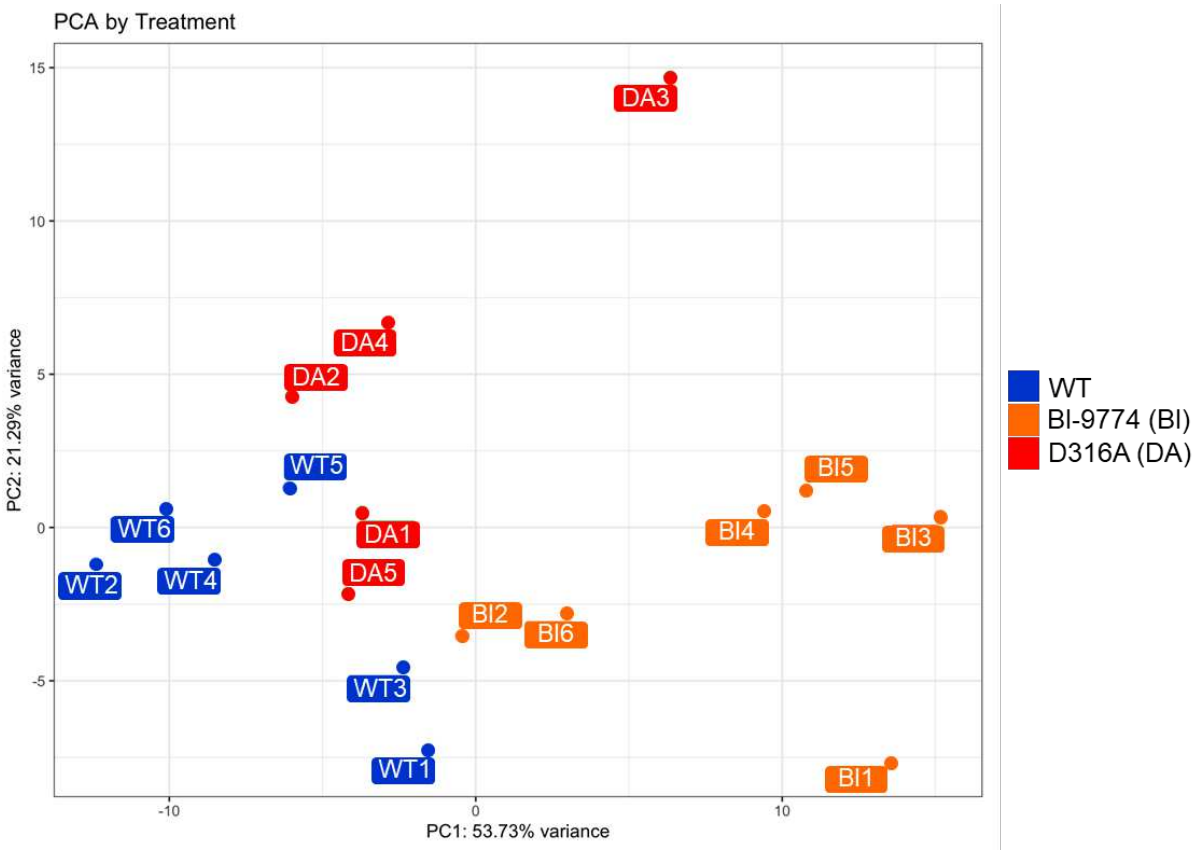


Figure 4.21 Sample clustering of D316A, WT and BI-9774 SVF adipocytes

Principle component analysis (PCA) plot showing sample clustering of RNA sequencing samples.

Principle component analysis plots showed more separation between WT SVF adipocytes and BI-9774 SVF adipocytes, with D316A SVF adipocytes mostly sitting in between these (Figure 4.21). These relationships were illustrated with the volcano plots of the differentially expressed genes. There were many more differentially expressed genes between the BI-9774 SVF adipocytes and the WT SFV adipocytes compared to the D316A SVF adipocytes versus the WT SVF adipocytes (Figure 4.22A, B). The D316A versus WT SVF adipocyte volcano plot demonstrated the closeness of the populations, as there were very few significantly differentially expressed genes. Like with the WT SVF adipocytes, there were many more significantly differentially expressed genes between the D316A versus BI-9774 SVF adipocytes (Figure 4.22C). Whilst the WT and D316A SVF adipocytes had more similar gene expression, GSEA using the Hallmark gene set showed similar enrichment patterns between BI-9774 v WT SVF adipocytes and D316A v WT SVF adipocytes, indicating that AMPK genetic and pharmacological activation has a similar effect in adipocytes, albeit a weaker effect in the genetic model (Figure 4.23).

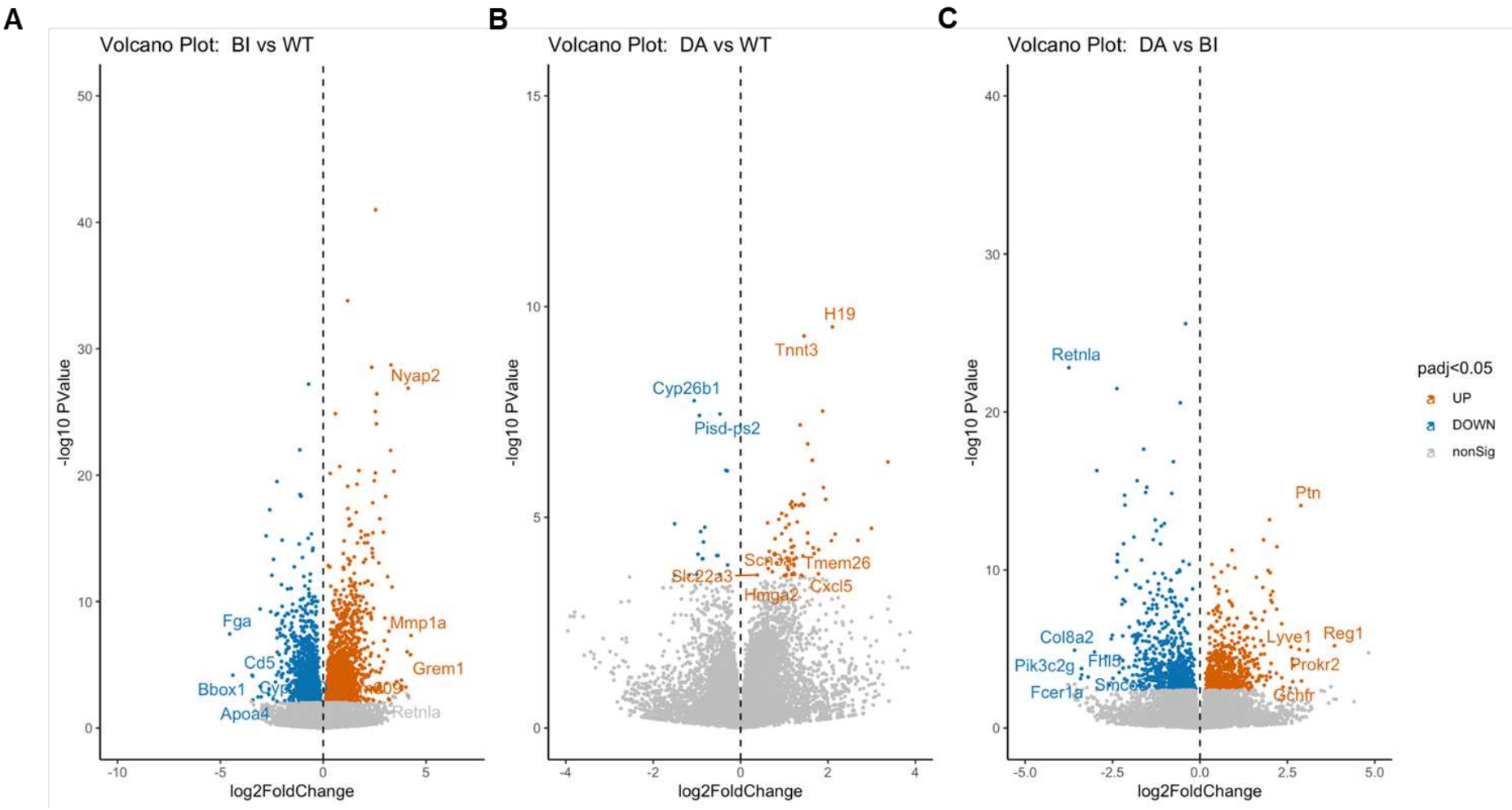


Figure 4.22 Volcano plots of differentially expressed genes

From the RNA sequencing data, volcano plots showing the differentially expressed genes between (A) BI-9774 v WT, (B) D316A v WT and (C) D316A v BI-9774. (BI, BI-9774; DA, D316A).

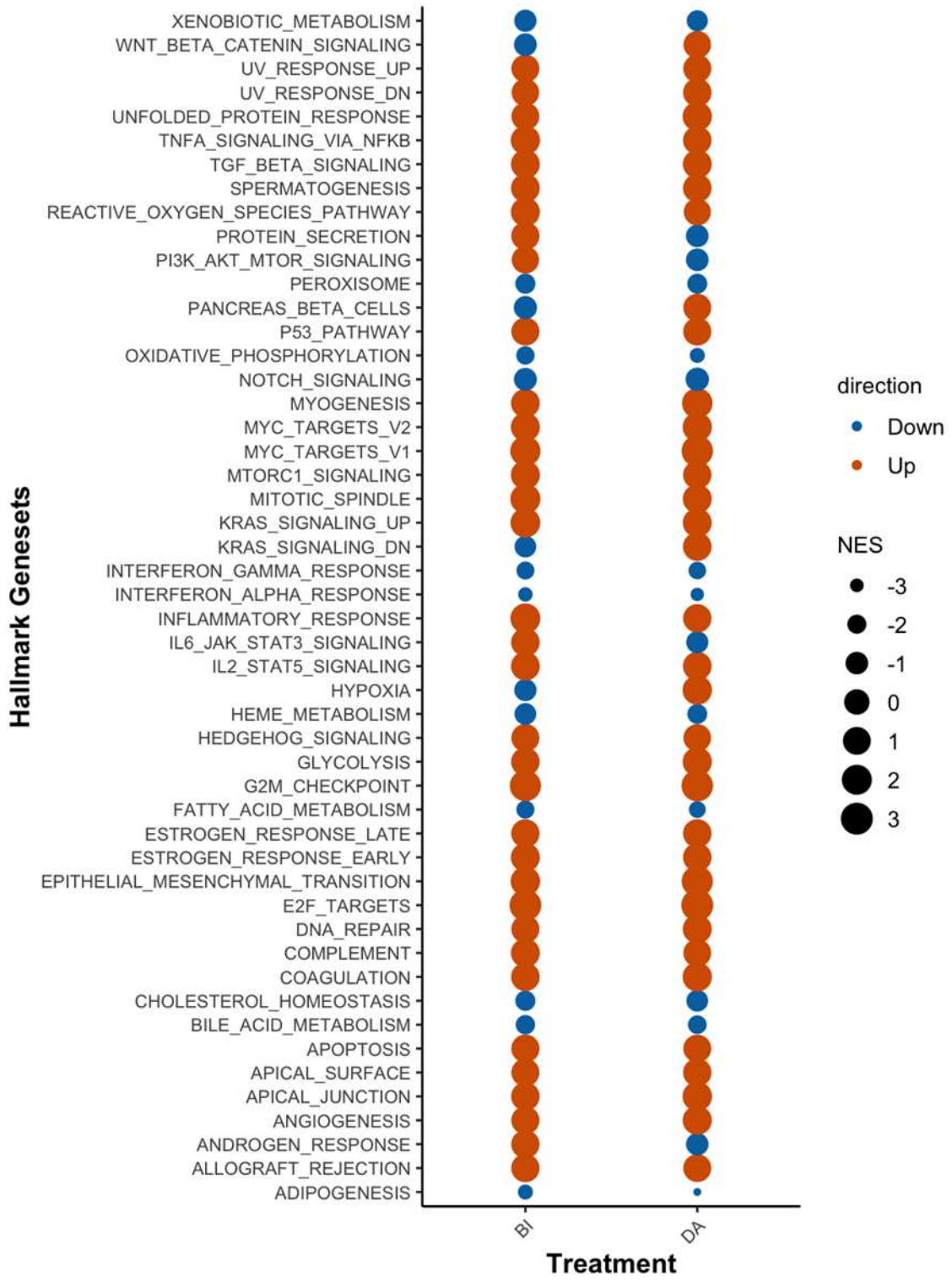


Figure 4.23 Bubblegum plot of the Hallmark gene sets for BI-9774 and D316A compared to WT

From the RNA sequencing data a bubblegum plot comparing the results of the GSEA for the Hallmark gene set between BI-9774 v WT and D316A v WT. (BI, BI-9774; DA, D316A; NES, normalised enrichment score).

The top gene ontology terms associated with the significantly upregulated genes in BI-9774 SVF compared to WT SVF were mostly related to cell cycle, which will be explored further later in this thesis (Figure 4.24A). Meanwhile, the top gene ontology terms associated with the significantly downregulated genes were related to immune response and also lipid and fatty acid metabolism (Figure 4.24B).

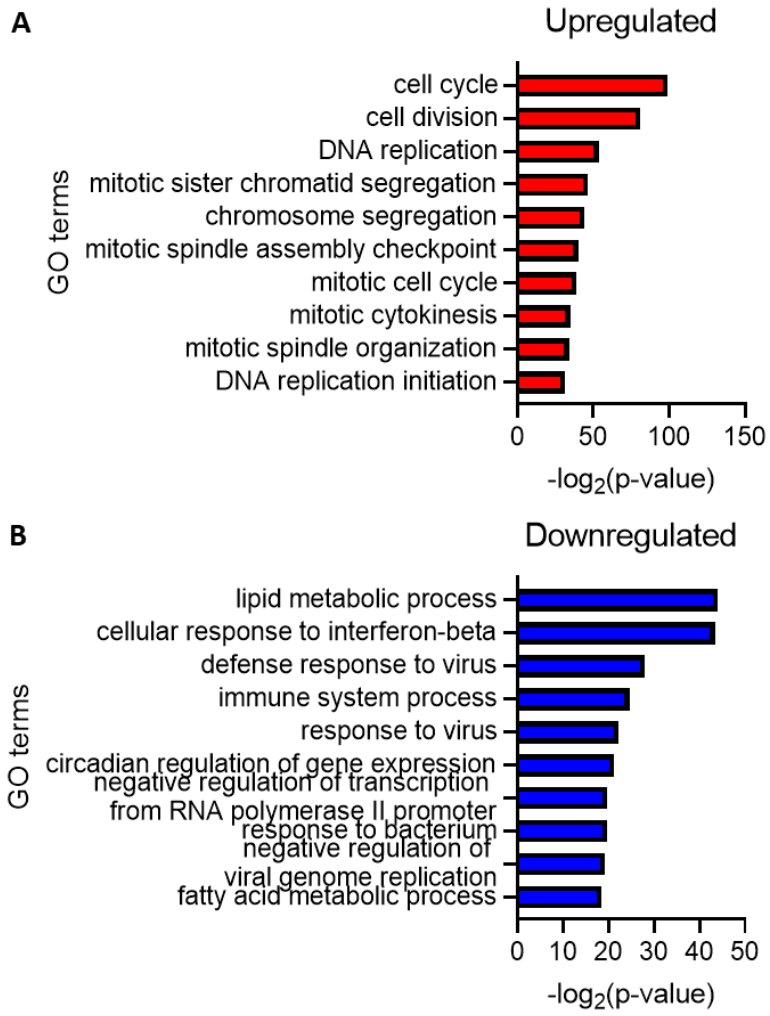


Figure 4.24 Most significantly changed GO terms

The most significantly (A) upregulated and (B) downregulated GO terms associated with the significantly differentially expressed genes in BI-9774 SVF adipocytes compared to WT SVF adipocytes.

4.2.4 Further investigation of AMPK activation by BI-9774 in adipogenesis

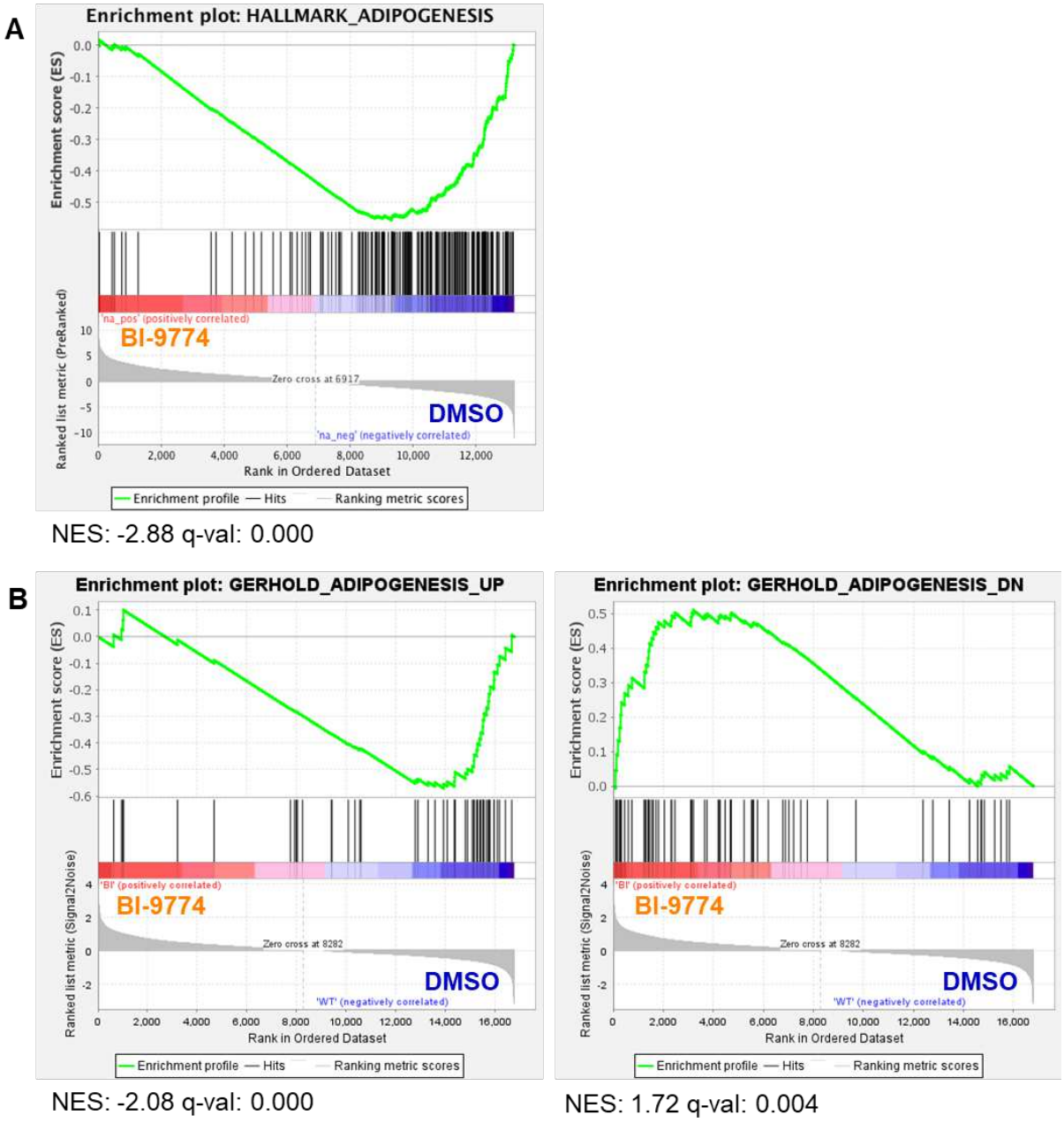


Figure 4.25 GSEA plots for adipogenesis in BI-9774 vs DMSO

From the RNA sequencing data set, enrichment plots for (A) the Hallmark Adipogenesis genes and (B) the Gerhold Adipogenesis Up and Down gene sets.

Titration of BI-9774 in adipogenesis showed that from 1.25μM there was a dose dependent reduction in adipogenic index (Figure 4.4). In support of this, the Hallmark Adipogenesis

gene set showed a reduction in the BI-9774 SVF adipocytes with normalised enrichment score (NES) -2.88 (Figure 4.25A). The Gerhold Adipogenesis gene sets showed enrichment of genes upregulated with adipogenesis in the untreated cells, and enrichment for genes that are downregulated in adipogenesis in the BI-9774 treated cells (Figure 4.25B). Assessment by qPCR on the same set of samples of individual genes associated with adipogenesis showed a reduction in *Pparγ*, *Cebpα*, *Lipoprotein lipase* (*Lpl*), *Perilipin1* (*Plin1*), *Adipoq* and *Leptin* expression with BI-9774 in adipogenesis, with all reductions except for *Cebpα* being significant (Figure 4.26). Protein levels of PPARγ and Perilipin1, as well as lipogenic machinery ACC and FAS which are associated with adipogenesis were characterised by Western blot (Figure 4.27A). There was a significant reduction in FAS, ACC and PPARγ with BI-9774 (Figure 4.27B-D), and a reduction in Perilipin1 that didn't quite reach significance (Figure 4.27E). These results backed up the adipogenic index data, showing that the presence of 1.25μM BI-9774 to activate AMPK throughout adipogenesis is enough to lead to a significant reduction in adipocyte formation.

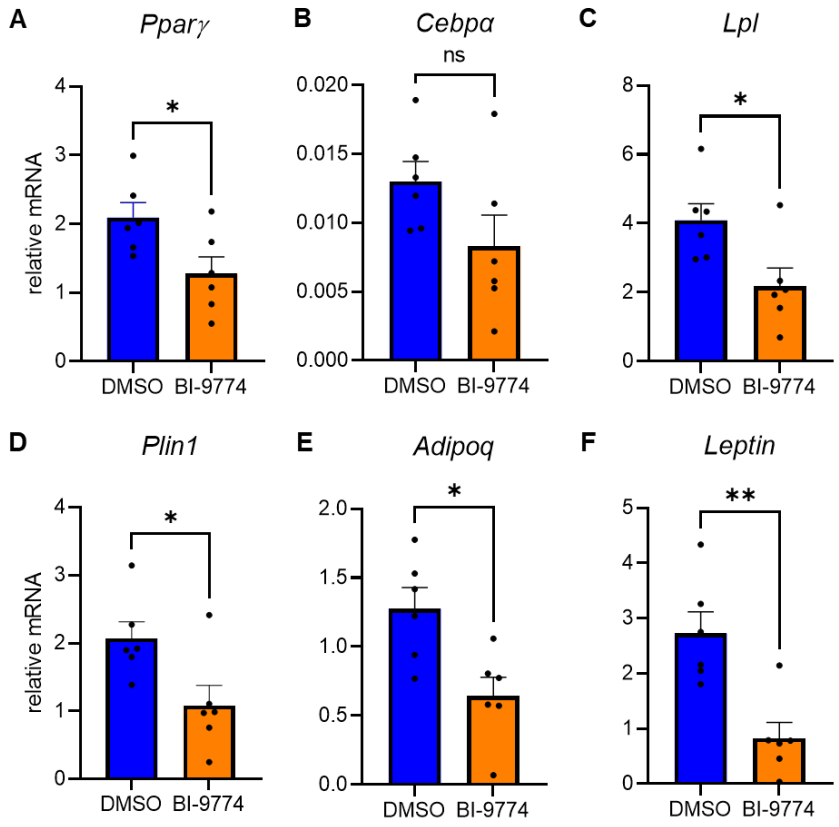


Figure 4.26 Characterisation of AMPK activation on adipocyte marker gene expression.

*(A-F) Adipocyte marker gene mRNA levels by qPCR at the end of SVF adipogenic differentiation with or without BI-9774. mRNA levels relative to housekeeping gene 36B4. Data are shown as mean ± SEM with statistical significance determined by Student's t-test, *p<0.05, **p<0.01, (n=6).*

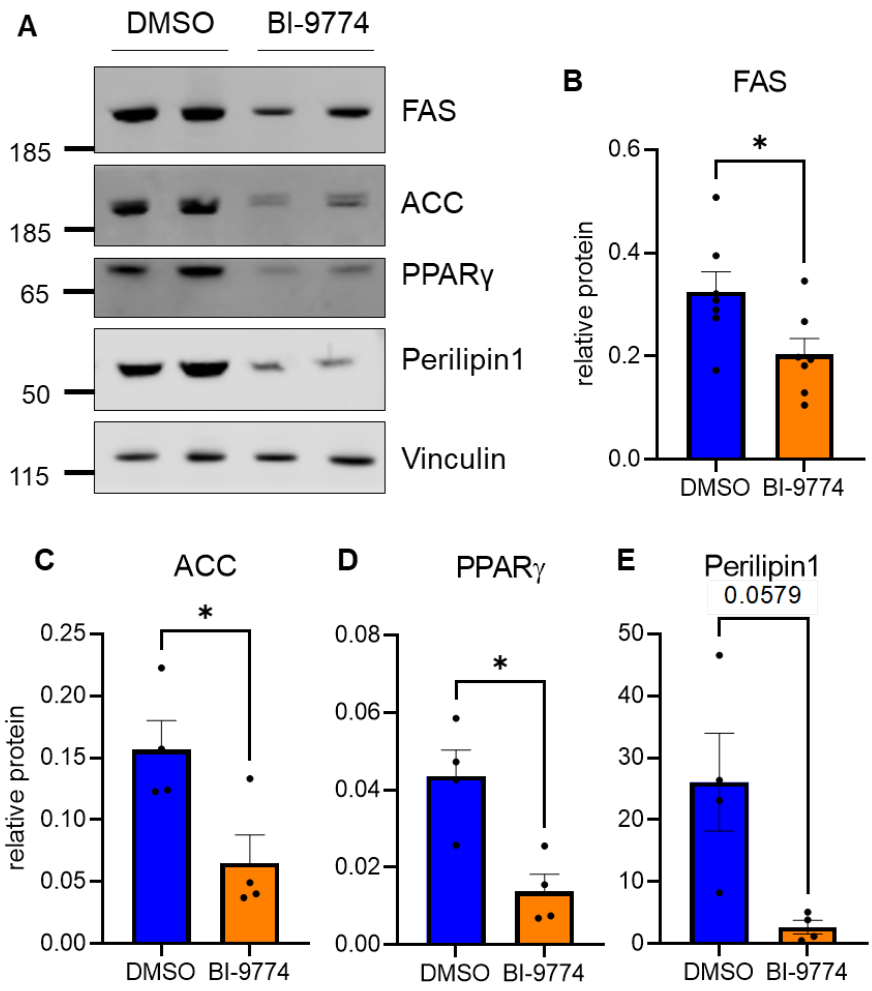


Figure 4.27 Characterisation of AMPK activation on adipocyte associated protein expression.

*Adipocyte marker protein levels at the end of SVF adipogenic differentiation with or without BI-9774. (A) Representative Western blot of adipocyte associated proteins with quantification for (B) FAS, (C) ACC, (D) PPARγ and (E) Perilipin1 all relative to vinculin. Data are shown as mean ± SEM with statistical significance determined by Student's two tailed t-test with Welch's correction applied for (E) Perilipin1, *p<0.05 (n=4).*

To see whether activation of AMPK in adipogenesis leads to the formation of SMART cells like in the D316A iWAT, cells were stimulated with the β-AR agonist isoprenaline for 4 hours at the end of differentiation. Isoprenaline can induce lipolysis in adipocytes via the β-AR signalling pathway which can fuel thermogenesis. However, the role of AMPK in lipolysis is

contended (Yin, Mu et al. 2003, Daval, Diot-Dupuy et al. 2005, Dagon, Avraham et al. 2006, Ahmadian, Abbott et al. 2011, Chuang, Johanns et al. 2021). Basal levels of lipolysis were investigated indirectly by looking at the PKA phosphorylation site on HSL. There was a reduction in total HSL protein levels with BI-9774 (Figure 4.28A), likely reflective of the reduction in the number of adipocytes as HSL expression is high in adipose tissue (Kraemer et al., 1993). There were subsequently lower levels of p-HSL with BI-9774. However, when the reduction in total HSL was accounted for, there was no difference in the levels of HSL activity with AMPK activation (Figure 4.28B). Isoprenaline induced a large increase in phosphorylation of HSL (Figure 4.28C, D). Still there was no difference in the level of p-HSL to total HSL and implicating that AMPK activation with BI-9774 had no effect on stimulated lipolysis in this model, although more direct studies would be needed to confirm this.

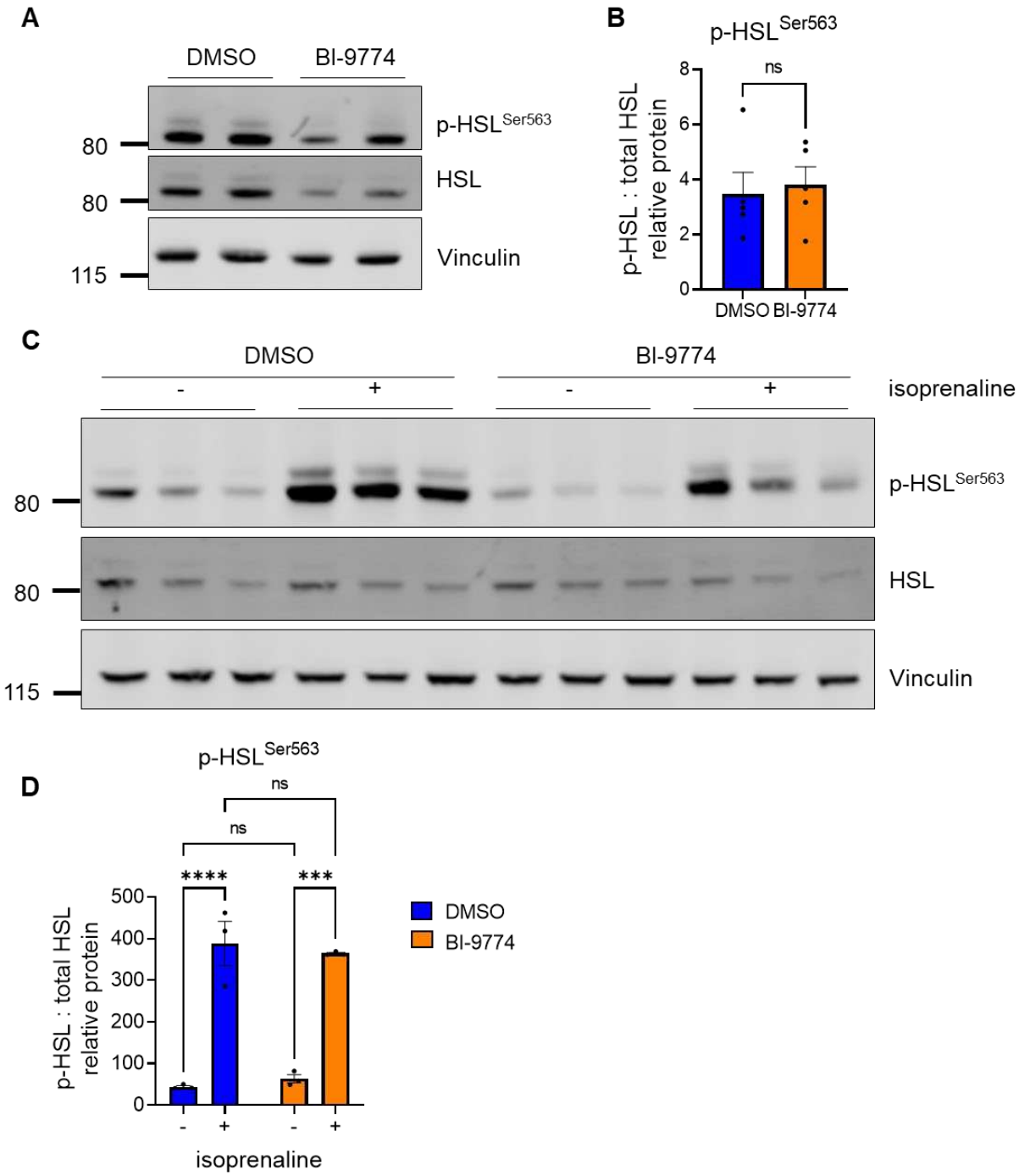


Figure 4.28 Effect of AMPK activation on an indirect readout of lipolysis in adipocytes

(A-B) The SVF was differentiated with BI-9774 and basal lipolysis was investigated by looking at levels of HSL phosphorylation. (A) Representative Western blot with quantification for (B) p-HSL relative to HSL, all relative to vinculin (n=5). (C-D) The SVF was differentiated

*with BI-9774 and after adipocyte formation lipolysis was stimulated with 10μM isoprenaline for 4 hours. (C) Western bot with quantification for (D) p-HSL relative to HSL, all relative to vinculin (n=3). Data are shown as mean ± SEM with statistical significance determined by Student's t-test (B) or two-way ANOVA with Tukey's correction for multiple comparisons, ***p<0.001, ****p<0.0001, (n=3).*

To see whether AMPK activation promoted adipocyte browning, thermogenic proteins were assessed with and without isoprenaline stimulation. Isoprenaline was unable to induce UCP1 protein expression, the classic indicator of beige and brown adipocyte formation (Figure 4.29A). There was also no increase in CKB expression which is involved in creatine futile cycling in adipocytes (Rahbani et al., 2021). Skeletal muscle associated proteins creatine kinase, mitochondrial 2 (CKMT2) and SERCA1 expression were both increased in the D316A iWAT in a high fat diet mouse (Pollard et al., 2019). However, they were not expressed in the SVF adipocytes and expression was not induced with isoprenaline (Figure 4.29B). SERCA2 appeared to be ubiquitously expressed in the SVF adipocytes, and although isoprenaline and BI-9774 appeared to increase its expression in WT untreated SVF adipocytes, this increase was not significant. Due to the likely lack of difference in stimulated or unstimulated lipolysis and thermogenesis with BI-9774, pharmacological activation of AMPK with stimulation of β-AR was not able to generate SMART cells.

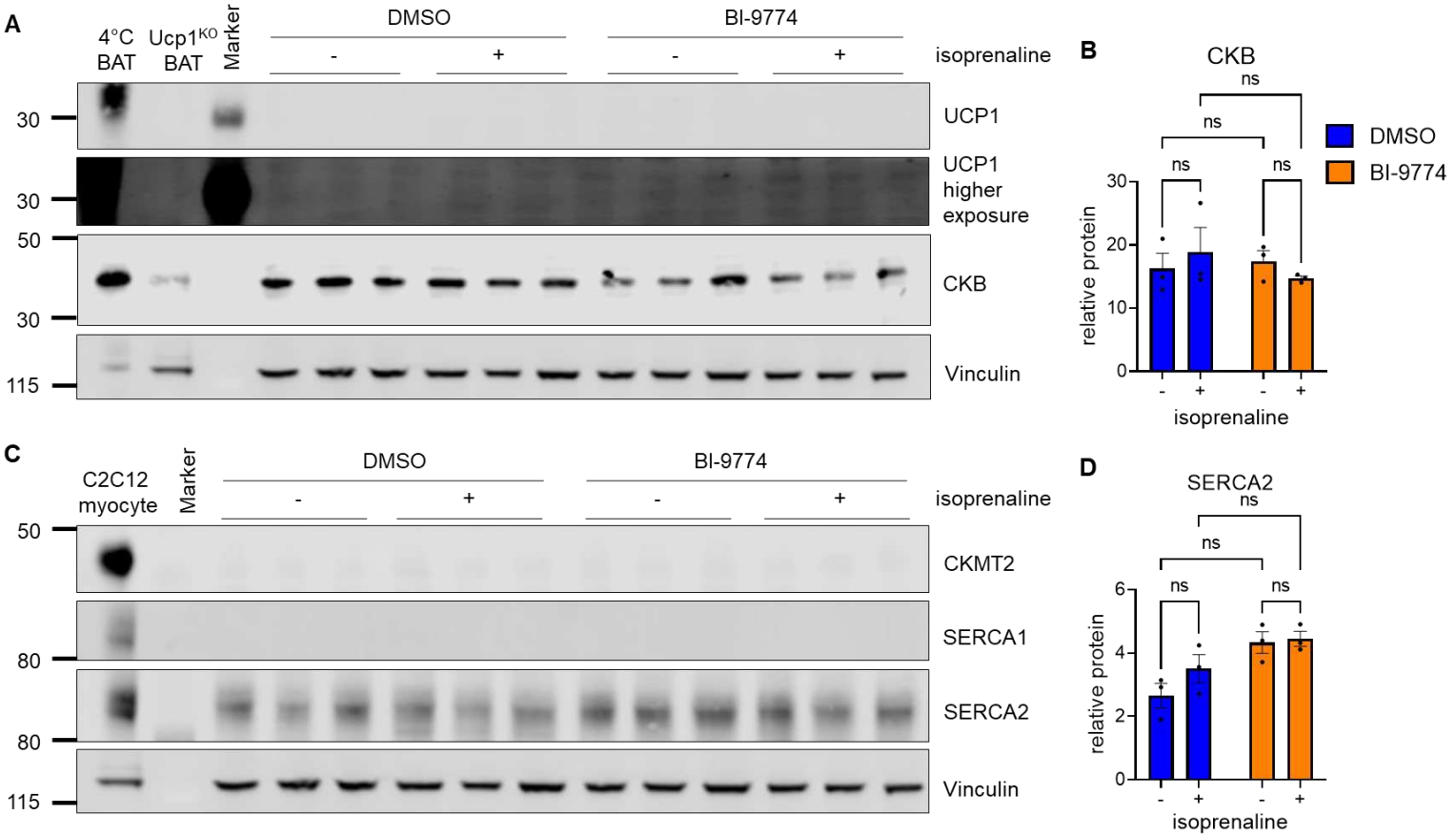


Figure 4.29 Characterisation of AMPK activation in adipogenesis on adipocyte thermogenesis

The SVF was differentiated with BI-9774 and after adipocyte formation lipolysis was stimulated with 10µM isoprenaline for 4 hours, after which proteins involved in thermogenesis in (A, B) adipose tissue and in (C, D) muscle were investigated. (A) Western blot of adipocyte associated thermogenic proteins with (B) quantification of CKB relative to vinculin. (C) Western blot of muscle associated thermogenic proteins with (D) quantification of SERCA2 relative to vinculin. Data are shown as mean ± SEM with statistical significance determined by two-way ANOVA with Tukey's correction for multiple comparisons (n=3).

4.2.5 Importance of timing of AMPK activation in adipogenesis

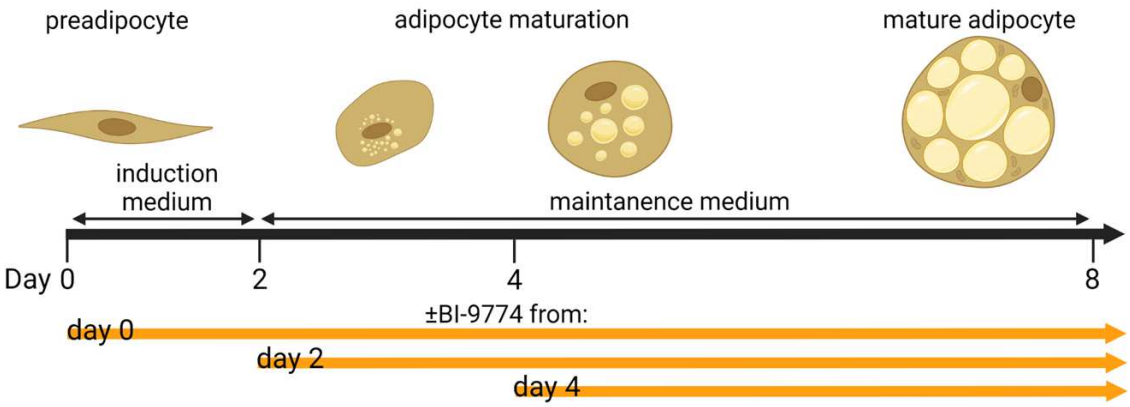


Figure 4.30 Timeline of adipogenesis with AMPK activated at different time points
SVF adipogenesis with BI-9774 added chronically from day 0, day 2 or day 4 onwards until the end point.

To try to understand how AMPK activation reduces adipogenesis, AMPK was chronically activated from different times throughout adipogenesis. BI-9774 was added from day 0, day 2 or day 4 onwards (Figure 4.30). Day 2 signifies the end of the induction phase, when cells should be committed to adipogenesis, but adipocytes have not yet formed. Meanwhile, day 4 is when lipid droplets should have started to form, and adipocytes are maturing. Snapshots were taken throughout adipogenesis on day 0, 2, 4 and 8 for each of the conditions (Figure 4.31). In the top row, normal progression of adipogenesis without AMPK activation can be seen, with the SVF at 90% confluence on day 0 when adipogenesis is initiated. At day 2 small lipid droplets were being synthesised from the ER around the nucleus. These become more visible on day 4 and then mature adipocytes are clearly visible at day 8. In the second row the effect of activating AMPK from day 0 was evident at day 2, where there were fewer cells with lipid droplets forming around the nucleus and by days 4 and 8 where there was a clear reduction in adipocytes. When AMPK was activated from day 2 in the third row there was no striking reduction in adipogenesis at days 4 and 8 as is seen when it is added at day 0, and in the bottom row when AMPK is activated from day 4 there is no visible difference in adipogenesis at day 8.

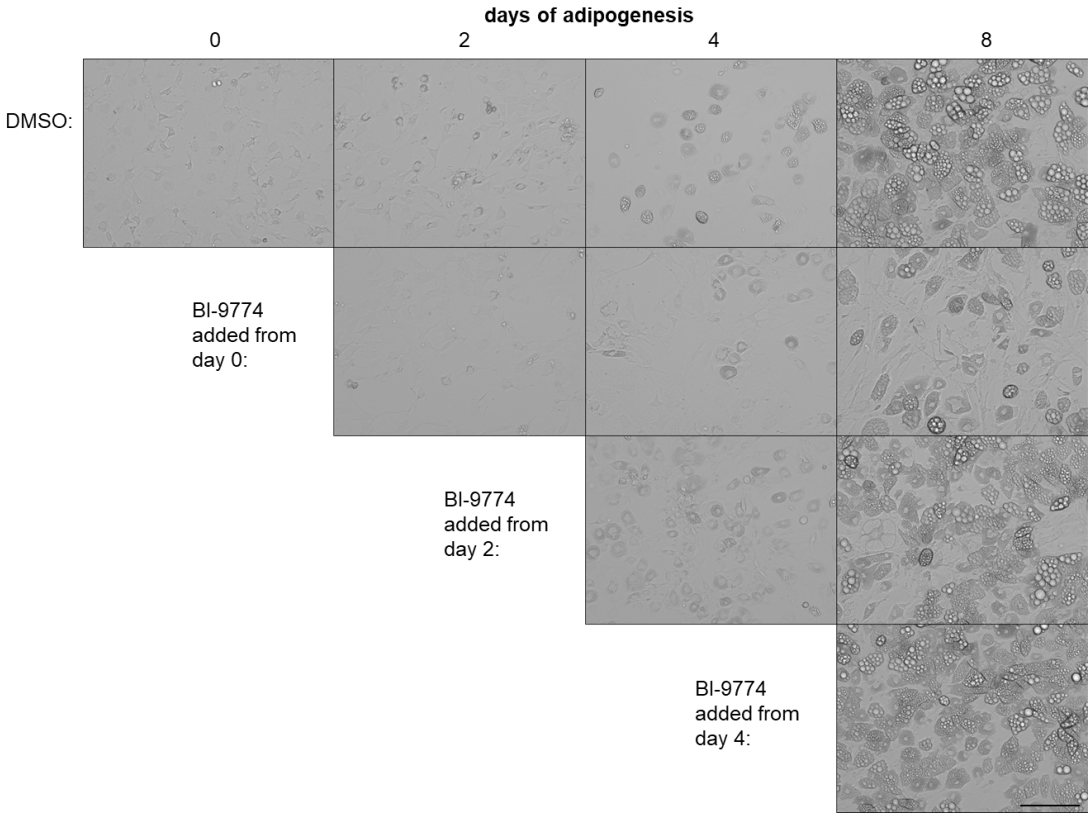


Figure 4.31 Progression of adipogenesis when AMPK is added at different time points

Representative images taken through adipogenesis on days 0, 2, 4 and 8 to see the onward effect of adding BI-9774 chronically from day 0, 2 and 4. Scale bar represents 150μm.

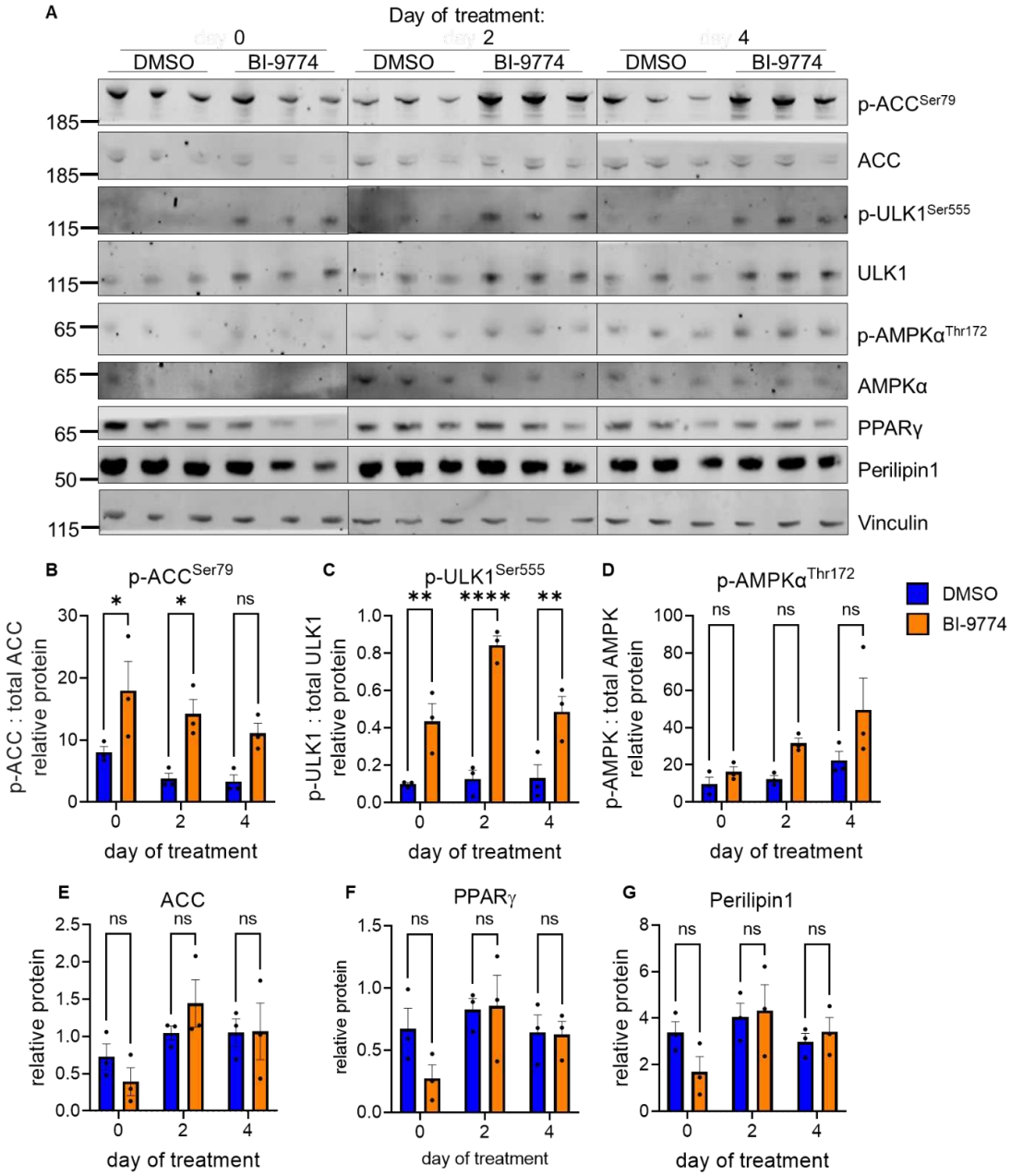


Figure 4.32 Characterisation of AMPK activation and adipogenesis when BI-9774 is added at different time points in adipogenesis

BI-9774 was added from day 0, 2 or 4 onwards in adipogenesis and AMPK activation was assessed at the end of adipocyte differentiation. (A) Western blot showing phosphorylation of AMPK targets and levels of adipocyte marker proteins. Quantification of (B) p-ACC relative to ACC, (C) p-ULK1 relative to ULK1 and (D) p-AMPKα relative to AMPKα, plus adipocyte associated proteins (E) ACC, (F) PPARγ and (G) Perilipin1 all normalised to

*vinculin. Data are shown as mean ± SEM with statistical significance determined by two-way ANOVA with Šidák's correction for multiple comparisons, *p<0.05, **p<0.01, ****p<0.0001, (n=3).*

BI-9774 activated AMPK as judged by increased phosphorylation of AMPK and its downstream targets regardless of which day it was added (Figure 4.32A-D). Levels of some adipocyte associated proteins were assessed. Although not significant, ACC, PPARγ and Perilipin1 protein expression was decreased when AMPK was activated from day 0 compared to DMSO, but not from day 2 or 4 (Figure 4.32A, E-G). To further investigate levels of adipogenesis, levels of adipocyte marker genes *Pparγ*, *Cebpα*, *Lpl*, *Plin1* and *Adipoq* showed reductions when AMPK was activated from day 0 but not day 2 or 4, although like with the protein levels, these were not significant (Figure 4.33A-E). In contrast to the other adipocyte marker genes, the levels of *leptin* showed reductions with AMPK activation regardless of the timing of activation (Figure 4.33F). Although not significant it suggests the effect of AMPK on leptin expression may be through a different mechanism to that of the other marker genes. The lack of significance is likely due to variability, particularly in the DMSO control.

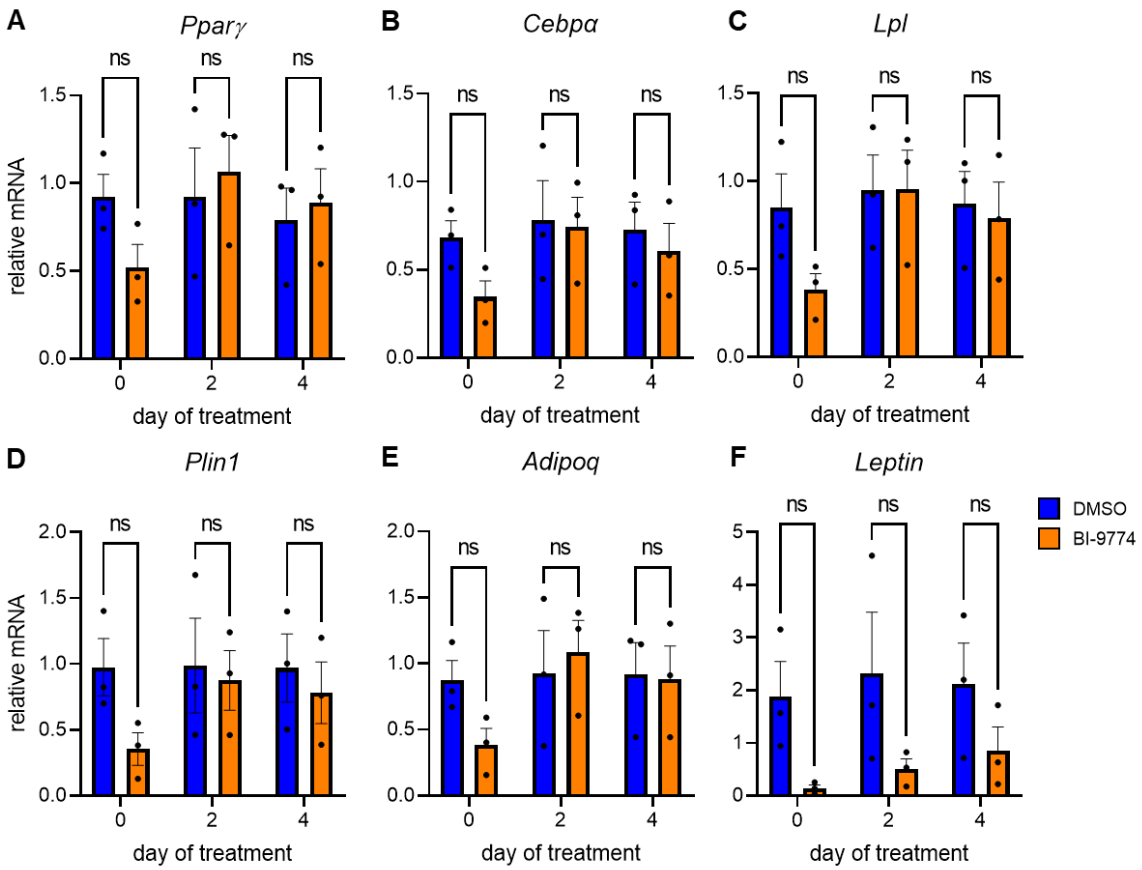


Figure 4.33 Effect of AMPK activation from different time points on adipocyte marker gene expression

(A-F) BI-9774 was added from day 0, 2 or 4 onwards in adipogenesis with adipocyte marker gene mRNA expression assessed at the end of differentiation. mRNA levels relative to housekeeping gene 36B4. Data are shown as mean ± SEM with statistical significance determined by two-way ANOVA with Šidák's correction for multiple comparisons (n=3).

The effect of activating AMPK at different time points in adipogenesis on the adipogenic index was determined (Figure 4.34). Here, representative images and quantification showed a significant reduction in lipid droplet staining when AMPK was activated from day 0, but not from days 2 or 4 (Figure 4.34A, B). There was a slight increase in lipid droplet staining when AMPK was activated on day 2 compared to DMSO. AMPK activation from day 0 and day 2 significantly reduced nuclei counts, although there was no effect when AMPK was activated

from day 4 (Figure 4.34C). The adipogenic index only showed a reduction when AMPK was activated from day 0 (Figure 4.34D). The slight increase in lipid droplet staining when AMPK was activated at day 2 was compounded by the reduction in nuclei counts, resulting in a significant increase in the adipogenic index. There was no difference in adipogenic index when AMPK was activated at day 4. These data show that in order to reduce adipogenesis AMPK must be activated from the initiation of differentiation.

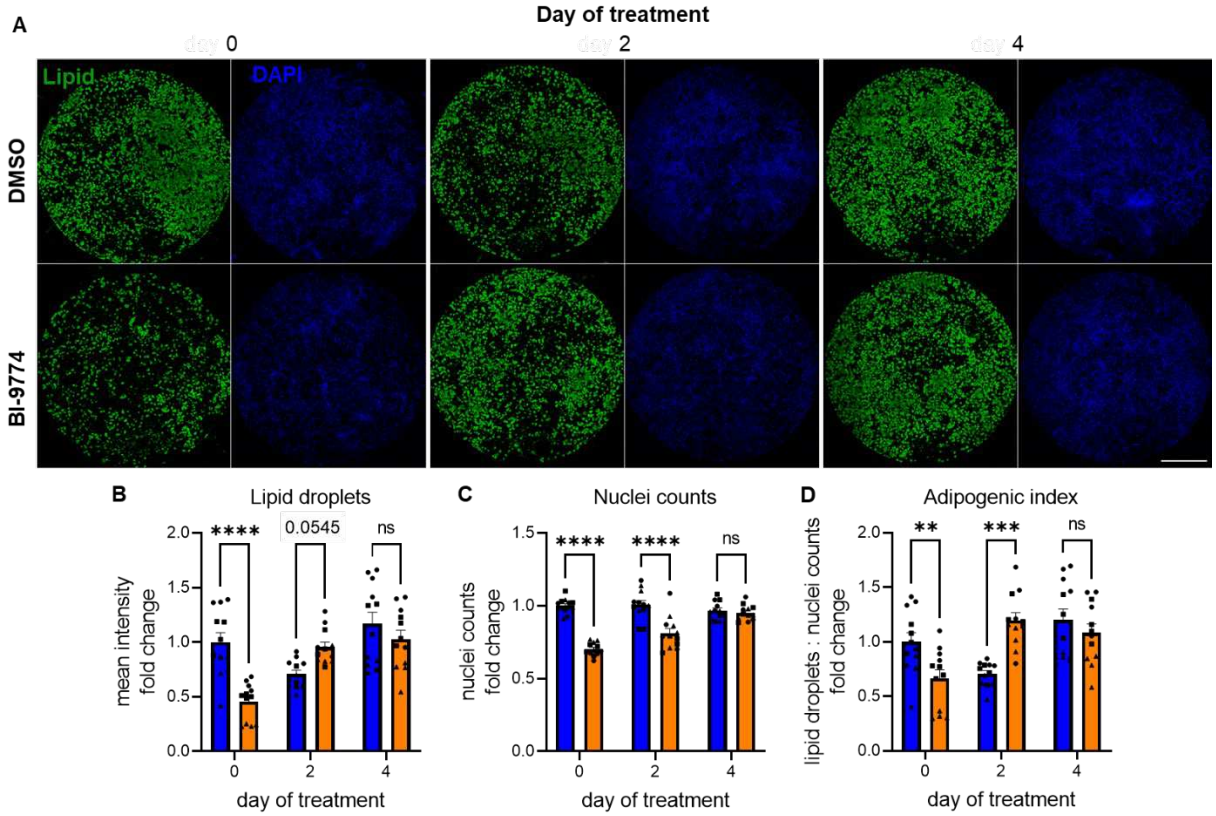


Figure 4.34 Effect of AMPK activation from different time points in adipogenesis on adipocyte lipid accumulation

*BI-9774 was added from day 0, 2 or 4 onwards in adipogenesis. (A) Representative images of whole well scans with lipid droplet and DAPI staining. Quantification of (B) lipid droplet staining (C) nuclei counts and (D) adipogenic index. Data are shown as mean ± SEM, with biological replicates represented by different shaped symbols. Statistical significance is determined by two-way ANOVA with Šidák's correction for multiple comparisons, **p<0.01, ***p<0.001, ****p<0.0001, (n=3 mice, each represented by a different shaped symbol, SVF isolated on the same day, 4 technical replicates per mouse). Scale bar represents 1500μm.*

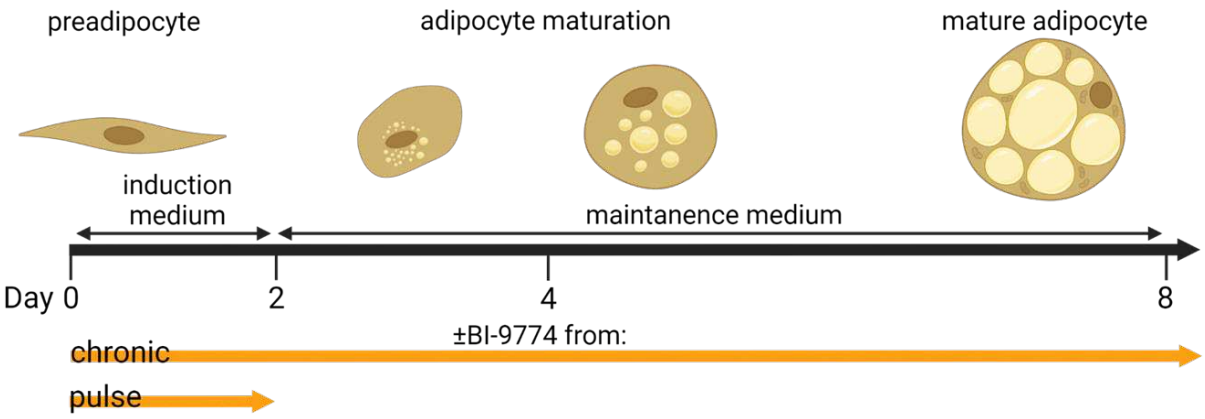


Figure 4.35 Timeline of adipogenesis with chronic and pulse activation of AMPK
SVF adipogenesis with BI-9774 added chronically from day 0 to the end or pulse from day 0 to day 2.

Next, it was investigated whether AMPK needed to be active throughout the entirety of adipogenesis to reduce adipocyte differentiation. To do this, AMPK was added at day 0 upon initiation of adipogenesis and then either maintained chronically throughout the whole of adipogenesis or removed after the induction phase of adipogenesis at day 2 to give a pulse treatment (Figure 4.35). Chronic activation of AMPK with BI-9774 gave an increase in p-ACC, p-ULK1 and p-AMPKα, as has been previously observed (Figure 4.36A-D). The pulse activation of AMPK from day 0 to 2 did not lead to increased phosphorylation of AMPK or its downstream targets, meaning that AMPK was only active in the early stages of adipogenesis and BI-9774 had been successfully washed from the cells. There was a significant reduction in PPARγ expression with chronic and pulse activation of AMPK compared to DMSO (Figure 4.36G). There were non-significant reductions in ACC, FAS and Perilipin1 with both chronic and pulse activation of AMPK (Figure 4.36F, H).

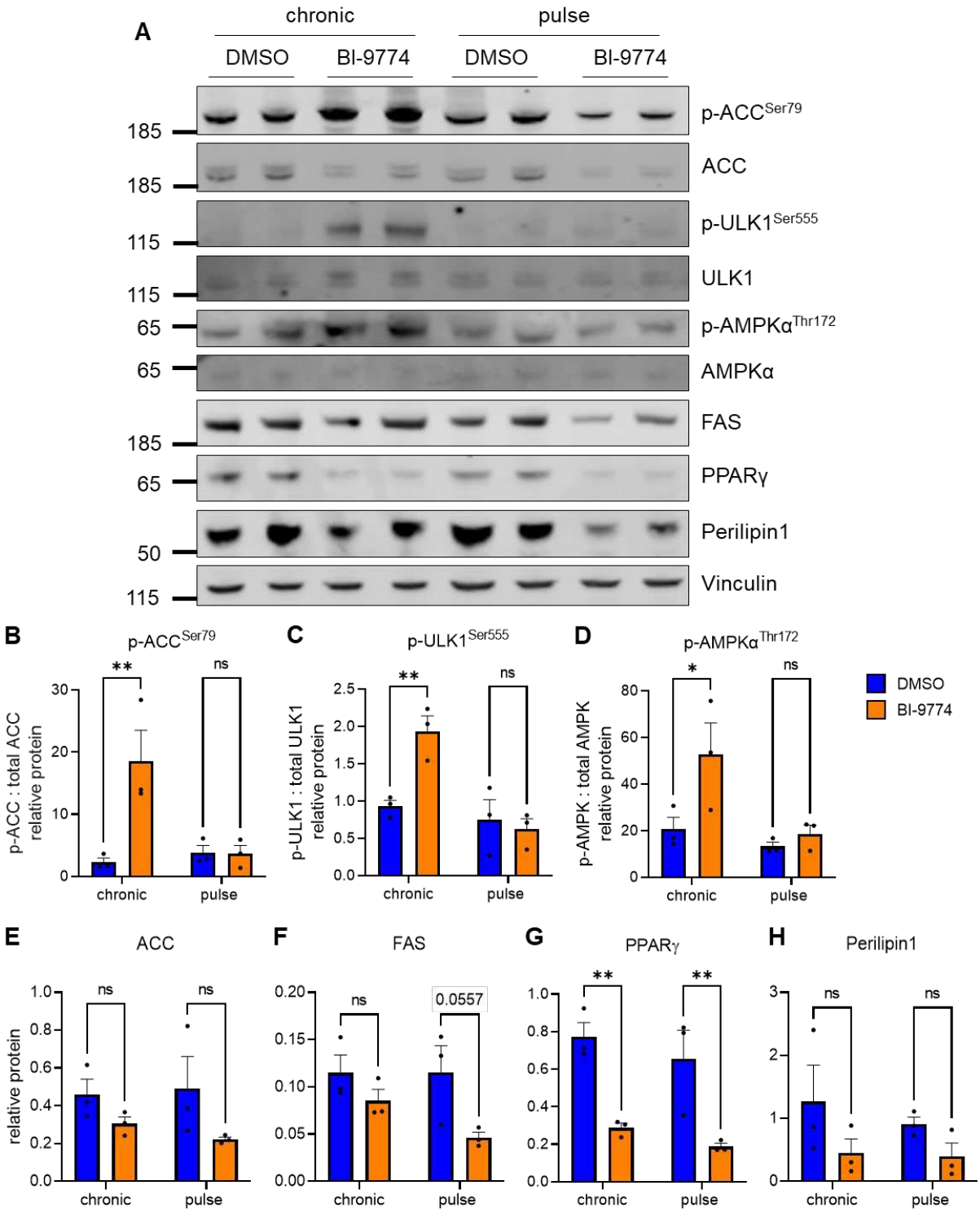


Figure 4.36 Effect of pulse AMPK activation in adipogenesis on AMPK activation and adipocyte associated proteins

*To pulse treat, BI-9774 was added from day 0 to day 2 in adipogenesis and then removed, whilst for chronic treatment it was kept in throughout adipogenesis, with protein levels assessed at the end of adipogenesis. (A) Representative Western blot showing phosphorylation of AMPK targets and proteins associated with adipocytes. Quantification of (B) p-ACC relative to ACC, (C) p-ULK1 relative to ULK1 and (D) p-AMPKα relative to AMPKα, plus adipocyte associated proteins (E) ACC, (F) FAS and (G) PPARγ and (H) Perilipin1 all normalised to vinculin. Data are shown as mean ± SEM with statistical significance determined by two-way ANOVA with Šidák's correction for multiple comparisons, *p<0.05, **p<0.01 (n=3).*

Gene expression levels of adipocyte marker proteins gave mixed results in terms of significance; however, the general pattern was that there was a reduction with chronic and pulse activation of AMPK (Figure 4.37).

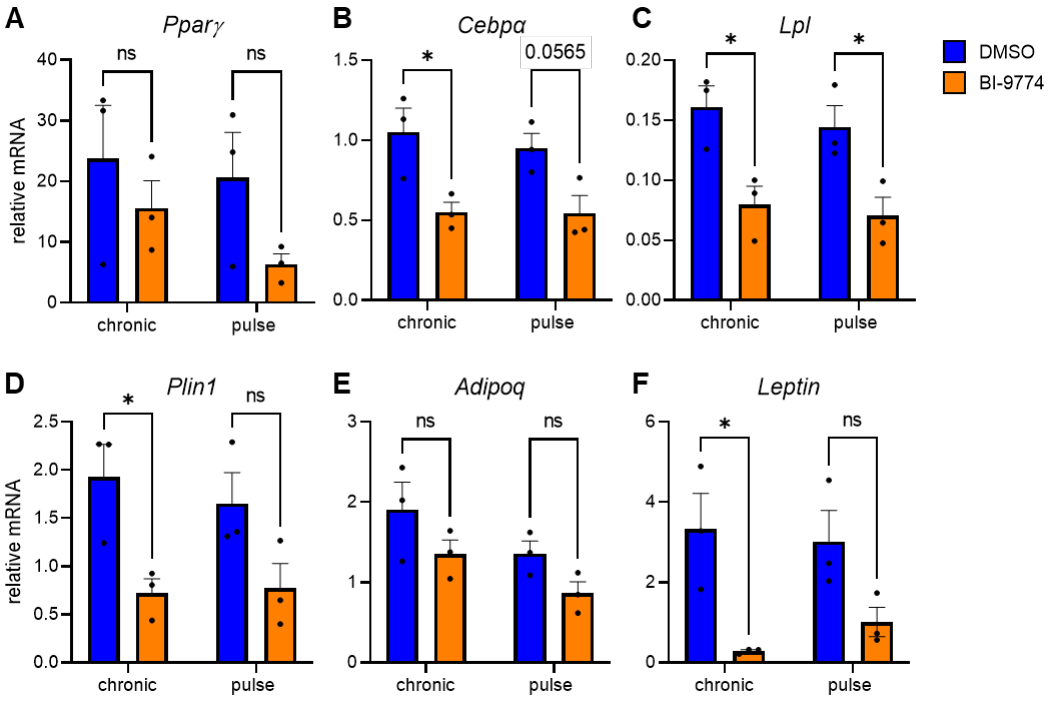


Figure 4.37 Effect of pulse AMPK activation in adipogenesis on adipocyte marker gene expression

(A-F) To pulse treat, BI-9774 was added from day 0 to day 2 in adipogenesis and then removed, whilst for chronic treatment it was kept in throughout adipogenesis, with adipocyte

*marker gene mRNA expression assessed at the end of adipogenesis. mRNA levels relative to housekeeping gene 36B4. Data are shown as mean ± SEM with statistical significance determined by two-way ANOVA with Šidák's correction for multiple comparisons, *p<0.05, (n=3).*

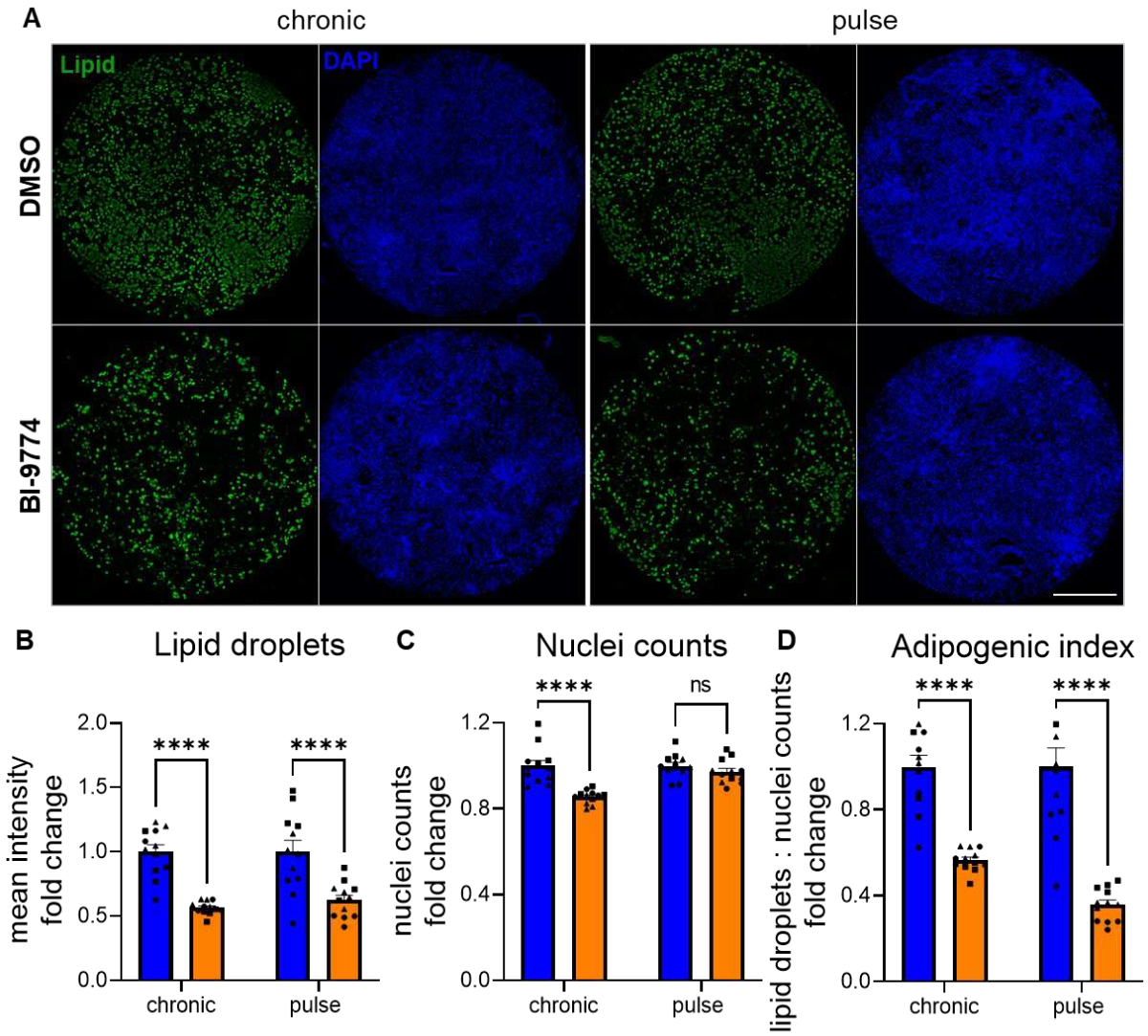


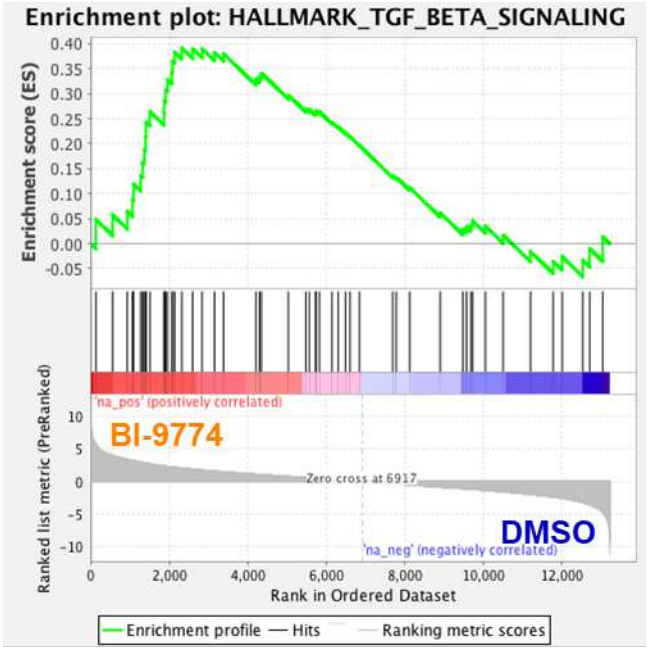
Figure 4.38 Effect of pulse AMPK activation in adipogenesis on adipocyte formation *To pulse treat, BI-9774 was added from day 0 to day 2 in adipogenesis and then removed, whilst for chronic treatment it was kept in throughout adipogenesis. (A) Representative images of whole well scans with lipid droplet and DAPI staining. Quantification of (B) lipid droplet staining (C) nuclei counts and (D) adipogenic index. Data are shown as mean ±*

*SEM, with different biological replicates represented by different shaped symbols. Statistical significance is determined by two-way ANOVA with Šidák's correction for multiple comparisons, ****p<0.0001, (n=3 mice, each represented by a different shaped symbol, SVF isolated on the same day, 4 technical replicates per mouse). Scale bar represents 1500μm.*

There was an obvious reduction in lipid droplet staining with both chronic and pulse activation of AMPK compared to DMSO (Figure 4.38A), which was supported by quantification of lipid droplet staining (Figure 4.38B). Nuclei counts only showed a reduction when AMPK was activated chronically (Figure 4.38C), and the adipogenic index supported the trend, with significant reduction when AMPK was activated both chronically and pulse compared to DMSO (Figure 4.38D). These data show that AMPK must be activated from the initiation of adipogenesis to reduce adipocyte formation, but it is only essential that it is activated in the initial stages of adipogenesis to have an effect. Therefore, it is the events in the early stages of adipogenesis that are affected by AMPK activation.

4.3 INVESTIGATING THE MECHANISM OF AMPK REDUCTION OF ADIPOGENESIS

4.3.1 TGFβ and WNT signalling pathways

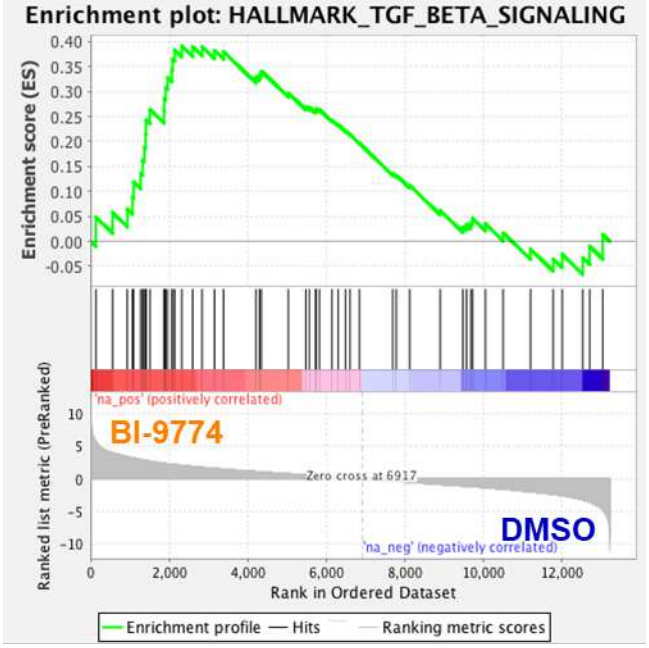


NES: 1.48 q-val: 0.033

Figure 4.39 GSEA plot for TGFβ signalling in BI-9774 vs WT

From the RNA sequencing data set the Hallmark TGFβ signalling gene set enrichment plot showing an increase with BI-9774 treatment.

TGFβ has been implicated in inhibiting progression of adipocyte progenitors to committed precursor cells and promoting progenitor proliferation (Merrick et al., 2019). Interestingly, from the RNA sequencing data the Hallmark TGFβ signalling gene set showed enrichment in BI-9774 treated SVF adipocytes (



NES: 1.48 q-val: 0.033

Figure 4.39). The genes that are part of the core enrichment for this gene set are listed in Table 4.3 and include TGFβ itself, its receptor TGFβR, suppressor of mothers against decapentaplegic (SMAD) 3- one of its downstream signalling proteins involved in inhibition of adipogenesis, and associated proteins LTBP2, ACVR1 and TGIF1. In contrast, the latter TGIF1 forms a repressor complex with SMAD2 to inhibit TGFβ signalling. In addition SMURF1 ubiquitinates SMAD3.

Table 4.3 List of genes in the core enrichment of the Hallmark TGFβ Signalling gene set enriched in the BI-9774 treated SVF adipocytes

Symbol	Gene Name	Rank in Gene List	Rank Metric Score	Running enrichment score

ACVR1	activin A receptor, type 1	139	5.725	0.0486
TGIF1	TGFB-induced factor homeobox 1	564	3.993	0.0577
TGFB1	transforming growth factor, beta 1	940	3.404	0.0645
SMAD3	SMAD family member 3	1071	3.237	0.0881
SMURF2	SMAD specific E3 ubiquitin protein ligase 2	1101	3.189	0.1189
SLC20A1	solute carrier family 20, member 1	1280	2.951	0.1359
SMURF1	SMAD specific E3 ubiquitin protein ligase 1	1330	2.897	0.1621
IFNGR2	interferon gamma receptor 2	1374	2.849	0.1883
SERPINE1	serine (or cysteine) peptidase inhibitor, clade E, member 1	1406	2.818	0.215
LTBP2	latent transforming growth factor beta binding protein 2	1416	2.811	0.2434
THBS1	thrombospondin 1	1515	2.724	0.2641
TGFBR1	transforming growth factor, beta receptor I	1876	2.395	0.2616
FKBP1A	FK506 binding protein 1a	1879	2.393	0.2862
NCOR2	nuclear receptor co-repressor 2	1916	2.358	0.3078
SKI	ski sarcoma viral oncogene homolog (avian)	1965	2.317	0.3281
ID2	inhibitor of DNA binding 2	2073	2.235	0.3431
CTNNB1	catenin (cadherin associated protein), beta	2090	2.222	0.3649
PMEPA1	prostate transmembrane protein, androgen induced 1	2146	2.194	0.3834
ENG	endoglin	2328	2.069	0.391

To confirm whether there were changes in TGFβ signalling an ELISA was used to determine TGFβ protein levels (Figure 4.40). Within the cells there was a large decrease in TGFβ levels. Although this is contradictory to what it shown by RNA sequencing, it is in line with literature whereby activation of AMPK negates the pro-fibrotic and pro-tumorigenic effects of TGFβ (Gao et al., 2018; Lu et al., 2015; Mishra et al., 2008). As TGFβ is a secreted factor that works on the extracellular TGFβR, measurements of the levels of TGFβ in the SVF adipocyte conditioned media was attempted by ELISA but without success (data not shown), either due to the low relative concentrations of TGFβ in the media or because the TGFβ isn't secreted. Attempts to concentrate the media were also unsuccessful, as TGFβ was still undetected (data not shown).

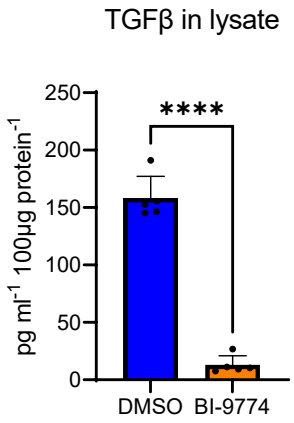


Figure 4.40 Characterisation of the effect of AMPK activation on TGFβ in SVF adipocytes

*Cellular TGFβ protein levels were assessed in SVF derived adipocytes at the end of adipogenesis by ELISA (n=5). Data are shown as mean ± SEM with statistical significance determined by Student's t-test, ****p<0.0001.*

Although in opposition to the effect on adipogenesis, the reductions in TGFβ protein levels were still interesting. TGFβ exerts its effects mainly through the extracellular signal-regulated kinases (ERK) or the SMAD signalling pathways (Figure 4.41A). AMPK has been previously shown to not reduce phosphorylation of SMAD3 when disrupting the TGFβ signalling pathway. However, SMAD3 signalling is the main pathway through which TGFβ exerts its

anti-adipogenic role (Lu et al., 2015; Mishra et al., 2008). There were no changes in the levels of total or p-ERK (Figure 4.41B-D). Again, there were no changes in SMAD2 or SMAD3 protein levels (Figure 4.41B, F, G). Phosphorylation of SMAD3 was barely detectable, and although there was a slight increase in p-SMAD2 levels, the increase was not significant (Figure 4.41A, E).

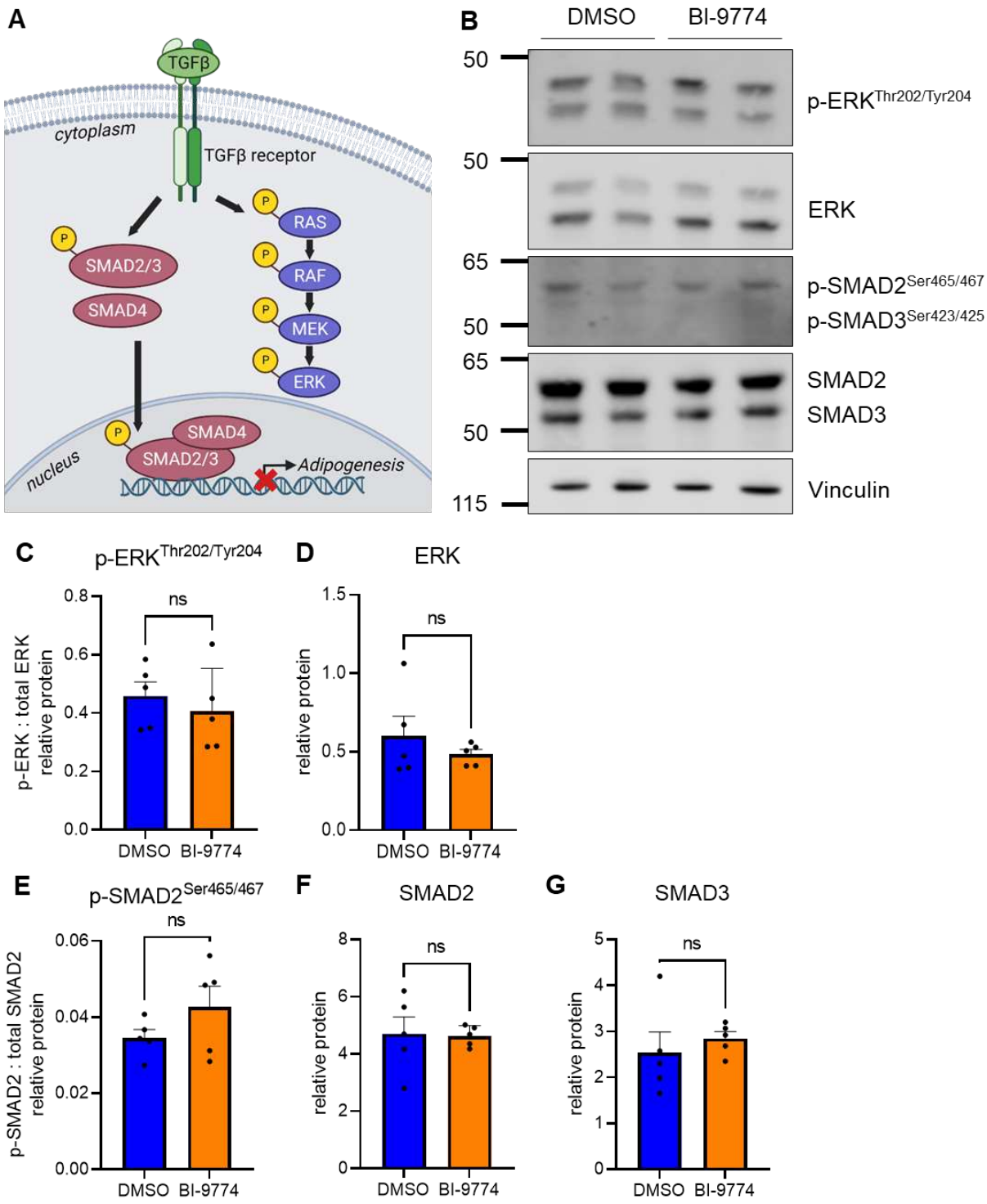


Figure 4.41 Assessing the effect of BI-9774 on the downstream targets of TFGβ

TGFβ downstream targets ERK and SMAD2/3 were assessed at the end of SVF adipocyte differentiation with BI-9774. (A) TGFβ main downstream signalling pathways ERK and

SMAD (adapted from Principe, Diaz et al. 2017). (B) Representative Western blot of the downstream targets of TGFβ with quantification of (C) p-ERK relative to ERK, (D) ERK, (E) p-SMAD2 relative to SMAD2, (F) SMAD2 and (G) SMAD3, all relative to vinculin. Data are shown as mean ± SEM with statistical significance determined by Student's t-test (n=5). (ERK, extracellular signal-regulated kinases; MEK, Mitogen-activated protein kinase kinase; RAF rapidly accelerated fibrosarcoma; RAS, Renin-angiotensin-system; SMAD, suppressor of mothers against decapentaplegic; TGFβ, Transforming growth factor β).

The WNT pathway has been shown to be anti-adipogenic and important for the maintenance and proliferation of preadipocytes and mesenchymal stem cells, acting in an autocrine manner (de Winter and Nusse, 2021). Upon treatment with AICAR, 3T3-L1 cells show increased β-catenin accumulation in the nucleus (Lee et al., 2011a). The β-catenin gene also appeared in the core enrichment of the Hallmark TGFβ gene set (Table 4.3). Therefore SMAD2/3 and β-catenin nuclear translocation was assessed upon AMPK activation. As activation of AMPK during the induction of adipogenesis is essential for its suppressive effect, cytosolic to nuclear translocation was looked at during the day 2 time point in adipogenesis, but at this time point there appeared to be no β-catenin in the nucleus, and very low levels of SMAD2/3 (Figure 4.42A). By the end of adipogenesis all three proteins were detected in both the cytoplasm and the nucleus, with nuclear SMAD3 being phosphorylated whilst there was no evidence of cytosolic SMAD3 phosphorylation (Figure 4.42B). However, there was no clear difference between protein levels or cytosolic to nuclear translocation with BI-9774. Unfortunately, one of the DMSO nuclear protein samples from the end of adipogenesis was lost, and so statistical analysis was not possible. Nevertheless, it appears that the TGFβ or WNT/β-catenin pathways are involved in inhibition of adipogenesis with AMPK activation.

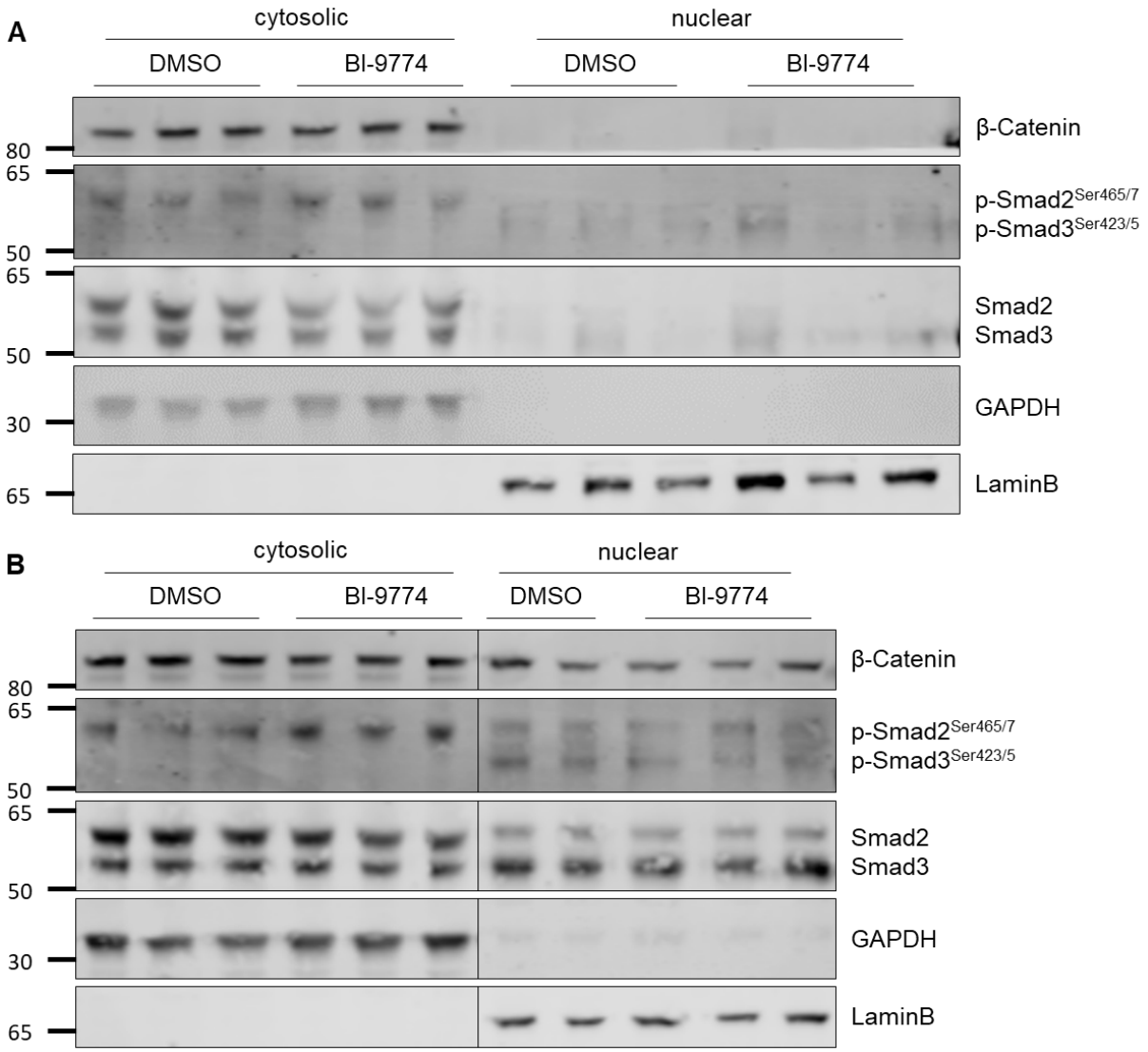


Figure 4.42 Characterising the subcellular localisation of TGFβ and WNT downstream signalling proteins after AMPK activation

Cytosolic and nuclear fractionation to determine the localisation of TGFβ and WNT downstream signalling proteins after AMPK activation. (A) Western blot showing cytosolic and nuclear expression 2 days after adipogenic induction with AMPK activation (n=3). (B) Western blot showing cytosolic and nuclear expression at the end of adipogenesis with AMPK activation. Downstream targets ERK and SMAD2/3 were assessed at the end of SVF adipocyte differentiation with BI-9774 (DMSO n=3, BI-9774 n=2).

4.3.2 Inhibition of lipogenesis

It is often suggested that inhibition of lipogenesis is the mechanism of AMPK inhibition of adipogenesis (Choi et al., 2015; Habinowski and Witters, 2001; He et al., 2013). AMPK inhibits fatty acid synthesis through the phosphorylation and inhibition of ACC. To see whether inhibition of ACC was the mechanism by which AMPK inhibits adipogenesis the pan-ACC inhibitor PF-05175157 was used. PF-05175157 has previously been submitted for clinical trials as an inhibitor of lipogenesis in T2D and to treat acne vulgaris (Batchuluun et al., 2022). It binds to the carboxyl transferase domain of ACC and blocks its ability to synthesise malonyl-CoA. PF-05175157 was titrated from 50 to 0.05μM throughout adipogenesis alongside BI-9774 to see if it was able to give a reduction in adipogenesis. At the end of adipogenesis, levels of adipocyte marker genes were assessed by qPCR (Figure 4.43). As a control, BI-9774 was used and caused the expected reduction in adipocyte markers, although in this case *Pparγ*, *Cebpα* and *Adipoq* did not reach significance. PF-05175157 gave a significant reduction in the more mature adipocyte markers *Plin1*, *Adipoq* and *Leptin* at 5 and 50μM. To investigate the effect of ACC inhibition on lipid droplet formation, the adipogenic index was determined (Figure 4.44). Inhibition of ACC led to a reduction in lipogenesis and lipid droplet formation, greater than with BI-9774 (Figure 4.44A, B, D). The modest reduction in nuclei counts with BI-9774 did not reach significance in this data set, likely due to the spread in the data, and there was no significant difference in nuclei counts with ACC inhibition (Figure 4.44C). So it appears as though inhibition of lipogenesis is also able to reduce lipid droplet formation and expression of functional markers of adipocytes similar to AMPK activation.

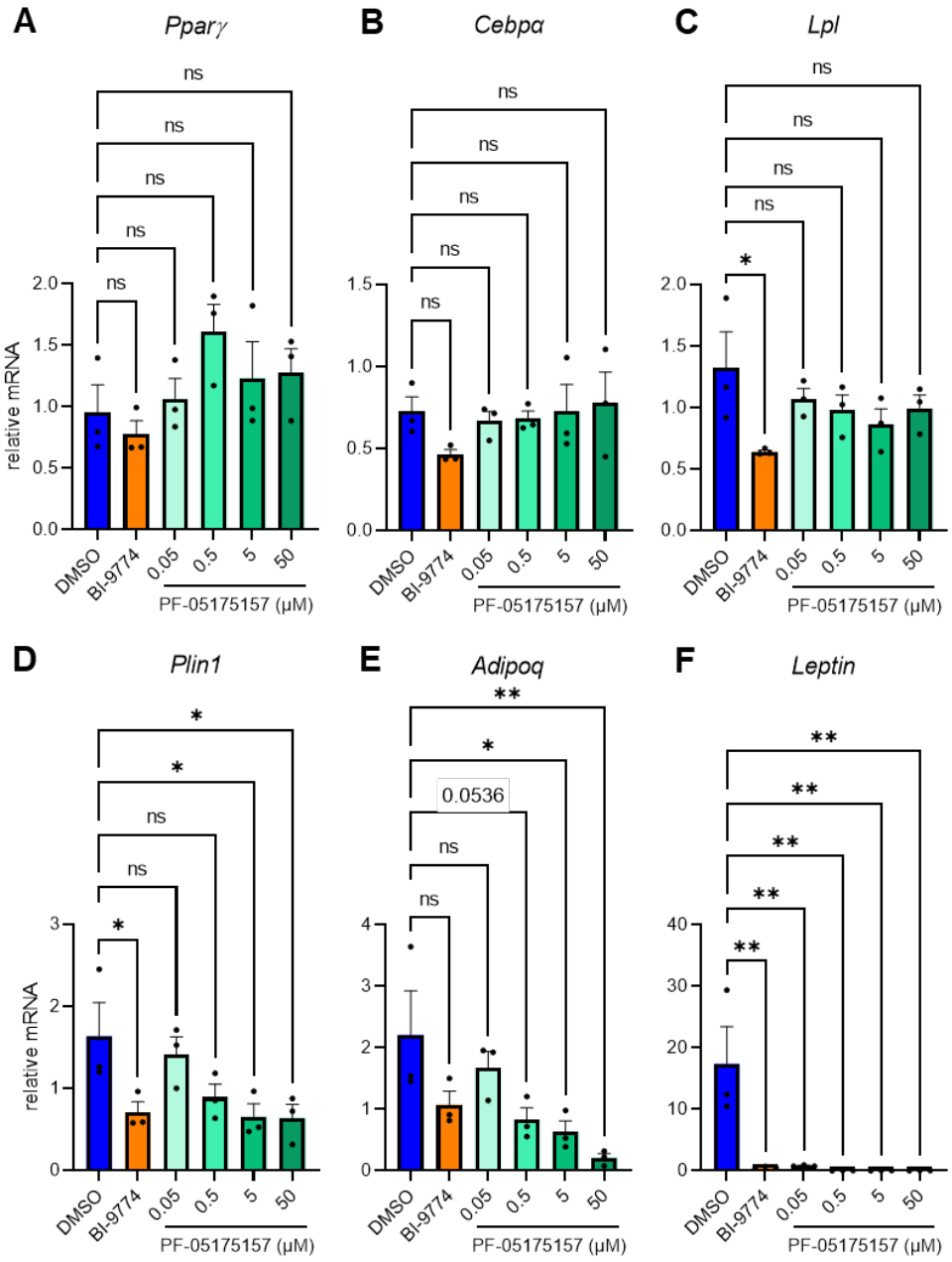


Figure 4.43 Comparative effect of AMPK activation with ACC inhibition in adipogenesis

*(A-F) 0.05 to 50μM ACC inhibitor PF-05175157 or 1.25μM BI-9774 were added to the SVF through adipogenesis to compare its effects on the expression of adipocyte marker genes. mRNA levels relative to housekeeping gene 36B4. Data are shown as mean ± SEM with statistical significance determined by one-way ANOVA with Dunnett's correction for multiple comparisons, *p<0.05, **p<0.01, (n=3).*

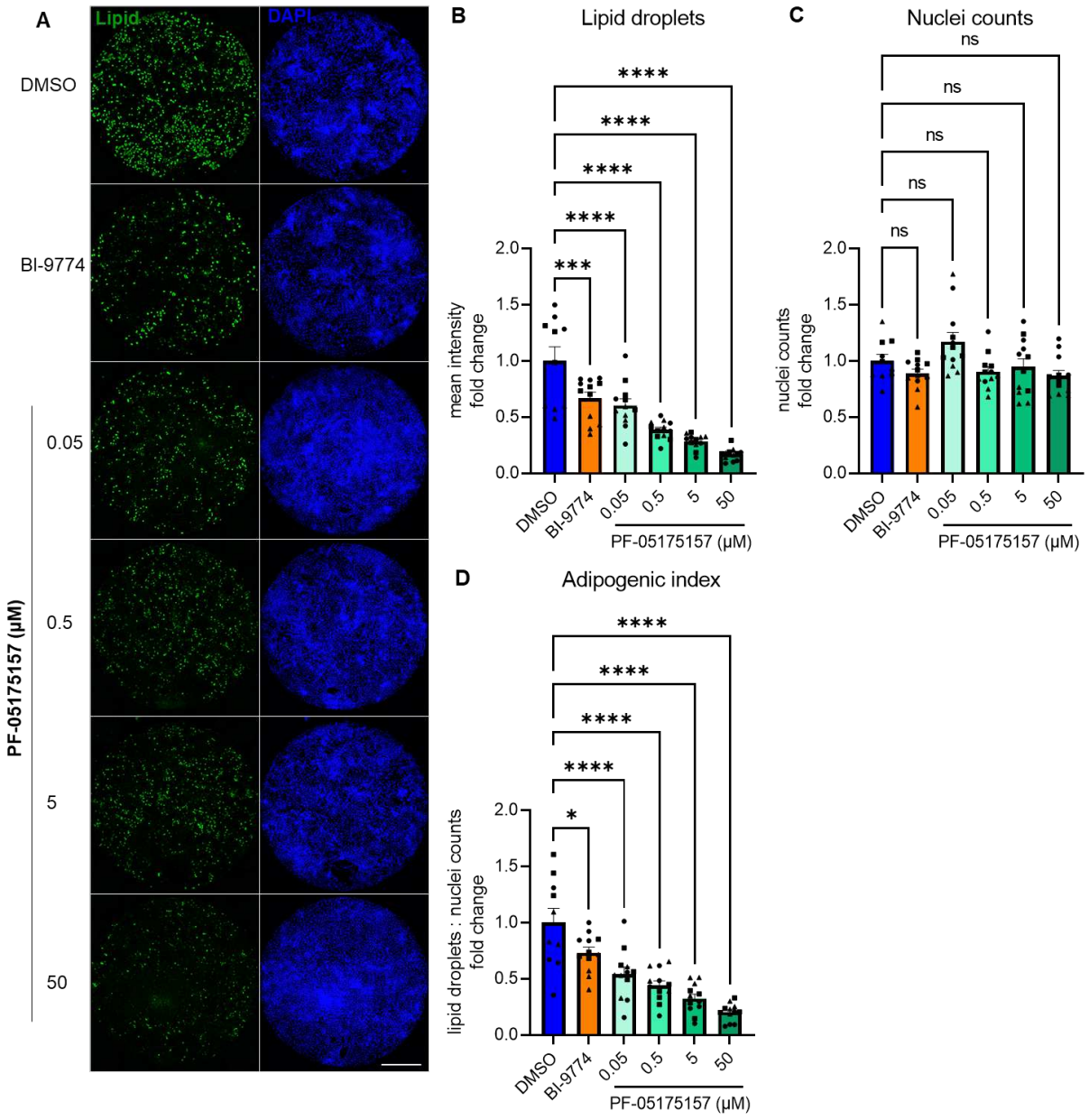


Figure 4.44 Titration of PF-05175157 in SVF adipogenesis

*0.05 to 50μM ACC inhibitor PF-05175157 or 1.25μM BI-9774 were added to the SVF through adipogenesis. (A) Representative images of whole well scans with lipid droplet and DAPI staining Quantification of (B) lipid droplet staining (C) nuclei counts and (D) adipogenic index. Data are shown as mean ± SEM, with different biological replicates represented by different shaped symbols. Statistical significance is determined by one-way ANOVA with Dunnett's correction for multiple comparisons, *p<0.05, ***p<0.001, ****p<0.0001 (n=3 mice,*

each represented by a different shaped symbol, SVF isolated on the same day, 8 technical replicates per mouse). Scale bar represents 1500μm.

To see whether ACC inhibition is the mechanism for suppression of adipogenesis in response to AMPK activation, both PF-05175157 and BI-9774 were added chronically, and in a pulse treatment from day 0 to day 2. 5μM PF-05175157 was chosen as in the titration it was the lowest concentration to give consistent, significant reduction in adipogenesis (Figure 4.44). As previously observed, BI-9774 gave a reduction in adipocyte marker gene expression (Figure 4.45). Once more, chronic pharmacological inhibition of ACC gave a reduction in the genes associated with the later stages of adipogenesis, this time including *Lpl* (Figure 4.45C). However, once again chronic inhibition of ACC did not lead to a reduction in *Pparγ* or *Cebpα*. Pulse inhibition of ACC did not mirror the effects of pulse activation of AMPK, and did not lead to reductions in any of the adipocyte marker genes. To visualise the effect on lipid droplet formation, lipid droplets and nuclei were stained and the adipogenic index was calculated (Figure 4.46). Lipid droplet staining and the adipogenic index support mRNA levels, where chronic treatment with BI-9774 or PF-05175157 led to reductions, but only pulse treatment with BI-9774 led to a reduction in lipid droplet formation or adipogenic index (Figure 4.46A, B, D). Pulse inhibition of ACC did not lead to reductions in lipid droplet quantification or adipogenic index. Interestingly, chronic treatment with PF-05175157 did cause a slight reduction in nuclei counts, matching that seen in BI-9774 (Figure 4.46A, C). This could be through slowed proliferation. However, neither had an effect when pulse treated, reflecting what was previously seen with pulse treatment of BI-9774. These data indicate that AMPK's inhibition of adipogenesis is independent of its inhibition of ACC and lipogenesis.

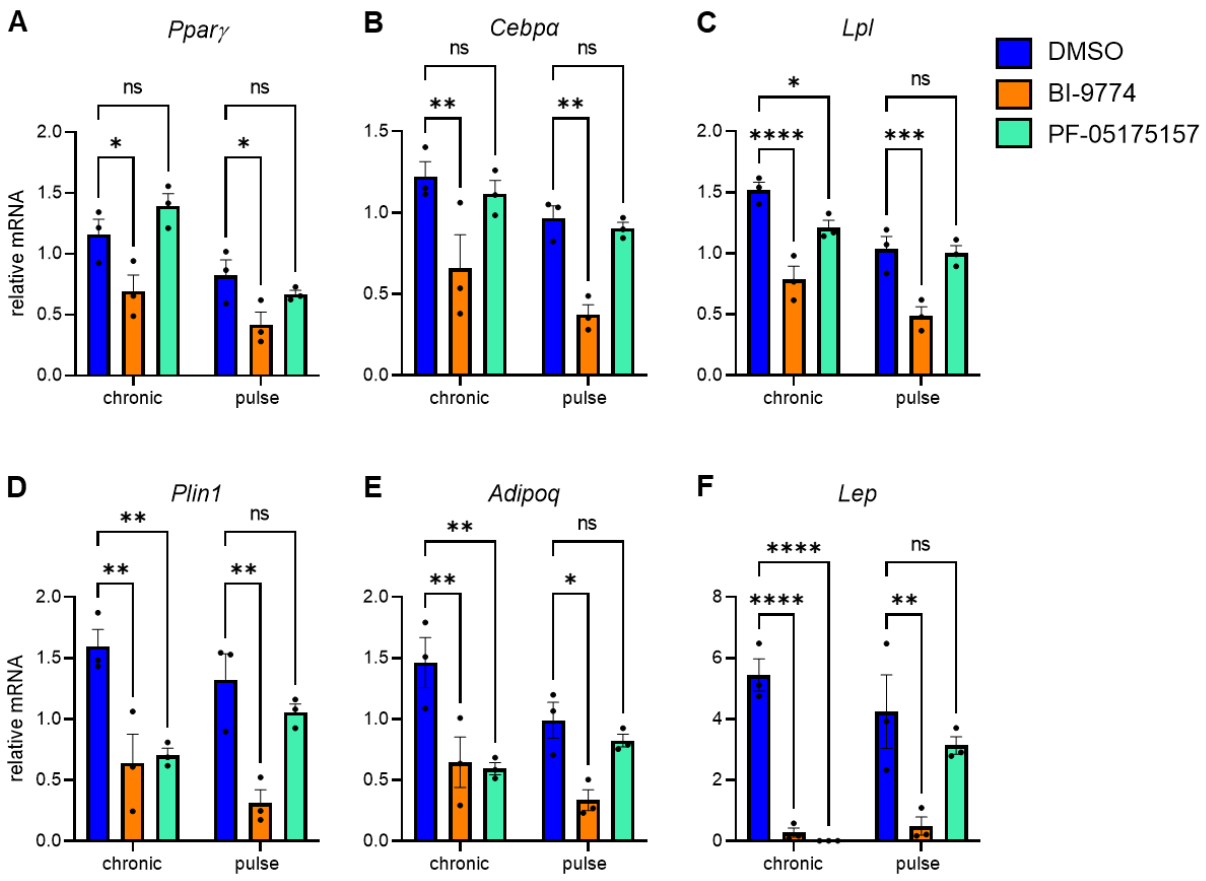


Figure 4.45 Comparative effect of pulse AMPK activation tp pulse ACC inhibition in adipogenesis on adipocyte marker gene expression

*(A-F) To pulse treat, either 1.25μM BI-9774 or 5μM PF-051575157 was added from day 0 to day 2 in adipogenesis and then removed, whilst for chronic treatment it was kept in throughout adipogenesis. Adipocyte marker gene expression is assessed at the end of adipogenesis. mRNA levels relative to housekeeping gene 36B4. Data are shown as mean ± SEM with statistical significance determined by two-way ANOVA with Šidák's correction for multiple comparisons, *p<0.05, **p<0.01, ***p<0.001, ****p<0.0001 (n=3).*

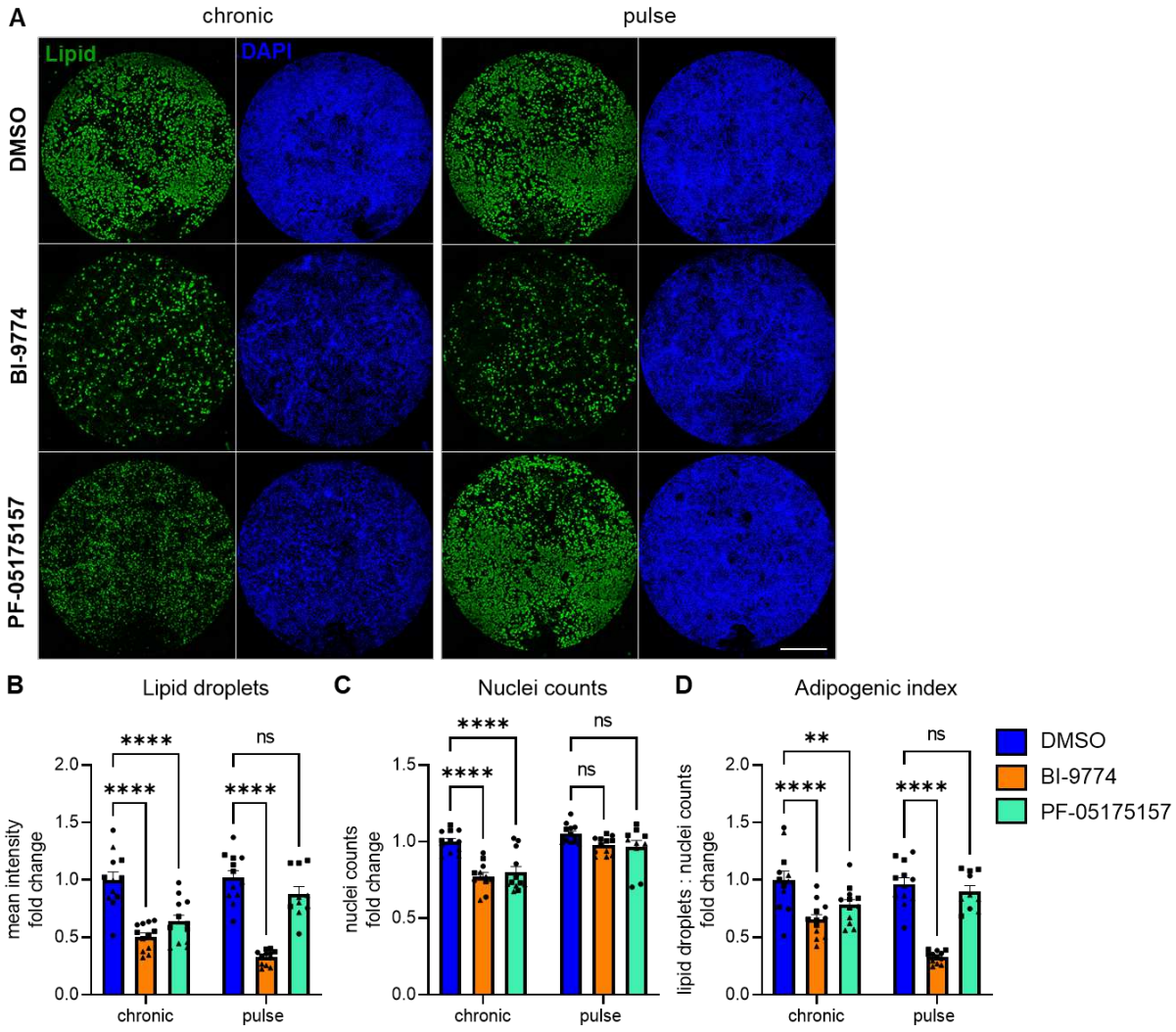
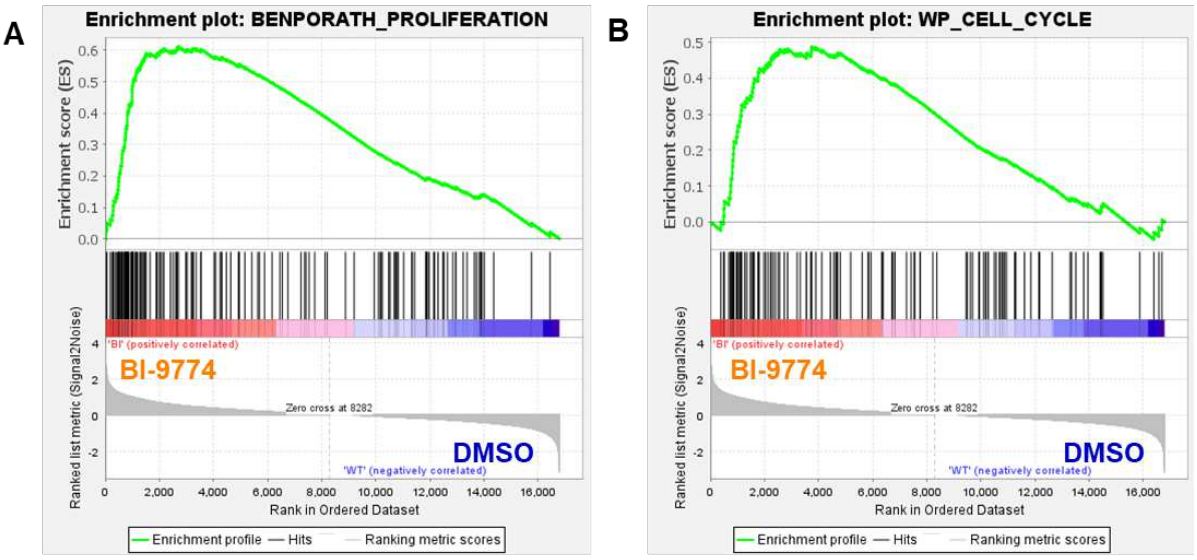


Figure 4.46 Effect of pulse ACC inhibition in adipogenesis on adipocyte formation

*To pulse treat, 1.25μM BI-9774 or 5μM PF-051575157 was added from day 0 to day 2 in adipogenesis and then removed, whilst for chronic treatment it was kept in throughout adipogenesis. (A) Representative images of whole well scans with lipid droplet and DAPI staining. Quantification of (B) lipid droplet staining (C) nuclei counts and (D) adipogenic index. Data are shown as mean ± SEM, with different biological replicates represented by different shaped symbols. Statistical significance is determined by two-way ANOVA with Šidák's correction for multiple comparisons, **p<0.01, ****p<0.0001, (n=3 mice, each represented by a different shaped symbol, SVF isolated on the same day, 8 technical replicates per mouse). Scale bar represents 1500μm.*

4.4 EFFECT OF AMPK ACTIVATION ON PROLIFERATION

From the RNA sequencing data, the Hallmark Gene sets (Figure 4.23) and the most significantly upregulated GO terms associated with differentially expressed genes (Figure 4.24A) show an increase in markers of the cell cycle. Further GSEA with the Benporath Proliferation gene set derived from proliferative tumour profiles (Ben-Porath et al., 2008; Hu et al., 2006) (Figure 4.47A) and the Wikipathway Cell Cycle gene set from Wikipathway 179 (Figure 4.47B) also showed enrichment in BI-9774 compared to WT SVF adipocytes. This was contradictory to what was seen with DAPI staining, where there were reductions in nuclei counts with BI-9774 (Figure 4.6 Characterisation of AMPK activation by BI-9774 in adipocytesFigure 4.6C).



NES: 2.33 q-val: 0.000

NES: 1.82 q-val: 0.000

Figure 4.47 GSEA plots for proliferation in BI-9774 vs WT

From the RNA sequencing data set the Benporath Proliferation and the WP Cell Cycle gene set enrichment plots showing enrichment with BI-9774 treatment.

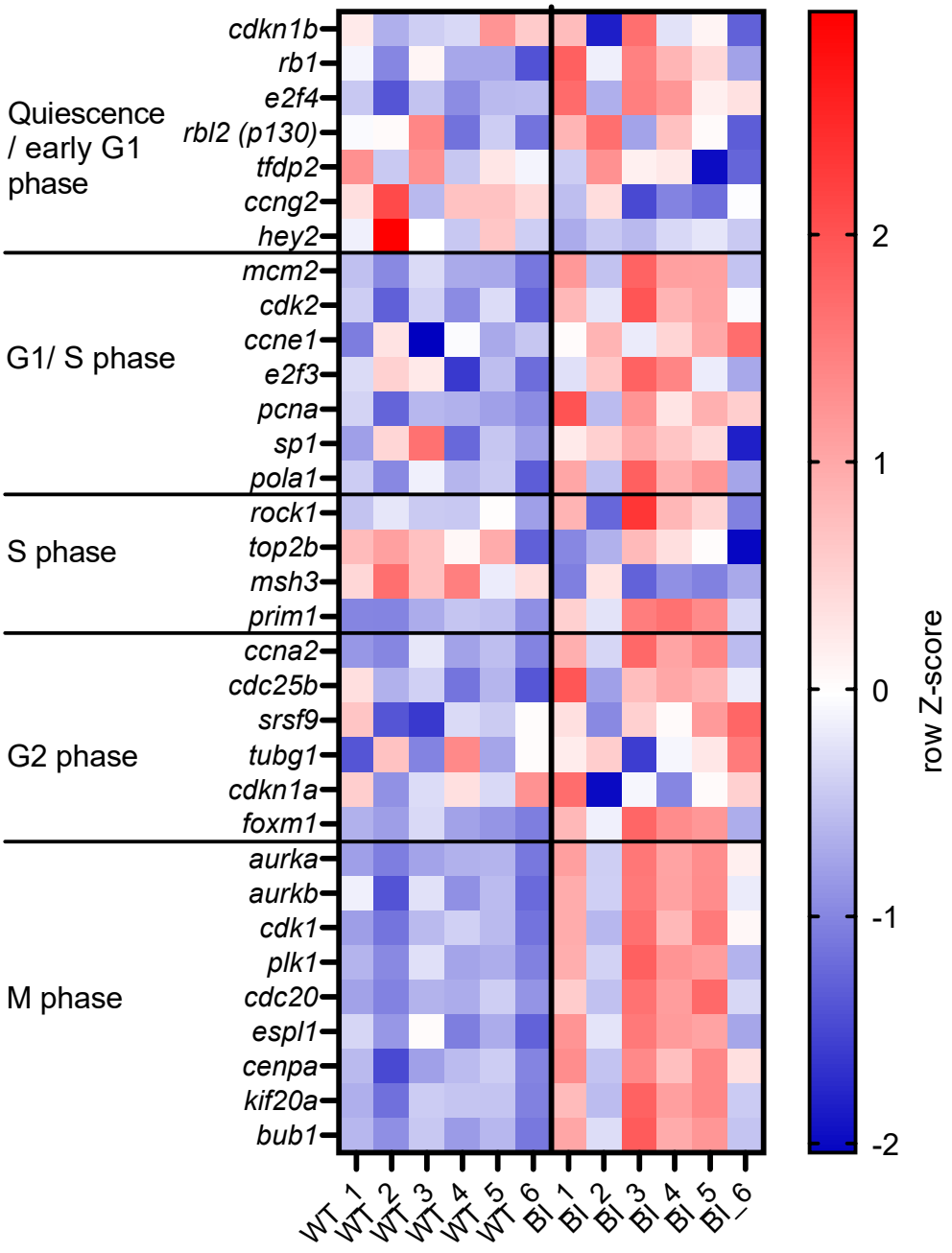


Figure 4.48 Cell cycle phases in SVF adipocytes

From the RNA sequencing data set, a heat map showing expression of adipocyte cell cycle phase markers in day 8 BI-9774 SVF adipocytes compared to WT SVF adipocytes. Dataset from Li, Hagberg et al.

It could be that the BI-9774 treated cells are paused in a particular stage of the cell cycle. The Whitfield gene sets for specific cell cycle stages were determined by thoroughly investigating the gene expression profiles of different cell cycle phases in HeLa cells (Whitfield et al., 2002). Using these gene sets for GSEA showed there was enrichment in BI-9774 treatment at every phase of the cell cycle (Table 4.4). Another more relevant published gene set obtained from cycling adipocytes (Li et al., 2021a) also showed increased expression with BI-9774 treatment in all cell cycle phases (Figure 4.48). Li, Hagberg et al. analysed a pure mature adipocyte population and there was a lack of expression of mitosis markers, and so it is likely that the proliferative signature is coming from the non-adipocyte cells.

Table 4.4 Whitfield gene set for cell cycle stages

Gene set	NES	q-value	Outcome
WHITFIELD_CELL_CYCLE_G1_S	1.57	0.004	enriched in BI-9774
WHITFIELD_CELL_CYCLE_S	1.69	0.002	enriched in BI-9774
WHITFIELD_CELL_CYCLE_G2	1.68	0.002	enriched in BI-9774
WHITFIELD_CELL_CYCLE_G2_M	2.05	0.000	enriched in BI-9774
WHITFIELD_CELL_CYCLE_M_G1	1.30	0.065	enriched in BI-9774

The nuclei counts from DAPI staining and the RNA sequencing data appear to be conflicting, therefore to assess proliferation throughout adipogenesis the IncuCyte cell imaging system with a live nuclear dye was employed. The effect of AMPK activation on cell number throughout adipogenesis was measured (Figure 4.49A) and from this the percentage increase or decrease over different growth phases was calculated (Figure 4.49B). Due to the high variability between replicates, none of the differences between BI-9774 and DMSO were significant. After the induction of differentiation up to day 2 the number of cells increased in both conditions, although at a slower rate in BI-9774 treatment leading to a lower nuclear count by day 2. Media was then exchanged for maintenance media and this is indicated with the black error bars. Media changes led to small reductions in cell number as some cells were washed away. Between day 2 and day 4 the number of cells increased in both conditions and at a similar rate so there are still fewer cells with BI-9774. After refreshing the maintenance media from day 4 to day 5 there was a reduction in cell number as some of the primary cells that were not proliferating or differentiating died, so that there

was a similar number of cells in both conditions. Whilst the nuclei counts in both the BI-9774 and the DMSO conditions initially increased at the same rate from day 5, the DMSO condition appeared to plateau whilst the BI-9774 condition appeared to reduce slightly.

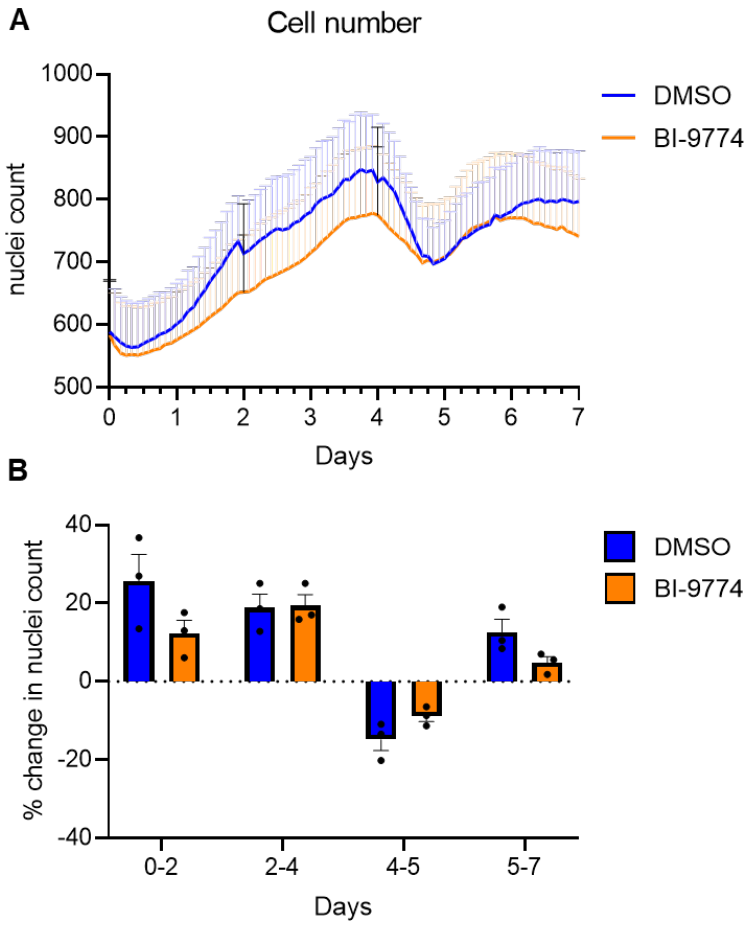


Figure 4.49 Change in nuclei counts throughout adipogenesis with AMPK activation
A live nuclear dye was incorporated into cells to measure nuclei count throughout adipogenesis with or without BI-9774 on the IncuCyte. (A) Changes in nuclei counts over time with black error bars indicating media changes. (B) Percentage change in nuclei counts over different days. Data are shown as mean ± SEM with statistical significance determined by two-way ANOVA with Šidák's correction for multiple comparisons (n=3).

Interestingly, although there were lower nuclei counts at day 2 of differentiation with activation of AMPK (Figure 4.50A), when BI-9774 was removed in a pulse treatment the nuclei counts likely fall to the same level as in the DMSO treatment and so there was no

significant difference in nuclei counts compared to the DMSO (Figure 4.38C, Figure 4.42C, Figure 4.50B). This again indicates that the events at the beginning of adipogenesis are important in determining the outcome. An improvement in the RNA sequencing study would have been to have conducted it on the pulse treated cells instead of the chronically treated cells as this may have removed the differences in cell cycle at the end point, allowing other changes to be more prominent.

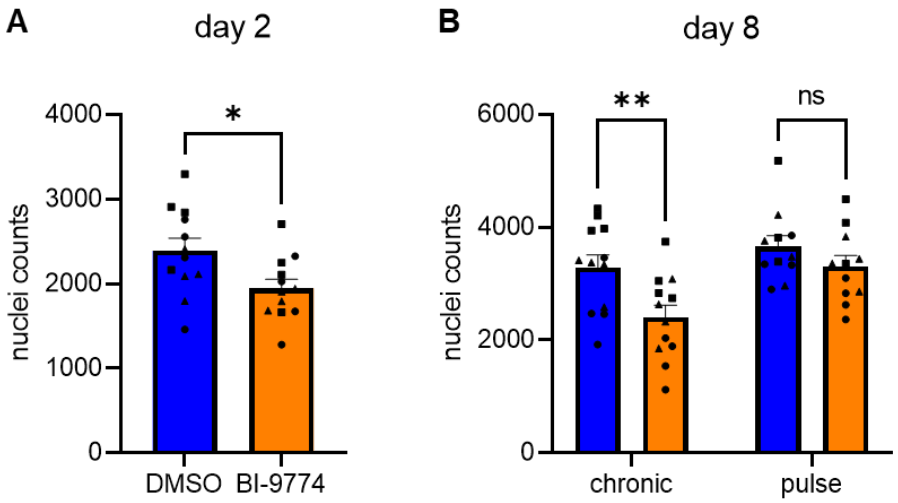


Figure 4.50 Effect of AMPK activation on proliferation throughout differentiation. *The SVF was differentiated to adipocytes with chronic and pulse treatment with BI-9774 and nuclei counts were assessed at (A) day 2 of adipogenesis and (B) day 8 at the end of adipogenesis. Data are shown as ± SEM with different biological replicates represented by different shaped symbols and statistical significance determined by (A) Student's t-test and (B) two-way ANOVA with Šidák's correction for multiple comparisons, *p<0.05, **p<0.01, (n=3 mice, each represented by a different shaped symbol, SVF isolated on the same day, 4 technical replicates per mouse).*

To see whether differences in cell number could also be accounted for by apoptosis, the number of caspase-3/7 expressing apoptotic cells were also measured throughout adipogenesis (Figure 4.51). Due to the high variability between replicates, none of the differences between BI-9774 and DMSO were significant. Of note, compared to the live nuclear counts the apoptotic nuclei counts seem relatively high, likely because these are primary cells, many of which don't survive long in culture. The apoptosis curve showed an

opposite path to the proliferative curve (Figure 4.49), as apoptotic rates remained steady up to day 2 and then decreased between days 2 and 4 as nuclear counts increased. The big drop in nuclear counts between days 4 to 5 corresponded to an increase in apoptosis at this time point, possibly due to undifferentiated cells being cleared. Apoptotic rate then stayed steady for the rest of adipogenesis. Overall there were fewer apoptotic events in the BI-9774 treated cells, and so apoptosis does not explain the reduction in nuclear counts.

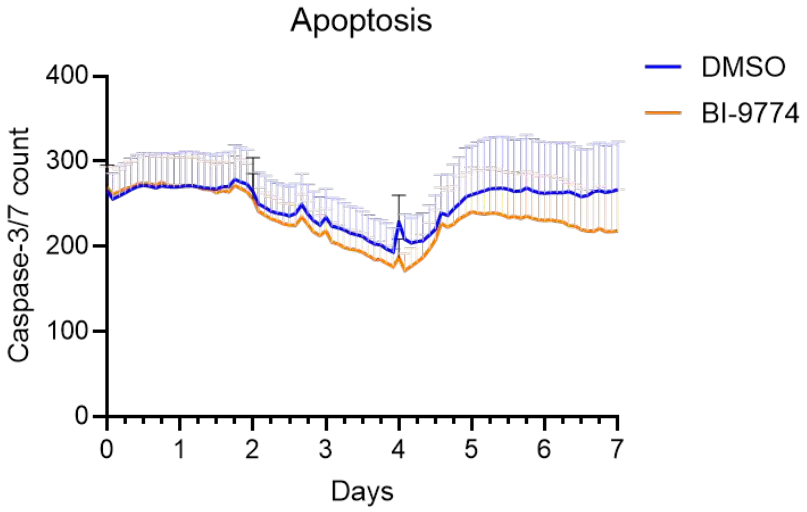


Figure 4.51 Live measurement of apoptosis throughout adipogenesis with AMPK activation

A live caspase-3/7 nuclear dye was incorporated into cells to measure apoptosis throughout adipogenesis with or without BI-9774 on the IncuCyte with black error bars indicating media changes. Apoptosis measured by caspase-3/7 dye count. Data are shown as mean ± SEM with statistical significance determined by two-way ANOVA with Šidák's correction for multiple comparisons (n=3).

One other possible growth event that may explain a reduction in cell number is if AMPK activation increases the number of cells exiting the cell cycle and entering senescence. Senescence has been described in adipose tissue, usually in response to stress from high fat diet or ageing (Le Pelletier et al., 2021; Li et al., 2021a; Pini et al., 2021; Smith et al., 2021). Exercise or metformin, both of which activate AMPK have been found to reduce adipose tissue senescence. SA-β-Gal staining along with DAPI staining was employed to determine the number of senescent cells at the end of differentiation. Representative images

show the adipocytes with Oil Red O stained lipid droplets and senescent cells in stained blue (Figure 4.52A). Quantification shows that there was a slight yet significant decrease in the proportion of senescent cells with BI-9774 (Figure 4.52B), in agreement with previous reports (Le Pelletier et al., 2021).

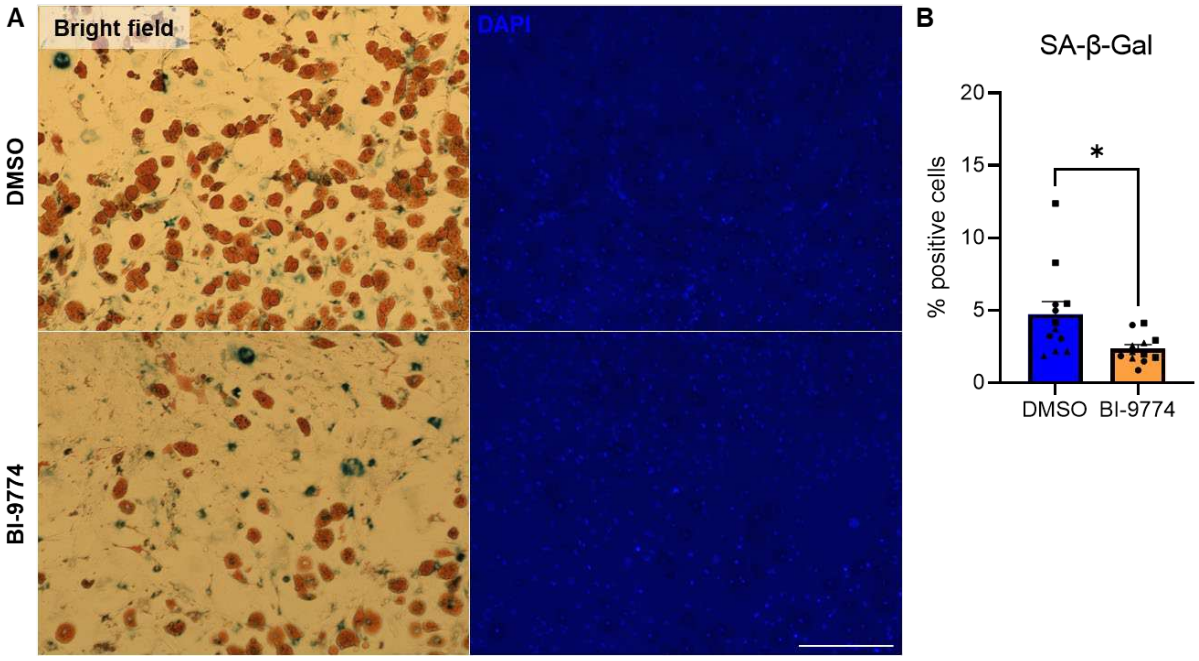


Figure 4.52 Effect of AMPK activation on senescence in adipogenesis

The SVF was differentiated to adipocytes with BI-9774 and the SA-β-gal assay was used to determine levels of senescence. (A) Representative images of senescence assay with SA-β-gal positive cells in blue and Oil Red O staining adipocyte lipid droplets. (B) Quantification of senescence with numbers of SA-β-gal positive cells normalised to total cell number. Data are shown as mean ± SEM with different biological replicates represented by different shaped symbols and statistical significance determined by Student's t-test with Welch's correction (n=3 mice, each represented by a different shaped symbol, SVF isolated on the same day, 4 technical replicates per mouse). Scale bar represents 275μm.

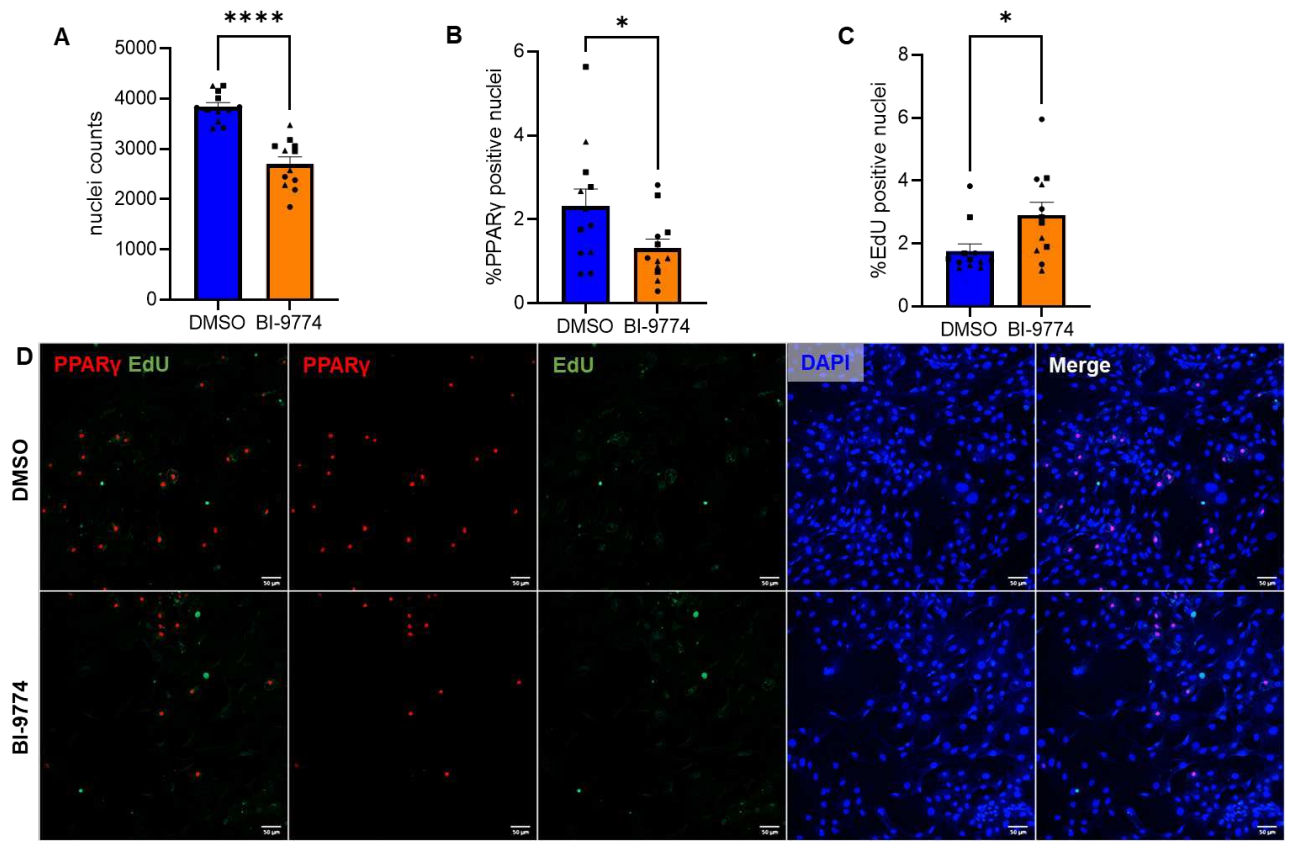


Figure 4.53 Effect of AMPK activation on proportion of proliferating cells

*The SVF was differentiated to adipocytes with BI-9774 and were incubated with EdU at the end of differentiation. (A) Nuclei counts and percentage of (B) PPARγ and (C) EdU positive nuclei. (D) Representative images showing non-overlapping PPARγ and EdU expressing nuclei in DMSO and BI-9774 treated cells. Data are shown as ± SEM with different biological replicates represented by different shaped symbols and statistical significance determined by Student's t-test with Welch's correction for (B), *p<0.05, ****p<0.0001 (n=3 mice, each represented by a different shaped symbol, SVF isolated on the same day, 4 technical replicates per mouse). Scale bar represents 50µm.*

It is most likely that BI-9774 reduces nuclei counts by slowing proliferation. However, this is still at odds with RNA sequencing data showing an increase in markers of the cell cycle. One theory to explain this discrepancy is that the increase in cell cycle and proliferative gene expression is a side effect of there being more differentiated adipocytes, and therefore fewer dividing cells in the DMSO control compared to the BI-9774 treated group. To look at the effect of AMPK activation on the amount of dividing cells at the end of differentiation, labelling of incorporated EdU at the end of differentiation was assessed. As expected, there were fewer cells with BI-9774 treatment (Figure 4.53A), as well as a smaller proportion of PPARγ expressing cells with BI-9774 treatment (Figure 4.53B). Meanwhile, there was a greater proportion of EdU labelled nuclei with BI-9774 treatment (Figure 4.53C). Representative images show that the PPARγ expressing cells are not the same population as the EdU expressing cells, and so the proliferative signature is coming from the non-adipocyte population (Figure 4.53D). So even though AMPK activation slows proliferation leading to lower nuclear counts at the end of differentiation, there are fewer differentiated cells and more cells with proliferative ability.

4.5 EFFECT OF AMPK ACTIVATION ON LIPID DROPLET SIZE

4.5.1 AMPK activation reduces lipid droplet size

In addition to reducing adipogenesis, pharmacological activation of AMPK in adipocyte differentiation alters adipocyte morphology by reducing lipid droplet size in a dose dependent manner (Figure 4.54). For an indirect measurement of lipid content, SVF adipocytes differentiated with 1.25 and 10μM BI-9774 or with DMSO were stained with Oil Red O. There was a visible reduction in Oil Red O staining with BI-9774 treatment in whole well scans and in x10 magnification images (Figure 4.55). Quantification of Oil Red O staining showed a dose dependent reduction with pharmacological activation of AMPK, indicating reduced lipid content in the wells (Figure 4.55B).

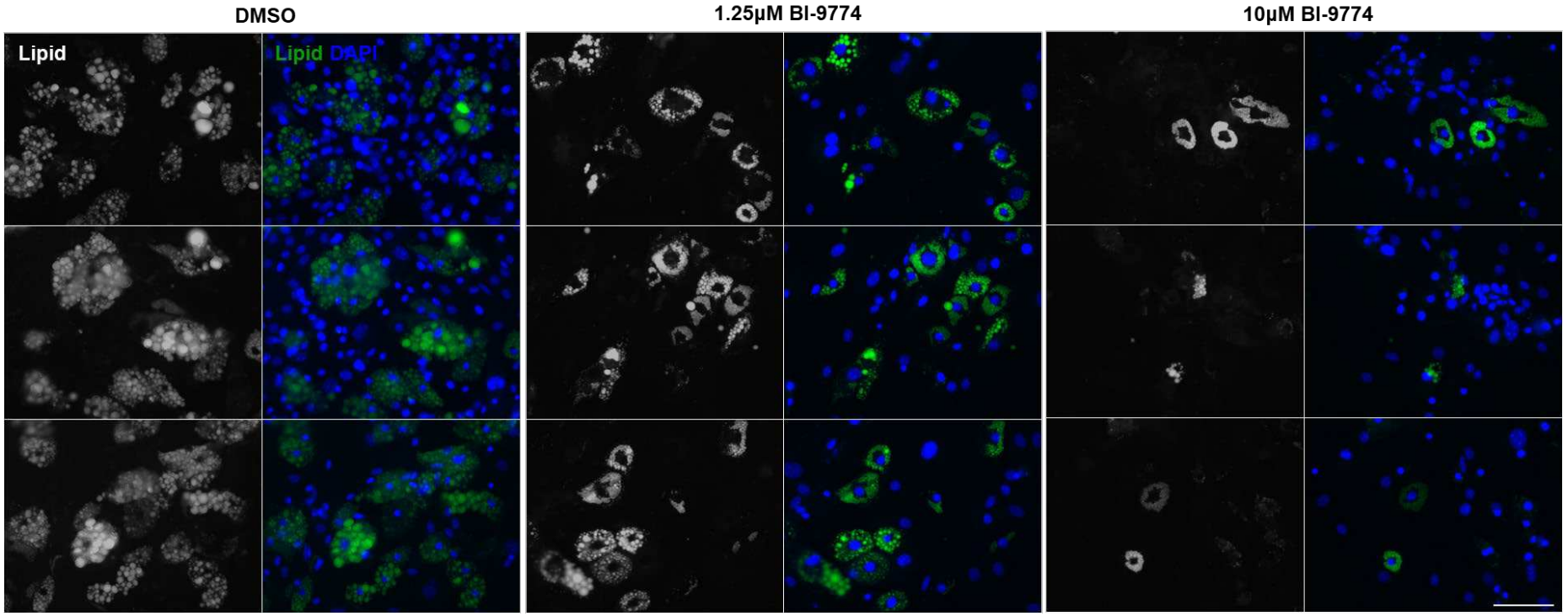


Figure 4.54 Effect of AMPK activation on adipocyte lipid droplet size

Representative images showing SVF derived adipocytes differentiated with 1.25μM and 10μM BI-9774 with lipid droplet and nuclear staining. Scale bar represents 75μm.

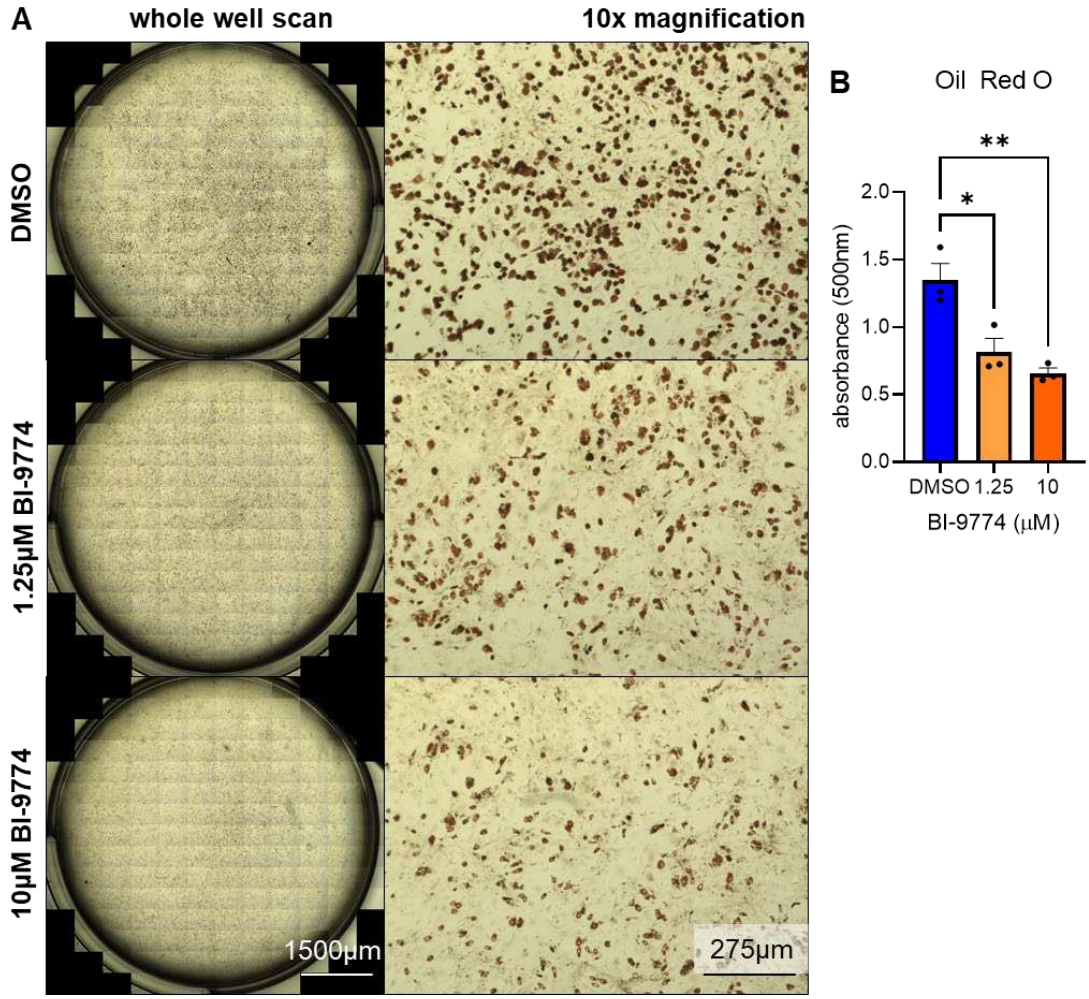


Figure 4.55 Characterisation of AMPK activation on lipid content in SVF adipocytes *Representative images showing SVF derived adipocytes differentiated with 1.25µM and 10µM BI-9774 and lipid is stained with Oil Red O. (A) Representative whole well scan and 10x magnification of Oil Red O stained adipocytes. (B) Quantification of total Oil Red O. Data are shown as mean ± SEM with statistical significance determined by one-way ANOVA with Dunnett's correction for multiple comparisons, *p<0.05, **p<0.01, (n=3). Scale bar represents 1500µm for the whole well scans and 275µm for the 10x magnifications.*

Due to their 3D nature, adipocytes are challenging to image. Lipid droplets in an adipocyte may be on top of one another, and usually large lipid droplet edges are blurred by many small lipid droplets that sit on their edges. However, quantification of lipid droplet size is essential to know the effect of AMPK activation and so Harmony, the high-content image analysis software was used to evaluate x10 magnification images of DAPI and lipid droplet stained cells acquired on the Operetta high-content imaging system (Figure 4.56). Firstly, nuclei were used to locate cells and any positioned on the edges of an image were

discarded. Then lipid droplet staining around the nucleus was used to identify the adipocytes and within the adipocytes individual lipid droplets were distinguished and their parameters determined. Whilst this method is not perfect, it is capable of capturing most of the adipocyte lipid droplets. Using this method, it was determined that AMPK activation reduced the average area of lipid droplets (Figure 4.57A). 1.25μM BI-9774 almost reached significance and 10μM BI-9774 led to a significant decrease. 1.25μM BI-9774 caused there to be a greater proportion of lipid droplets between 50-100μm^2 and a lower proportion that are greater than 100μm^2 in comparison to the DMSO treatment (Figure 4.57B). Meanwhile, 10μM BI-9774 shifted the lipid droplet size distribution so that there was an increase in the proportion of lipid droplets below 50μm^2 and reduction in the proportion of lipid droplets over 100μm^2. So, activation of AMPK reduces the average lipid droplet size by impeding the formation of large lipid droplets so that there is a greater amount of small lipid droplets.

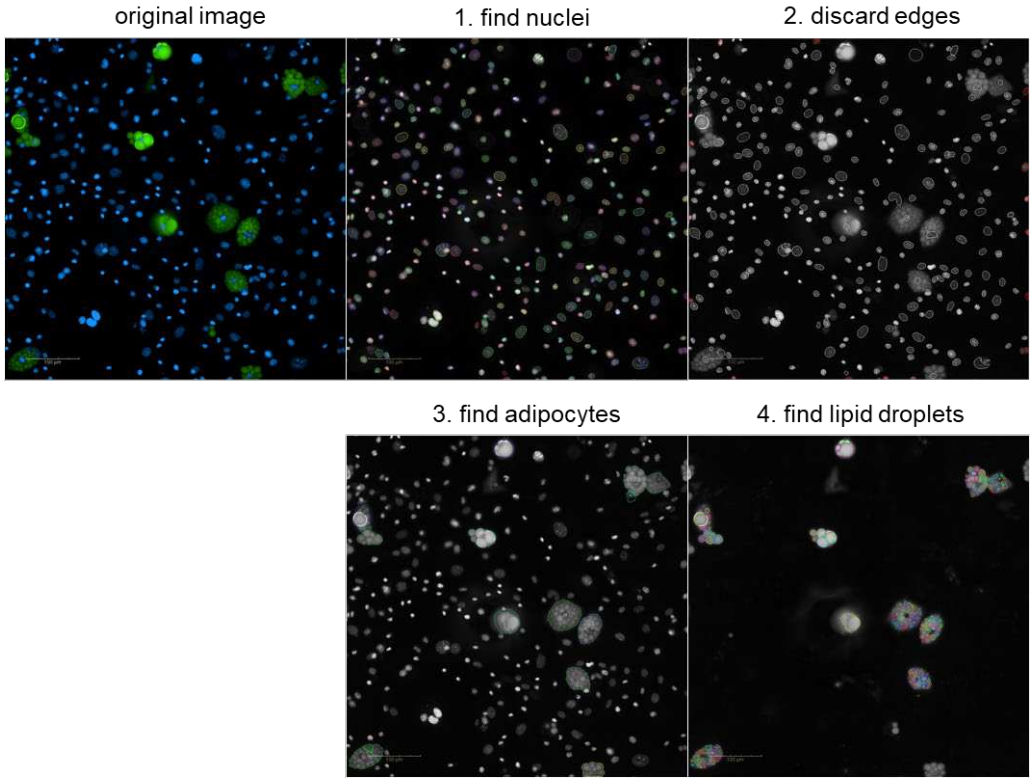


Figure 4.56 Method for measuring lipid droplet parameters

SVF adipocytes were stained for lipid droplets and nuclei and scanned on the Operetta. Harmony software was used to derive lipid droplet parameters. To identify lipid droplets, nuclei were identified and any on the edges were discarded. Then the adipocytes were

identified by selecting the cells with green surrounding the nucleus, and then individual lipid droplets within the cytoplasm were identified. Scale bar represents 100µm.

There are several potential explanations for why an adipocyte could have smaller lipid droplets. Reduction in lipid droplet size occurs during lipolysis which provides fatty acids to fuel thermogenesis. It was also a feature of the D316A iWAT and in browning of adipose tissue where fatty acids released from lipolysis fuels thermogenesis (Pollard et al., 2019). However, there was no increase in HSL activity or thermogenic protein expression in the BI-9774 SVF adipocytes (Figure 4.28, Figure 4.29).

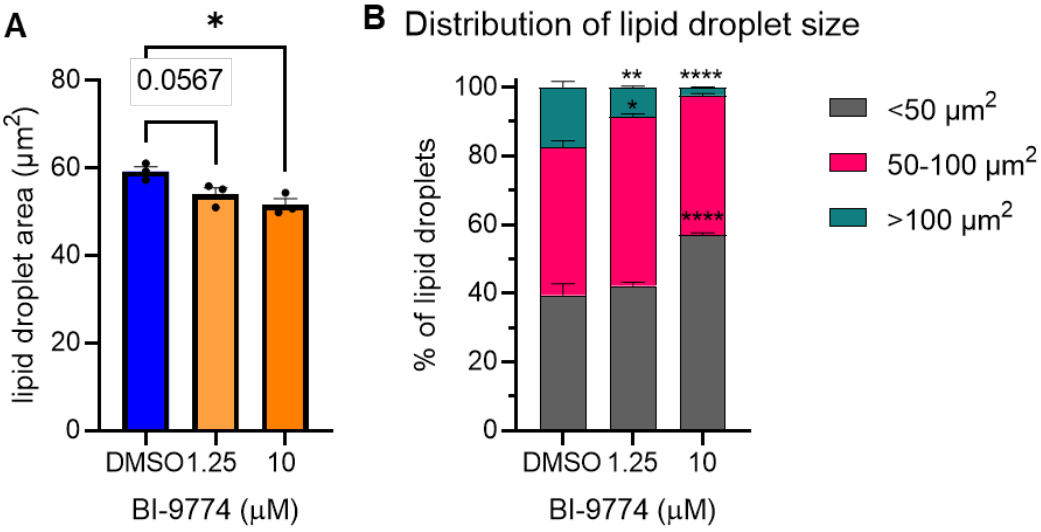


Figure 4.57 Quantification of effect of BI-9774 on lipid droplet size
*The SVF was differentiated to adipocytes with 1.25µM and 10µM BI-9774 with lipid droplet and nuclear staining imaged on the Operetta. Lipid droplet size was quantified with Harmony. (A) Mean average lipid droplet size at a lower and higher concentration of BI-9774. (B) Distribution of lipid droplet size. Data are shown as mean ± SEM with statistical significance determined by (A) one-way ANOVA with Dunnett's correction for multiple comparisons or (B) two-way ANOVA with Dunnett's correction for multiple comparisons, *p<0.05, **p<0.01, ****p<0.0001 (n=3).*

Lipid droplet expansion is controlled by CIDEC which regulates formation of pores for neutral lipid transfer from smaller to larger lipid droplets (Figure 4.58A) (Jambunathan et al., 2011).

From the RNA sequencing data, normalised counts showed a reduction in *Cidec* with AMPK activation (Figure 4.58B), which was reflected in mRNA levels (Figure 4.58C). CIDEC is an adipocyte associated protein, and so reductions in *Cidec* may reflect a reduction in overall adipocyte levels as opposed to a reduction in *Cidec* expression per adipocyte. To account for the reduction in adipocytes, *Cidec* normalised counts and mRNA levels were normalised to expression of adipocyte marker genes *Pparγ*, *Cebpα*, *Lpl*, *Plin1*, *Adipoq* and *Leptin*. Relative to adipocyte markers the significant reduction in *Cidec* normalised counts (Figure 4.58D) and mRNA (Figure 4.58E) remained.

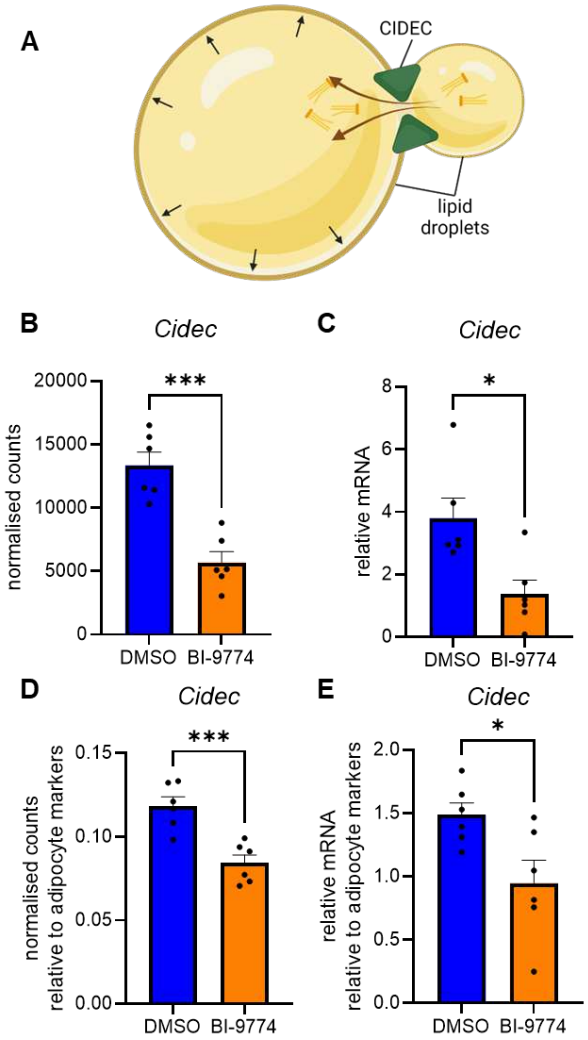


Figure 4.58 Effect of AMPK activation on Cidec in adipocytes

The SVF was differentiated to adipocytes with BI-9774 and expression of Cidec was assessed at the end of differentiation. (A) Diagram of CIDEC function in adipocytes. (B)

*Cidec normalised counts from RNA sequencing and (C) Cidec mRNA expression. To account for a reduction in adipocytes, (D) normalised counts when averaged over normalised counts of adipocyte marker genes and (E) Cidec mRNA expression when averaged over mRNA expression of adipocyte marker genes to account for the reduction in adipogenesis with BI-9774. All mRNA normalised to housekeeping gene 36B4. Adipocyte marker genes for normalization are Pparγ, Cebpα, Lpl, Plin1, Adipoq and Leptin. Data are shown as mean ± SEM with statistical significance determined by Student's t-test, *p<0.05, ***p<0.001, (n=6).*

Whilst the reductions of *Cidec* gene expression levels is interesting, knowing the whether this effect of AMPK activation translates to a reduction in CIDEC protein levels is important. Two commercial anti-CIDEC antibodies were tested: Abcam 213693 and Novus NB100-430. Both antibodies tended to give faint and non-specific bands (Figure 4.59A, B). When tested on a different set of samples, the Novus NB100-430 antibody detected a single band with ECL, and whilst there was a reduction with 10μM BI-9774, it was not significant (Figure 4.59C, D). Subsequently, immunocytochemistry with the NB100-430 antibody didn't show lipid droplet membrane specific staining (Figure 4.59E). Instead, there was general cytoplasmic staining and nuclear staining. The Abcam 213693 antibody datasheet states that due to sequence homology, the antibody may cross-react with CIDEA, which exhibits nuclear expression (Konige et al., 2014). It may be that the antibodies are detecting both CIDE isoforms. The inconsistency of the antibodies in this system made investigating CIDEC protein levels unreliable.

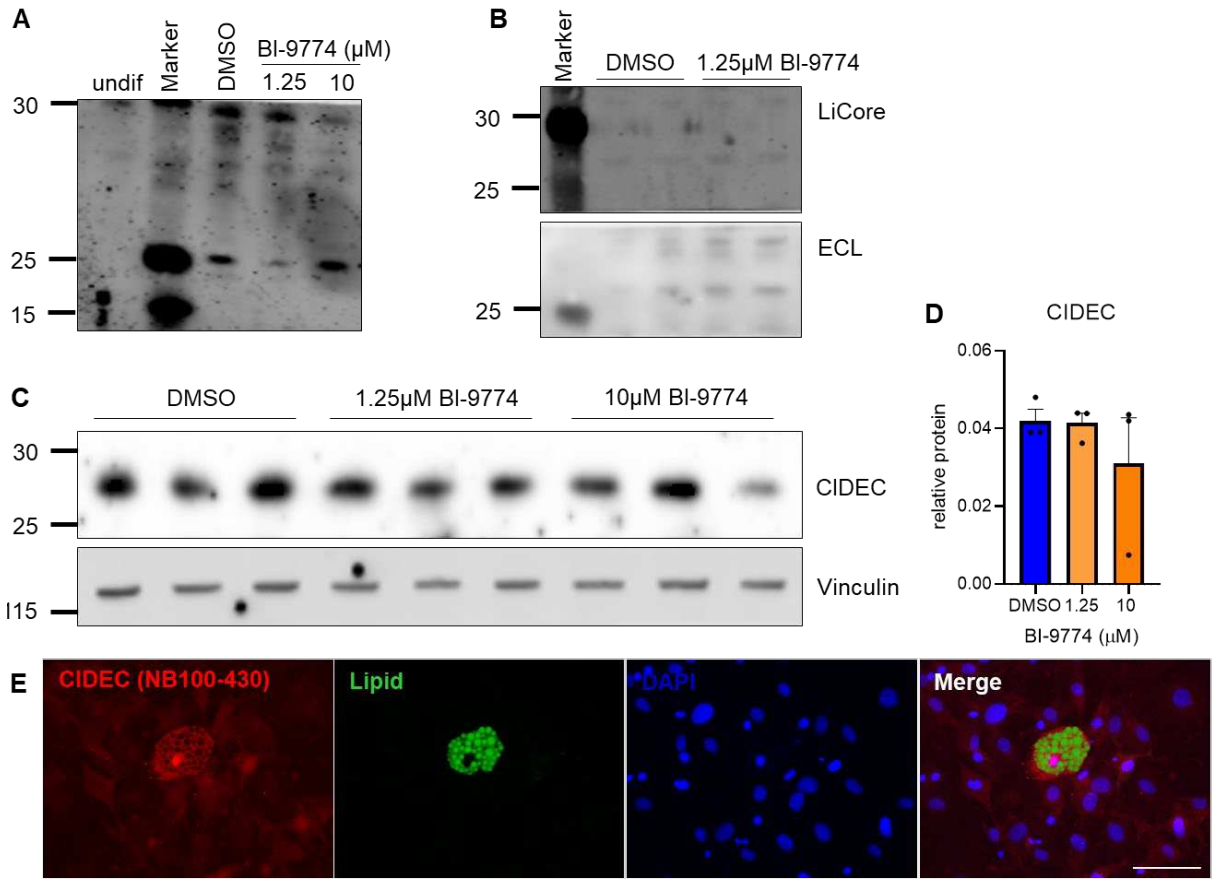


Figure 4.59 Effect of AMPK activation on CIDEC in adipocytes

The SVF was differentiated to adipocytes with BI-9774 and expression of CIDEC was assessed at the end of differentiation. (A) Abcam 213693 antibody detected on LiCore with 1.25 and 10μM BI-9774, with an undifferentiated control that should be negative for CIDEC expression. (B) Novus NB100-430 antibody detected on LiCore (above) and ECL (below) with 1.25μM BI-9774. (C) Novus NB100-430 antibody detected on ECL with 1.25 and 10μM BI-9774 with (D) quantification relative to vinculin. (E) Immunocytochemistry with the Novus NB100-430 antibody in a DMSO treated adipocyte. Data are shown as mean ± SEM with statistical significance determined by one-way ANOVA with Dunnett's correction for multiple comparisons (n=3). Scale bar represents 75μm.

AMPK's inhibition of lipogenesis could also explain the reduction of lipid droplet size. Chronic treatment with 5μM ACC inhibitor PF-05175157 to reduce fatty acid synthesis gave a strong visible reduction in lipid droplet size which was significant upon quantification (Figure 4.60A, B). There was a strong shift in the lipid droplet size distribution with PF-05175157, with an

increase in lipid droplets 50μm^2 and a decrease in lipid droplets over 50μm^2 (Figure 4.60C). 5μM PF-05175157 gave a much greater reduction in lipid droplet size compared to 10μM BI-9774 and may be a more potent inhibitor of fatty acid synthesis than the AMPK activator (Figure 4.54, Figure 4.60A). So reduction in lipid droplet size could be due reductions in CIDEC, reductions in lipogenesis or both.

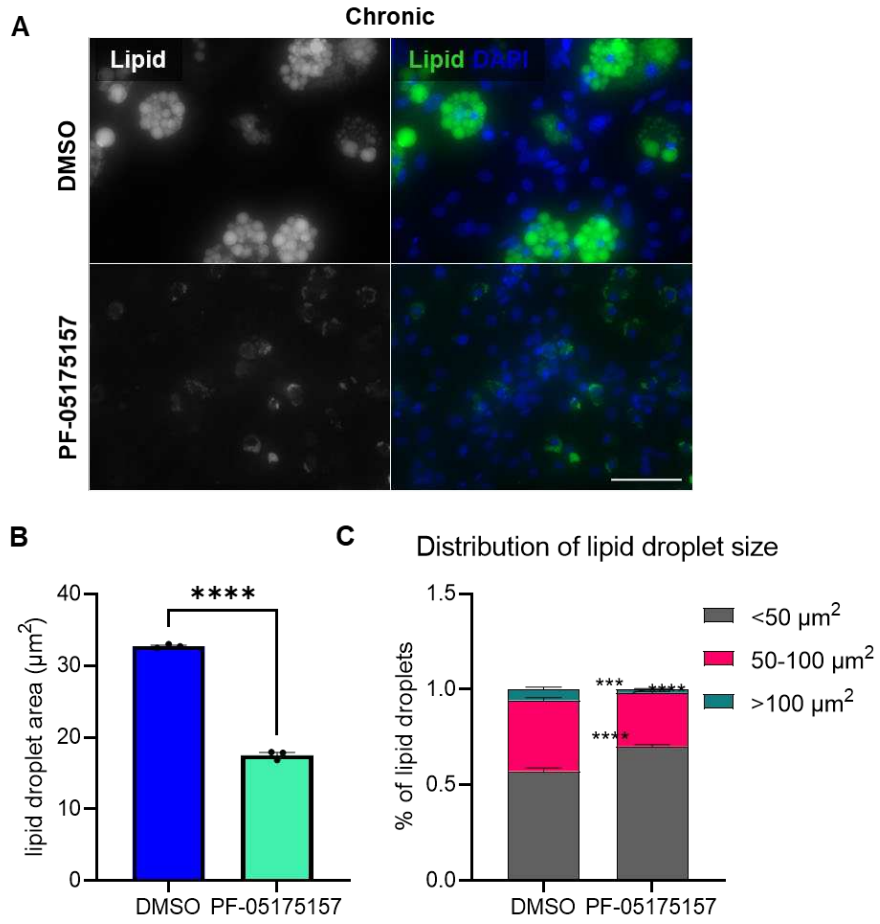


Figure 4.60 Effect of inhibition of ACC on lipid droplet size

*The SVF was differentiated to adipocytes with chronic treatment with PF-05175157 with lipid droplet and nuclear staining imaged on the Operetta. Lipid droplet size was quantified with Harmony. (A) Representative images of adipocytes with chronic treatment of PF-05175157. (B) Mean average lipid droplet size quantification. (C) Lipid droplet size distribution. Data are shown as mean ± SEM with statistical significance determined by Student's t-test (B) or two-way ANOVA with Dunnett's correction for multiple comparisons (C), ***p<0.001, ****p<0.0001, (n=3). Scale bar represents 75μM.*

4.5.2 Lipid droplet size as a measure of adipocyte maturity

Adipocytes with smaller lipid droplets may indicate stunted maturation (Figure 4.57). The Burton Adipogenesis gene sets group together genes associated with different stages of 3T3-L1 adipogenesis (Burton et al., 2004). In the RNA sequencing data there was enrichment in WT SVF adipocytes in gene sets associated with the final stages of adipogenesis, as expected (Table 4.5). There was enrichment in gene sets associated with the early and middle stages of adipogenesis in the BI-9774 SVF adipocytes. This could be an artefact of there being more mature adipocytes in the DMSO conditions. However, there was no significant enrichment for either group in the 0 hour or 2 hour upregulated gene sets. Therefore, it's possible that the AMPK activated cells are arrested in a less mature adipocyte stage, and one output of this is smaller lipid droplets.

Table 4.5 Burton Adipogenesis gene sets for stages of adipogenesis

Gene set	Time point	NES	q-value	Outcome
BURTON_ADIPOGENESIS_PEAK_AT_0_HR	0 hours	-1.10	0.326	no enrichment
BURTON_ADIPOGENESIS_1	2 hours	1.05	0.432	no enrichment
BURTON_ADIPOGENESIS_2	8 hours	1.16	0.231	enriched in BI-9774
BURTON_ADIPOGENESIS_3	16-24 hours	2.57	0.000	enriched in BI-9774
BURTON_ADIPOGENESIS_4	8-48 hours	-1.40	0.045	enriched in DMSO
BURTON_ADIPOGENESIS_5	48-96 hours	-2.71	0.000	enriched in DMSO
BURTON_ADIPOGENESIS_6	96 hours	-2.87	0.000	enriched in DMSO

If AMPK activation stunts adipocyte maturation and this is linked to its mechanism of suppressing adipogenesis, it may be that the effect on lipid droplet size is observed with the pulse treatment with BI-9774 in adipogenesis. Representative images demonstrate that there may still be a reduction in lipid droplet size with pulse activation of AMPK (Figure 4.61A). Compared to chronic activation of AMPK, pulse treatment did not lead to a significant reduction in the mean lipid droplet area, although there was a tendency for smaller lipid droplets (Figure 4.61B). The distribution of lipid droplet size in the pulse treatment showed minor changes, with negligible differences with 1.25μM BI-9774 and a slight but significant increase in lipid droplets under 50μm^2 with 10μM BI-9774 compared to

DMSO treated cells (Figure 4.61C). Whilst the small change in lipid droplet size distribution may point to the smaller lipid droplets being an effect from earlier activation of AMPK, AMPK needs to be activated throughout adipogenesis with higher concentrations of activator to significantly reduce lipid droplet size.

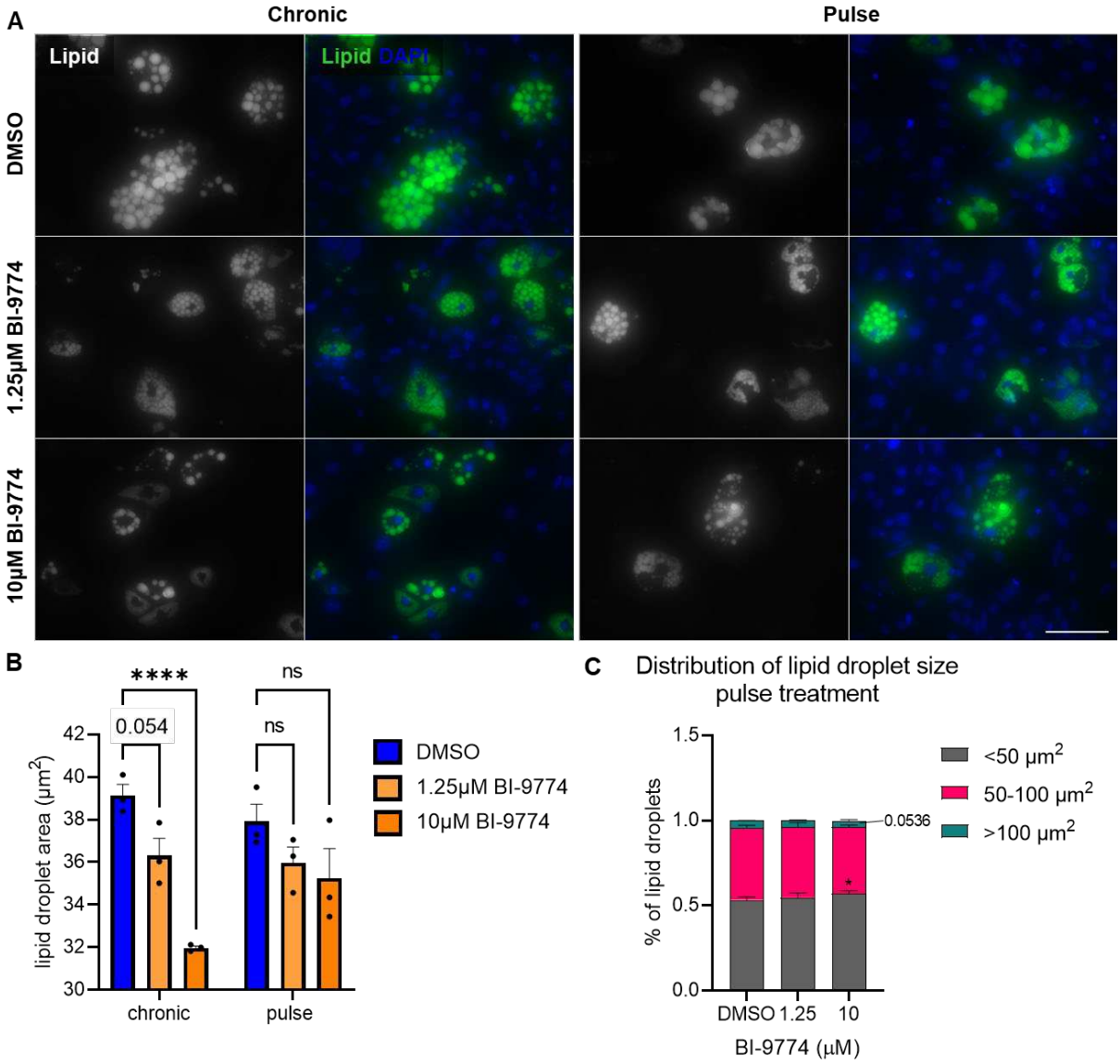


Figure 4.61 Comparison of chronic and pulse BI-9774 treatments

The SVF was differentiated to adipocytes with chronic or pulse treatment with BI-9774 with lipid droplet and nuclear staining imaged on the Operetta. Lipid droplet size was quantified with Harmony. (A) Representative images of adipocytes with chronic and pulse treatment of BI-9774. (B) Mean average lipid droplet size quantification. (C) Lipid droplet size distribution.

*Data are shown as mean ± SEM with statistical significance determined by one-way ANOVA with Dunnett's correction for multiple comparisons (B) or two-way ANOVA with Dunnett's correction for multiple comparisons (C), *p<0.0332, ****p<0.0001, (n=3). Scale bar represents 75μM.*

4.6 EFFECT OF AMPK ACTIVATION IN MATURE ADIPOCYTES

Pharmacological activation of adipose tissue AMPK in a clinically relevant *in vivo* setting would target mature adipocytes as well as adipocyte progenitors. In addition, in the D316A mouse AMPK would have been constitutively active in the mature adipocytes. To look at the effect of AMPK activation in mature adipocytes, the SVF of WT mice was differentiated and once mature adipocytes had developed, they were treated with 1.25 and 10μM BI-9774 for 3 days. Firstly, level of AMPK activation was assessed by Western blotting (Figure 4.62A). Both concentrations of BI-9774 gave a significant increase in phosphorylation of ACC (Figure 4.62B). They also both led to increases in phosphorylation of ULK1 and AMPKα, although not significant (Figure 4.62C, D). However, as ACC phosphorylation is significantly increased, there was enough evidence to say that AMPK was activated with 1.25 and 10μM BI-9774.

Activation of AMPK in mature adipocytes did not affect the number of cells or the adipogenic index (Figure 4.63), neither did it effect adipocyte morphology, as there was no difference in lipid droplet size (Figure 4.63A). Here, x20 magnification images and Columbus software was used to calculate the adipogenic index.

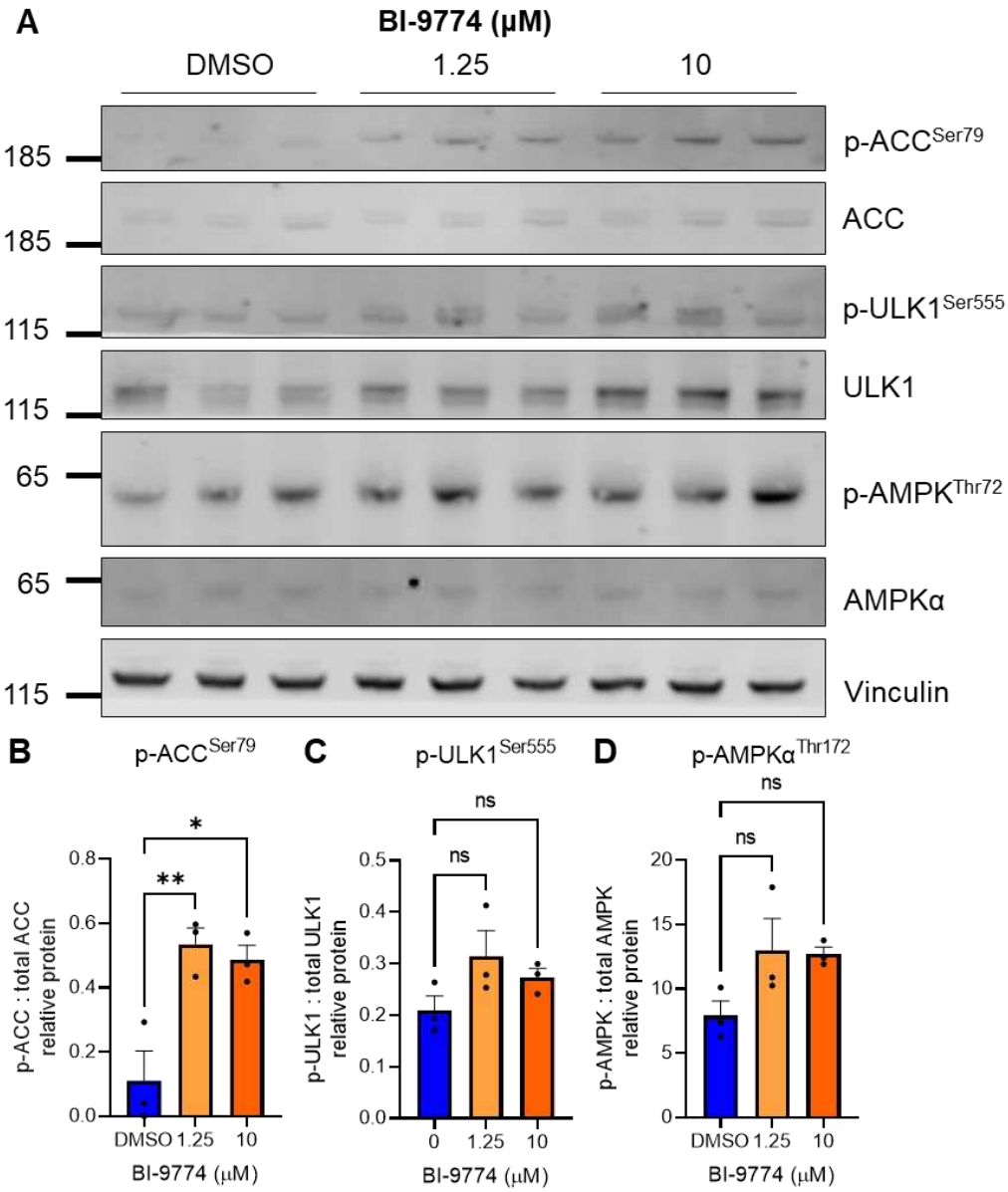


Figure 4.62 AMPK activation in mature adipocytes

*The SVF was differentiated and after mature adipocyte formation was treated with 1.25 or 10μM BI-9774 for 3 days. (A) Western blot showing phosphorylation of AMPK targets with quantification of (B) p-ACC relative to ACC, (C) p-ULK1 relative to ULK1 and (D) p-AMPK relative to AMPK, all relative to vinculin. Data are shown as mean ± SEM with statistical significance determined by one-way ANOVA with Dunnett's correction for multiple comparisons, *p<0.05, **p<0.01 (n=3).*

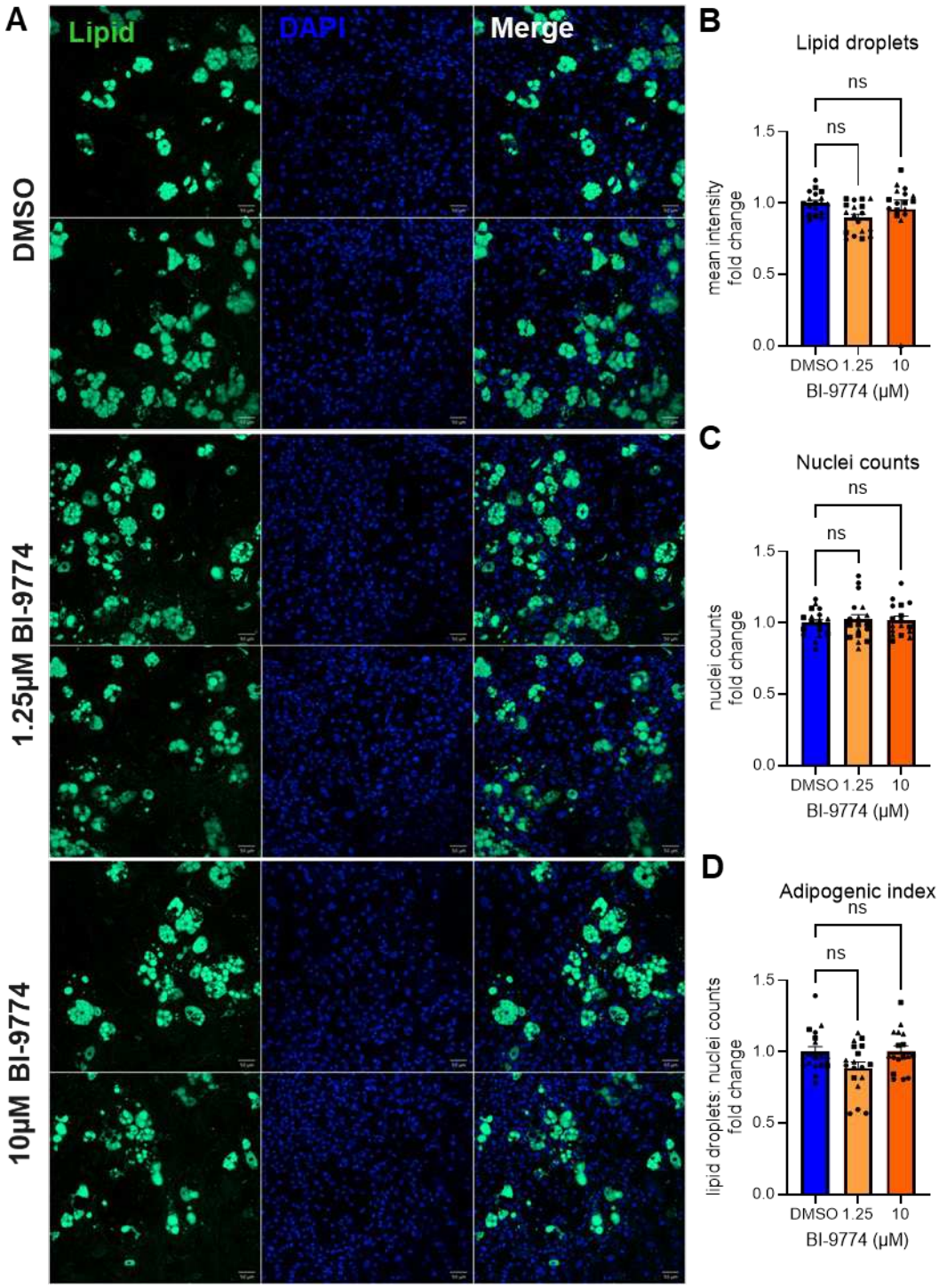


Figure 4.63 Effect of AMPK on adipogenesis in mature adipocytes

The SVF was differentiated and after mature adipocyte formation was treated with 1.25µM and 10µM BI-9774 for 3 days. (A) Representative images of adipocytes with lipid droplet and

DAPI staining. Quantification of (B) lipid droplet staining (C) nuclei counts and (D) adipogenic index. Data are shown as mean ± SEM with statistical significance determined by one-way ANOVA with Dunnett's correction for multiple comparisons (n=3 mice, each represented by a different shaped symbol, SVF isolated on the same day, 6 technical replicates per mouse). Scale bar represents 50μm.

Adipocytes in culture have the potential to dedifferentiate and this can be stimulated for example by expression of the immortalisation agent Simian Virus 40-Large T antigen, or by the addition of rapamycin to inhibit mTOR (Kim and Chen, 2004; Liu et al., 2019). Early-stage adipocyte markers *Pparγ* and *Cebpα* showed no change in expression with 3 days of activation of AMPK (Figure 4.64A, B). Mid and late-stage markers *Lpl*, *Plin1* and *Adipoq* all show reductions with 10μM BI-9774, although not significant (Figure 4.64C-E). *Leptin* once again stands out from the other adipocyte markers and shows a significant reduction in expression with 10μM BI-9774 (Figure 4.64F). It may be that longer activation of AMPK could stimulate dedifferentiation and significant reduction in adipocyte markers. However, it does not appear that this is occurring within 3 days. On the other hand, AMPK may be able to regulate leptin by an unexplored mechanism that is separate to its regulation of adipogenesis.

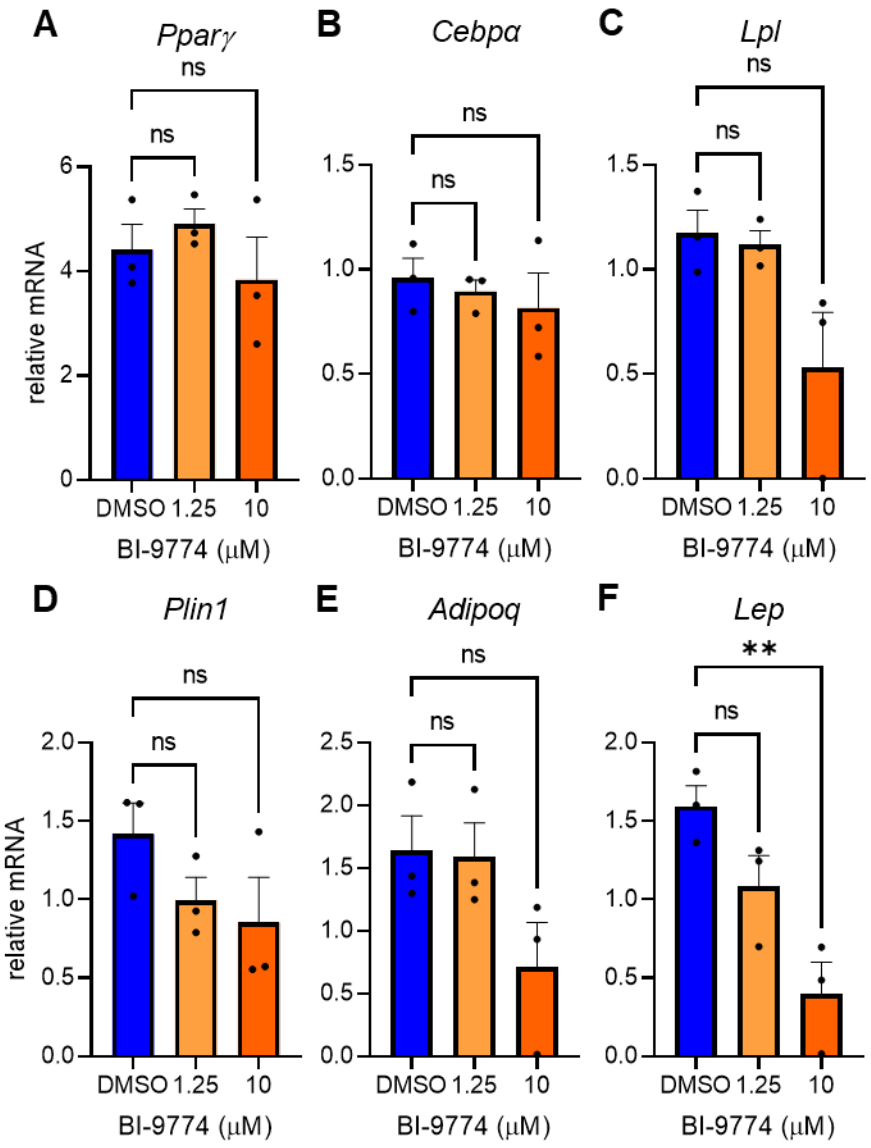


Figure 4.64 Effect of AMPK activation in mature adipocytes on adipocyte marker genes

*(A-F) The SVF was differentiated and after mature adipocyte formation was treated with 1.25μM and 10μM BI-9774 for 3 days, with adipocyte marker gene mRNA expression assessed. mRNA levels relative to housekeeping gene 36B4. Data are shown as mean ± SEM with statistical significance determined by one-way ANOVA with Dunnett's correction for multiple comparisons, **p<0.01, (n=3).*

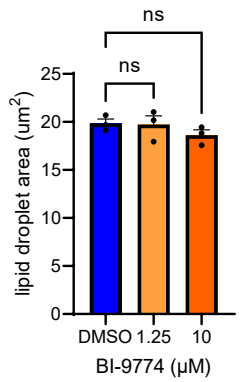


Figure 4.65 Effect of AMPK on lipid droplet size in mature adipocytes

The SVF was differentiated and after mature adipocyte formation was treated with 1.25µM and 10µM BI-9774 for 3 days. Quantification of lipid droplet size. Data are shown as mean ± SEM with statistical significance determined by one-way ANOVA with Dunnett's correction for multiple comparisons (n=3).

AMPK activation has been shown to induce browning in adipocytes (Pollard et al., 2019; Wang et al., 2015; Wu et al., 2018; Yan et al., 2016; Zhao et al., 2017). Whilst there was no change in lipid droplet size (Figure 4.65), this is not the most straightforward read out for browning in 2D culture where cells are already multilocular. Browning of adipocytes is accompanied by the expression of thermogenic genes. AMPK activation led to slight reductions in p-HSL when assessed by Western blotting. However, the reduction was not significant (Figure 4.66A, B). In addition, it did not lead to adipocyte browning or stimulation of thermogenesis (Figure 4.66C). There was no expression of UCP1 or SERCA1. There were also no changes in levels of CKB or SERCA2 with AMPK activation (Figure 4.66D, E). Because of the previous unsuccessful induction of thermogenic gene expression by β-AR stimulation, this was not investigated further here.

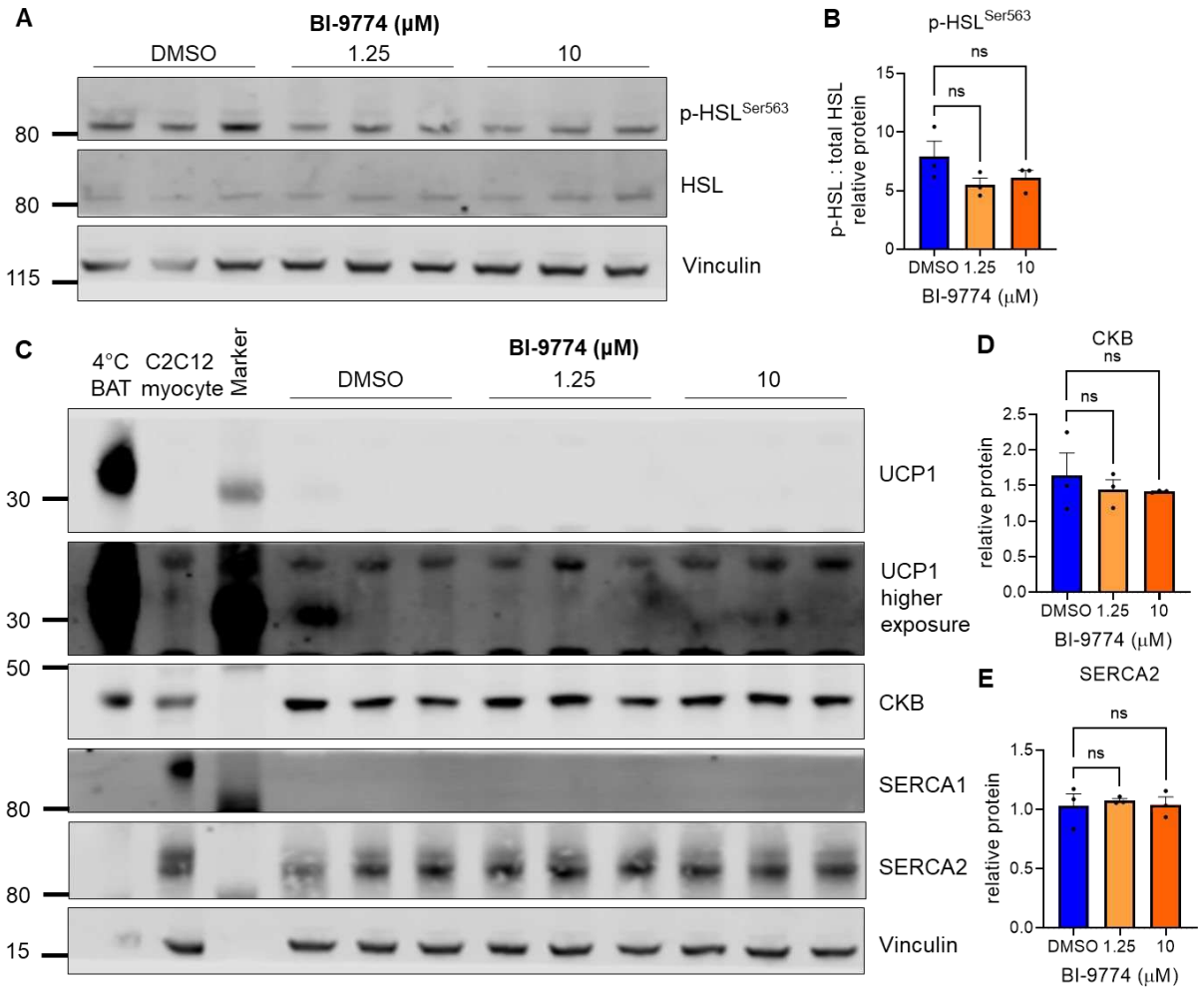


Figure 4.66 Effect of AMPK in mature adipocytes

The SVF was differentiated and after mature adipocyte formation was treated with 1.25μM and 10μM BI-9774 for 3 days. (A) Western blot for phosphorylation of HSL with quantification of (B) p-HSL relative to HSL all relative to vinculin. (C) Western blot for thermogenesis with quantification of (D) CKB and (E) SERCA2 relative to vinculin. Data are shown as mean ± SEM with statistical significance determined by one-way ANOVA with Dunnett's correction for multiple comparisons (n=3).

4.7 DISCUSSION

This study evolved from an endeavour to generate SMART cells *in vitro* to learn more about their origins and mechanism of ATP uncoupling. Activation of AMPK in the mature adipocyte

failed to induce SMART cells as determined by the lack of increase in SERCA1 or other thermogenic proteins (Figure 4.66C). This was not surprising given that in the D316A mouse AMPK activation precedes the formation of a mature adipocyte (Pollard et al., 2019). Furthermore, expression of the D316A construct in mature adipocytes using an adiponectin Cre failed to protect mice against diet induced obesity. It is important to note that the mature adipocytes were never stimulated to undergo thermogenesis due to the difficulties in finding the appropriate conditions (Figure 4.29), and in the D316A mouse thermogenesis is induced with a high fat diet (Pollard et al., 2019).

AMPK activation in the adipogenesis of E14 cells was investigated. Whilst this provided insight into the requirement for AMPK activation during the earlier time points in differentiation, it was not a feasible model of adipogenesis due to the 24-day time frame which meant overgrowth of cells and often whole layer detachment from the plate. Additionally, there were concerns about the relevance of activating AMPK in an ES cell, when adult stem cells would likely be the therapeutic target. Therefore, primary SVF derived was investigated as a model. Whilst again this did not appear to yield SMART cells as skeletal muscle associated thermogenesis was not induced (Figure 4.29C), the recurring reduction in adipogenesis upon AMPK activation during differentiation warranted further investigation. Clarity on the mechanism of AMPK activation would give insight into whether adipose tissue is a suitable target for AMPK activators, as generally inhibition of adipogenesis is not desirable. One challenge presented when using the primary SVF is overcoming the variability in differentiation efficiency that exists between wells, between mice, and between cell isolation days. When differentiation efficiency is low then the differences seen with activation of AMPK are less substantial and so the differentiation efficiency effects the level of significance. Whilst measures are taken to minimise the differences in differentiation efficiency, such as replicating the level of confluence and number of days in culture between each experiment, some factors, such as media batches, are not as easy to control. Whilst a general trend will be present, some of the variability then impacts the statistical significance of the results.

4.7.1 Pharmacological activation of AMPK does not suppress adipogenesis through inhibition of lipogenesis

There is vast literature pertaining to the inhibition of adipogenesis through activation of AMPK (Ahmad et al., 2020). Many natural ligands have been found to reduce adipogenesis

which coincides with an increase in AMPK phosphorylation. Only one study uses a direct activator of AMPK, A-769662, in 3T3-L1 adipogenesis (Zhou et al., 2009). Some studies point to AMPK's inhibition of de novo lipogenesis as being the mechanism responsible for the inhibition of adipogenesis (Choi et al., 2015; Habinowski and Witters, 2001; He et al., 2013).

In adipose tissue de novo lipogenesis is mostly controlled at a transcriptional level through insulin responsive transcription factors SREBP1c and ChREBP, with ChREBP being the major regulator of lipogenesis in adipose tissue (Song et al., 2018). Constitutive activation of ChREBP increases adipogenesis in 3T3-L1 and other mouse fibroblast models (Witte et al., 2015). In addition, in mice constitutive activation of ChREBP increases adipogenic gene expression in eWAT (Nuotio-Antar et al., 2015). It is thought that ChREBP can increase PPARγ activity by modulating the synthesis of a lipid derived PPARγ ligand, thereby inducing adipogenesis (Witte et al., 2015). When ChREBP is absent, there is a reduction in adipogenesis and PPARγ target genes. Further investigation into the role of the PPARγ binding ligand in adipogenesis reveals that is it synthesised through the de novo lipogenesis pathway and plays an important role in the first 2 days after adipogenic induction (Lodhi et al., 2012; Tzameli et al., 2004). One model of ChREBP knock out in primary adipose tissue SVF showed that it did not reduce adipogenic gene expression or impairment of *in vitro* adipogenesis (Vijayakumar et al., 2017). However, there may have been compensation from SREBP in this model as levels of *Srebp1* and *Srebp2* were increased, and SREBP1 has also been found to be capable of modulating the synthesis of a PPARγ lipid ligand (Kim et al., 1998).

In the current study, it was observed that mimicking AMPK's inhibition of lipogenesis through pharmacological inhibition of ACC, which catalyses the initial and irreversible step in fatty acid synthesis, reduced adipogenesis and impaired lipid droplet synthesis (Figure 4.44). Whilst AMPK phosphorylation of ACC leads to conformational changes which cause dimer dissociation, the pharmacological inhibitor PF-05175157 works by binding to the carboxyl transferase domain and preventing the synthesis of malonyl-CoA (Batchuluun et al., 2022). They both simultaneously inhibit de novo lipogenesis and promote fatty acid β-oxidation. The reduction in lipid droplet synthesis and size was much greater with inhibition of ACC than AMPK activation (Figure 4.44, Figure 4.60A). Nevertheless, the inhibition of ACC in the first 2 days of adipogenesis did not cause the reduction of adipogenesis that is seen with AMPK

activation (Figure 4.46). A previous study saw that inhibition of ACC with soraphen A, a first generation ACC inhibitor, had a potent effect on 3T3-L1 adipogenesis when added from days 0 to 8, reminiscent of the chronic activation in this study, but not when added from day 8 onwards (Cordonier et al., 2016). In that study, earlier time points were not included, and 3T3-L1 adipocytes will have already formed by day 8.

It would seem that the inhibition of de novo lipogenesis may not be the mechanism of action for AMPK in the reduction of adipogenesis. But, more investigation of this link would need to be undertaken to rule this out completely. A useful study would have been the comparison of the inhibition of ACC indirectly with 1.25μM BI-9774 and directly with PF-05175157 on lipogenesis with labelled ^{3}H-acetate and on fatty acid oxidation with ^{14}C-palmitate. It could be that a lipid species required for PPARγ ligand binding is not synthesised through ACC, although this is unlikely as it is the irreversible step in de novo lipogenesis. It is also important to note that AMPK can alter TAG synthesis through inhibition of glycerol-3-phosphate acetyl transferase, and this would be another important avenue to explore in the future (Steinberg and Carling, 2019).

Although ChREBP regulates adipogenesis, in preadipocytes its gene expression and protein levels are low, with expression increasing throughout adipogenesis (He et al., 2004; Hurtado del Pozo et al., 2011; Vijayakumar et al., 2017; Witte et al., 2015). In terminally differentiated adipocytes it is a highly expressed protein and plays a major role in lipokine synthesis and insulin sensitisation (Hurtado del Pozo et al., 2011; Nuotio-Antar et al., 2015; Vijayakumar et al., 2017). This low level of expression in the early stages of differentiation would make it difficult to investigate whether it is held in the cytoplasm during AMPK activation in early adipogenesis by conventional blotting or immunocytochemistry techniques. Instead, more invasive techniques such as transcription factor activity reporter systems would need to be used, which are more difficult to establish in primary SVF.

Studies show rosiglitazone and other PPARγ ligands can rescue the reduction in adipogenesis when there is loss of the lipid ligand (Kim et al., 1998; Lodhi et al., 2012), which would suggest that if AMPK suppression of adipogenesis was through a reduction in ChREBP mediated lipogenesis, that rosiglitazone could overcome this. However, even in the presence of rosiglitazone in the media, AMPK still reduces adipogenesis (Chen et al., 2017). In the E14 adipogenesis model, rosiglitazone is used in the adipogenic maintenance and induction media, yet AMPK activation still suppresses adipogenesis (Figure 4.13). In

addition, it was observed that adipogenic cocktail component IBMX was able to increase PPARγ activity indirectly through its ligand binding domain (Tzameli et al., 2004), and so loss of a PPARγ ligand does not appear to be the key to AMPK's mechanism of action.

Leptin showed an independent pattern of gene expression compared to other adipocyte markers in response to AMPK activation. It was often the most significantly reduced in response to chronic AMPK activation as well as chronic ACC inhibition (Figure 4.26F, Figure 4.43F). Like with the other adipocyte markers, its expression was still reduced with pulse AMPK activation but not with pulse ACC inhibition (Figure 4.45F). Unlike the other markers, it also appears to be reduced when AMPK is activated after the induction phase (Figure 4.33F), and it is also reduced when AMPK is activated in mature adipocytes (Figure 4.64F), both being conditions where there is no change in the number of adipocytes. This suggests a role for AMPK in regulating leptin independently of its broader suppression of adipogenesis. There is plenty of literature on leptin's regulation of AMPK; it activates AMPK in peripheral tissues e.g. skeletal muscle, whereas in the hypothalamus leptin inhibits AMPK (López et al., 2016; Steinberg and Carling, 2019). Meanwhile, there is an absence of literature on the effects of AMPK activation on leptin expression. The D316A mouse has reduced circulating leptin when on a high fat diet although there are no changes in appetite (Pollard, 2017). Reduced leptin levels are a symptom of lipodystrophies (Lim et al., 2021). Adipocyte subtypes display differences in expression levels of leptin, and it is possible that activation of AMPK leads to a change in adipocyte function to a subtype of adipocyte that expresses low levels of leptin (Bäckdahl et al., 2021). An initial follow up would be to determine the effects of AMPK on leptin expression and secretion which can be done by ELISA. If the gene expression pattern followed through to a protein level, then the effect of AMPK activator administration in *ex vivo* WAT or *in vivo* should be assessed.

4.7.2 Activation of AMPK slows proliferation in adipogenesis

AMPK activation reduces proliferation in the mitotic clonal expansion phase of adipogenesis, and so this may be the mechanism by which it reduces adipocyte differentiation (Vingtdeux et al., 2011; Zhou et al., 2009). Studies reporting these findings were carried out in 3T3-L1 cells, where the phases of adipogenesis are clearly defined. One disadvantage of using 3T3-L1 cells to study adipogenesis is that they are a fibroblastic cell line and don't accurately reflect the adipocyte precursors found in mice or humans. In these studies activation of AMPK inhibits proliferation completely, blocking cell cycle progression to G2/M phase (Zhou

et al., 2009). Another study shows that resveratrol perturbs proliferation by preventing G2/M phase progression cell cycle progression. However, it does not link its effects to activation of AMPK (Kwon et al., 2012). In the work presented here, there is a reduction in proliferation with BI-9774 (Figure 4.49). One of the caveats of using the SVF was that the effects on the other cell types can skew the effects on adipocytes. For instance, there is an increase in cell cycle and proliferative genes in the BI-9774 treated cells even though there is a reduction in proliferation, as the proportion of differentiated cells which have exited the cell cycle are higher in the untreated cells and so there is a greater proportion of proliferating cells in the BI-9774 treated cells (Figure 4.53). However, this also is advantageous as adipose tissue is highly heterogeneous and so retaining other cell types gives a better overall reflection of the complexity *in vivo*.

Whether the mitotic clonal expansion phase is essential *in vitro* is debated, with inhibition of mitotic clonal expansion coinciding with a reduction in adipogenesis (Lyle et al., 1998; Tang et al., 2003b), and degradation of cyclin-dependent kinase inhibitor 1B is shown to be essential for adipogenesis (Patel and Lane, 2000). On the other hand, adipogenesis still occurred when cell cycle progression was blocked with use of serum starvation or inhibition of mitogen activated protein kinase kinase (Entenmann and Hauner, 1996; Qiu et al., 2001). It is even less clear whether mitotic clonal expansion is required *in vivo*, although the study showing serum starvation pauses cell growth but doesn't suppress adipogenesis was carried out in human primary preadipocytes (Entenmann and Hauner, 1996). In this study, carried out in primary mouse adipocytes which again are a more translational model, AMPK activation clearly reduces cell proliferation (Figure 4.49). Even if cells can recover from the initial suppression in cell growth there is still a reduction in adipogenesis (Figure 4.38), supporting the theory that AMPK's disruption of the mitotic clonal expansion phase is important for the suppression of adipogenesis.

AMPK can block cell cycle progression through the mTOR signalling pathway. One study shows that insulin mediated phosphorylation and inhibition of the mTOR inhibitory TSC1-TSC2 complex via the phosphoinositide 3-kinase-AKT increases adipogenesis, and that loss of TSC2 also increases adipogenesis (Zhang et al., 2009). mTOR also leads to increased PPARγ activity independently of the influence of insulin, as its inhibitor rapamycin reduces PPARγ promoter activity (Kim and Chen, 2004). One group reported that metformin suppresses adipogenesis independently of AMPK through the mTOR-p70S6K pathway,

suggesting a reduction in cell growth via a reduction in protein synthesis (Chen et al., 2017). The effect of mTOR on adipogenesis has been investigated using rapamycin, and chronic treatment with rapamycin reduces 3T3-L1 cell adipocyte differentiation (Cho et al., 2004; Kim and Chen, 2004; Yeh et al., 1995). Pulse treatment of 3T3-L1 cells with rapamycin at the earliest time points in adipogenesis, from days 0 to 1 up to days 0 to 5, changes adipocyte morphology with smaller lipid droplets. However, in this study imaging alone was used to determine this effect, but adipocyte markers were not assessed and no quantification was carried out (Cho et al., 2004). Adding rapamycin for longer periods inhibits adipogenesis. Adding rapamycin after the initiation of adipogenesis and even towards the end of adipogenesis reduced lipid droplet size and appeared to reduce the expression of adipocyte markers with the effect becoming less substantial the later in adipogenesis rapamycin is added (Cho et al., 2004; Kim and Chen, 2004). This deviates from what was seen in this study as addition of AMPK after the day 2 time point had no effect on the number or morphology of adipocytes. This avenue is important to follow up on, and inhibition of mTOR should be assessed at the early time points in adipogenesis with BI-9774 treatment.

4.7.3 Activation of AMPK in adipogenesis effects adipocyte morphology

Activation of AMPK during adipogenesis leads to the formation of adipocytes with smaller lipid droplets (Figure 4.57). Interestingly, reduced lipid droplet size was a phenotype of the D316A mouse (Pollard et al., 2019). In the D316A mouse this was accompanied by an increase in multilocularity and was part of the non-canonical browning of iWAT. Smaller lipid droplets and increased number of lipid droplets are important for fuelling futile cycling and thermogenesis in adipocytes. Unlike their *in vivo* counterparts, *in vitro* white adipocytes in 2D culture are already multilocular, but 3D cultures can provide the ECM support network needed to generate unilocular adipocytes (Gerlach et al., 2011; Hsiao et al., 2016). This makes locularity a less defined characteristic of browning in 2D culture and so whilst it could be that the smaller lipid droplets indicate there is browning, more evidence is needed to support this. There are well defined gene sets for browning and beige adipocytes. However, given the general reduction in adipogenesis, transcriptomic approaches may be skewed and so is not the best way to determine if there is browning of adipocytes. If AMPK has induced browning of primary adipocytes there should be an increase in thermogenesis. UCP1 mediated thermogenesis is usually stimulated by β-AR receptor agonists and isoprenaline is a commonly used one. Unfortunately, although isoprenaline was able to stimulate HSL phosphorylation, it was unable to stimulate UCP1 mediated thermogenesis, or

thermogenesis by any other reported mechanism for adipose tissue (Figure 4.29). This suggests that browning is not the reason for the reduced lipid droplet size in adipocytes with AMPK activation. A limitation of the investigations into the effect of AMPK activation on HSL activity and thermogenesis is that 1.25μM BI-9774 is used. Whilst 1.25μM BI-9774 did give significant activation of AMPK, and a reduction in lipid droplet size that was close to significance, it was the 10μM concentration that gave the significant reduction in mean lipid droplet area (Figure 4.57). Although 10μM BI-9774 in mature adipocytes did not affect basal HSL activity or expression of thermogenic proteins (Figure 4.66), it also did not lead to changes in lipid droplet size (Figure 4.65) and is a different model. Another disadvantage of this study is that lipolysis was not directly measured by quantification of glycerol release, and other proteins involved in lipolysis, such as ATGL, were not assessed to determine their phosphorylation levels. Confirmation of the effect of 10μM BI-9774 in adipogenesis on lipolysis and thermogenic protein expression is an important follow up study.

The distribution of lipid droplet size indicates that AMPK activation prevented the formation of larger adipocytes, and this effect was dose dependent (Figure 4.57). CIDEC regulates lipid droplet size and growth by facilitating the transfer of neutral lipids from smaller to larger adipocytes (Gong et al., 2011). A tenuous and indirect link between AMPK and CIDEC has been drawn in skeletal muscle cells, where CIDEC levels increase in conditions where AMPK is inhibited, and silencing of CIDEC coincides with an increase in p-AMPK (Wang et al., 2010). In liver, SREBP1c, an inhibitory target of AMPK, was found to bind to the CIDEC promoter to increase expression (Chen et al., 2018). Very recently, and more relevant to adipocytes, metformin was found to inhibit lipid droplet growth along with reducing CIDEC expression whilst increasing AMPK activation in rat primary iWAT and eWAT SVF adipocytes (Yang et al., 2022). However, this study did not account for the effect that the total reductions in adipogenesis upon metformin treatment would have had on overall levels of CIDEC. A potential mechanism for AMPK regulating CIDEC expression was through promotion of CIDEC proteasomal degradation, as indirect activators of AMPK stabilised CIDEC levels when proteasomal degradation was blocked (Zhang et al., 2014). AICAR was found to reduce iWAT CIDEC levels when injected into mice. In the work presented here, AMPK activation in adipogenesis led to reduced CIDEC mRNA levels even when the reduction in adipogenesis was accounted for. However, due to inconsistencies with the antibodies tested, it was not possible to determine the effect of AMPK activation on CIDEC protein levels in this study (Figure 4.58).

Adipocyte maturation is the final stage of adipogenesis and is signified by the growth of lipid droplets into large lipid droplets and expression of adipokines. The Burton gene sets were determined from thorough examination of gene expression at different time points in 3T3-L1 differentiation to determine genes associated with different stages of adipogenesis (Burton et al., 2004). Whilst there are caveats in this gene set mainly due to it being based on time points in 3T3-L1 adipogenesis that may not directly reflect the time points in SVF adipogenesis, it was still interesting to note the suggestion that there was enrichment in genes associated with a mid-early phase of differentiation in BI-9774 treated adipocytes (Table 4.4). It was also interesting to see that AMPK activation in E14 cells not only prevented adipocyte differentiation but also showed elevations in the levels of pluripotency markers, suggesting a role for AMPK in maintaining a level of stemness (Figure 4.14).

Due to a lack of significant difference in lipid droplet area but the small yet the significant increase in lipid droplets under 50μm^2 with 10μM BI-9774 (Figure 4.61), it is difficult to conclude the effect of pulse treatment on lipid droplet size. It may be that more replicates are needed to determine significance. If it truly reduces lipid droplet size, then it could be that early-stage AMPK activation not only suppresses adipogenesis but also pauses adipocyte maturation. Even if pulse activation of AMPK does not affect lipid droplet size, this does not rule out AMPK activation stunting adipocyte maturation, it may just be that it needs to be active for a longer time and at a later stage in adipogenesis to observe this effect. Using a method like RNA FISH it would be interesting to see whether there are reductions in expression of markers of terminal differentiation in each cell, or whether the reduction is an overall reflection of reduced numbers of adipocytes. Also, further investigation of lipid droplet dynamics could be carried out with high resolution live cell imaging to monitor lipid droplet formation and growth with AMPK activation.

4.7.4 Conclusion

Activation of AMPK in the initial stages of adipocyte differentiation suppresses adipogenesis, and the mechanism is not linked to its inhibition of lipogenesis. Delving further into the changes that occur in the first two days with AMPK activation will elucidate its mechanism of action. Epigenetic approaches at this stage may answer more about whether AMPK plays a role in maintaining a level of stemness in adipocyte precursors. A benefit of narrowing in on the early time points is that there will be less heterogeneity and so less skewing of results.

Investigating how AMPK suppresses proliferation during the mitotic clonal expansion phase, and whether inhibition of mTOR plays a role will be important.

In addition, determining the relevance of pharmacological activation of AMPK's suppression of proliferation in adipogenesis *in vivo* is imperative. This could be done using *ex vivo* or *in vivo* models. Whilst we know from the D316A mouse that chronic, constitutive activation of AMPK does not impair development of a whole mouse, *in vitro* the activation of AMPK has a subtle effect on adipocytes. 3D culture would also be a potential model for investigation, combining the flexibility of *in vitro* models with the closer replication of an *in vivo* adipocyte.

The suppression of adipogenesis, alteration adipocyte morphology and effect on leptin gene expression could suggest that activation of AMPK in adipose tissue may lead to lipodystrophy, meaning that adipose tissue AMPK is not a suitable therapeutic target. This would be in opposition to the metabolic benefits of AMPK activators in the liver in T2D and NAFLD. Therefore, it is important to clarify whether these effects are relevant *in vivo*. As AMPK has different isoform expression in different cells and tissues, and small molecule activators show selectivity towards different isotypes (Steinberg and Carling, 2019), it may be possible to target specific tissues using different small molecules.

5. GENETIC ACTIVATION OF AMPK AND THE ADIPOSE-MUSCLE LINK

5.1 INTRODUCTION

The AMPKγ1 D316A mutation induces conformational changes resulting in weak binding of AMP to the CBS4 domain which in turn reduces AMPKα^{Thr172} dephosphorylation giving constitutive AMPK activation (Woods et al., 2017). Mice harbouring the whole body D316A mutation driven by a β-actin Cre possess protection from diet induced obesity through increased iWAT energy expenditure from UCP1-independent, skeletal muscle associated mechanisms of thermogenesis (Pollard et al., 2019). AMPK activation inducing adipose tissue energy expenditure has interesting implications for alleviating obesity which as of yet has proved difficult to provide a long term remedy for. The adipose tissue of the D316A mouse had smaller lipid droplets and increased mitochondrial content. In the mouse, genes associated with the skeletal muscle were upregulated in the D316A iWAT including the skeletal muscle associated SERCA1, which mediates calcium futile cycling novel to adipose tissue, so these new adipocytes were called SMART cells. Animal models are limited in terms of mechanistic studies and investigating cell biology is aided by good cell based models. Having an *in vitro* model of SMART cells would allow for exploration of SERCA1 calcium futile cycling in adipose tissue as well as other changes induced by AMPK activation and may help to determine the developmental origins of SMART cells. However, the exact cell type that gives rise to the SMART cells has not been previously identified, making it difficult to generate a cell based model. Expressing the D316A mutation in mature adipocytes with an Adiponectin Cre didn't confer high fat diet induced obesity protection, so it may be that a specific precursor cell which needs to have constitutive AMPK activation to generate SMART cells. Unexpectedly, using the PDGFRα Cre still didn't recapitulate the phenotype of the β-actin Cre mouse, which means either that the precursor cell type is PDGFRα negative, that AMPK needs to be activated in an earlier adipocyte progenitor such as in the mesenchymal stem cells, or alternatively that the effect is not cell autonomous, and that there are extrinsic factors that contribute to the environment in the iWAT of the D316A mouse to lead to increased thermogenesis. Combining the D316A mutation with a myocyte enhancing factor 2C Cre for skeletal muscle expression also failed to reproduce the β-actin Cre phenotype, so the skeletal muscle alone isn't the extrinsic tissue type required if the effect is not cell autonomous. Isolating the β-actin Cre D316A SVF for *in vitro* adipogenesis could provide a cell based model of SMART cells to probe mechanisms and origins, and can

help to answer whether the protection from diet induced obesity lies solely in a SVF residing precursor.

WAT, BAT and skeletal muscle all share a common mesenchymal stem cell progenitor. BAT is more closely related to skeletal muscle and both share a MYF5 expressing precursor. The expression of PRDM16 and euchromatic histone lysine methyltransferase 1 distinguish the differentiation of brown adipocytes over skeletal muscle (Kajimura et al., 2009; Ohno et al., 2013; Seale et al., 2008). It is possible to induce fate switching of myoblasts to adipocytes and this has been investigated by many groups over the last 3 decades with almost all studies looking in mouse models using either primary myoblasts or myoblast cell lines G8 or C2C12 (Wang and Shan, 2021). Proteins PPARγ, CEBPα and WNT10b which are strongly associated with adipogenesis have been shown to play an important role in the transdifferentiation of myoblasts to adipocytes (Hu et al., 1995; Vertino et al., 2005) and can increase transdifferentiation when added directly, or through stimulation by external factors such as rosiglitazone or mechanical stretch (Aguiari et al., 2008; Akimoto et al., 2005; Itoigawa et al., 2010; Lee et al., 2011b; Luo et al., 2015; Mancini et al., 2007; Qi et al., 2016; Sharma et al., 2014; Yeow et al., 2001). In addition, myoblast to adipocyte transdifferentiation can also occur when there is targeted loss of muscle stem cell factors (An et al., 2017; Chen et al., 2019a; Gao et al., 2019; Wang et al., 2017). Fate switching was also observed when myocytes appeared in the iWAT of cold exposed mice lacking β-AR signalling. Under these conditions an alternative adipocyte with high glucose oxidative capacity called the glycolytic beige cell was identified, originating from a myogenic precursor cell that expresses MYOD, a major muscle differentiation regulatory factor (Chen et al., 2019b). The differentiation of glycolytic beige cells is controlled by transcription factor GABPα, and overexpression of GABPα in C2C12 cells leads to an increase in adipogenesis. We know that AMPK activation can upregulate expression of muscle associated genes and induce both cardiac and skeletal muscle-associated mechanisms of thermogenesis in adipose tissue through SERCA2b and SERCA1 respectively (Aquilano et al., 2020; Pollard et al., 2019). The link with muscle mechanisms of thermogenesis also introduces interesting questions about the role of AMPK in the link between adipose tissue and muscle tissue and makes the D316A adipose tissue a potential model to study this mechanism through.

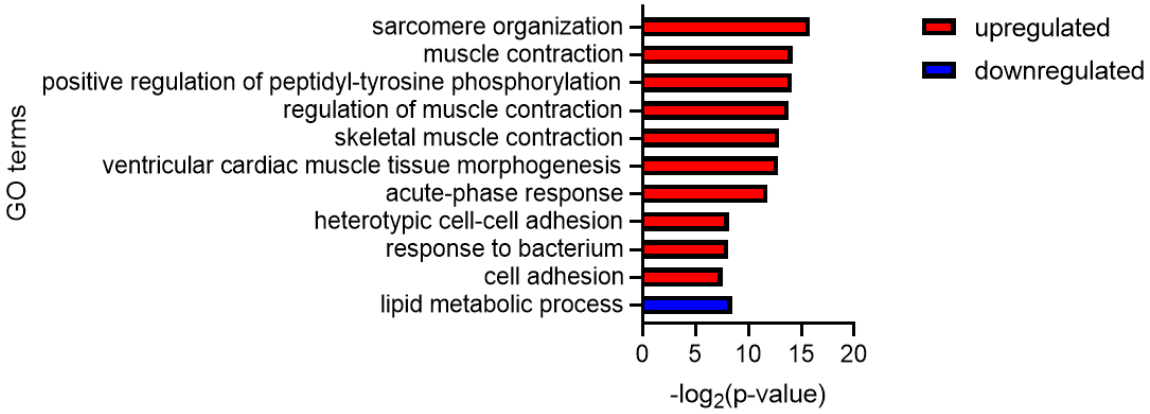
Chapter 4 delved into the effects of pharmacological activation on adipogenesis. This chapter looks at whether the effects of the D316A mutation on adipose tissue observed *in*

vivo remain present *in vitro* as well as how genetic activation compares to pharmacological activation in its effects on adipogenesis. In addition, the link between adipose tissue and muscle cells and the role of AMPK in this relationship is studied using D316A SVF adipocytes and the C2C12 mouse myoblast cell line.

5.2 D316A SVF ADIPOCYTES

The SVF of the D316A mouse as well as control WT mice were isolated, plated *in vitro* and differentiated to adipocytes. These adipocytes were submitted for RNA sequencing which revealed that the D316A SVF adipocytes were very similar to the WT SVF adipocytes (Figure 4.21), although they had greater AMPK activity (Figure 4.17). The changes seen with BI-9774 activation of AMPK were reflected with the D316A mutation, although the effects were far less pronounced. The D316A SVF adipocytes will now be investigated further.

5.2.1 Adipogenesis of D316A SVF



To

Figure 5.1 Analysis of D316A and WT SVF adipocyte RNA sequencing

The topmost significant gene ontology terms associated with the significantly differentially expressed genes between the D316A and WT SVF adipocytes.

demonstrate how similar the WT and D316A SVF adipocytes are, there were 19,593 differentially expressed genes between the D316A and WT SVF adipocytes. However, only 103 of these were significantly different as defined by an adjusted p-value below 0.05, with 21 significantly upregulated and 82 significantly downregulated. Exploring these significantly differentially expressed genes by looking at the topmost significant GO terms associated with them shows that many of the upregulated differentially expressed genes were

associated with muscle function, with a few related to immune response, whilst lipid metabolism was the only GO term that was associated with the downregulated differentially expressed genes (Figure 5.1).

As AMPK activation was associated with a reduction of adipogenesis *in vitro*, and lipid metabolism which is important for adipocytes was downregulated, the effect of the D316A mutation on adipogenesis was supported by GSEA. The Hallmark Adipogenesis gene set showed a strong reduction in genes related to adipogenesis in the D316A SVF adipocytes compared to WT with NES of -3.42 (Figure 5.2A). Out of 189 genes in the Hallmark Adipogenesis gene set, 161 were part of the core enrichment. Additionally, the Gerhold Adipogenesis gene sets showed significant enrichment in the WT SVF adipocytes for genes associated with increased adipogenesis, and significant enrichment in the D316A SVF adipocytes for genes associated with decreased adipogenesis (Figure 5.2B) (Gerhold et al., 2002). When individual adipocyte marker mRNA levels were assessed independently by qPCR there was a persistent trend for reduced expression in the D316A derived SVF (Figure 5.3). There is always mouse to mouse variation in *in vitro* adipogenesis and so many biological replicates were assessed to determine a pattern. There was great variability between replicates, and so none of the individual marker genes showed statistically significant reductions in the D316A SVF adipocytes, even though when looking at the adipogenesis gene set as a whole there was reduction.

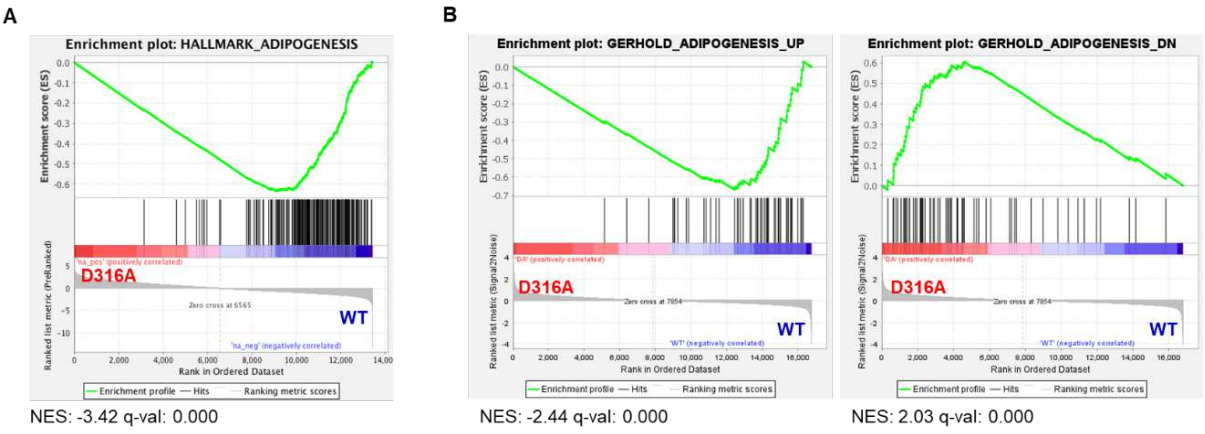


Figure 5.2 GSEA plot for adipogenesis in D316A vs WT

From the RNA sequencing data set, the enrichment plots for (A) the Hallmark Adipogenesis gene set and (A) the Gerhold Adipogenesis up and down gene sets (B) for D316A vs WT SVF adipocytes.

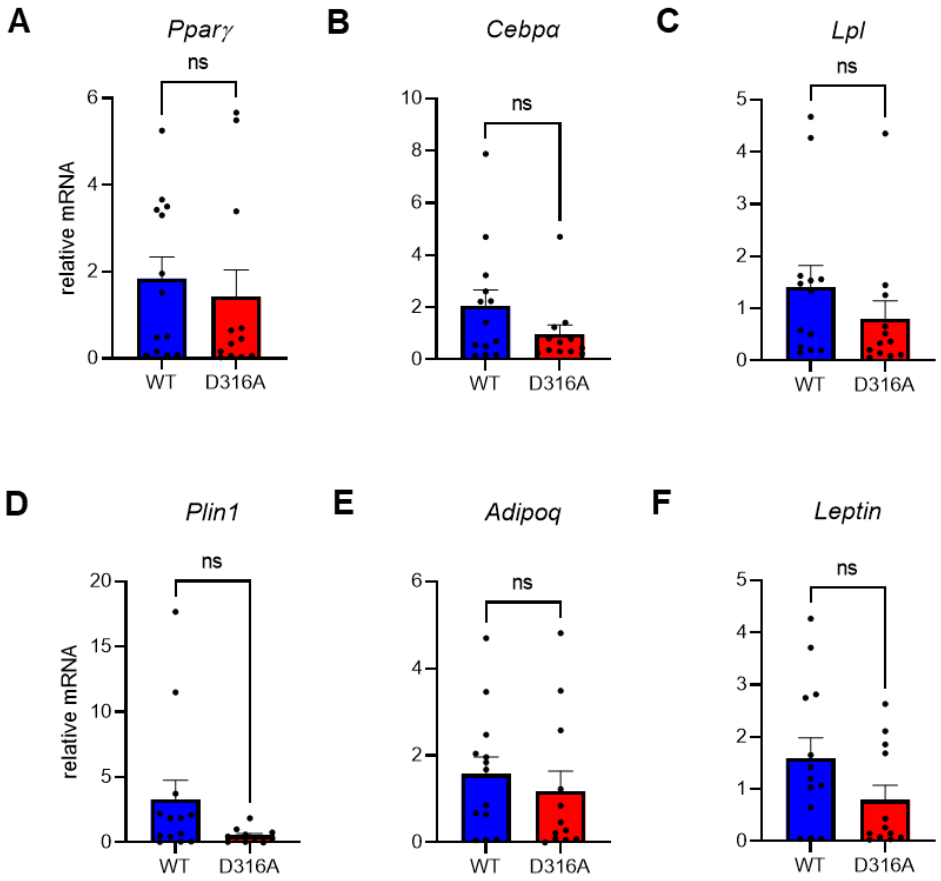


Figure 5.3 Effect of D316A mutation on adipocyte marker genes

(A-F) Adipocyte marker gene mRNA expression in WT and D316A SVF adipocytes. mRNA levels relative to housekeeping gene 36B4. Data are shown as mean ± SEM with statistical significance determined by Student's t-test with Welch's correction for (D) Plin1, (WT n=13, D316A n=12).

To further investigate levels of adipogenesis in D316A SVF compared to WT, adipogenic differentiation with quantification of lipid droplet staining and DAPI was done to determine the adipogenic index (Figure 5.4). Quantification showed that there was more lipid droplet staining in D316A SVF (Figure 5.4B). However, the nuclei counts in the D316A SVF were also greater (Figure 5.4C), so overall there were more cells in the D316A SVF but a similar proportion of adipocytes, meaning that the adipogenic index showed no difference between the WT and D316A SVF (Figure 5.4D). The D316A mouse iWAT adipocytes had smaller,

more multilocular lipid droplets than WT adipocytes. Pharmacological activation of AMPK during *in vitro* adipogenesis also reduced lipid droplet size, with higher concentrations increasing the number of lipid droplets (Figure 4.54). Despite this, *in vitro* adipogenesis of D316A SVF didn't lead to any obvious difference in lipid droplet morphology compared to WT (Figure 5.5), although quantification would be needed to confirm this.

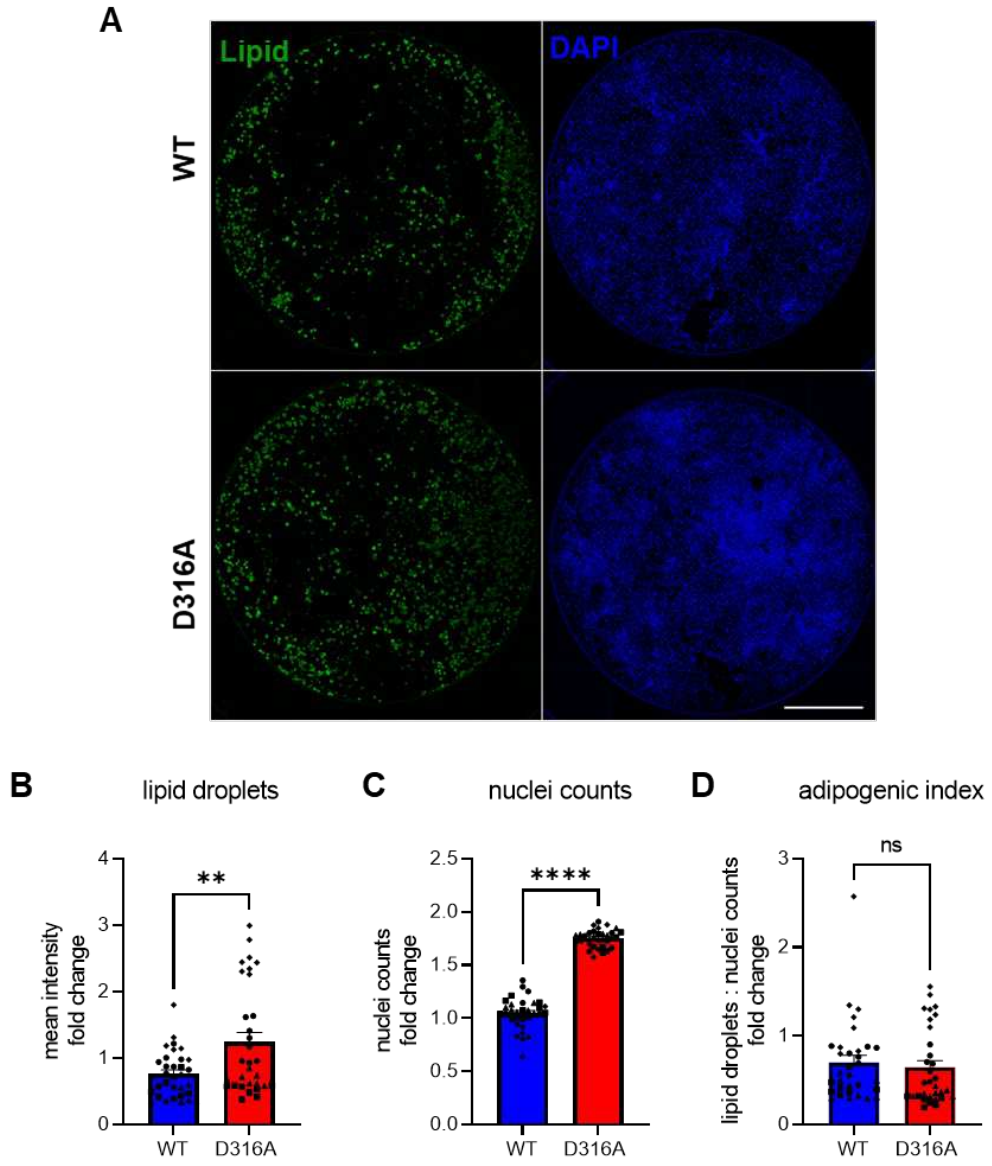


Figure 5.4 The effect of the D316A mutation on adipogenesis

Lipid droplet and DAPI staining of WT and D316A SVF adipocytes to determine adipogenic index. (A) Representative images of whole well scans with lipid droplet and DAPI staining.

*(B) Quantification of lipid droplet staining from whole well scans. (C) Nuclei counts from whole well scans. (D) Normalisation of lipid droplet staining to nuclei counts to calculate the adipogenic index. Data are shown as mean ± SEM, with different biological replicates represented by different shaped symbols. Statistical significance is determined by Student's t-test with Welch's correction for (B) and (C), **p<0.01, ****p<0.0001, (n=4 mice, each represented by a different shaped symbol, SVF isolated on the same day, 8 technical replicates per mouse). Scale bar represents 1500μm.*

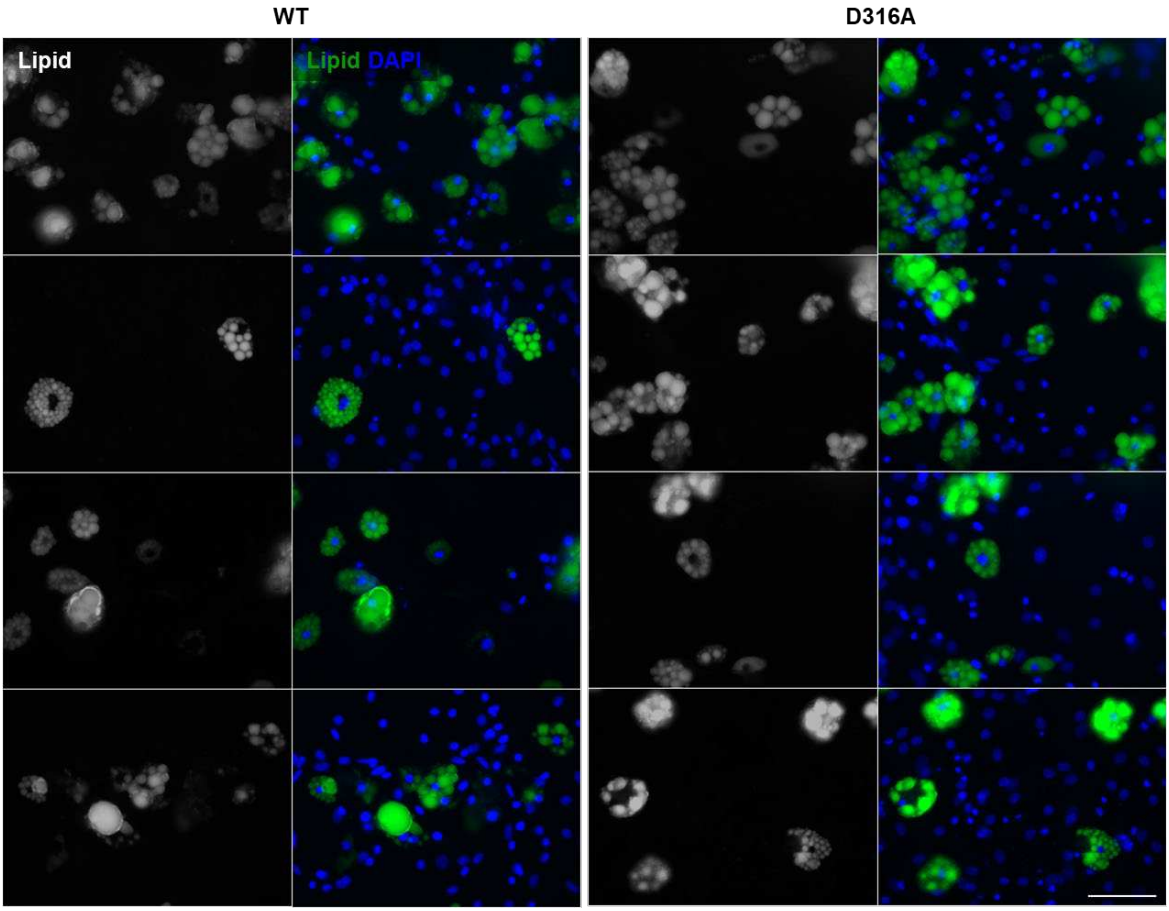


Figure 5.5 Morphology of WT and D316A SVF adipocytes
Representative images of WT and D316A SVF adipocytes with lipid droplet and DAPI staining. Scale bar represents 75μm.

Parameters that further distinguished the D316A iWAT from WT were the increased mitochondrial content visualised with TOMM20 staining and Western blotting (Pollard et al.,

2019). To see whether the mitochondrial phenotype remained in the isolated D316A SVF adipocytes, mitochondrial content was probed by Western blotting for PGC1α, TOMM20 and members of the mitochondrial oxidative phosphorylation complex (Figure 5.6). The change was subtle, but quantification showed an increase in PGC1α meaning there was maybe more mitochondrial biogenesis (Figure 5.6B), as well as an increase in TOMM20 (Figure 5.6C) and oxidative phosphorylation complexes (Figure 5.6D-H). Therefore, the D316A cells are able to retain some of their characteristics *ex vivo*.

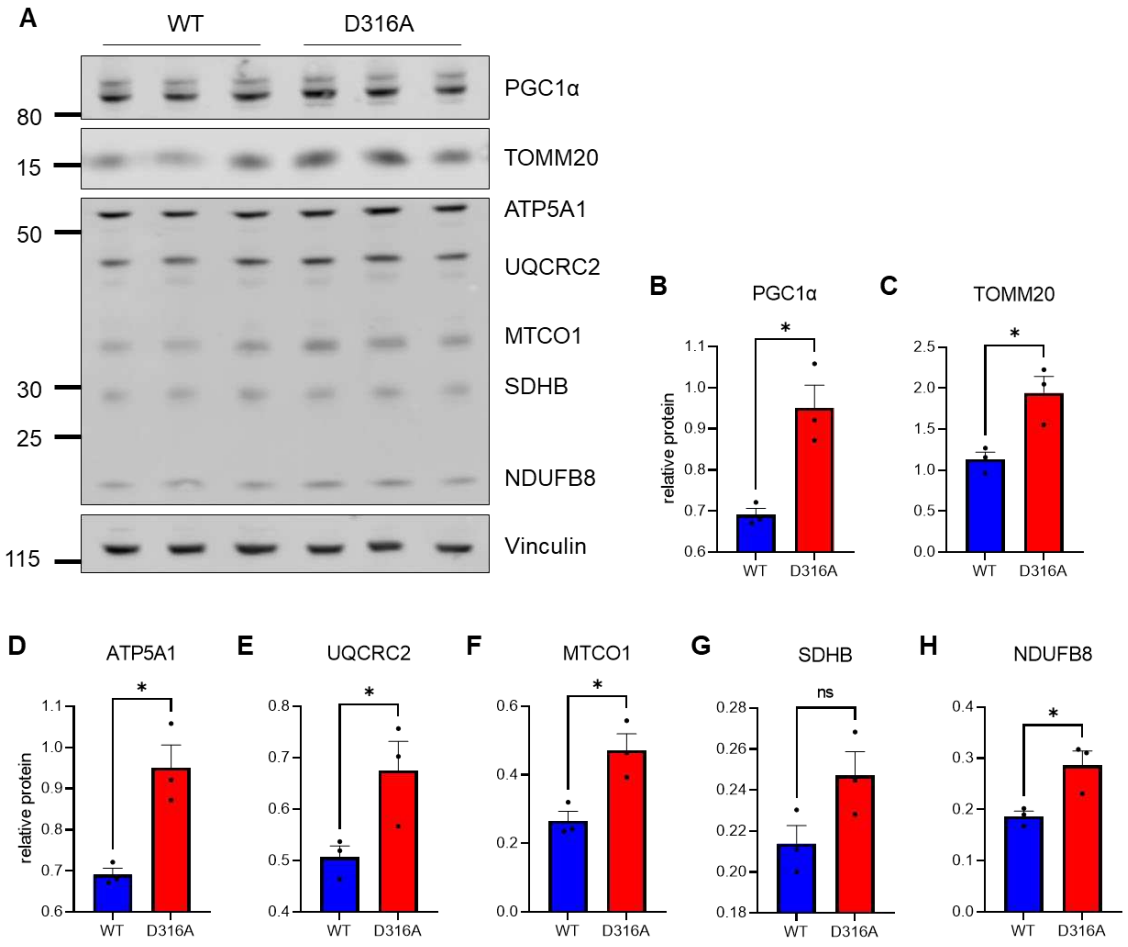


Figure 5.6 Characterising the effect of the D316A mutation on mitochondria in SVF adipocytes

Levels of mitochondrial associated proteins in WT and D316A SVF adipocytes. (A) Western blot for mitochondrial associated proteins with quantification of (B) PGC1α, (C) TOMM20 and (D-H) the mitochondrial oxidative phosphorylation proteins all relative to vinculin. Data

*are shown as mean ± SEM with statistical significance determined by Student's t-test, *p<0.05, (n=3).*

The defining feature of SMART cells was the upregulation of skeletal muscle associated genes as well as SERCA1 mediated thermogenesis. To test whether there was potential for muscle-associated thermogenesis in the D316A SVF adipocytes as was seen in the mouse adipose tissue, D316A and WT SVF adipocytes were stimulated with the β-AR agonist norepinephrine at 1μM over a 24-hour period, as this classically induces thermogenesis (Figure 5.7). There was an increase in *Ucp1* mRNA expression after 4 hours of norepinephrine expression (Figure 5.7A), although this did not lead to detectable expression at the protein level even up to 24 hours with stimulation (data not shown). There was an increase in a PKA phosphorylation site of HSL (S660), although not significant, it further indicated successful stimulation of the adrenergic receptors with the induction of HSL phosphorylation, with p-HSL levels peaking between 2 to 4 hours after stimulation falling at 24 hours (Figure 5.7C). Norepinephrine was unable to stimulate SERCA1 expression in either D316A or WT SVF adipocytes (Figure 5.7B), and SERCA2 expression was not affected over the 24 hour treatment course (Figure 5.7D).

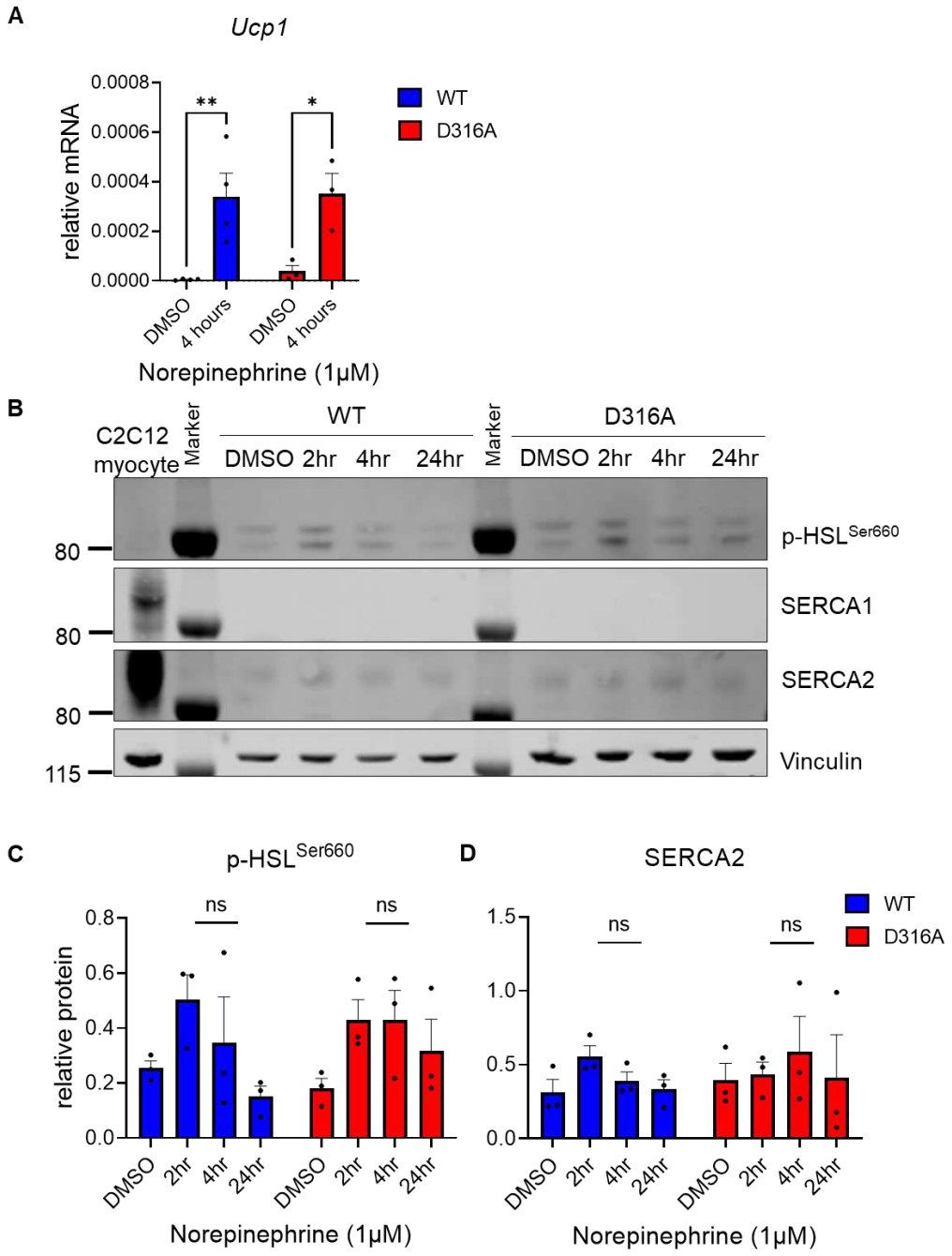


Figure 5.7 Stimulation of adrenergic receptors in WT and D316A SVF adipocytes

The WT and D316A SVF adipocytes were stimulated with 1μM norepinephrine for 2, 4 and 24 hours. (A) Ucp1 mRNA expression levels after 4 hours of norepinephrine relative to Gapdh. (B) Representative Western blot with quantification of (C) p-HSL and (D) SERCA2, relative to vinculin. Data are shown as mean ± SEM with statistical significance determined

*by two-way ANOVA with (A) Šídák's correction for multiple comparisons *p<0.05, **p<0.01, (WT n=4, D316A n=3) and (C, D) Tukey's correction for multiple comparisons, (n=3).*

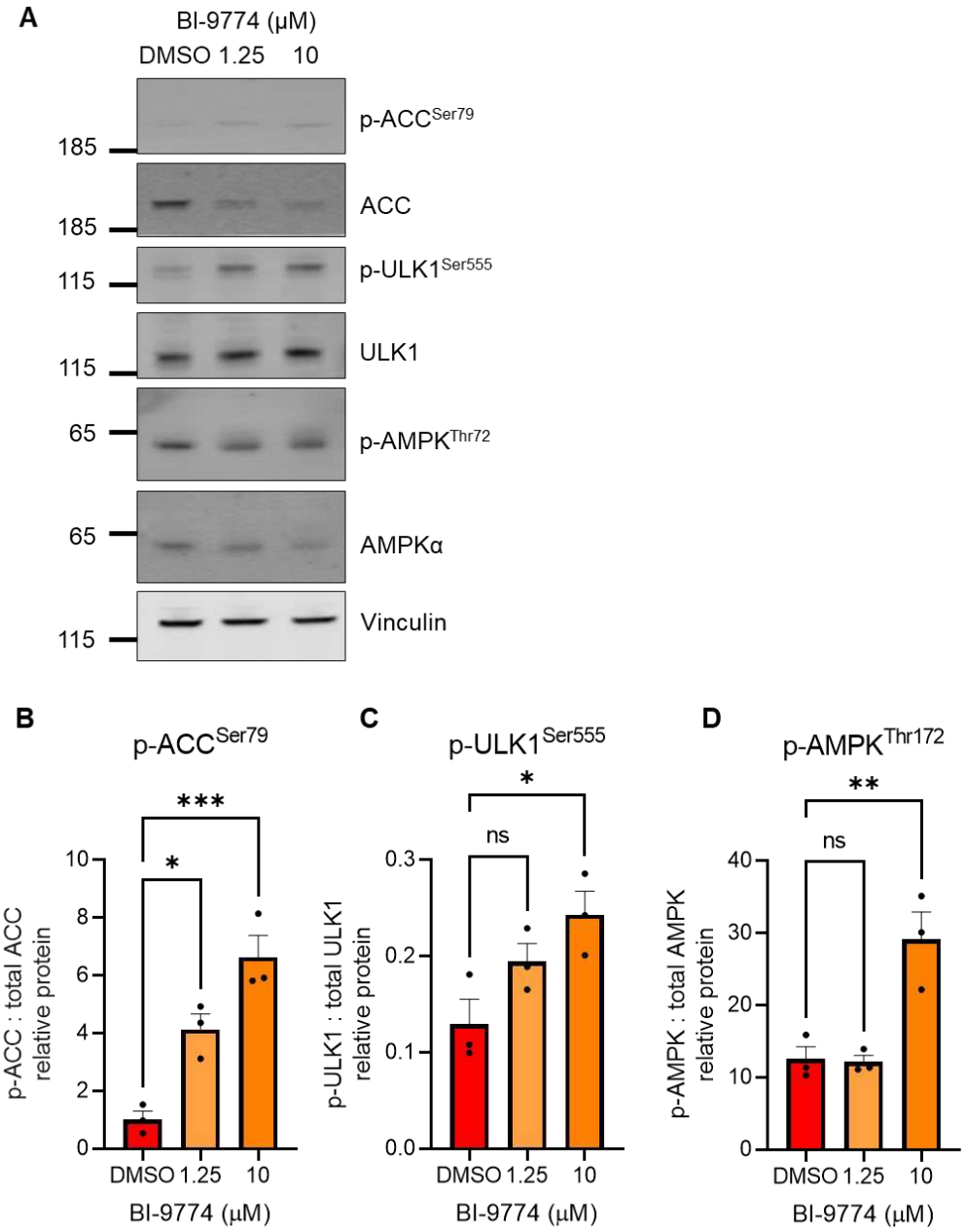


Figure 5.8 Effect of BI-9774 in the D316A SVF adipocytes

The D316A SVF was differentiated to adipocytes in the presence 1.25 and 10μM BI-9774. (A) Representative Western blot showing phosphorylation of AMPK targets with quantification of (B) p-ACC relative to ACC, (C) p-ULK1 relative to ULK1 and (D) p-AMPK

*relative to AMPK, all relative to vinculin. Data are shown as mean ± SEM with statistical significance determined by one-way ANOVA with Dunnett's correction for multiple comparisons, *p<0.05, **p<0.01, ***p<0.001, (n=3).*

The lack of effect on lipid droplet size and inability to stimulate SERCA1 expression differs from what was observed in the mouse. In addition, the lack of reduction adipogenic index or significant reduction of mRNA levels of individual adipocyte markers with the D316A mutation is also at odds with the effect of chronic *in vitro* pharmacological activation. The differences between the pharmacological and genetic models of AMPK activation could be due to the lower activation of downstream targets in the D316A model (Figure 4.18), as the effects from BI-9774 were dose dependent. BI-9774 may be able to further activate AMPK and lead to reduction in adipogenesis and adipocyte lipid droplet size that is observed with the WT SVF. To test this, D316A SVF was put through adipogenic differentiation with 1.25 and 10μM BI-9774, like with the WT SVF (Figure 5.8). Assessing AMPK activation, it appeared that BI-9774 was able to enhance the phosphorylation of downstream targets. There was a significant increase in p-ACC at both concentrations of BI-9774 (Figure 5.8B). There was also a reduction in ACC with BI-9774 treatment, as has been previously seen with AMPK activation in adipogenesis, although this did not reach significance (Figure 5.8E). Although there was an increase in p-ULK1 with 1.25μM BI-9774, this increase only became significant with 10μM BI-9774 (Figure 5.8C), and there was only a significant increase in p-AMPKα with 10μM BI-9774 (Figure 5.8D), so activation was stronger with the higher concentration. The mechanism of allosteric activation of AMPK by BI-9774 could explain why there was greater phosphorylation of downstream targets than AMPK itself. It follows suit that both concentrations of BI-9774 led to a reduction in lipid droplet staining (Figure 5.9B), as well as a reduction in nuclei count that was observed in WT SVF adipogenesis with BI-9774 (Figure 5.9C). The adipogenic index showed a reduction with the 1.25μM of BI-9774, but it was 10μM that was necessary to attain a significant reduction (Figure 5.9D). So further activation of AMPK in the D316A derived SVF gave a similar reduction in adipogenesis to what was seen with WT derived SVF. Inclusion of a WT control would have been useful to compare to the levels of activation achieved in the WT SVF.

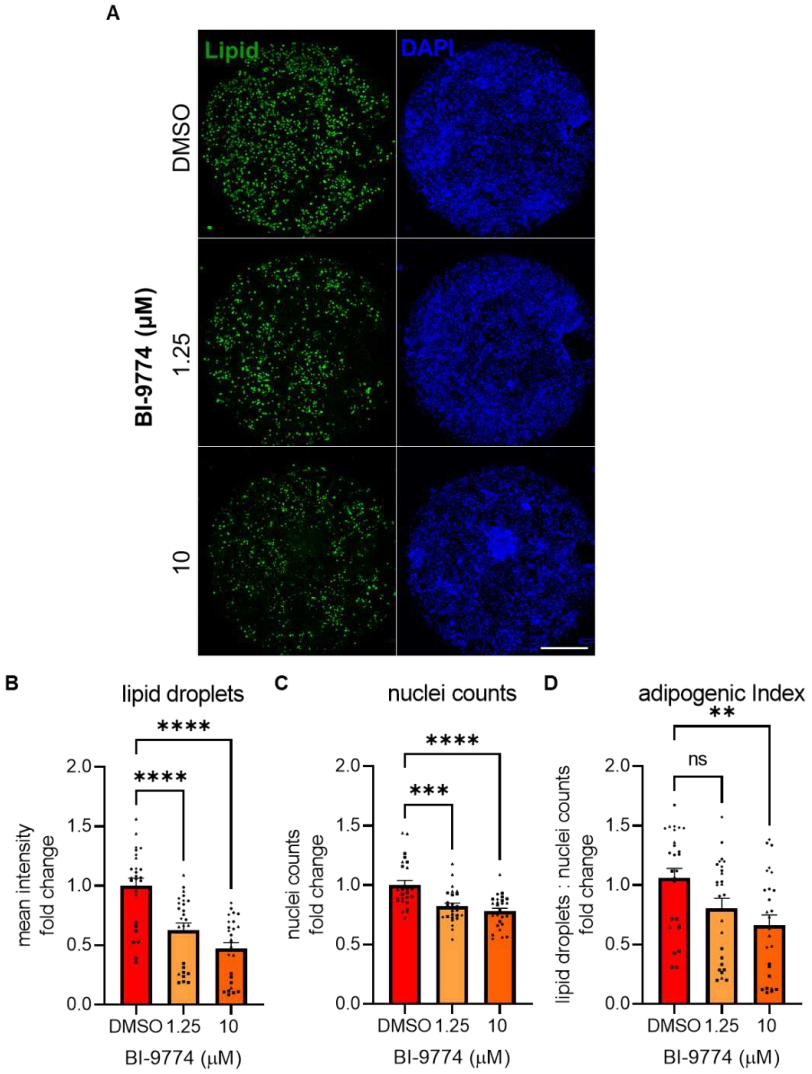


Figure 5.9 The effect of pharmacological activation of AMPK in D316A SVF adipocytes

*The D316A SVF was differentiated to adipocytes in the presence 1.25 and 10μM BI-9774 with lipid droplet and DAPI staining. (A) Representative images of whole well scans with lipid droplet and DAPI staining. (B) Quantification of lipid droplet staining from whole well scans. (C) Nuclei counts from whole well scans. (D) Normalisation of lipid droplet staining to nuclei counts to calculate the adipogenic index. Data are shown as mean ± SEM, with different biological replicates represented by different shaped symbols. Statistical significance is determined by one-way ANOVA with Dunnett's correction for multiple comparisons, **p<0.01, ***p<0.001, ****p<0.0001, (n=3 mice, each represented by a different shaped symbol, SVF isolated on the same day, 8 technical replicates per mouse). Scale bar represents 1500μm.*

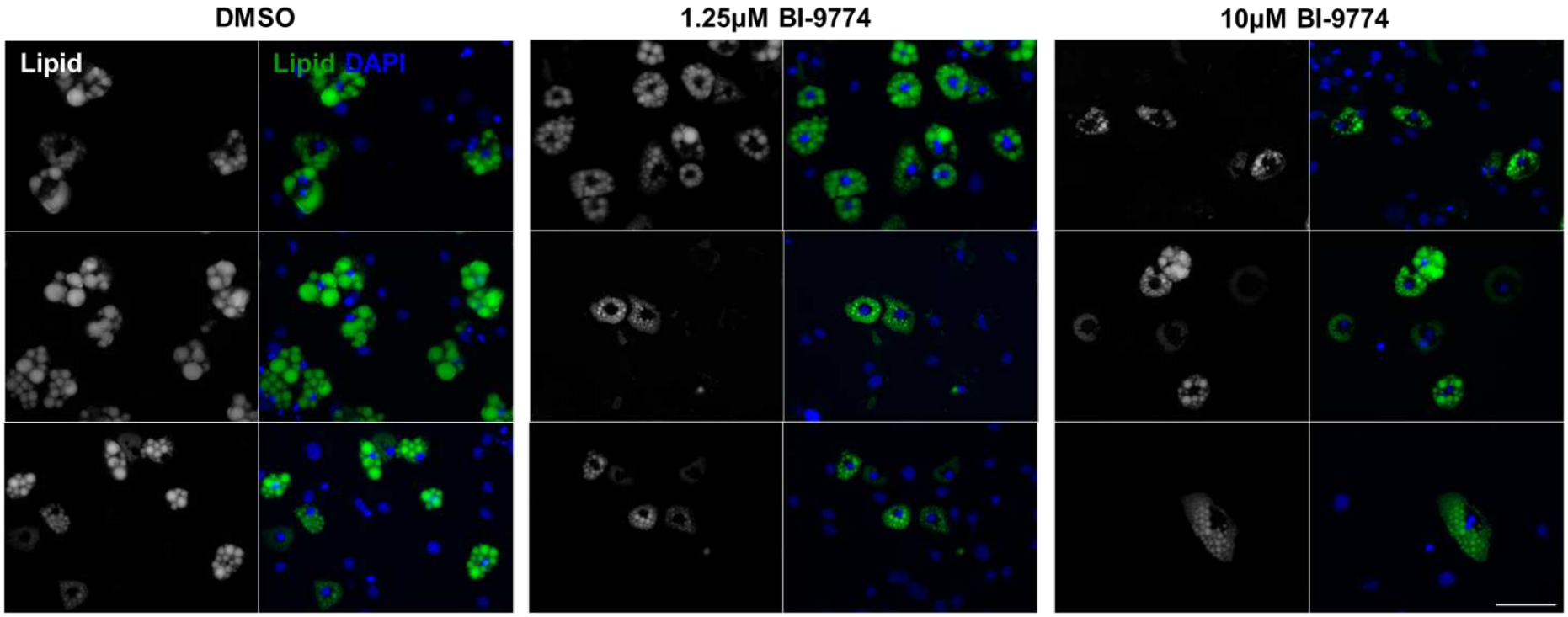


Figure 5.10 Effect of AMPK activation on adipocyte morphology in D316A SVF adipocytes

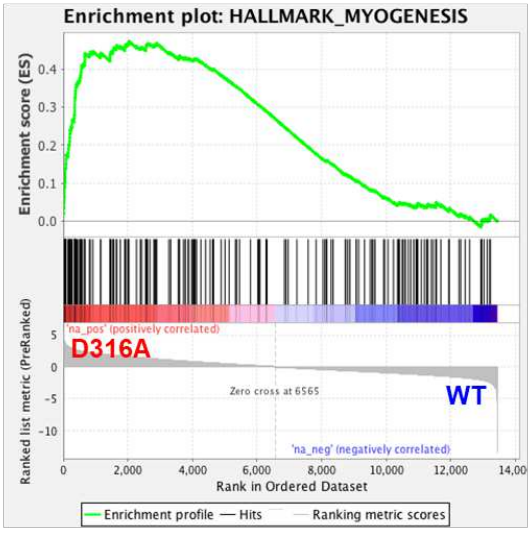
Representative images of D316A SVF adipocytes differentiated in the presence of 1.25 and 10μM BI-9774 with lipid droplet and DAPI staining. Scale bar represents 75μm.

In the WT SVF adipocytes BI-9774 reduced lipid droplet size in a dose dependent manner. As the D316A derived SVF seemed to have similar sized lipid droplets to the WT SVF, the effect of BI-9774 on D316A lipid droplet size was investigated. It appeared that the D316A adipocytes saw some reduction in lipid droplet size with the addition of BI-9774, with the greatest effect seen at 10μM (Figure 5.10), just as was seen in the WT SVF adipocytes. However, quantification is necessary before this can be determined.

5.2.2 Muscle gene expression with AMPK activation

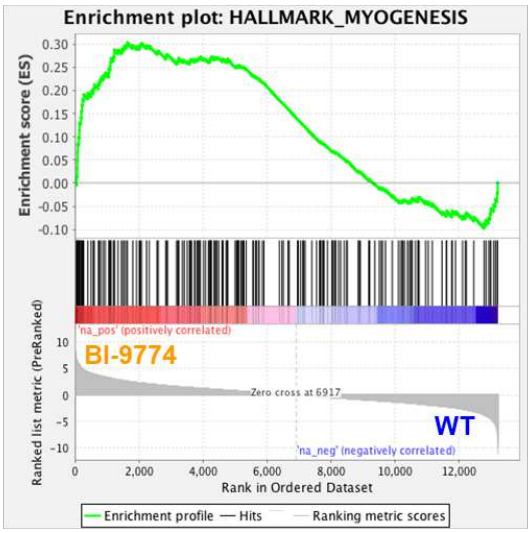
The D316A mouse showed links to skeletal muscle with skeletal muscle associated genes being upregulated in the iWAT. In the SVF adipocytes, muscle function was amongst the top GO terms associated with the genes upregulated in the D316A cells (Figure 5.1). To further investigate whether there were associations with muscle in the SVF adipocytes with AMPK activation, either through the D316A mutation or from BI-9774, the Hallmark Myogenesis gene set was used (Figure 5.11). For D316A compared to WT SVF adipocytes there was a significant enrichment in genes associated with myogenesis (Figure 5.11A). When comparing BI-9774 treated SVF adipocytes to WT cells, there was also a significant enrichment in genes associated with myogenesis, but the GSEA plot had a lower enrichment score than the plot comparing D316A to WT SVF adipocytes (Figure 5.11B). Finally, comparing D316A SVF adipocytes to BI-9774 treated SVF adipocytes there was significant enrichment in the Hallmark Myogenesis gene set in D316A cells, making it the most myogenic of the three (Figure 5.11C).

A D316A vs WT



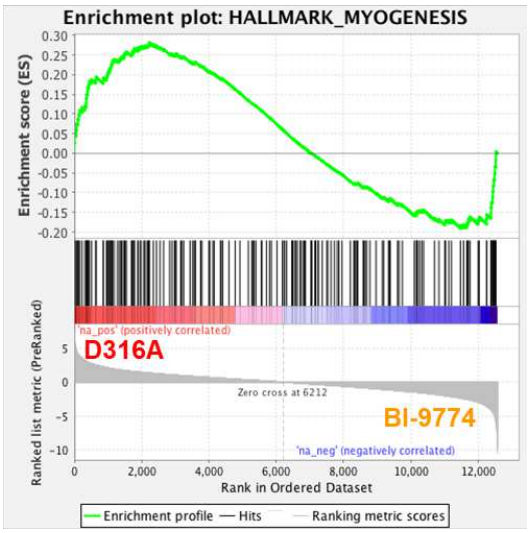
NES: 0.47 q-val: 0.000

B BI vs WT



NES: 0.30 q-val: 0.056

C D316A vs BI



NES: 0.28 q-val: 0.111

Figure 5.11 GSEA plots for myogenesis

From the RNA sequencing data set, the enrichment plots for the Myogenesis Hallmark gene set for (A) D316A compared to WT SVF adipocytes, (B) BI-9774 treated compared to untreated WT SVF adipocytes and (C) BI-9774 treated WT SVF adipocytes compared to D316A SVF adipocytes.

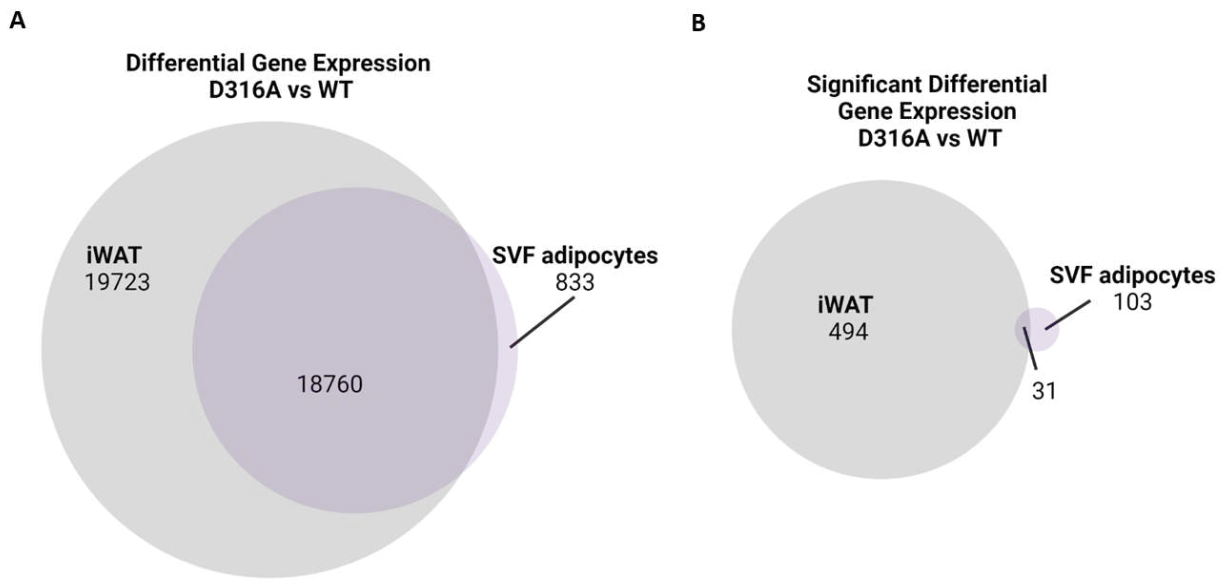


Figure 5.12 Number of overlapping differentially expressed genes between tissue and cell RNA sequencing data

Venn diagrams illustrating amount of overlap of (A) differentially expressed genes and (B) significantly differentially expressed genes from RNA sequencing data of D316A vs WT iWAT and D316A vs WT SVF adipocytes, tissue RNA sequencing data from (Pollard, 2017).

To see how the increased expression of muscle associated genes in the D316A SVF adipocytes compared to the established muscle association in the D316A iWAT, the differentially expressed genes from the published D316A vs WT iWAT transcriptomic analysis (Pollard, 2017) were compared with those of the D316A vs WT SVF adipocyte RNA sequencing in Chapter 4. Most of the genes that were differentially expressed in the SVF adipocytes were also differentially expressed in the tissue, with there being fewer differentially expressed genes in the SVF adipocytes overall (Figure 5.12A). However, when looking at those that are significantly different, as mentioned previously, there were far fewer differentially expressed genes in the SVF adipocytes (Figure 5.12B). 31 genes were overlapping between the D316A vs WT iWAT and D316A vs WT SVF adipocyte data, many of them relating to muscle (Table 5.1). GO term analysis shows that there were 15 significantly enriched GO terms relating to the list of 31 overlapping genes, most of them associated with cell-cell adhesion and signalling or with muscle function (Figure 5.13). This further supports the link between AMPK activation with the D316A mutation and muscle cell

development. There were 947 overlapping significant differentially expressed genes D316A vs WT iWAT compared to the BI-9774 treated vs WT untreated SVF adipocytes and GO term analysis showed that the top 15 significantly enriched terms were not related to muscle, but to an array of functions (Figure 4.24). The overlapping differentially expressed genes and the GSEA Hallmark Myogenesis gene set plots suggest that the link to muscle was stronger with the D316A mutation than pharmacological AMPK activation with BI-9774.

Table 5.1 List of overlapping significant differentially expressed genes between D316A vs WT iWAT and D316A vs WT SVF adipocytes

Symbol	**Gene Name**
ACTA1	actin, alpha 1, skeletal muscle
ACTN2	actinin alpha 2
AADAC	arylacetamide deacetylase (esterase)
CPXM1	carboxypeptidase X 1 (M14 family)
CD24A	CD24a antigen
CD4	CD4 antigen
CDR2	cerebellar degeneration-related 2
CFI	complement component factor i
ENO3	enolase 3, beta muscle
GANC	glucosidase, alpha; neutral C
GCHFR	GTP cyclohydrolase I feedback regulator
HMGA2	high mobility group AT-hook 2
ITGAX	integrin alpha X
ITGB7	integrin beta 7
ITGAD	integrin, alpha D
MORN4	MORN repeat containing 4
MEGF6	multiple EGF-like-domains 6
MYH7	myosin, heavy polypeptide 7, cardiac muscle, beta
NRN1	neuritin 1
OSTN	osteocrin
PGM5	phosphoglucomutase 5
PLCB2	phospholipase C, beta 2
PROX1	prospero homeobox 1

RGS5	regulator of G-protein signalling 5
SAA1	serum amyloid A 1
SAA4	serum amyloid A 4
SCN3A	sodium channel, voltage-gated, type III, alpha
STAB2	stabilin 2
TGM1	transglutaminase 1, K polypeptide
TNNC2	troponin C2, fast
TNNT3	troponin T3, skeletal, fast

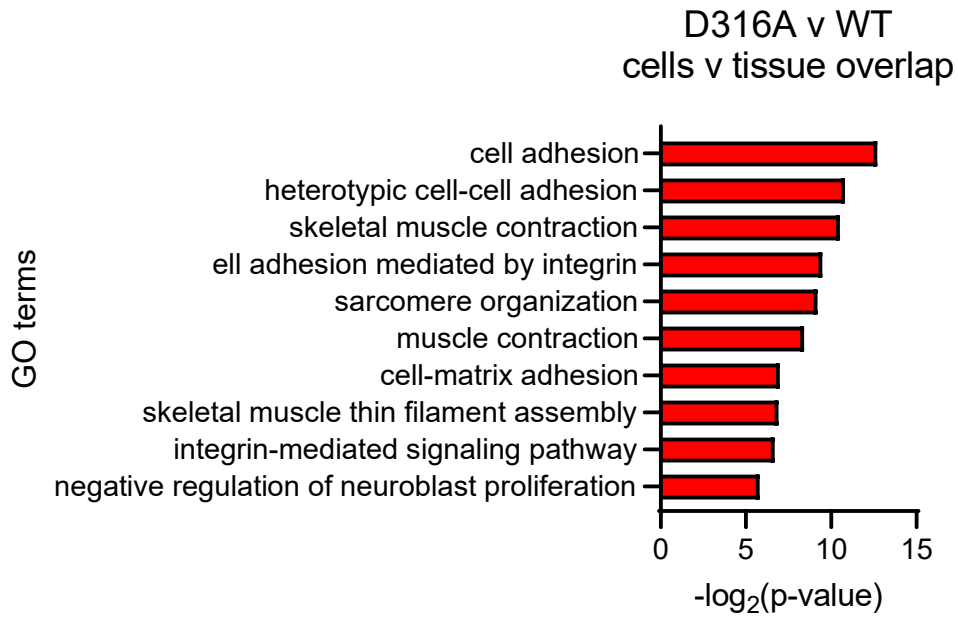


Figure 5.13 Muscle association of overlapping differentially expressed genes between tissue and cell RNA sequencing data

Top significantly enriched GO terms from the list of overlapping significantly differentially expressed genes from RNA sequencing data of D316A vs WT iWAT and D316A vs WT SVF adipocytes.

5.3 MYOBLAST ADIPOGENIC DIFFERENTIATION WITH AMPK ACTIVATION

To follow on from AMPK activation creating an adipocyte expressing muscle-associated proteins, it was investigated whether AMPK can increase the formation of adipocytes from a skeletal muscle precursor cell.

5.3.1 C2C12 adipogenic differentiation with AMPK

C2C12 cells were put through adipogenesis with a standard adipogenic protocol used for the SVF, with AMPK activators 991 and BI-9774 present throughout adipogenesis. Two AMPK activators were used to see if the effect was consistent. Based on the optimal concentrations in E14 cells (Figure 4.11) and the SVF (Figure 4.8), 991 was used at 10μM and BI-9774 was used at 1.25μM. Firstly, their effect on AMPK activation was assessed by looking at the phosphorylation of downstream targets of AMPK (Figure 5.14). Both BI-9774 and 991 led to significant increases in phosphorylation of ACC (Figure 5.14B). Whilst both activators led to an increase in phosphorylation of ULK1, the change didn't reach significance, and there was no change in p-AMPKα as the levels of AMPKα seemed to change (Figure 5.14C, D). This may be due to an increase in levels of total ULK1 (Figure 5.14A) which although is not significant (data not shown), could have impeded changes in phosphorylation being significant. However, there was enough evidence to show that AMPK was active with the concentrations of activators used.

To assess the effects of AMPK activation on C2C12 adipogenesis, cells were stained for lipid droplets and DAPI at the end of adipogenic differentiation to calculate the adipogenic index (Figure 5.15). An increase in lipid droplet staining with AMPK activation was visible in the whole well scans (Figure 5.15A), and quantification of lipid droplet staining supports the visual increase (Figure 5.15B). Clustering of the different shaped symbols which represent different biological replicates on the bar charts shows that there was strong variation in levels of lipid droplet staining between the biological replicates, but the pattern remained the same. The increase in lipid droplet staining was only significant with 991. Consistent with previous data, AMPK activation with 991 or BI-9774 led to a significant reduction in cell number as AMPK slowed proliferation (Figure 5.15C). The adipogenic index reflected the quantification of lipid droplet staining with a significant increase with 991 and the increase with BI-9774 not being significant (Figure 5.15D).

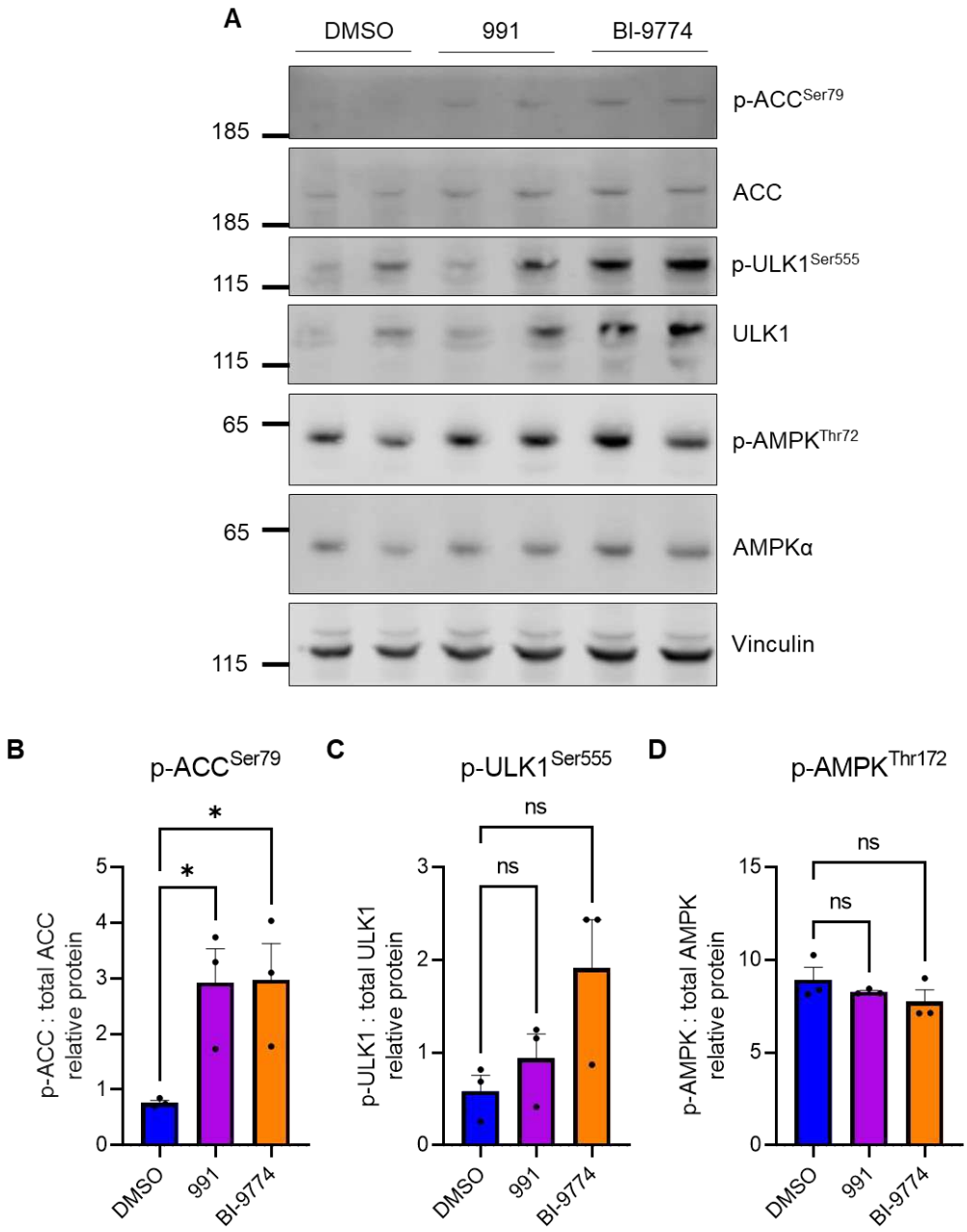


Figure 5.14 Characterising AMPK activation in C2C12 cell adipogenesis

*C2C12 cells were differentiated to adipocytes with 10μM 991 or 1.25μM BI-9774. (A) Representative Western blot showing phosphorylation of AMPK targets with quantification of (B) p-ACC relative to ACC, (C) p-ULK1 relative to ULK1 and (D) p-AMPK relative to AMPK, all relative to vinculin. Data are shown as mean ± SEM with statistical significance determined by one-way ANOVA with Dunnett's correction for multiple comparisons, *p<0.05, (n=3).*

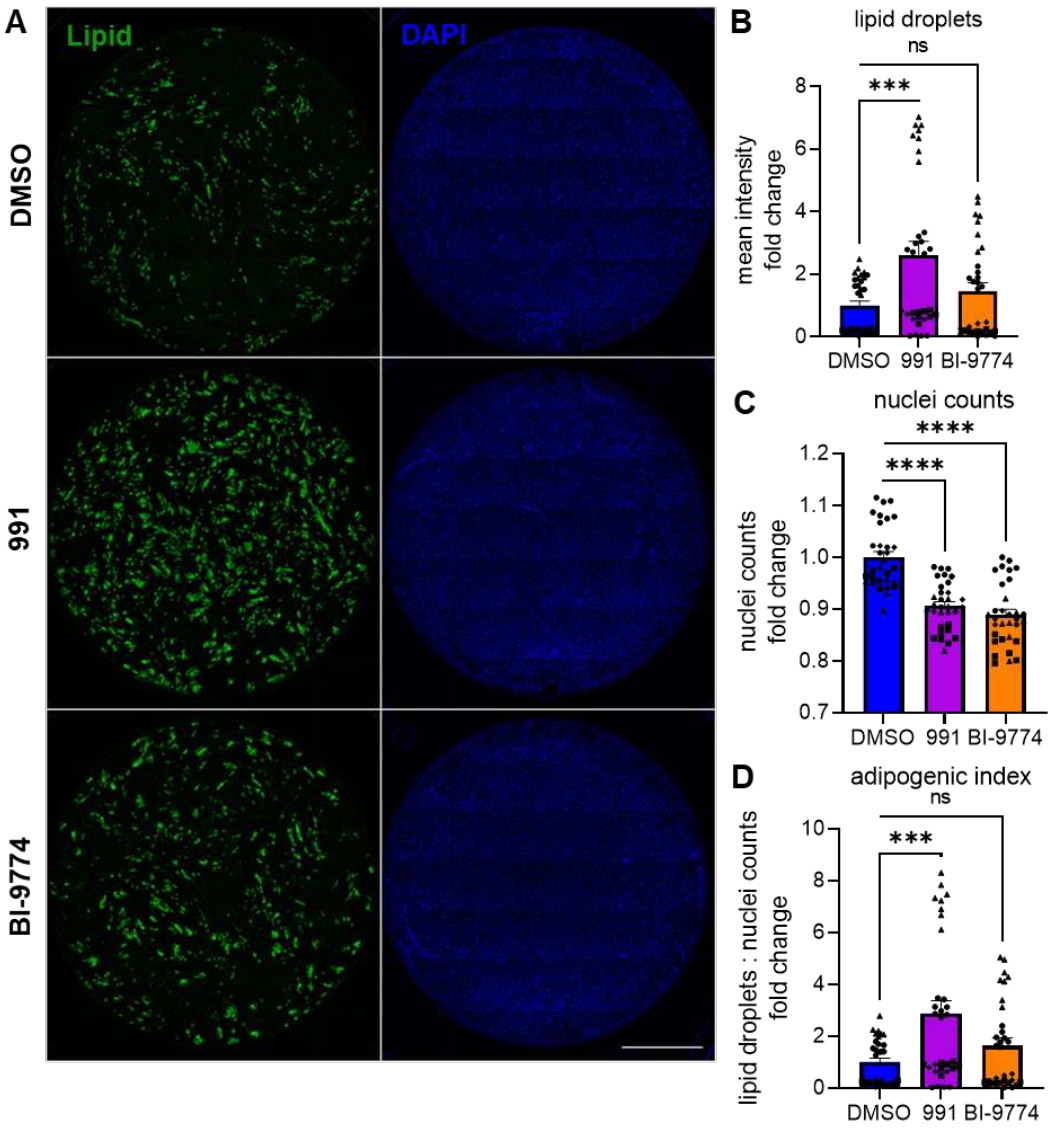


Figure 5.15 The effect of activating AMPK in C2C12 adipogenesis

*C2C12 cells were differentiated to adipocytes with 10μM 991 or 1.25μM BI-9774. (A) Representative images of whole well scans with lipid droplet and DAPI staining. (B) Quantification of lipid droplet staining from whole well scans. (C) Nuclei counts from whole well scans. (D) Normalisation of lipid droplet staining to nuclei counts to calculate the adipogenic index. Data are shown as mean ± SEM, with different biological replicates represented by different shaped symbols. Statistical significance is determined by one-way ANOVA with Dunnett's correction for multiple comparisons, ***p<0.001, ****p<0.0001, (n=5, biological replicates represented by different shaped symbols, 4 technical replicates each). Scale bar represents 1500μm.*

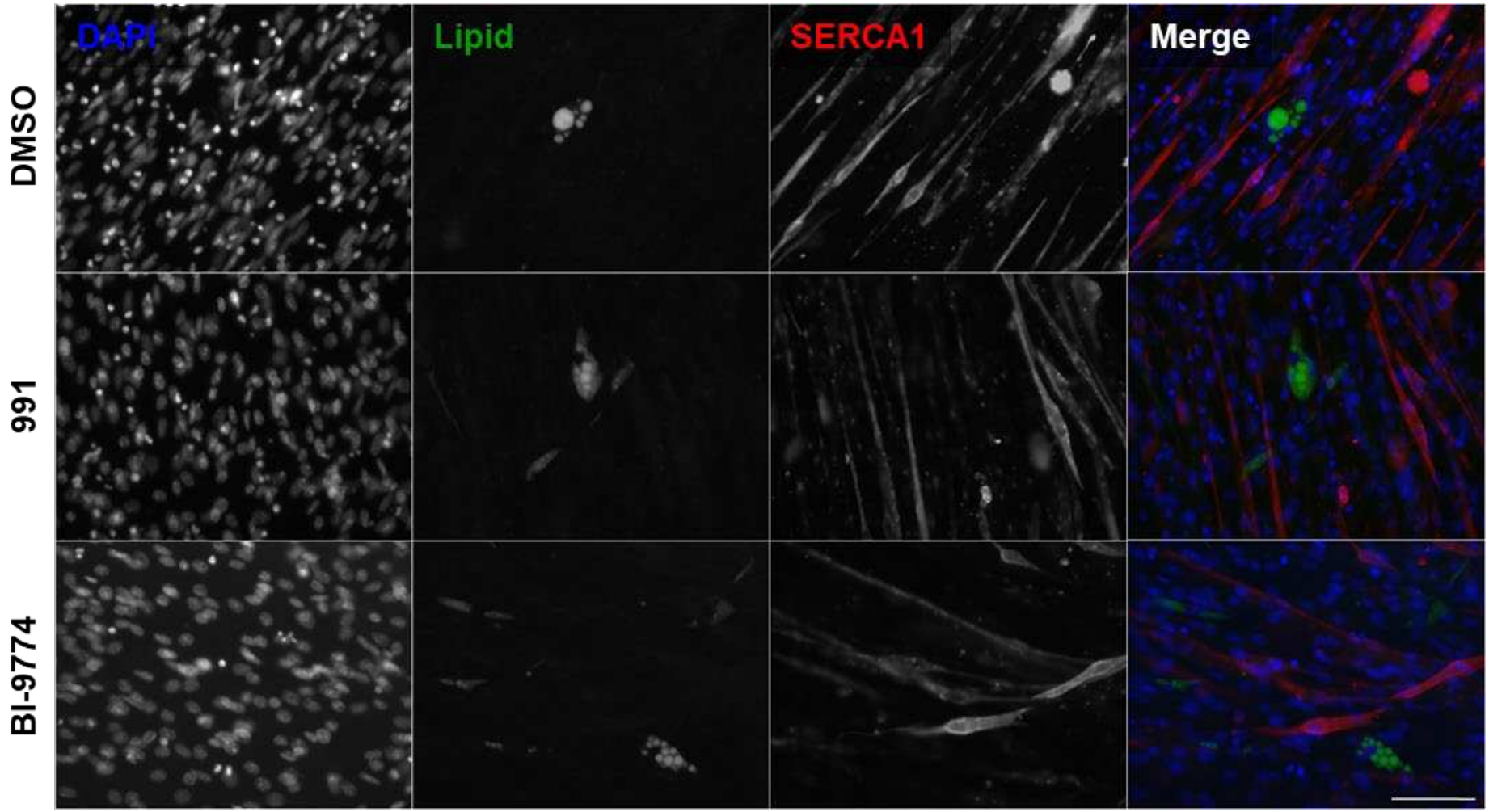


Figure 5.16 C2C12 derived adipocytes

Representative images of C2C12 derived adipocytes differentiated in the presence of 10μM 991 or 1.25μM BI-9774 stained for lipid droplets, DAPI and SERCA1. Scale bar represents 75μm.

High magnification images showed the appearance of the adipocytes formed in C2C12 cells, with their lipid droplets stained (Figure 5.16). Whilst some of them resembled the morphology of the primary adipocytes derived from the SVF, more rounded with larger lipid droplets, some of the adipocytes appeared more elongated with smaller lipid droplets. These could be less mature adipocytes. The mature skeletal muscle cells expressed SERCA1 and were morphologically distinct from the adipocytes, forming longer and multinucleated fibres. It was interesting to note that the adipocytes formed did not express SERCA1.

Following up on the adipogenic index, mRNA levels of adipocyte markers were investigated in the C2C12 adipocytes (Figure 5.17). Again there was substantial variation between replicates, and as a consequence most of the changes did not reach statistical significance. *Pparγ*, *Lpl*, *Plin1* and *Adipoq* followed the trend seen with the adipogenic index with increased expression following AMPK activation with 991, whilst there was only an increase in expression with BI-9774 for *Pparγ* and *Lpl*. *Cebpα* expression appeared to reduce with AMPK activation, whilst *leptin* followed an unclear pattern but with little difference upon AMPK activation. *Gabpα,* which was shown to be important in driving the generation of an adipocyte from a myoblast (Chen et al., 2019b), showed little increase with AMPK activation. In general, individual adipocyte markers did not give substantial evidence of an increase in adipogenesis with AMPK activation.

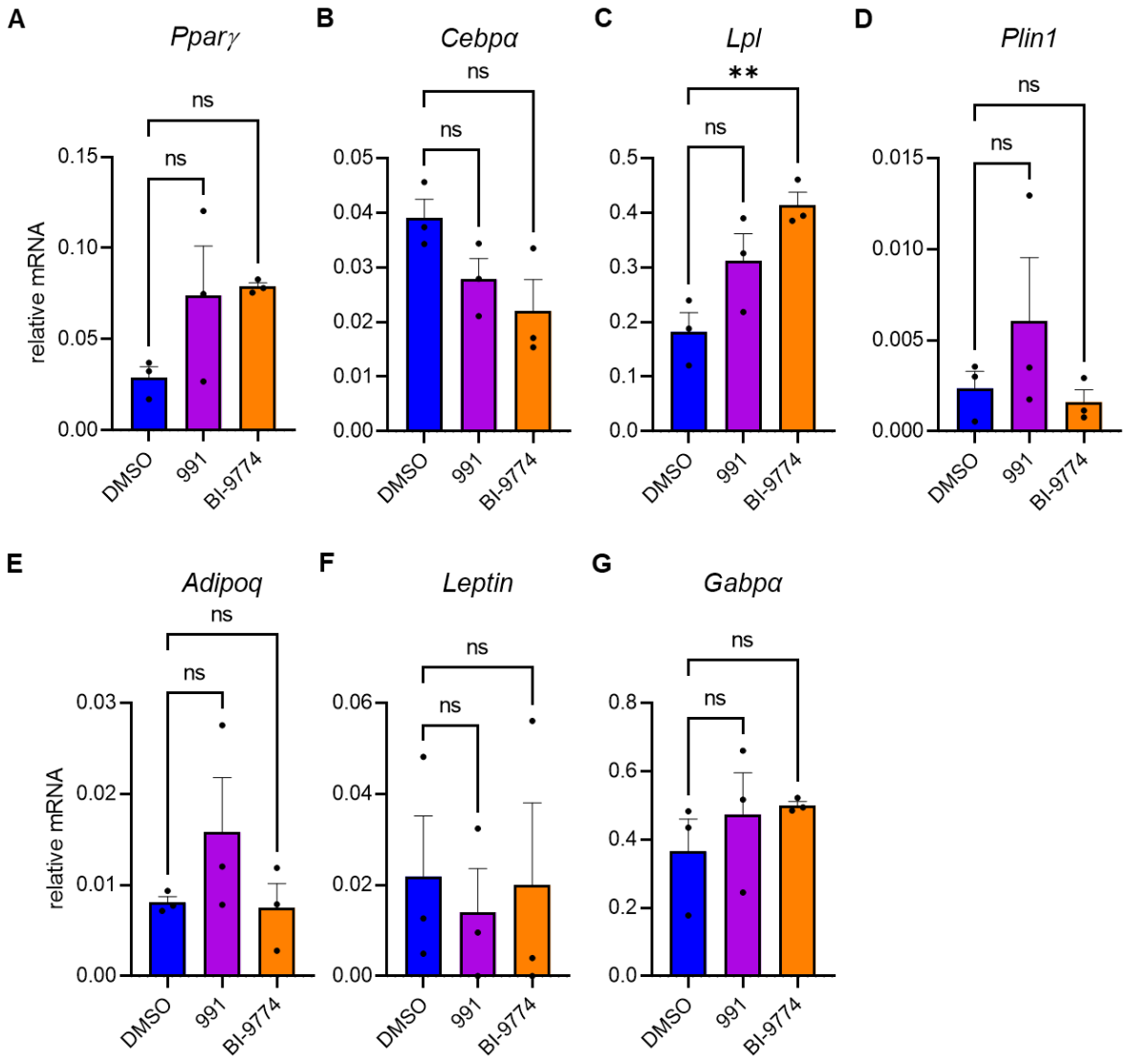


Figure 5.17 Effect of AMPK activation during C2C12 adipogenesis on adipocyte marker genes

*(A-G) C2C12 cells were differentiated to adipocytes with 10μM 991 or 1.25μM BI-9774, with adipocyte marker gene mRNA expression assessed. mRNA levels relative to housekeeping gene 36B4. Data are shown as mean ± SEM with statistical significance determined by one-way ANOVA with Dunnett's correction for multiple comparisons, **p<0.01, (n=3).*

5.3.2 Human skeletal muscle myoblast adipogenic differentiation with AMPK

This mixed set of data hints that AMPK activation may increase lipid droplet accumulation in C2C12 cells, with unclear effects . To see whether this is possible in human skeletal muscle

myoblasts, CC-2580 cells were used. These are myoblasts isolated from healthy donor upper arm or leg biopsies that can be passaged and differentiated to human skeletal muscle cells. Unlike with mouse myoblasts cells, there is very limited literature on the adipogenic differentiation of human myoblasts. For the first attempt, the usual adipogenic differentiation protocol was used as it worked with C2C12 cells, with 10μM 991 or 1.25μM BI-9774 present throughout adipogenesis. This protocol yielded no mature adipocytes (Figure 5.18). Wheat germ agglutinin (WGA) was used to visualise the whole cell with lipid droplet and DAPI staining. Representative images showed that the cells take on a more myocyte-like morphology with an elongated shape and multinucleated cells visible. There was no striking difference in the appearance of the cells with AMPK activation resulting from either activator. One study showed adipogenic differentiation of human muscle satellite cells was possible with the addition of rosiglitazone (De Coppi et al., 2006). In a repeat adipogenic differentiation of the CC-2580 cells, 10μmol/l rosiglitazone was added to the differentiation cocktail (Figure 5.19). However, this did not lead to the formation of mature adipocytes. Again the cells possessed a more elongated, myocyte-like morphology and there was no visible difference between cells treated with 991 or BI-9774 compared to untreated cells.

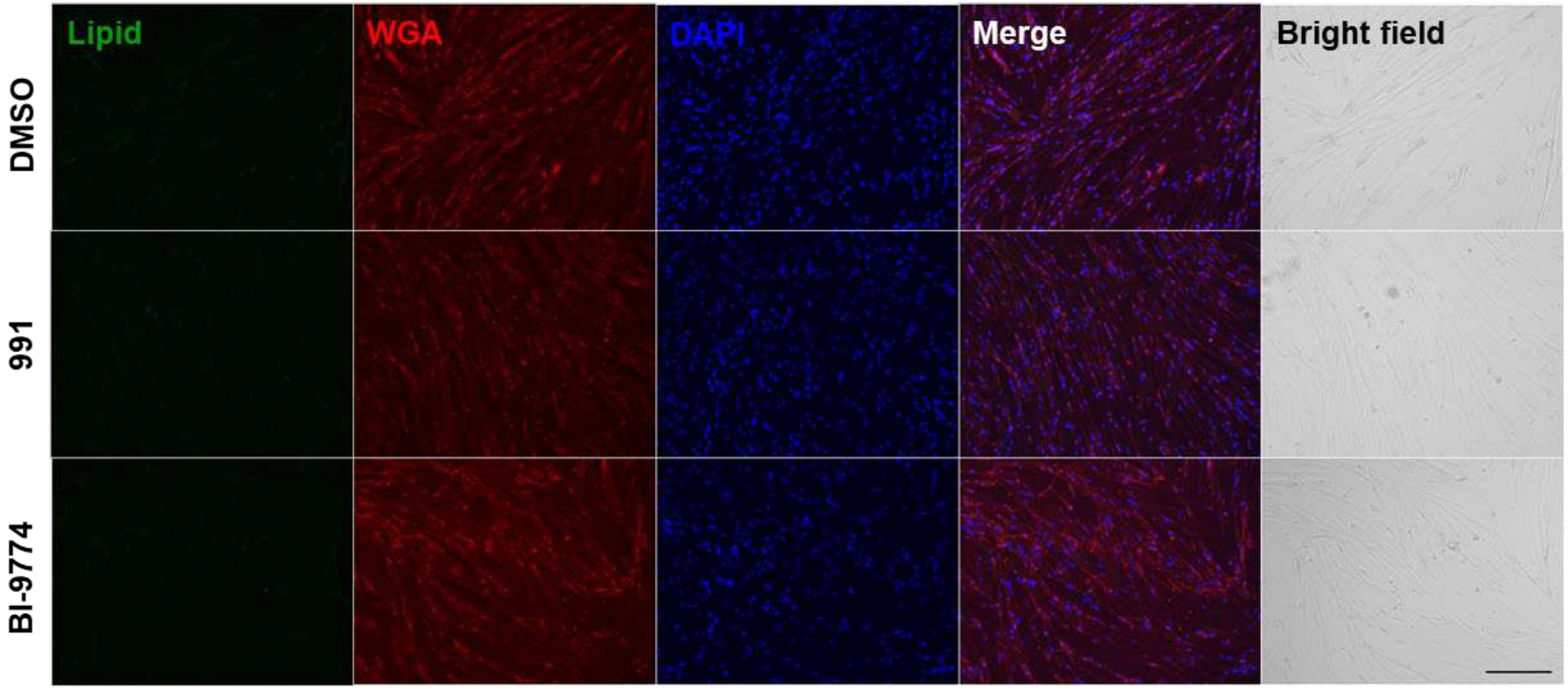


Figure 5.18 Effect of AMPK activation in human skeletal muscle myoblast adipogenic differentiation

Human skeletal muscle myoblasts CC-2580 were put through adipogenic differentiation with 10μM 991 or 1.25μM BI-9774, with lipid droplet, wheat germ agglutinin (WGA) and DAPI staining at the end of adipogenesis. Representative images shown. Scale bar represents 275μm.

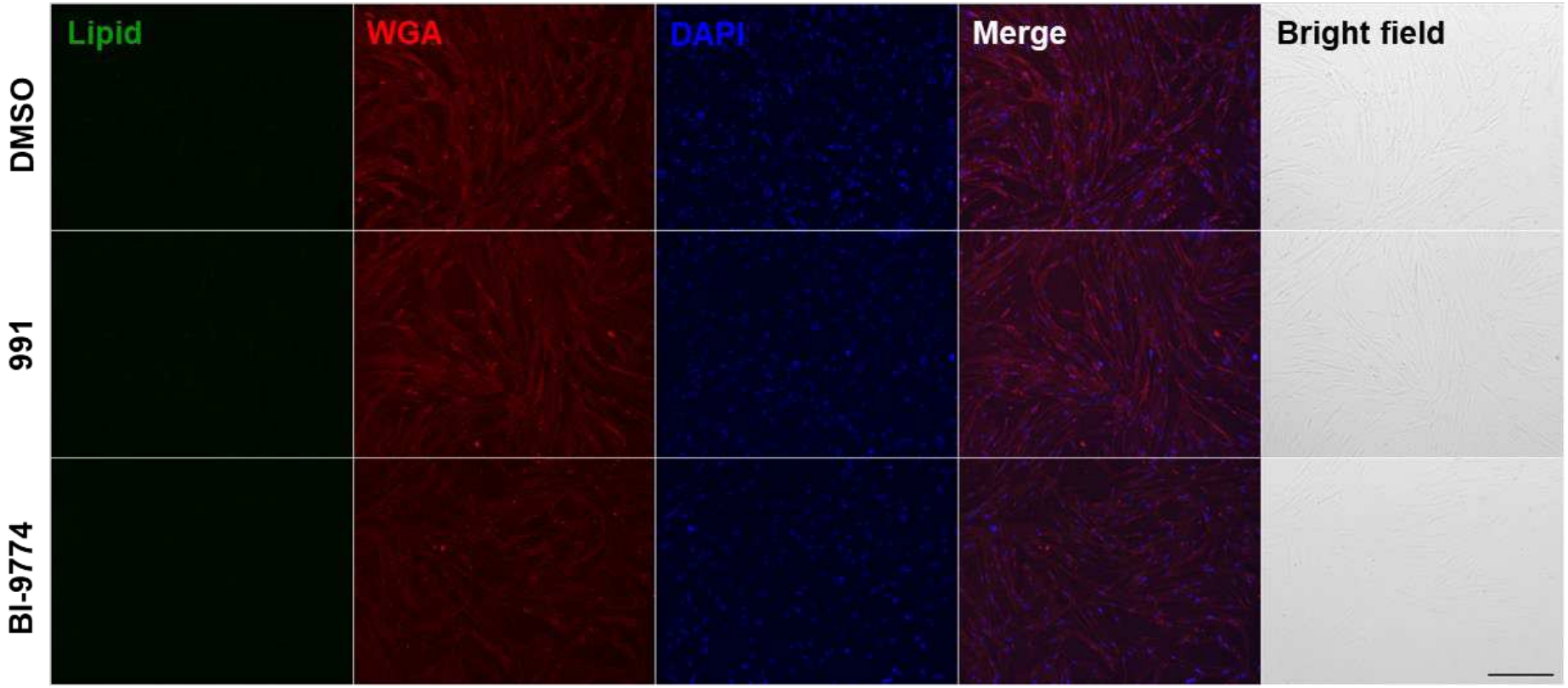


Figure 5.19 Effect of AMPK activation in human skeletal muscle myoblast adipogenic differentiation with rosiglitazone

Human skeletal muscle myoblasts CC-2580 were put through adipogenic differentiation with rosiglitazone and 10μM 991 or 1.25μM BI-9774, with lipid droplet, WGA and DAPI staining at the end of adipogenesis. Representative images shown. Scale bar represents 275μm.

5.4 DISCUSSION

Isolating the D316A SVF for adipogenesis gives clues to the origins of SMART cells, allows the determination of their autonomy and may provide a cell based model to study AMPK activation in adipose tissue. To assess whether it is a good cell based model to interrogate SMART cells it is important to know how well the phenotype observed in the mouse iWAT was preserved in the isolated SVF.

The D316A SVF adipocytes retained the increase in mitochondria biogenesis (Figure 5.6), although the effect was much more subtle than in the tissue (Pollard et al., 2019). It would be good to investigate this further to see whether the change in mitochondrial content plays a role in mitochondrial function. Mouse iWAT explants showed increased basal and spare respiratory capacity in the D316A tissue (Pollard et al., 2019). The Seahorse XF Analyzer could be utilised to assess the mitochondrial capacity of the primary SVF adipocytes to see if these differences are retained, and if the increased mitochondrial content in the D316A SVF adipocytes effect's mitochondrial function. It would also be interesting to assess the freshly isolated and plated D316A and WT SVF before adipogenic differentiation to see whether there are differences in mitochondrial metabolism at this stage, as it has been shown that mitochondrial metabolism effects progenitor cell fate and determines the subtype of adipocyte formed (Joffin et al., 2021). Differences in mitochondrial metabolism in progenitor cells with AMPK activation may affect the function of the adipocyte that is formed and may be a factor influencing the differentiation of SMART cells.

The D316A SVF adipocytes also preserved the muscle link observed in the iWAT, as was seen with GSEA of RNA sequencing data (Figure 5.11). Nevertheless, generation of an active SMART cell was not achieved here *in vitro*. β-AR agonists such as norepinephrine classically stimulate UCP1 mediated ATP futile cycling for thermogenesis in adipocytes and have also been shown to induce calcium futile cycling through the cardiac isoform of SERCA, SERCA2b, in adipose tissue (Ikeda et al., 2017). However, treatment with norepinephrine did not stimulate increased SERCA1 or SERCA2 mediated thermogenesis in the D316A SVF adipocytes (Figure 5.7). In these studies, β-AR agonists have not been able to induce UCP1 mediated thermogenesis in white adipocytes, which is contrary to literature. The concentrations and time frames used are in line with published literature. Although not all shown here, several β-AR agonists at a range of concentrations and times were tested

which increased *Ucp1* mRNA levels but these changes never translated to an increase in protein levels, for which a range of anti-UCP1 antibodies were tried which successfully detected UCP1 expression in BAT. It may be that there was a systematic issue with the treatment. However, norepinephrine was able to increase phosphorylation of HSL on its PKA phosphorylation sites which are downstream of β-AR signalling (Figure 5.7). This finding demonstrates a positive response to treatment with β-AR agonists. In the D316A mouse it is high fat diet that triggers the expression of SERCA1, so it may be that β-AR signalling is not the correct way to stimulate SERCA1 expression and another method is needed to stimulate thermogenesis in these cells *in vitro* such as palmitate feeding. It may also be that the SMART cell progenitors are recruited upon high fat diet feeding, so stimulation may be required throughout differentiation.

The retention of the increased muscle gene expression and higher mitochondrial content show that the D316A can retain some of its *in vivo* characteristics *in vitro* (Figure 5.11). However, the changes are subtle. RNA sequencing shows only 31 genes significantly differ in expression levels between the D316A and WT SVF adipocytes, and so there is little differentiating them (Table 5.1). The morphology of the D316A SVF adipocytes was also indistinguishable to that of the WT (Figure 5.5), which is a departure from what is observed in the tissue.

In this study it has not been possible to generate a SMART cell with active thermogenesis. As the SVF from the β-actin Cre mouse was used to generate primary adipocytes, it is unlikely that the SMART cell progenitor is absent from the starting pool of cells. There is some evidence of adipocytes arising from endothelial or hematopoietic precursors (Sera et al., 2009; Tran et al., 2012) which often don't adapt well to growth on plastic without special media, and are outcompeted by other cells in the SVF (Min et al., 2016). It could be that the cells arise from one of these progenitors. However, whether endothelial or hematopoietic cells can truly give rise to adipocytes is heavily disputed (Kanda et al., 2009). As discussed, it could also be that the correct stimuli were not present to induce SMART cells.

It may be that the SMART cell progenitors make up a relatively small proportion of the SVF and that environmental factors promote their expansion and differentiation over other adipocyte subpopulation progenitors. However, even on a regular chow diet the D316A iWAT had smaller and more multilocular lipid droplets than WT iWAT (Pollard et al., 2019),

yet the D316A SVF adipocytes were morphologically indistinguishable from the WT cells (Figure 5.5). More accurate quantification of lipid droplet size would have been advantageous. However, this was not possible at the time of these experiments. Nevertheless, there should be observable differences between the D316A and WT SVF adipocytes without stimulation if they are to be a reliable and robust model for SMART cells.

Finally, it may be that some, or all of the SMART cell phenotype is not cell autonomous, and that there are other environmental cues present *in vivo* that are lacking in the cell culture environment which are essential for SMART cell generation. Investigating this could be more difficult. It could be investigated through transplantation of WT mouse SVF into the D316A iWAT to see whether the WT cells take on the morphology and function of the D316A adipose tissue. However, if AMPK activation is needed in an earlier precursor cell type, then using the SVF would not be possible.

A benefit of isolating the D316A SVF is to compare the effect of the genetic activation with pharmacological activation of AMPK in cells. In chapter 4 it was observed that whilst both BI-9774 treatment and the D316A mutation had similar levels of AMPK activity (Figure 4.17), BI-9774 had a stronger effect on AMPK downstream targets (Figure 4.18), and this parallels with the RNA sequencing data showing that the pharmacological activation of AMPK lead to more changes in the SVF adipocytes than the D316A mutation, which was more similar to untreated WT SVF adipocytes (Figure 4.21). The main effects of BI-9774 activation of AMPK on *in vitro* adipogenesis was reduced adipocyte differentiation and a reduction in proliferation and adipocyte lipid droplet size. GSEA for the Hallmark Adipogenesis gene set showed significant reduction in adipogenesis in the D316A SVF adipocytes compared to WT SVF adipocytes (Figure 5.2). When individual adipocyte marker genes are assessed there is a consistent trend for reduced expression, although none are significant (Figure 5.3). The significant reduction in the Hallmark Adipogenesis gene set is therefore due to small consistent decreases in many of the associated genes which on their own do not show a statistically significant reduction.

When looking at adipogenic index there was no apparent reduction in adipocyte differentiation from D316A SVF compared to WT SVF (Figure 5.4). Although there did appear to be an increase in lipid droplet staining, there was also an increase in nuclei in the D316A SVF. This result on cell number was unexpected as it differs from the typical effect of

AMPK activation *in vitro* in which there is slowed proliferation, observed in this work with BI-9774 in the SVF, and also widely reported in the literature (Steinberg and Carling, 2019). However, when under conditions of stress, AMPK activation gives the cell a survival advantage and can increase proliferation (Jeon et al., 2012; Vincent et al., 2015), so it may be that the D316A SVF is more able to survive the stress of isolation and adaptation to growing on plastic. The increased proliferation with the D316A mutation may be a compensatory mechanism occurring when there is chronic constitutive activation of AMPK throughout development, to allow for the formation of a viable mouse, as if the reduced proliferation and adipogenesis remained as strongly *in vivo* it may perturb development. It is possible that there is also an increase in number of adipocytes in the iWAT of the D316A mouse compared to WT, as this was not measured. Increased proliferative ability is an advantage in obesity, allowing for healthy hyperplasic expansion of the adipose tissue with recruitment of new adipocytes instead of the hyperplasic growth that is associated with inflammation and fibrosis, and this may have an additive beneficial effect in combination with the increased energy expenditure in the D316A mouse.

The D316A SVF adipocytes more closely resemble WT SVF adipocytes than adipocytes with pharmacological AMPK activation when looking at the RNA sequencing data and at the morphology of the adipocytes themselves. Whilst the D316A mutation confers constitutive activation of AMPK through weakened binding of AMP, BI-9774 is an ADaM site ligand whose binding leads to conformational changes protecting AMPKα^{Thr172} from dephosphorylation. Further AMPK activation in the D316A cells with chronic BI-9774 treatment throughout differentiation led to the same reduction in adipogenesis and formation of adipocytes with smaller lipid droplets as is seen in WT SVF (Figure 5.10). So, it may be that the smaller effect from the D316A mutation is due to the lower levels of AMPK activation, as increased activation leads to a greater change in adipocyte number and morphology.

Whether the D316A SVF adipocytes are a good cell model to study AMPK activation in adipose tissue is unclear. However, given the little difference between D316A and WT SVF adipocytes, pharmacological activation of AMPK in WT SVF adipocytes is likely the better and more clinically relevant cell model.

The link between AMPK and muscle associated gene expression in adipose tissue has been previously established. In addition to the D316A mutation inducing SERCA mediated thermogenesis, a low protein and high carbohydrate diet has also been found to activate AMPK, which was essential to induce muscle associated gene expression during cold induced browning (Aquilano et al., 2020). Again, in the *in vitro* D316A SVF adipocytes there is still expression of muscle associated genes which overlap with the differentially expressed genes from the iWAT (Figure 5.13). The reason for the less muscle-like phenotype in the BI-9774 treated adipocytes compared to the D316A SVF adipocytes may be that AMPK needs to be activated at an earlier precursor cell stage and that the progenitors in the SVF are already too committed to their lineage by the time AMPK is activated. It could also be that exposure to AMPK activation is not long enough in the *in vitro* model, where the mature cells are only present for a few days before they are harvested, or that there is not appropriate stimulation, as the other studies observed changes after diet stimulation.

AMPK is essential for myogenesis through modification of the myoblasts epigenetic landscape via regulation of chromatin modifiers HDAC5 and TET2 (Fu et al., 2013; Zhang et al., 2019a). In the absence of AMPK, myogenesis is impaired both *in vitro* and *in vivo.* However, like what seen in adipogenesis, activation of AMPK can prevent myogenesis through interruption of the cell cycle (Williamson et al., 2009). AMPK subunit levels and activity increase throughout myogenesis, so it may be that whilst AMPK is essential for complete myogenesis, the timing of AMPK activation is significant for regulating the process (Niesler et al., 2007; Zhang et al., 2019a).

The adipogenic differentiation of C2C12 cells previously has been shown to be linked to GABPα (Chen et al., 2019b). Novel adipocytes were derived from a myoblast precursor, and under specialised conditions of cold exposure without β-AR signalling, myotubes were formed in adipose tissue. As AMPK activation gives rise a specialised adipocyte with an association with skeletal muscle, it was of interest to see if a similar effect could be observed. Without AMPK activation it is possible to induce some fate switching to promote a proportion of C2C12 cells to become adipocytes using an adipogenic cocktail. AMPK activation did further increase adipogenesis although only when looking at the adipogenic index, and there was high variability in the data which made it difficult to draw a conclusion (Figure 5.15). If AMPK activation can increase adipogenic differentiation from a myoblast

precursor, this would be different to its ability to reduce adipogenesis from an adipocyte precursor. Increasing lipogenesis which is essential for lipid droplet formation also seems at odds with the canonical effect of AMPK to inhibit ACC. AMPK is needed for reduced methylation at transcriptional start sites and more open chromatin in myoblasts and myotubes (Zhang et al., 2019a). It could be that increased AMPK activation leads to increased de-methylation and more chromatin opening allowing for increased fate switching by enhancing the effects of the adipogenic cocktail which will promote adipogenesis through increased expression of adipogenic genes. If the effect of AMPK activation on C2C12 adipogenesis was more robust and consistent, then it would be interesting to follow this up by looking at whether there are genome-wide changes in DNA methylation with AMPK activation in the initial stages of differentiation using a method such as methylated DNA immunoprecipitation and high throughput sequencing. It was not possible to induce adipogenesis of human skeletal muscle myoblasts and it may be that human cells are less flexible to fate switching than mouse cells.

In conclusion, AMPK may play a role in the link between adipocytes and muscle cells, although more investigation is needed to conclusively draw the connection. It appears as though the D316A SVF adipocytes weakly retain some of the features seen in the tissue, but as of yet have not been able to provide a cell based model of SMART cells which appear to not be fully cell autonomous. D316A SVF adipocytes are overall closer to WT SVF adipocytes and their AMPK activation has a weaker effect *in vitro* compared to BI-9774 treatment. It will be interesting to see the effects of BI-9774 *in vivo*, as it may be more similar to the D316A mutation and is of clinical relevance.

6. SUMMARY AND FUTURE PERSPECTIVES

The first aim of the study was to determine the cell autonomy of adipocytes isolated from D316A mice and their therapeutic potential in protection against diet induced obesity following adipose tissue allograft transplantation. Direct transplantation of adipose tissue from a D316A mouse did not lead to significant therapeutic benefits in the recipient in terms of diet induced obesity (Chapter 3). Allograft transplantation of D316A adipose tissue (Chapter 3), as well as isolation and differentiation of D316A SVF (Chapter 5), suggests that the effects observed in the D316A mouse are not fully cell autonomous. Interestingly, a patch of multilocular adipocytes was detected in one of the D316A allografts, suggesting that there could be some tissue autonomy, but that it is not a robust response (Chapter 3). Further evidence from isolation and differentiation of D316A SVF showed that there was a slight increase in mitochondrial content of adipocytes, and there was retention of the skeletal muscle gene expression. However, again this was not a robust phenotype and overall D316A SVF adipocytes closely resembled WT SVF adipocytes (Chapter 5). This suggests that external factors brought about by whole body activation of AMPK might influence the adipose tissue phenotype *in vivo*. Determining these factors will give more insight into the beneficial effect of constitutive, whole body activation of AMPK. Whilst some investigation into the serum of the D316A mouse was done, deeper probing of the serum components with proteomics and metabolomics may reveal differences between WT and D316A mice. In addition, adipose tissue denervation studies may help to determine whether it is neuronal signalling that influences the D316A adipose tissue phenotype. However, these are more complex and invasive studies. As previously discussed, allograft transplantation of WT adipose tissue into a D316A recipient would confirm whether it is extrinsic factors that determine the D316A adipose tissue phenotype. In addition, transplantation of progenitors derived from the adipose tissue SVF of a mouse expressing RFP to allow for tracking of the transplanted cells could confirm whether this is a developmental effect or whether adult stem cells can undergo the changes required to produce SMART cells.

The third aim of the study was to explore the role of AMPK in adipose tissue and muscle cell fate determination. The D316A SVF derived adipocytes retained some of the skeletal muscle characteristics in the D316A iWAT transcriptome, and there was an increase in adipogenesis with pharmacological AMPK activation in C2C12 myocytes (Chapter 5). The D316A SVF derived adipocytes seemed to be able to initiate a more robust myogenic program than BI-

9774 treatment of SVF adipocytes, which may be due to a threshold of AMPK activation being required, which BI-9774 goes beyond. However, this link was weak and more robust data would be needed to support investigating any further. Gaining further understanding of the role of AMPK in the early stages of adipogenesis may give more clues about its involvement in cell fate determination.

The second aim of the study was to determine the effects of pharmacological AMPK activation in adipogenesis. The main finding from this study was that AMPK's previously described suppression of adipogenesis occurred in the SVF derived adipocytes with BI-9774, and that it was not linked to its inhibition of ACC (Chapter 4). This disproves one of the suggested but not deeply investigated theories that it is AMPK's inhibition of fatty acid synthesis that is responsible for its suppression of adipogenesis (Choi et al., 2015; Habinowski and Witters, 2001; He et al., 2013). AMPK inhibition of fatty acid synthesis through ACC inhibition may be relevant in the reduction of lipid droplet size (Figure 6.1). However, further lipid tracing studies to determine the fate of lipids into triglycerides would be needed to conclude this. AMPK inhibition of TAG synthesis through glycerol-3-phosphate acetyl transferase may also cause the reduction in lipid droplet size, and this could be followed up.

This study supports work showing that AMPK suppresses adipogenesis in the early stages of the process (Vingtdeux et al., 2011; Zhou et al., 2009). Addition of BI-9774 from the beginning of E14 adipogenesis led to higher levels of stem cell markers. Additionally, morphology and transcriptomes of BI-9774 in SVF adipogenesis hinted at a less mature, more stem cell-like state. These suggest that AMPK activation is important in stem cell maintenance and differentiation. It may be that maintaining the AMPK-mTOR balance is important for this (Cho et al., 2004; Kim and Chen, 2004; Yeh et al., 1995). Further study into the changes effected by activation of AMPK in the early stages of differentiation will be important to determine how it exerts its effects. AMPK activation slows proliferation, and this is suggested to be the mechanism by which it suppresses adipogenesis (Vingtdeux et al., 2011; Zhou et al., 2009) (Figure 6.1). However, the role of proliferation and specifically the mitotic clonal expansion phase in adipogenesis in vivo still not fully understood due to the complexity in studying it. Cellular labelling and tracing studies in mouse adipose tissue which

use fluorescent reporters currently require culling of mice to detect the labelled populations, meaning that live in vivo tracing is not yet possible.

Further investigation into the role of AMPK in adipogenesis could involve studying the changes induced in the earliest stages of adipogenesis, between days 0 to 2. Phosphoproteomic studies could indicate what the immediate effectors of AMPK are in the preadipocytes. As epigenetic reprogramming is an essential part of differentiation, looking at the epigenetic changes brought about by AMPK activation in the first two days could also give a better idea of how it exerts its effects. This may help to determine whether AMPK activation does hold cells in a more stem-like and less mature state, as transcriptomic analysis and effect on lipid droplet size seem to suggest (Chapter 4). Incorporating 3D cell culture models to allow for unilocular adipocyte formation (Gerlach et al., 2011; Hsiao et al., 2016) will be more reflective of *in vivo adipose tissue* and will give more accurate insight into the effect of AMPK activation on adipocyte morphology. However, for investigating the earlier stages, simpler 2D models may be relevant enough as there is less requirement for the 3D support structure needed for development of a fully differentiated adipocyte.

Based on the effect of AMPK on suppression of adipogenesis, formation of adipocytes with reduced lipid droplet size, and also the potential reduction in leptin levels (Figure 6.1) suggests that BI-9774 may cause lipodystrophy (Chapter 4). Determining whether this is an artefact of in vitro differentiation is very important to follow up on in 3D cell culture models and also with direct targeting of AMPK in adipose tissue with BI-9774. It would also be interesting to see the effects of activating AMPK with BI-9774 in progenitor populations derived from a fluorescent reporter mouse before transplantation to allow for cell tracking. Activation of AMPK in the D316A mouse leads to protection from diet induced obesity, and AMPK is a good therapeutic target for NAFLD and T2D (Cusi et al., 2021; Fouqueray et al., 2021; Pollard et al., 2019; Steneberg et al., 2018). However, if BI-9774 does indeed lead to lipodystrophy then it is important to consider that the adipose tissue may not be a good target for AMPK activation.

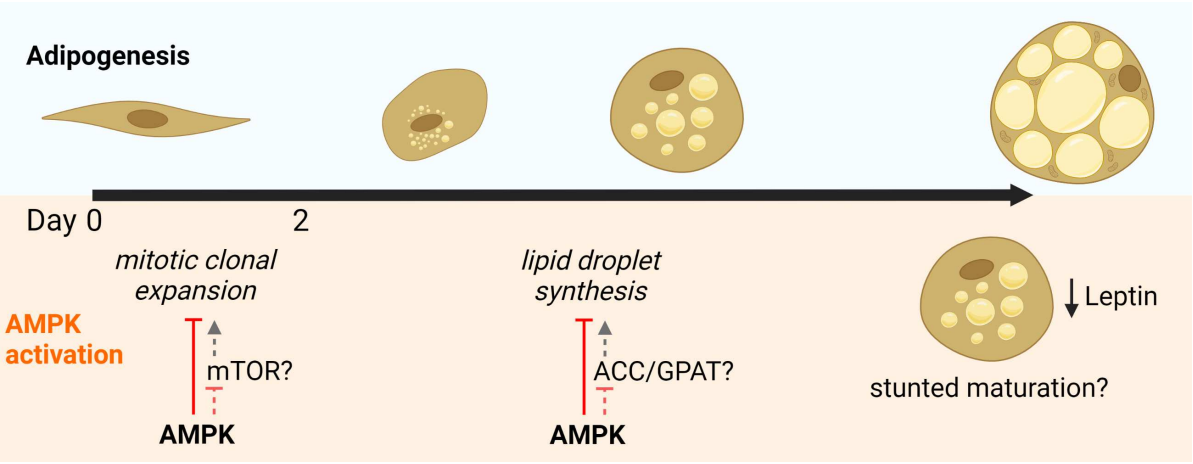


Figure 6.1 Activation of AMPK in adipogenesis

Activation of AMPK during adipogenesis leads to interruption of proliferation in the mitotic clonal expansion phase, possibly occurring through AMPK's inhibition of growth regulator mammalian target of rapamycin (mTOR). It also leads to the formation of adipocytes with smaller lipid droplets, possibly through reduction in lipid droplet synthesis through its inhibition of fatty acid synthesis via phosphorylation of acetyl co-A carboxylase (ACC), or inhibition of triacylglycerol synthesis via phosphorylation of glycerol-3-phosphate acetyl transferase (GPAT). The resulting adipocyte has smaller lipid droplets than a canonical adipocyte and has reduced leptin expression.

REFERENCES

Abdelaal, M., le Roux, C.W., and Docherty, N.G. (2017). Morbidity and mortality associated with obesity. Ann Transl Med *5*, 161-161.

Aguiari, P., Leo, S., Zavan, B., Vindigni, V., Rimessi, A., Bianchi, K., Franzin, C., Cortivo, R., Rossato, M., Vettor, R.*, et al.* (2008). High glucose induces adipogenic differentiation of muscle-derived stem cells. Proceedings of the National Academy of Sciences of the United States of America *105*, 1226-1231.

Ahmad, B., Serpell, C.J., Fong, I.L., and Wong, E.H. (2020). Molecular Mechanisms of Adipogenesis: The Anti-adipogenic Role of AMP-Activated Protein Kinase. Frontiers in molecular biosciences *7*, 76.

Ahmadian, M., Abbott, M.J., Tang, T., Hudak, C.S.S., Kim, Y., Bruss, M., Hellerstein, M.K., Lee, H.-Y., Samuel, V.T., Shulman, G.I.*, et al.* (2011). Desnutrin/ATGL is regulated by AMPK and is required for a brown adipose phenotype. Cell Metab *13*, 739-748.

Ahmadian, M., Suh Jm Fau - Hah, N., Hah N Fau - Liddle, C., Liddle C Fau - Atkins, A.R., Atkins Ar Fau - Downes, M., Downes M Fau - Evans, R.M., and Evans, R.M. (2013). PPARγ signaling and metabolism: the good, the bad and the future.

Akimoto, T., Ushida, T., Miyaki, S., Akaogi, H., Tsuchiya, K., Yan, Z., Williams, R.S., and Tateishi, T. (2005). Mechanical stretch inhibits myoblast-to-adipocyte differentiation through Wnt signaling. Biochem Biophys Res Commun *329*, 381-385.

Albers, P.H., Bojsen-Møller, K.N., Dirksen, C., Serup, A.K., Kristensen, D.E., Frystyk, J., Clausen, T.R., Kiens, B., Richter, E.A., Madsbad, S.*, et al.* (2015). Enhanced insulin signaling in human skeletal muscle and adipose tissue following gastric bypass surgery. American Journal of Physiology-Regulatory, Integrative and Comparative Physiology *309*, R510-R524.

Ali, M., M; Hassan, Chandra; Masrur, Mario; Bianco, Francesco, M; Naquiallah, Dina; Mirza, Imaduddin; Frederick, Patrice; Fernandes, Eduardo, T; Giulianotti, Cristoforo, P; Gangemi, Antonio; Phillips, Shane, A; Mahmoud, Abeer, M; (2021).

Adipose Tissue Hypoxia Correlates with Adipokine Hypomethylation and Vascular Dysfunction. In Biomedicines.
An, Y., Wang, G., Diao, Y., Long, Y., Fu, X., Weng, M., Zhou, L., Sun, K., Cheung, T.H., Ip, N.Y.*, et al.* (2017). A Molecular Switch Regulating Cell Fate Choice between Muscle Progenitor Cells and Brown Adipocytes. Developmental Cell *41*, 382-391.e385.
Andersson, U., Filipsson, K., Abbott, C.R., Woods, A., Smith, K., Bloom, S.R., Carling, D., and Small, C.J. (2004). AMP-activated Protein Kinase Plays a Role in the Control of Food Intake. Journal of Biological Chemistry *279*, 12005-12008.
Angelidi, A.M., Belanger, M.J., Kokkinos, A., Koliaki, C.C., and Mantzoros, C.S. (2022). Novel Noninvasive Approaches to the Treatment of Obesity: From Pharmacotherapy to Gene Therapy. Endocrine Reviews *43*, 507-557.
Angueira, A.R., Sakers, A.P., Holman, C.D., Cheng, L., Arbocco, M.N., Shamsi, F., Lynes, M.D., Shrestha, R., Okada, C., Batmanov, K.*, et al.* (2021). Defining the lineage of thermogenic perivascular adipose tissue. Nature Metabolism.
Aquilano, K., Sciarretta, F., Turchi, R., Li, B.-H., Rosina, M., Ceci, V., Guidobaldi, G., Arena, S., D'Ambrosio, C., Audano, M.*, et al.* (2020). Low-protein/high-carbohydrate diet induces AMPK-dependent canonical and non-canonical thermogenesis in subcutaneous adipose tissue. Redox Biology *36*, 101633.
Arita, Y., Kihara, S., Ouchi, N., Takahashi, M., Maeda, K., Miyagawa, J.-i., Hotta, K., Shimomura, I., Nakamura, T., Miyaoka, K.*, et al.* (1999). Paradoxical Decrease of an Adipose-Specific Protein, Adiponectin, in Obesity. Biochem Biophys Res Commun *257*, 79-83.
Aschenbach, W.G., Hirshman, M.F., Fujii, N., Sakamoto, K., Howlett, K.F., and Goodyear, L.J. (2002). Effect of AICAR Treatment on Glycogen Metabolism in Skeletal Muscle. Diabetes *51*, 567-573.
Assembly, W.H. (2013). Follow-up to the Political Declaration of the High-level Meeting of the General Assembly on the Prevention and Control of Non-communicable Diseases. WHA66.10 W.H. Assembly, ed.

Azoury, S.C., Shakir, S., Bucky, L.P., and Percec, I. (2021). Modern Fat Grafting Techniques to the Face and Neck. *148*, 620e-633e.
Bäckdahl, J., Franzén, L., Massier, L., Li, Q., Jalkanen, J., Gao, H., Andersson, A., Bhalla, N., Thorell, A., Rydén, M.*, et al.* (2021). Spatial mapping reveals human adipocyte subpopulations with distinct sensitivities to insulin. Cell Metab *33*, 1869-1882.e1866.
Bal, N.C., Maurya, S.K., Sopariwala, D.H., Sahoo, S.K., Gupta, S.C., Shaikh, S.A., Pant, M., Rowland, L.A., Bombardier, E., Goonasekera, S.A.*, et al.* (2012). Sarcolipin is a newly identified regulator of muscle-based thermogenesis in mammals. Nature medicine *18*, 1575-1579.
Barbatelli, G., Murano, I., Madsen, L., Hao, Q., Jimenez, M., Kristiansen, K., Giacobino, J.P., De Matteis, R., and Cinti, S. (2010). The emergence of cold-induced brown adipocytes in mouse white fat depots is determined predominantly by white to brown adipocyte transdifferentiation. American journal of physiology Endocrinology and metabolism *298*, E1244-1253.
Barrett, S., Begg, S., O'Halloran, P., and Kingsley, M. (2018). Integrated motivational interviewing and cognitive behaviour therapy for lifestyle mediators of overweight and obesity in community-dwelling adults: a systematic review and meta-analyses. BMC Public Health *18*, 1160-1160.
Batchuluun, B., Pinkosky, S.L., and Steinberg, G.R. (2022). Lipogenesis inhibitors: therapeutic opportunities and challenges. Nature Reviews Drug Discovery *21*, 283-305.
Baur, J.A., Pearson, K.J., Price, N.L., Jamieson, H.A., Lerin, C., Kalra, A., Prabhu, V.V., Allard, J.S., Lopez-Lluch, G., Lewis, K.*, et al.* (2006). Resveratrol improves health and survival of mice on a high-calorie diet. Nature *444*, 337-342.
Ben-Porath, I., Thomson, M.W., Carey, V.J., Ge, R., Bell, G.W., Regev, A., and Weinberg, R.A. (2008). An embryonic stem cell–like gene expression signature in poorly differentiated aggressive human tumors. Nature Genetics *40*, 499-507.

Benziane, B., Björnholm, M., Lantier, L., Viollet, B., Zierath, J.R., and Chibalin, A.V. (2009). AMP-activated protein kinase activator A-769662 is an inhibitor of the Na+-K+-ATPase. American Journal of Physiology-Cell Physiology *297*, C1554-C1566.
Berry, D.C., Jiang, Y., and Graff, J.M. (2016). Mouse strains to study cold-inducible beige progenitors and beige adipocyte formation and function. Nature Communications *7*, 10184.
Berry, R., Jeffery, E., and Rodeheffer, Matthew S. (2014). Weighing in on Adipocyte Precursors. Cell Metab *19*, 8-20.
Berry, R., and Rodeheffer, M.S. (2013). Characterization of the adipocyte cellular lineage in vivo. Nature cell biology *15*, 302.
Bertholet, A.M., Kazak, L., Chouchani, E.T., Bogaczyńska, M.G., Paranjpe, I., Wainwright, G.L., Bétourné, A., Kajimura, S., Spiegelman, B.M., and Kirichok, Y. (2017). Mitochondrial Patch Clamp of Beige Adipocytes Reveals UCP1-Positive and UCP1-Negative Cells Both Exhibiting Futile Creatine Cycling. Cell Metab *25*, 811-822.e814.
Bilal, M., Nawaz, A., Kado, T., Aslam, M.R., Igarashi, Y., Nishimura, A., Watanabe, Y., Kuwano, T., Liu, J., Miwa, H.*, et al.* (2021). Fate of adipocyte progenitors during adipogenesis in mice fed a high-fat diet. Mol Metab *54*, 101328.
Billon, N., Iannarelli, P., Monteiro, M.C., Glavieux-Pardanaud, C., Richardson, W.D., Kessaris, N., Dani, C., and Dupin, E. (2007). The generation of adipocytes by the neural crest. Development (Cambridge, England) *134*, 2283-2292.
Blaszkiewicz, M., Willows, J.W., Johnson, C.P., and Townsend, K.L. (2019). The Importance of Peripheral Nerves in Adipose Tissue for the Regulation of Energy Balance. Biology (Basel) *8*, 10.
Blondin, D.P., Nielsen, S., Kuipers, E.N., Severinsen, M.C., Jensen, V.H., Miard, S., Jespersen, N.Z., Kooijman, S., Boon, M.R., Fortin, M.*, et al.* (2020). Human Brown Adipocyte Thermogenesis Is Driven by β2-AR Stimulation. Cell Metab *32*, 287-300.e287.

Blüher, M. (2019). Obesity: global epidemiology and pathogenesis. Nature Reviews Endocrinology *15*, 288-298.
Borén, J., Taskinen, M.R., Olofsson, S.O., and Levin, M. (2013). Ectopic lipid storage and insulin resistance: a harmful relationship. Journal of Internal Medicine *274*, 25-40.
Braun, K., Oeckl, J., Westermeier, J., Li, Y., and Klingenspor, M. (2018). Non-adrenergic control of lipolysis and thermogenesis in adipose tissues. The Journal of Experimental Biology *221*, jeb165381.
Bray, G.A., Frühbeck, G., Ryan, D.H., and Wilding, J.P.H. (2016). Management of obesity. The Lancet *387*, 1947-1956.
Britton, K.A., and Fox, C.S. (2011). Perivascular adipose tissue and vascular disease. Clinical lipidology *6*, 79-91.
Brownstein, A.J., Veliova, M., Acin-Perez, R., Liesa, M., and Shirihai, O.S. (2022). ATP-consuming futile cycles as energy dissipating mechanisms to counteract obesity. Reviews in endocrine & metabolic disorders *23*, 121-131.
Buhl, E.S., Jessen, N., Pold, R., Ledet, T., Flyvbjerg, A., Pedersen, S.B., Pedersen, O., Schmitz, O., and Lund, S. (2002). Long-Term AICAR Administration Reduces Metabolic Disturbances and Lowers Blood Pressure in Rats Displaying Features of the Insulin Resistance Syndrome. Diabetes *51*, 2199.
Bultot, L., Guigas, B., Von Wilamowitz-Moellendorff, A., Maisin, L., Vertommen, D., Hussain, N., Beullens, M., Guinovart, J.J., Foretz, M., Viollet, B.*, et al.* (2012). AMP-activated protein kinase phosphorylates and inactivates liver glycogen synthase. Biochem J *443*, 193-203.
Bultot, L., Jensen, T.E., Lai, Y.-C., Madsen, A.L.B., Collodet, C., Kviklyte, S., Deak, M., Yavari, A., Foretz, M., Ghaffari, S.*, et al.* (2016). Benzimidazole derivative small-molecule 991 enhances AMPK activity and glucose uptake induced by AICAR or contraction in skeletal muscle. American journal of physiology Endocrinology and metabolism *311*, E706-E719.

Burl, R.B., Ramseyer, V.D., Rondini, E.A., Pique-Regi, R., Lee, Y.H., and Granneman, J.G. (2018). Deconstructing Adipogenesis Induced by beta3-Adrenergic Receptor Activation with Single-Cell Expression Profiling. Cell Metab *28*, 300-309 e304.
Burton, G.R., Nagarajan, R., Peterson, C.A., and McGehee, R.E. (2004). Microarray analysis of differentiation-specific gene expression during 3T3-L1 adipogenesis. Gene *329*, 167-185.
Calejman, C.M., Doxsey, W.G., Fazakerley, D.J., and Guertin, D.A. (2022). Integrating adipocyte insulin signaling and metabolism in the multi-omics era. Trends in biochemical sciences *47*, 531-546.
Cantó, C., Gerhart-Hines, Z., Feige, J.N., Lagouge, M., Noriega, L., Milne, J.C., Elliott, P.J., Puigserver, P., and Auwerx, J. (2009). AMPK regulates energy expenditure by modulating NAD+ metabolism and SIRT1 activity. Nature *458*, 1056-1060.
Cao, W., Daniel, K.W., Robidoux, J., Puigserver, P., Medvedev, A.V., Bai, X., Floering, L.M., Spiegelman, B.M., and Collins, S. (2004). p38 mitogen-activated protein kinase is the central regulator of cyclic AMP-dependent transcription of the brown fat uncoupling protein 1 gene. Mol Cell Biol *24*, 3057-3067.
Capurso, C., and Capurso, A. (2012). From excess adiposity to insulin resistance: The role of free fatty acids. Vascular Pharmacology *57*, 91-97.
Carling, D. (2017). AMPK signalling in health and disease. Current opinion in cell biology *45*, 31-37.
Carling, D., Clarke, P.R., Zammit, V.A., and Hardie, D.G. (1989). Purification and characterization of the AMP-activated protein kinase. European journal of biochemistry *186*, 129-136.
Carling, D., Zammit, V.A., and Hardie, D.G. (1987). A common bicyclic protein kinase cascade inactivates the regulatory enzymes of fatty acid and cholesterol biosynthesis. FEBS letters *223*, 217-222.

Cattaneo, P., Mukherjee, D., Spinozzi, S., Zhang, L., Larcher, V., Stallcup, W.B., Kataoka, H., Chen, J., Dimmeler, S., Evans, S.M.*, et al.* (2020). Parallel Lineage-Tracing Studies Establish Fibroblasts as the Prevailing In Vivo Adipocyte Progenitor. Cell Rep *30*, 571-582.e572.

Chatterjee, S., Khunti, K., and Davies, M.J. (2017). Type 2 diabetes. The Lancet *389*, 2239-2251.

Chau, Y.-Y., Bandiera, R., Serrels, A., Martínez-Estrada, O.M., Qing, W., Lee, M., Slight, J., Thornburn, A., Berry, R., McHaffie, S.*, et al.* (2014). Visceral and subcutaneous fat have different origins and evidence supports a mesothelial source. Nature cell biology *16*, 367-375.

Chen, A., Chen, X., Cheng, S., Shu, L., Yan, M., Yao, L., Wang, B., Huang, S., Zhou, L., Yang, Z.*, et al.* (2018). FTO promotes SREBP1c maturation and enhances CIDEC transcription during lipid accumulation in HepG2 cells. Biochimica et biophysica acta Molecular and cell biology of lipids *1863*, 538-548.

Chen, J., Wang, C., and Kuang, S. (2019a). Transdifferentiation of Muscle Satellite Cells to Adipose Cells Using CRISPR/Cas9-Mediated Targeting of MyoD. Methods Mol Biol *1889*, 25-41.

Chen, L., Xin, F.-J., Wang, J., Hu, J., Zhang, Y.-Y., Wan, S., Cao, L.-S., Lu, C., Li, P., Yan, S.F.*, et al.* (2013). Conserved regulatory elements in AMPK. Nature *498*, E8-E10.

Chen, S., Liu, X., Peng, C., Tan, C., Sun, H., Liu, H., Zhang, Y., Wu, P., Cui, C., Liu, C.*, et al.* (2021). The phytochemical hyperforin triggers thermogenesis in adipose tissue via a Dlat-AMPK signaling axis to curb obesity. Cell Metab *33*, 565-580.e567.

Chen, S.C., Brooks, R., Houskeeper, J., Bremner, S.K., Dunlop, J., Viollet, B., Logan, P.J., Salt, I.P., Ahmed, S.F., and Yarwood, S.J. (2017). Metformin suppresses adipogenesis through both AMP-activated protein kinase (AMPK)-dependent and AMPK-independent mechanisms. Mol Cell Endocrinol *440*, 57-68.

Chen, Y., Ikeda, K., Yoneshiro, T., Scaramozza, A., Tajima, K., Wang, Q., Kim, K., Shinoda, K., Sponton, C.H., Brown, Z.*, et al.* (2019b). Thermal stress induces glycolytic beige fat formation via a myogenic state. Nature *565*, 180-185.
Cheng, S.W., Fryer, L.G., Carling, D., and Shepherd, P.R. (2004). Thr2446 is a novel mammalian target of rapamycin (mTOR) phosphorylation site regulated by nutrient status. J Biol Chem *279*, 15719-15722.
Cheung, P.C., Salt, I.P., Davies, S.P., Hardie, D.G., and Carling, D. (2000). Characterization of AMP-activated protein kinase gamma-subunit isoforms and their role in AMP binding. Biochem J *346 Pt 3*, 659-669.
Chiquette, E., Oral, E.A., Garg, A., Araújo-Vilar, D., and Dhankhar, P. (2017). Estimating the prevalence of generalized and partial lipodystrophy: findings and challenges. Diabetes, metabolic syndrome and obesity : targets and therapy *10*, 375-383.
Cho, H.J., Park, J., Lee, H.W., Lee, Y.S., and Kim, J.B. (2004). Regulation of adipocyte differentiation and insulin action with rapamycin. Biochem Biophys Res Commun *321*, 942-948.
Choi, H.-S., Jeon, H.-J., Lee, O.-H., and Lee, B.-Y. (2015). Dieckol, a major phlorotannin in Ecklonia cava, suppresses lipid accumulation in the adipocytes of high-fat diet-fed zebrafish and mice: Inhibition of early adipogenesis via cell-cycle arrest and AMPKα activation. Molecular Nutrition & Food Research *59*, 1458-1471.
Choi, R.H., McConahay, A., Johnson, M.B., Jeong, H.-W., and Koh, H.-J. (2019). Adipose tissue-specific knockout of AMPKα1/α2 results in normal AICAR tolerance and glucose metabolism. Biochem Biophys Res Commun *519*, 633-638.
Chondronikola, M., Volpi, E., Børsheim, E., Porter, C., Annamalai, P., Enerbäck, S., Lidell, M.E., Saraf, M.K., Labbe, S.M., Hurren, N.M.*, et al.* (2014). Brown adipose tissue improves whole-body glucose homeostasis and insulin sensitivity in humans. Diabetes *63*, 4089-4099.
Chuang, S.-J., Johanns, M., Pyr dit Ruys, S., Steinberg, G.R., Kemp, B.E., Viollet, B., and Rider, M.H. (2021). AMPK activation by SC4 inhibits noradrenaline-induced

lipolysis and insulin-stimulated lipogenesis in white adipose tissue. Biochemical Journal *478*, 3869-3889.
Cinti, S., Mitchell, G., Barbatelli, G., Murano, I., Ceresi, E., Faloia, E., Wang, S., Fortier, M., Greenberg, A.S., and Obin, M.S. (2005). Adipocyte death defines macrophage localization and function in adipose tissue of obese mice and humans. Journal of lipid research *46*, 2347-2355.
Clemmensen, C., Müller, T.D., Woods, S.C., Berthoud, H.-R., Seeley, R.J., and Tschöp, M.H. (2017). Gut-Brain Cross-Talk in Metabolic Control. Cell *168*, 758-774.
Cokorinos, E.C., Delmore, J., Reyes, A.R., Albuquerque, B., Kjøbsted, R., Jørgensen, N.O., Tran, J.-L., Jatkar, A., Cialdea, K., Esquejo, R.M.*, et al.* (2017). Activation of Skeletal Muscle AMPK Promotes Glucose Disposal and Glucose Lowering in Non-human Primates and Mice. Cell Metab *25*, 1147-1159.e1110.
Collaborators, T.G.O. (2017). Health Effects of Overweight and Obesity in 195 Countries over 25 Years. New England Journal of Medicine *377*, 13-27.
Cool, B., Zinker, B., Chiou, W., Kifle, L., Cao, N., Perham, M., Dickinson, R., Adler, A., Gagne, G., Iyengar, R.*, et al.* (2006). Identification and characterization of a small molecule AMPK activator that treats key components of type 2 diabetes and the metabolic syndrome. Cell Metab *3*, 403-416.
Cordonier, E.L., Jarecke, S.K., Hollinger, F.E., and Zempleni, J. (2016). Inhibition of acetyl-CoA carboxylases by soraphen A prevents lipid accumulation and adipocyte differentiation in 3T3-L1 cells. European journal of pharmacology *780*, 202-208.
Corton, J.M., Gillespie, J.G., Hawley, S.A., and Hardie, D.G. (1995). 5-Aminoimidazole-4-Carboxamide Ribonucleoside, A Specific Method for Activating AMP-Activated Protein Kinase in Intact Cells? European journal of biochemistry *229*, 558-565.
Cousin, B., Cinti, S., Morroni, M., Raimbault, S., Ricquier, D., Penicaud, L., and Casteilla, L. (1992). Occurrence of brown adipocytes in rat white adipose tissue: molecular and morphological characterization. Journal of Cell Science *103*, 931.

Crewe, C., An, Y.A., and Scherer, P.E. (2017). The ominous triad of adipose tissue dysfunction: inflammation, fibrosis, and impaired angiogenesis. J Clin Invest *127*, 74-82.
Cuaranta-Monroy, I., Simandi, Z., Kolostyak, Z., Doan-Xuan, Q.M., Poliska, S., Horvath, A., Nagy, G., Bacso, Z., and Nagy, L. (2014). Highly efficient differentiation of embryonic stem cells into adipocytes by ascorbic acid. Stem Cell Res *13*, 88-97.
Cuevas-Ramos, D., Mehta, R., and Aguilar-Salinas, C.A. (2019). Fibroblast Growth Factor 21 and Browning of White Adipose Tissue. Frontiers in physiology *10*, 37-37.
Cusi, K., Alkhouri, N., Harrison, S.A., Fouqueray, P., Moller, D.E., Hallakou-Bozec, S., Bolze, S., Grouin, J.-M., Jeannin Megnien, S., Dubourg, J.*, et al.* (2021). Efficacy and safety of PXL770, a direct AMP kinase activator, for the treatment of non-alcoholic fatty liver disease (STAMP-NAFLD): a randomised, double-blind, placebo-controlled, phase 2a study. The Lancet Gastroenterology & Hepatology *6*, 889-902.
Cypess, A.M., Lehman, S., Williams, G., Tal, I., Rodman, D., Goldfine, A.B., Kuo, F.C., Palmer, E.L., Tseng, Y.-H., Doria, A.*, et al.* (2009). Identification and importance of brown adipose tissue in adult humans. N Engl J Med *360*, 1509-1517.
Cypess, A.M., Weiner, L.S., Roberts-Toler, C., Franquet Elía, E., Kessler, S.H., Kahn, P.A., English, J., Chatman, K., Trauger, S.A., Doria, A.*, et al.* (2015). Activation of human brown adipose tissue by a β3-adrenergic receptor agonist. Cell Metab *21*, 33-38.
Cypess, A.M., White, A.P., Vernochet, C., Schulz, T.J., Xue, R., Sass, C.A., Huang, T.L., Roberts-Toler, C., Weiner, L.S., Sze, C.*, et al.* (2013). Anatomical localization, gene expression profiling and functional characterization of adult human neck brown fat. Nature medicine *19*, 635-639.
Dagon, Y., Avraham, Y., and Berry, E.M. (2006). AMPK activation regulates apoptosis, adipogenesis, and lipolysis by eIF2alpha in adipocytes. Biochem Biophys Res Commun *340*, 43-47.

Dahlman, I., Elsen, M., Tennagels, N., Korn, M., Brockmann, B., Sell, H., Eckel, J., and Arner, P. (2012). Functional annotation of the human fat cell secretome. Archives of physiology and biochemistry *118*, 84-91.
Danforth, E. (2000). Failure of adipocyte differentiation causes type II diabetes mellitus? Nature Genetics *26*, 13-13.
Dani, C., Smith, A.G., Dessolin, S., Leroy, P., Staccini, L., Villageois, P., Darimont, C., and Ailhaud, G. (1997). Differentiation of embryonic stem cells into adipocytes in vitro. Journal of Cell Science, 1279-1285.
Darimont, C., Gaillard, D., Ailhaud, G., and Negrel, R. (1993). Terminal differentiation of mouse preadipocyte cells: adipogenic and antimitogenic role of triiodothyronine. Molecular and Cellular Endocrinology *98*, 67-73.
Daval, M., Diot-Dupuy, F., Bazin, R., Hainault, I., Viollet, B., Vaulont, S., Hajduch, E., Ferré, P., and Foufelle, F. (2005). Anti-lipolytic Action of AMP-activated Protein Kinase in Rodent Adipocytes. Journal of Biological Chemistry *280*, 25250-25257.
Day, E.A., Ford, R.J., and Steinberg, G.R. (2017). AMPK as a Therapeutic Target for Treating Metabolic Diseases. Trends in Endocrinology & Metabolism *28*, 545-560.
De Coppi, P., Milan, G., Scarda, A., Boldrin, L., Centobene, C., Piccoli, M., Pozzobon, M., Pilon, C., Pagano, C., Gamba, P*., et al.* (2006). Rosiglitazone modifies the adipogenic potential of human muscle satellite cells. Diabetologia *49*, 1962-1973.
de Jong, J.M.A., Larsson, O., Cannon, B., and Nedergaard, J. (2015). A stringent validation of mouse adipose tissue identity markers. American Journal of Physiology-Endocrinology and Metabolism *308*, E1085-E1105.
de Sá, P.M., Richard, A.J., Hang, H., and Stephens, J.M. (2017). Transcriptional Regulation of Adipogenesis. In Comprehensive Physiology, pp. 635-674.
de Winter, T.J.J., and Nusse, R. (2021). Running Against the Wnt: How Wnt/β-Catenin Suppresses Adipogenesis. Frontiers in cell and developmental biology *9*, 627429.

Denton, N.F., Eghleilib, M., Al-Sharifi, S., Todorčević, M., Neville, M.J., Loh, N., Drakesmith, A., Karpe, F., and Pinnick, K.E. (2019). Bone morphogenetic protein 2 is a depot-specific regulator of human adipogenesis. Int J Obes *43*, 2458-2468.
Dong, Y., Zhang, M., Liang, B., Xie, Z., Zhao, Z., Asfa, S., Choi, H.C., and Zou, M.-H. (2010). Reduction of AMP-activated protein kinase alpha2 increases endoplasmic reticulum stress and atherosclerosis in vivo. Circulation *121*, 792-803.
Duncan, R.E., Ahmadian, M., Jaworski, K., Sarkadi-Nagy, E., and Sul, H.S. (2007). Regulation of lipolysis in adipocytes. Annual review of nutrition *27*, 79-101.
Emont, M.P., Jacobs, C., Essene, A.L., Pant, D., Tenen, D., Colleluori, G., Di Vincenzo, A., Jørgensen, A.M., Dashti, H., Stefek, A.*, et al.* (2022). A single-cell atlas of human and mouse white adipose tissue. Nature.
Entenmann, G., and Hauner, H. (1996). Relationship between replication and differentiation in cultured human adipocyte precursor cells. American Journal of Physiology-Cell Physiology *270*, C1011-C1016.
Farmer, S.R. (2006). Transcriptional control of adipocyte formation. Cell Metab *4*, 263-273.
Farooqi, I.S., Jebb, S.A., Langmack, G., Lawrence, E., Cheetham, C.H., Prentice, A.M., Hughes, I.A., McCamish, M.A., and O'Rahilly, S. (1999). Effects of Recombinant Leptin Therapy in a Child with Congenital Leptin Deficiency. New England Journal of Medicine *341*, 879-884.
Fasshauer, M., and Blüher, M. (2015). Adipokines in health and disease. Trends in pharmacological sciences *36*, 461-470.
Fedorenko, A., Lishko, Polina V., and Kirichok, Y. (2012). Mechanism of Fatty-Acid-Dependent UCP1 Uncoupling in Brown Fat Mitochondria. Cell *151*, 400-413.
Ferren, L. (1966). Morphological Differentiation of Implanted Brown and White Fats. Transactions of the Kansas Academy of Science (1903-) *69*, 350-353.
Fingar Diane, C., Richardson Celeste, J., Tee Andrew, R., Cheatham, L., Tsou, C., and Blenis, J. (2004). mTOR Controls Cell Cycle Progression through Its Cell Growth

Effectors S6K1 and 4E-BP1/Eukaryotic Translation Initiation Factor 4E. Molecular and Cellular Biology *24*, 200-216.
Fisher, F.M., Kleiner, S., Douris, N., Fox, E.C., Mepani, R.J., Verdeguer, F., Wu, J., Kharitonenkov, A., Flier, J.S., Maratos-Flier, E.*, et al.* (2012). FGF21 regulates PGC-1α and browning of white adipose tissues in adaptive thermogenesis. Genes Dev *26*, 271-281.
Fock, K.M., and Khoo, J. (2013). Diet and exercise in management of obesity and overweight. Journal of Gastroenterology and Hepatology *28*, 59-63.
Forcet, C., Etienne-Manneville, S., Gaude, H., Fournier, L., Debilly, S., Salmi, M., Baas, A., Olschwang, S., Clevers, H., and Billaud, M. (2005). Functional analysis of Peutz–Jeghers mutations reveals that the LKB1 C-terminal region exerts a crucial role in regulating both the AMPK pathway and the cell polarity. Human Molecular Genetics *14*, 1283-1292.
Foretz, M., Even, P.C., and Viollet, B. (2018). AMPK Activation Reduces Hepatic Lipid Content by Increasing Fat Oxidation In Vivo. Int J Mol Sci *19*, 2826.
Fouqueray, P., Bolze, S., Dubourg, J., Hallakou-Bozec, S., Theurey, P., Grouin, J.-M., Chevalier, C., Gluais-Dagorn, P., Moller, D.E., and Cusi, K. (2021). Pharmacodynamic effects of direct AMP kinase activation in humans with insulin resistance and non-alcoholic fatty liver disease: A phase 1b study. Cell Reports Medicine *2*, 100474.
Fritzen, A.M., Lundsgaard, A.-M., Jordy, A.B., Poulsen, S.K., Stender, S., Pilegaard, H., Astrup, A., Larsen, T.M., Wojtaszewski, J.F.P., Richter, E.A.*, et al.* (2015). New Nordic Diet–Induced Weight Loss Is Accompanied by Changes in Metabolism and AMPK Signaling in Adipose Tissue. The Journal of Clinical Endocrinology & Metabolism *100*, 3509-3519.
Fu, X., Zhao, J.-X., Liang, J., Zhu, M.-J., Foretz, M., Viollet, B., and Du, M. (2013). AMP-activated protein kinase mediates myogenin expression and myogenesis via histone deacetylase 5. American Journal of Physiology-Cell Physiology *305*, C887-C895.

Fukumura, D., Ushiyama, A., Duda, D.G., Xu, L., Tam, J., Krishna, V., Chatterjee, K., Garkavtsev, I., and Jain, R.K. (2003). Paracrine regulation of angiogenesis and adipocyte differentiation during in vivo adipogenesis. Circulation research *93*, e88-97.
Fullerton, M.D., Galic, S., Marcinko, K., Sikkema, S., Pulinilkunnil, T., Chen, Z.-P., O'Neill, H.M., Ford, R.J., Palanivel, R., O'Brien, M.*, et al.* (2013). Single phosphorylation sites in Acc1 and Acc2 regulate lipid homeostasis and the insulin-sensitizing effects of metformin. Nature medicine *19*, 1649-1654.
Gao, J., Ye, J., Ying, Y., Lin, H., and Luo, Z. (2018). Negative regulation of TGF-β by AMPK and implications in the treatment of associated disorders. Acta biochimica et biophysica Sinica *50*, 523-531.
Gao, L., Yang, M., Wang, X., Yang, L., Bai, C., and Li, G. (2019). Mstn knockdown decreases the trans-differentiation from myocytes to adipocytes by reducing Jmjd3 expression via the SMAD2/SMAD3 complex. Bioscience, Biotechnology, and Biochemistry *83*, 2090-2096.
Gao, S., Kinzig, K.P., Aja, S., Scott, K.A., Keung, W., Kelly, S., Strynadka, K., Chohnan, S., Smith, W.W., Tamashiro, K.L.K.*, et al.* (2007). Leptin activates hypothalamic acetyl-CoA carboxylase to inhibit food intake. Proceedings of the National Academy of Sciences *104*, 17358.
Gao, Z., Zhang, X., Zuberi, A., Hwang, D., Quon, M.J., Lefevre, M., and Ye, J. (2004). Inhibition of Insulin Sensitivity by Free Fatty Acids Requires Activation of Multiple Serine Kinases in 3T3-L1 Adipocytes. Molecular Endocrinology *18*, 2024-2034.
García-Niño, W.R., and Zazueta, C. (2021). New insights of Krüppel-like transcription factors in adipogenesis and the role of their regulatory neighbors. Life Sciences *265*, 118763.
Garcia, D., Hellberg, K., Chaix, A., Wallace, M., Herzig, S., Badur, M.G., Lin, T., Shokhirev, M.N., Pinto, A.F.M., Ross, D.S.*, et al.* (2019). Genetic Liver-Specific

AMPK Activation Protects against Diet-Induced Obesity and NAFLD. Cell Rep *26*, 192-208.e196.
Garcia, D., and Shaw, R.J. (2017). AMPK: Mechanisms of Cellular Energy Sensing and Restoration of Metabolic Balance. Molecular Cell *66*, 789-800.
Gauthier, M.-S., O'Brien, E.L., Bigornia, S., Mott, M., Cacicedo, J.M., Xu, X.J., Gokce, N., Apovian, C., and Ruderman, N. (2011). Decreased AMP-activated protein kinase activity is associated with increased inflammation in visceral adipose tissue and with whole-body insulin resistance in morbidly obese humans. Biochem Biophys Res Commun *404*, 382-387.
Geng, L., Lam, K.S.L., and Xu, A. (2020). The therapeutic potential of FGF21 in metabolic diseases: from bench to clinic. Nature Reviews Endocrinology *16*, 654-667.
Gerhold, D.L., Liu, F., Jiang, G., Li, Z., Xu, J., Lu, M., Sachs, J.R., Bagchi, A., Fridman, A., Holder, D.J.*, et al.* (2002). Gene expression profile of adipocyte differentiation and its regulation by peroxisome proliferator-activated receptor-gamma agonists. Endocrinology *143*, 2106-2118.
Gerlach, J.C., Lin, Y.-C., Brayfield, C.A., Minteer, D.M., Li, H., Rubin, J.P., and Marra, K.G. (2011). Adipogenesis of Human Adipose-Derived Stem Cells Within Three-Dimensional Hollow Fiber-Based Bioreactors. Tissue Engineering Part C: Methods *18*, 54-61.
Giordanetto, F., and Karis, D. (2012). Direct AMP-activated protein kinase activators: a review of evidence from the patent literature. Expert Opinion on Therapeutic Patents *22*, 1467-1477.
Gluais-Dagorn, P., Foretz, M., Steinberg, G.R., Batchuluun, B., Zawistowska-Deniziak, A., Lambooij, J.M., Guigas, B., Carling, D., Monternier, P.A., Moller, D.E.*, et al.* (2022). Direct AMPK Activation Corrects NASH in Rodents Through Metabolic Effects and Direct Action on Inflammation and Fibrogenesis. Hepatology communications *6*, 101-119.

Gong, J., Sun, Z., Wu, L., Xu, W., Schieber, N., Xu, D., Shui, G., Yang, H., Parton, R.G., and Li, P. (2011). Fsp27 promotes lipid droplet growth by lipid exchange and transfer at lipid droplet contact sites. Journal of Cell Biology *195*, 953-963.
Gonzaga-Jauregui, C., Ge, W., Staples, J., Van Hout, C., Yadav, A., Colonie, R., Leader, J.B., Kirchner, H.L., Murray, M.F., Reid, J.G.*, et al.* (2019). Clinical and Molecular Prevalence of Lipodystrophy in an Unascertained Large Clinical Care Cohort. Diabetes *69*, 249-258.
Gowans, Graeme J., and Hardie, D.G. (2014). AMPK: a cellular energy sensor primarily regulated by AMP. Biochemical Society Transactions *42*, 71-75.
Gowans, G.J., Hawley, S.A., Ross, F.A., and Hardie, D.G. (2013). AMP is a true physiological regulator of AMP-activated protein kinase by both allosteric activation and enhancing net phosphorylation. Cell Metab *18*, 556-566.
Granneman, J.G., Burnazi, M., Zhu, Z., and Schwamb, L.A. (2003). White adipose tissue contributes to UCP1-independent thermogenesis. American Journal of Physiology-Endocrinology and Metabolism *285*, E1230-E1236.
Greer, E.L., Oskoui, P.R., Banko, M.R., Maniar, J.M., Gygi, M.P., Gygi, S.P., and Brunet, A. (2007). The Energy Sensor AMP-activated Protein Kinase Directly Regulates the Mammalian FOXO3 Transcription Factor*. Journal of Biological Chemistry *282*, 30107-30119.
Grempler, R., Wolff, M., Simon, E., Schmid, R., Eisele, C., Rieber, K., Fischer, E., Mettel, S., Gabrielyan, O., Delic, D.*, et al.* (2018). Discovery and translation of a target engagement marker for AMP-activated protein kinase (AMPK). PLoS One *13*, e0197849.
Guilherme, A., Yenilmez, B., Bedard, A.H., Henriques, F., Liu, D., Lee, A., Goldstein, L., Kelly, M., Nicoloro, S.M., Chen, M.*, et al.* (2020). Control of Adipocyte Thermogenesis and Lipogenesis through β3-Adrenergic and Thyroid Hormone Signal Integration. Cell Rep *31*, 107598.
Gunawardana, S.C., and Piston, D.W. (2012). Reversal of Type 1 Diabetes in Mice by Brown Adipose Tissue Transplant. Diabetes *61*, 674.

Gunawardana, S.C., and Piston, D.W. (2015). Insulin-independent reversal of type 1 diabetes in nonobese diabetic mice with brown adipose tissue transplant. American Journal of Physiology-Endocrinology and Metabolism *308*, E1043-E1055.
Gupta, Rana K., Mepani, Rina J., Kleiner, S., Lo, James C., Khandekar, Melin J., Cohen, P., Frontini, A., Bhowmick, Diti C., Ye, L., Cinti, S.*, et al.* (2012). Zfp423 Expression Identifies Committed Preadipocytes and Localizes to Adipose Endothelial and Perivascular Cells. Cell Metab *15*, 230-239.
Gwinn, D.M., Shackelford, D.B., Egan, D.F., Mihaylova, M.M., Mery, A., Vasquez, D.S., Turk, B.E., and Shaw, R.J. (2008). AMPK phosphorylation of raptor mediates a metabolic checkpoint. Mol Cell *30*, 214-226.
Habinowski, S.A., and Witters, L.A. (2001). The Effects of AICAR on Adipocyte Differentiation of 3T3-L1 Cells. Biochem Biophys Res Commun *286*, 852-856.
Hadad, S.M., Hardie, D.G., Appleyard, V., and Thompson, A.M. (2014). Effects of metformin on breast cancer cell proliferation, the AMPK pathway and the cell cycle. Clinical and Translational Oncology *16*, 746-752.
Hagberg, C.E., Li, Q., Kutschke, M., Bhowmick, D., Kiss, E., Shabalina, I.G., Harms, M.J., Shilkova, O., Kozina, V., Nedergaard, J.*, et al.* (2018). Flow Cytometry of Mouse and Human Adipocytes for the Analysis of Browning and Cellular Heterogeneity. Cell Rep *24*, 2746-2756.e2745.
Han, J., Lee, J.-E., Jin, J., Lim, J.S., Oh, N., Kim, K., Chang, S.-I., Shibuya, M., Kim, H., and Koh, G.Y. (2011). The spatiotemporal development of adipose tissue. Development (Cambridge, England) *138*, 5027.
Hardin, J., McLennan, A.K., and Brewis, A. (2018). Body size, body norms and some unintended consequences of obesity intervention in the Pacific islands. Annals of Human Biology *45*, 285-294.
Hasenour, C.M., Ridley, D.E., Hughey, C.C., James, F.D., Donahue, E.P., Shearer, J., Viollet, B., Foretz, M., and Wasserman, D.H. (2014). 5-Aminoimidazole-4-carboxamide-1-β-D-ribofuranoside (AICAR) effect on glucose production, but not

energy metabolism, is independent of hepatic AMPK in vivo. The Journal of biological chemistry *289*, 5950-5959.
Hawley, S.A., Boudeau, J., Reid, J.L., Mustard, K.J., Udd, L., Mäkelä, T.P., Alessi, D.R., and Hardie, D.G. (2003). Complexes between the LKB1 tumor suppressor, STRADα/β and MO25α/β are upstream kinases in the AMP-activated protein kinase cascade. Journal of Biology *2*, 28.
Hawley, S.A., Davison, M., Woods, A., Davies, S.P., Beri, R.K., Carling, D., and Hardie, D.G. (1996). Characterization of the AMP-activated protein kinase kinase from rat liver and identification of threonine 172 as the major site at which it phosphorylates AMP-activated protein kinase. J Biol Chem *271*, 27879-27887.
Hawley, S.A., Fullerton, M.D., Ross, F.A., Schertzer, J.D., Chevtzoff, C., Walker, K.J., Peggie, M.W., Zibrova, D., Green, K.A., Mustard, K.J.*, et al.* (2012). The Ancient Drug Salicylate Directly Activates AMP-Activated Protein Kinase. Science *336*, 918-922.
Hawley, S.A., Pan, D.A., Mustard, K.J., Ross, L., Bain, J., Edelman, A.M., Frenguelli, B.G., and Hardie, D.G. (2005). Calmodulin-dependent protein kinase kinase-β is an alternative upstream kinase for AMP-activated protein kinase. Cell Metab *2*, 9-19.
Hawley, S.A., Selbert, M.A., Goldstein, E.G., Edelman, A.M., Carling, D., and Hardie, D.G. (1995). 5'-AMP activates the AMP-activated protein kinase cascade, and Ca2+/calmodulin activates the calmodulin-dependent protein kinase I cascade, via three independent mechanisms. J Biol Chem *270*, 27186-27191.
He, Y., Li, Y., Zhao, T., Wang, Y., and Sun, C. (2013). Ursolic acid inhibits adipogenesis in 3T3-L1 adipocytes through LKB1/AMPK pathway. PLoS One *8*, e70135.
He, Z., Jiang, T., Wang, Z., Levi, M., and Li, J. (2004). Modulation of carbohydrate response element-binding protein gene expression in 3T3-L1 adipocytes and rat adipose tissue. *287*, E424-E430.
Hebebrand, J., Holm, J.-C., Woodward, E., Baker, J.L., Blaak, E., Durrer Schutz, D., Farpour-Lambert, N.J., Frühbeck, G., Halford, J.G.C., Lissner, L.*, et al.* (2017). A

Proposal of the European Association for the Study of Obesity to Improve the ICD-11 Diagnostic Criteria for Obesity Based on the Three Dimensions Etiology, Degree of Adiposity and Health Risk. Obes Facts *10*, 284-307.
Hemminki, A., Markie, D., Tomlinson, I., Avizienyte, E., Roth, S., Loukola, A., Bignell, G., Warren, W., Aminoff, M., Höglund, P.*, et al.* (1998). A serine/threonine kinase gene defective in Peutz–Jeghers syndrome. Nature *391*, 184-187.
Hepler, C., Shan, B., Zhang, Q., Henry, G.H., Shao, M., Vishvanath, L., Ghaben, A.L., Mobley, A.B., Strand, D., Hon, G.C.*, et al.* (2018). Identification of functionally distinct fibro-inflammatory and adipogenic stromal subpopulations in visceral adipose tissue of adult mice. Elife *7*, e39636.
Herzig, S., and Shaw, R.J. (2018). AMPK: guardian of metabolism and mitochondrial homeostasis. Nat Rev Mol Cell Biol *19*, 121-135.
Himms-Hagen, J., Cui, J., E. Danforth, J., Taatjes, D.J., Lang, S.S., Waters, B.L., and Claus, T.H. (1994). Effect of CL-316,243, a thermogenic beta 3-agonist, on energy balance and brown and white adipose tissues in rats. *266*, R1371-R1382.
Hong, S.-P., Leiper, F.C., Woods, A., Carling, D., and Carlson, M. (2003). Activation of yeast Snf1 and mammalian AMP-activated protein kinase by upstream kinases. Proceedings of the National Academy of Sciences *100*, 8839.
Horman, S., Browne, G.J., Krause, U., Patel, J.V., Vertommen, D., Bertrand, L., Lavoinne, A., Hue, L., Proud, C.G., and Rider, M.H. (2002). Activation of AMP-Activated Protein Kinase Leads to the Phosphorylation of Elongation Factor 2 and an Inhibition of Protein Synthesis. Current Biology *12*, 1419-1423.
Houde, A.-A., Légaré, C., Biron, S., Lescelleur, O., Biertho, L., Marceau, S., Tchernof, A., Vohl, M.-C., Hivert, M.-F., and Bouchard, L. (2015). Leptin and adiponectin DNA methylation levels in adipose tissues and blood cells are associated with BMI, waist girth and LDL-cholesterol levels in severely obese men and women. BMC Medical Genetics *16*, 29.

Hsiao, A.Y., Okitsu, T., Teramae, H., and Takeuchi, S. (2016). 3D Tissue Formation of Unilocular Adipocytes in Hydrogel Microfibers. Advanced Healthcare Materials *5*, 548-556.
Hu, E., Tontonoz, P., and Spiegelman, B.M. (1995). Transdifferentiation of myoblasts by the adipogenic transcription factors PPAR gamma and C/EBP alpha. Proceedings of the National Academy of Sciences of the United States of America *92*, 9856-9860.
Hu, Z., Fan, C., Oh, D.S., Marron, J.S., He, X., Qaqish, B.F., Livasy, C., Carey, L.A., Reynolds, E., Dressler, L.*, et al.* (2006). The molecular portraits of breast tumors are conserved across microarray platforms. BMC Genomics *7*, 96.
Hudak, C.S., and Sul, H.S. (2013). Pref-1, a gatekeeper of adipogenesis. Front Endocrinol (Lausanne) *4*, 79.
Hudson, E.R., Pan, D.A., James, J., Lucocq, J.M., Hawley, S.A., Green, K.A., Baba, O., Terashima, T., and Hardie, D.G. (2003). A Novel Domain in AMP-Activated Protein Kinase Causes Glycogen Storage Bodies Similar to Those Seen in Hereditary Cardiac Arrhythmias. Current Biology *13*, 861-866.
Humphrey, Sean J., Yang, G., Yang, P., Fazakerley, Daniel J., Stöckli, J., Yang, Jean Y., and James, David E. (2013). Dynamic Adipocyte Phosphoproteome Reveals that Akt Directly Regulates mTORC2. Cell Metab *17*, 1009-1020.
Hung, C.-M., Lombardo, P.S., Malik, N., Brun, S.N., Hellberg, K., Van Nostrand, J.L., Garcia, D., Baumgart, J., Diffenderfer, K., Asara, J.M.*, et al.* (2021). AMPK/ULK1-mediated phosphorylation of Parkin ACT domain mediates an early step in mitophagy. Science Advances *7*, eabg4544.
Hurley, R.L., Anderson, K.A., Franzone, J.M., Kemp, B.E., Means, A.R., and Witters, L.A. (2005). The Ca2+/Calmodulin-dependent Protein Kinase Kinases Are AMP-activated Protein Kinase Kinases. Journal of Biological Chemistry *280*, 29060-29066.
Hurtado del Pozo, C., Vesperinas-García, G., Rubio, M.-Á., Corripio-Sánchez, R., Torres-García, A.J., Obregon, M.-J., and Calvo, R.M. (2011). ChREBP expression in the liver, adipose tissue and differentiated preadipocytes in human obesity.

Biochimica et Biophysica Acta (BBA) - Molecular and Cell Biology of Lipids *1811*, 1194-1200.
Hutchinson, D.S., Chernogubova, E., Dallner, O.S., Cannon, B., and Bengtsson, T. (2005). β-Adrenoceptors, but not α-adrenoceptors, stimulate AMP-activated protein kinase in brown adipocytes independently of uncoupling protein-1. Diabetologia *48*, 2386-2395.
Huypens, P., Sass, S., Wu, M., Dyckhoff, D., Tschöp, M., Theis, F., Marschall, S., de Angelis, M.H., and Beckers, J. (2016). Epigenetic germline inheritance of diet-induced obesity and insulin resistance. Nature Genetics *48*, 497-499.
Ikeda, K., Kang, Q., Yoneshiro, T., Camporez, J.P., Maki, H., Homma, M., Shinoda, K., Chen, Y., Lu, X., Maretich, P.*, et al.* (2017). UCP1-independent signaling involving SERCA2b-mediated calcium cycling regulates beige fat thermogenesis and systemic glucose homeostasis. Nature medicine *23*, 1454-1465.
Inoki, K., Zhu, T., and Guan, K.L. (2003). TSC2 mediates cellular energy response to control cell growth and survival. Cell *115*, 577-590.
Itoigawa, Y., Kishimoto, K.N., Okuno, H., Sano, H., Kaneko, K., and Itoi, E. (2010). Hypoxia induces adipogenic differentitation of myoblastic cell lines. Biochem Biophys Res Commun *399*, 721-726.
Izquierdo, A.G., and Crujeiras, A.B. (2019). Obesity-Related Epigenetic Changes After Bariatric Surgery. Front Endocrinol (Lausanne) *10*, 232-232.
Jäger, S., Handschin, C., St.-Pierre, J., and Spiegelman, B.M. (2007). AMP-activated protein kinase (AMPK) action in skeletal muscle via direct phosphorylation of PGC-1α. Proceedings of the National Academy of Sciences *104*, 12017-12022.
Jambunathan, S., Yin, J., Khan, W., Tamori, Y., and Puri, V. (2011). FSP27 promotes lipid droplet clustering and then fusion to regulate triglyceride accumulation. PLoS One *6*, e28614.
Jang, M., Park, R., Kim, H., Namkoong, S., Jo, D., Huh, Y.H., Jang, I.-S., Lee, J.I., and Park, J. (2018). AMPK contributes to autophagosome maturation and lysosomal fusion. Scientific reports *8*, 12637.

Jeffery, E., Wing, A., Holtrup, B., Sebo, Z., Kaplan, Jennifer L., Saavedra-Peña, R., Church, Christopher D., Colman, L., Berry, R., and Rodeheffer, Matthew S. (2016). The Adipose Tissue Microenvironment Regulates Depot-Specific Adipogenesis in Obesity. Cell Metab *24*, 142-150.
Jeon, H.-J., Choi, D.K., Choi, J., Lee, S., Lee, H., Yu, J.H., and Min, S.-H. (2021). D-Mannitol Induces a Brown Fat-like Phenotype via a β3-Adrenergic Receptor-Dependent Mechanism. Cells *10*.
Jeon, S.-M., Chandel, N.S., and Hay, N. (2012). AMPK regulates NADPH homeostasis to promote tumour cell survival during energy stress. Nature *485*, 661-665.
Joffin, N., Paschoal, V.A., Gliniak, C.M., Crewe, C., Elnwasany, A., Szweda, L.I., Zhang, Q., Hepler, C., Kusminski, C.M., Gordillo, R.*, et al.* (2021). Mitochondrial metabolism is a key regulator of the fibro-inflammatory and adipogenic stromal subpopulations in white adipose tissue. Cell Stem Cell *28*, 702-717.e708.
Jones, R.G., Plas, D.R., Kubek, S., Buzzai, M., Mu, J., Xu, Y., Birnbaum, M.J., and Thompson, C.B. (2005). AMP-Activated Protein Kinase Induces a p53-Dependent Metabolic Checkpoint. Molecular Cell *18*, 283-293.
Jönsson, C., Castor Batista, A.P., Kjølhede, P., and Strålfors, P. (2019). Insulin and β-adrenergic receptors mediate lipolytic and anti-lipolytic signalling that is not altered by type 2 diabetes in human adipocytes. Biochem J *476*, 2883-2908.
Kahn, C.R., Wang, G., and Lee, K.Y. (2019). Altered adipose tissue and adipocyte function in the pathogenesis of metabolic syndrome. J Clin Invest *129*, 3990-4000.
Kajimura, S., Seale, P., Kubota, K., Lunsford, E., Frangioni, J.V., Gygi, S.P., and Spiegelman, B.M. (2009). Initiation of myoblast to brown fat switch by a PRDM16-C/EBP-beta transcriptional complex. Nature *460*, 1154-1158.
Kajimura, S., Seale, P., Tomaru, T., Erdjument-Bromage, H., Cooper, M.P., Ruas, J.L., Chin, S., Tempst, P., Lazar, M.A., and Spiegelman, B.M. (2008). Regulation of the brown and white fat gene programs through a PRDM16/CtBP transcriptional complex. Genes Dev *22*, 1397-1409.

Kallas, A., Pook, M., Trei, A., and Maimets, T. (2014). SOX2 Is Regulated Differently from NANOG and OCT4 in Human Embryonic Stem Cells during Early Differentiation Initiated with Sodium Butyrate. Stem Cells International *2014*, 298163.
Kanda, T., Brown, J.D., Orasanu, G., Vogel, S., Gonzalez, F.J., Sartoretto, J., Michel, T., and Plutzky, J. (2009). PPARgamma in the endothelium regulates metabolic responses to high-fat diet in mice. J Clin Invest *119*, 110-124.
Karastergiou, K., and Mohamed-Ali, V. (2010). The autocrine and paracrine roles of adipokines. Mol Cell Endocrinol *318*, 69-78.
Kawaguchi, T., Osatomi, K., Yamashita, H., Kabashima, T., and Uyeda, K. (2002). Mechanism for fatty acid "sparing" effect on glucose-induced transcription: regulation of carbohydrate-responsive element-binding protein by AMP-activated protein kinase. J Biol Chem *277*, 3829-3835.
Kazak, L., Chouchani, E.T., Jedrychowski, M.P., Erickson, B.K., Shinoda, K., Cohen, P., Vetrivelan, R., Lu, G.Z., Laznik-Bogoslavski, D., Hasenfuss, S.C.*, et al.* (2015). A creatine-driven substrate cycle enhances energy expenditure and thermogenesis in beige fat. Cell *163*, 643-655.
Kazak, L., Chouchani, E.T., Lu, G.Z., Jedrychowski, M.P., Bare, C.J., Mina, A.I., Kumari, M., Zhang, S., Vuckovic, I., Laznik-Bogoslavski, D.*, et al.* (2017). Genetic Depletion of Adipocyte Creatine Metabolism Inhibits Diet-Induced Thermogenesis and Drives Obesity. Cell Metab *26*, 660-671.e663.
Kazak, L., Rahbani, J.F., Samborska, B., Lu, G.Z., Jedrychowski, M.P., Lajoie, M., Zhang, S., Ramsay, L., Dou, F.Y., Tenen, D.*, et al.* (2019). Ablation of adipocyte creatine transport impairs thermogenesis and causes diet-induced obesity. Nature Metabolism *1*, 360-370.
Kharitonenkov, A., Shiyanova, T.L., Koester, A., Ford, A.M., Micanovic, R., Galbreath, E.J., Sandusky, G.E., Hammond, L.J., Moyers, J.S., Owens, R.A.*, et al.* (2005). FGF-21 as a novel metabolic regulator. J Clin Invest *115*, 1627-1635.
Kim, J., Kundu, M., Viollet, B., and Guan, K.-L. (2011). AMPK and mTOR regulate autophagy through direct phosphorylation of Ulk1. Nature cell biology *13*, 132-141.

Kim, J.B., Wright, H.M., Wright, M., and Spiegelman, B.M. (1998). ADD1/SREBP1 activates PPARg through the production of endogenous ligand. *95*, 4333-4337.
Kim, J.E., and Chen, J. (2004). Regulation of Peroxisome Proliferator–Activated Receptor-γ Activity by Mammalian Target of Rapamycin and Amino Acids in Adipogenesis. Diabetes *53*, 2748-2756.
Kim, S.-J., Tang, T., Abbott, M., Viscarra, J.A., Wang, Y., and Sul, H.S. (2016). AMPK Phosphorylates Desnutrin/ATGL and Hormone-Sensitive Lipase To Regulate Lipolysis and Fatty Acid Oxidation within Adipose Tissue. Molecular and cellular biology *36*, 1961-1976.
Kishida, T., Ejima, A., Yamamoto, K., Tanaka, S., Yamamoto, T., and Mazda, O. (2015). Reprogrammed Functional Brown Adipocytes Ameliorate Insulin Resistance and Dyslipidemia in Diet-Induced Obesity and Type 2 Diabetes. Stem Cell Reports *5*, 569-581.
Kjøbsted, R., Munk-Hansen, N., Birk, J.B., Foretz, M., Viollet, B., Björnholm, M., Zierath, J.R., Treebak, J.T., and Wojtaszewski, J.F.P. (2017). Enhanced Muscle Insulin Sensitivity After Contraction/Exercise Is Mediated by AMPK. Diabetes *66*, 598.
Kjøbsted, R., Treebak, J.T., Fentz, J., Lantier, L., Viollet, B., Birk, J.B., Schjerling, P., Björnholm, M., Zierath, J.R., and Wojtaszewski, J.F.P. (2015). Prior AICAR Stimulation Increases Insulin Sensitivity in Mouse Skeletal Muscle in an AMPK-Dependent Manner. Diabetes *64*, 2042.
Klebanov, S., Astle, C.M., DeSimone, O., Ablamunits, V., and Harrison, D.E. (2005). Adipose tissue transplantation protects ob/ob mice from obesity, normalizes insulin sensitivity and restores fertility. Journal of Endocrinology *186*, 203-211.
Kleinendorst, L., Massink, M.P.G., Cooiman, M.I., Savas, M., van der Baan-Slootweg, O.H., Roelants, R.J., Janssen, I.C.M., Meijers-Heijboer, H.J., Knoers, N.V.A.M., Ploos van Amstel, H.K.*, et al.* (2018). Genetic obesity: next-generation sequencing results of 1230 patients with obesity. Journal of Medical Genetics *55*, 578.

Klemm, D.J., Leitner, J.W., Watson, P., Nesterova, A., Reusch, J.E., Goalstone, M.L., and Draznin, B. (2001). Insulin-induced adipocyte differentiation. Activation of CREB rescues adipogenesis from the arrest caused by inhibition of prenylation. J Biol Chem *276*, 28430-28435.
Koh, H.-J., Hirshman, M.F., He, H., Li, Y., Manabe, Y., Balschi, J.A., and Goodyear, L.J. (2007). Adrenaline is a critical mediator of acute exercise-induced AMP-activated protein kinase activation in adipocytes. Biochem J *403*, 473-481.
Konige, M., Wang, H., and Sztalryd, C. (2014). Role of adipose specific lipid droplet proteins in maintaining whole body energy homeostasis. Biochimica et Biophysica Acta (BBA) - Molecular Basis of Disease *1842*, 393-401.
Kontis, V., Mathers, C.D., Rehm, J., Stevens, G.A., Shield, K.D., Bonita, R., Riley, L.M., Poznyak, V., Beaglehole, R., and Ezzati, M. (2014). Contribution of six risk factors to achieving the 25×25 non-communicable disease mortality reduction target: a modelling study. The Lancet *384*, 427-437.
Kopietz, F., Alshuweishi, Y., Bijland, S., Alghamdi, F., Degerman, E., Sakamoto, K., Salt, I.P., and Göransson, O. (2021). A-769662 inhibits adipocyte glucose uptake in an AMPK-independent manner. Biochemical Journal *478*, 633-646.
Kozak, L.P., and Anunciado-Koza, R. (2008). UCP1: its involvement and utility in obesity. Int J Obes (Lond) *32* S32-S38.
Kraemer, F.B., Patel, S., Saedi, M.S., and Sztalryd, C. (1993). Detection of hormone-sensitive lipase in various tissues. I. Expression of an HSL/bacterial fusion protein and generation of anti-HSL antibodies. Journal of lipid research *34*, 663-671.
Kral, T.V.E., and Rolls, B.J. (2004). Energy density and portion size: their independent and combined effects on energy intake. Physiology & Behavior *82*, 131-138.
Kulkarni, S.S., and Cantó, C. (2015). The molecular targets of resveratrol. Biochimica et Biophysica Acta (BBA) - Molecular Basis of Disease *1852*, 1114-1123.

Kwon, J.Y., Seo, S.G., Yue, S., Cheng, J.-X., Lee, K.W., and Kim, K.-H. (2012). An inhibitory effect of resveratrol in the mitotic clonal expansion and insulin signaling pathway in the early phase of adipogenesis. Nutrition Research *32*, 607-616.
Lawlor, D.A., Relton, C., Sattar, N., and Nelson, S.M. (2012). Maternal adiposity—a determinant of perinatal and offspring outcomes? Nature Reviews Endocrinology *8*, 679-688.
Le Pelletier, L., Mantecon, M., Gorwood, J., Auclair, M., Foresti, R., Motterlini, R., Laforge, M., Atlan, M., Fève, B., Capeau, J.*, et al.* (2021). Metformin alleviates stress-induced cellular senescence of aging human adipose stromal cells and the ensuing adipocyte dysfunction. Elife *10*.
Lee, C.-W., Wong, L.L.-Y., Tse, E.Y.-T., Liu, H.-F., Leong, V.Y.-L., Lee, J.M.-F., Hardie, D.G., Ng, I.O.-L., and Ching, Y.-P. (2012a). AMPK Promotes p53 Acetylation via Phosphorylation and Inactivation of SIRT1 in Liver Cancer Cells. Cancer research *72*, 4394-4404.
Lee, C.W., Hsiao, W.T., and Lee, O.K. (2017). Mesenchymal stromal cell-based therapies reduce obesity and metabolic syndromes induced by a high-fat diet. Translational research : the journal of laboratory and clinical medicine *182*, 61-74.e68.
Lee, H., Kang, R., Bae, S., and Yoon, Y. (2011a). AICAR, an activator of AMPK, inhibits adipogenesis via the WNT/β-catenin pathway in 3T3-L1 adipocytes. Int J Mol Med *28*, 65-71.
Lee, J.E., Schmidt, H., Lai, B., and Ge, K. (2019). Transcriptional and Epigenomic Regulation of Adipogenesis. Mol Cell Biol *39*.
Lee, S.J., Lee, E.J., Kim, S.-H., Choi, I., Lee, D.-M., Lee, H.-J., Yoon, D., and Chun, T. (2011b). IL-17A promotes transdifferentiation of mouse myoblast cells (C2C12) into adipocytes by increasing the expression of peroxisome proliferator-activated receptor γ through CAAT/enhancer binding protein β signaling. Biotechnology Letters *33*, 229-235.

Lee, Y.-H., Petkova, A.P., Konkar, A.A., and Granneman, J.G. (2015). Cellular origins of cold-induced brown adipocytes in adult mice. FASEB J *29*, 286-299.
Lee, Y.-H., Petkova, A.P., Mottillo, E.P., and Granneman, J.G. (2012b). In vivo identification of bipotential adipocyte progenitors recruited by β3-adrenoceptor activation and high-fat feeding. Cell Metab *15*, 480-491.
Lefterova, M.I., Zhang, Y., Steger, D.J., Schupp, M., Schug, J., Cristancho, A., Feng, D., Zhuo, D., Stoeckert, C.J., Jr., Liu, X.S.*, et al.* (2008). PPARgamma and C/EBP factors orchestrate adipocyte biology via adjacent binding on a genome-wide scale. Genes Dev *22*, 2941-2952.
Lehnert, T., Sonntag, D., Konnopka, A., Riedel-Heller, S., and König, H.-H. (2013). Economic costs of overweight and obesity. Best Practice & Research Clinical Endocrinology & Metabolism *27*, 105-115.
Li, Q., Hagberg, C.E., Silva Cascales, H., Lang, S., Hyvönen, M.T., Salehzadeh, F., Chen, P., Alexandersson, I., Terezaki, E., Harms, M.J.*, et al.* (2021a). Obesity and hyperinsulinemia drive adipocytes to activate a cell cycle program and senesce. Nature Medicine *27*, 1941-1953.
Li, S., Gao, H., Hasegawa, Y., and Lu, X. (2021b). Fight against fibrosis in adipose tissue remodeling. American Journal of Physiology-Endocrinology and Metabolism *321*, E169-E175.
Li, Y., Li, Z., Ngandiri, D.A., Llerins Perez, M., Wolf, A., and Wang, Y. (2022). The Molecular Brakes of Adipose Tissue Lipolysis. Front Physiol *13*, 826314.
Li, Y., Xu, S., Mihaylova, M.M., Zheng, B., Hou, X., Jiang, B., Park, O., Luo, Z., Lefai, E., Shyy, J.Y.J.*, et al.* (2011). AMPK phosphorylates and inhibits SREBP activity to attenuate hepatic steatosis and atherosclerosis in diet-induced insulin-resistant mice. Cell Metab *13*, 376-388.
Liang, J., Shao, S.H., Xu, Z.-X., Hennessy, B., Ding, Z., Larrea, M., Kondo, S., Dumont, D.J., Gutterman, J.U., Walker, C.L.*, et al.* (2007). The energy sensing LKB1–AMPK pathway regulates p27kip1 phosphorylation mediating the decision to enter autophagy or apoptosis. Nature cell biology *9*, 218-224.

Lidell, M.E., Betz, M.J., Leinhard, O.D., Heglind, M., Elander, L., Slawik, M., Mussack, T., Nilsson, D., Romu, T., Nuutila, P.*, et al.* (2013). Evidence for two types of brown adipose tissue in humans. Nature Medicine *19*, 631-634.
Lim, K., Haider, A., Adams, C., Sleigh, A., and Savage, D.B. (2021). Lipodistrophy: a paradigm for understanding the consequences of “overloading” adipose tissue. *101*, 907-993.
Lindholm, C.R., Ertel, R.L., Bauwens, J.D., Schmuck, E.G., Mulligan, J.D., and Saupe, K.W. (2013). A high-fat diet decreases AMPK activity in multiple tissues in the absence of hyperglycemia or systemic inflammation in rats. J Physiol Biochem *69*, 165-175.
Liu, J., Kuipers, E.N., Sips, H.C.M., Dorleijn, J.C., van Dam, A.D., Christodoulides, C., Karpe, F., Zhou, G., Boon, M.R., Rensen, P.C.N.*, et al.* (2019). Conditionally immortalized brown preadipocytes can switch between proliferative and differentiated states. Biochimica et Biophysica Acta (BBA) - Molecular and Cell Biology of Lipids *1864*, 158511.
Liu, W., Li, D., Cao, H., Li, H., and Wang, Y. (2021a). Expansion and inflammation of white adipose tissue - focusing on adipocyte progenitors. Biological Chemistry *402*, 123-132.
Liu, X., Rossmeisl, M., McClaine, J., Riachi, M., Harper, M.-E., and Kozak, L.P. (2003). Paradoxical resistance to diet-induced obesity in UCP1-deficient mice. J Clin Invest *111*, 399-407.
Liu, X., Wang, S., You, Y., Meng, M., Zheng, Z., Dong, M., Lin, J., Zhao, Q., Zhang, C., Yuan, X.*, et al.* (2015). Brown Adipose Tissue Transplantation Reverses Obesity in Ob/Ob Mice. Endocrinology *156*, 2461-2469.
Liu, X., Zhang, Y., Chu, Y., Zhao, X., Mao, L., Zhao, S., Lin, S., Hui, X., Gu, P., Xu, Y.*, et al.* (2021b). The natural compound rutaecarpine promotes white adipocyte browning through activation of the AMPK-PRDM16 axis. Biochem Biophys Res Commun *545*, 189-194.

Liu, X., Zheng, Z., Zhu, X., Meng, M., Li, L., Shen, Y., Chi, Q., Wang, D., Zhang, Z., Li, C.*, et al.* (2013). Brown adipose tissue transplantation improves whole-body energy metabolism. Cell Research *23*, 851-854.
Locke, A.E., Kahali, B., Berndt, S.I., Justice, A.E., Pers, T.H., Day, F.R., Powell, C., Vedantam, S., Buchkovich, M.L., Yang, J.*, et al.* (2015). Genetic studies of body mass index yield new insights for obesity biology. Nature *518*, 197-206.
Lodhi, I.J., Yin, L., Jensen-Urstad, A.P., Funai, K., Coleman, T., Baird, J.H., El Ramahi, M.K., Razani, B., Song, H., Fu-Hsu, F.*, et al.* (2012). Inhibiting adipose tissue lipogenesis reprograms thermogenesis and PPARγ activation to decrease diet-induced obesity. Cell Metab *16*, 189-201.
Loh, R.K.C., Formosa, M.F., Eikelis, N., Bertovic, D.A., Anderson, M.J., Barwood, S.A., Nanayakkara, S., Cohen, N.D., La Gerche, A., Reutens, A.T.*, et al.* (2018). Pioglitazone reduces cold-induced brown fat glucose uptake despite induction of browning in cultured human adipocytes: a randomised, controlled trial in humans. Diabetologia *61*, 220-230.
Long, Jonathan Z., Svensson, Katrin J., Tsai, L., Zeng, X., Roh, Hyun C., Kong, X., Rao, Rajesh R., Lou, J., Lokurkar, I., Baur, W.*, et al.* (2014). A Smooth Muscle-Like Origin for Beige Adipocytes. Cell Metab *19*, 810-820.
López, M., Nogueiras, R., Tena-Sempere, M., and Diéguez, C. (2016). Hypothalamic AMPK: a canonical regulator of whole-body energy balance. Nature Reviews Endocrinology *12*, 421-432.
Lotta, L.A., Gulati, P., Day, F.R., Payne, F., Ongen, H., van de Bunt, M., Gaulton, K.J., Eicher, J.D., Sharp, S.J., Luan, J.a.*, et al.* (2017). Integrative genomic analysis implicates limited peripheral adipose storage capacity in the pathogenesis of human insulin resistance. Nature Genetics *49*, 17-26.
Lu, J., Shi, J., Li, M., Gui, B., Fu, R., Yao, G., Duan, Z., Lv, Z., Yang, Y., Chen, Z.*, et al.* (2015). Activation of AMPK by metformin inhibits TGF-β-induced collagen production in mouse renal fibroblasts. Life Sciences *127*, 59-65.

Luo, H., Zhou, Y., Hu, X., Peng, X., Wei, H., Peng, J., and Jiang, S. (2015). Activation of PPARγ2 by PPARγ1 through a functional PPRE in transdifferentiation of myoblasts to adipocytes induced by EPA. Cell Cycle *14*, 1830-1841.
Luo, T., Nocon, A., Fry, J., Sherban, A., Rui, X., Jiang, B., Xu, X.J., Han, J., Yan, Y., Yang, Q.*, et al.* (2016). AMPK Activation by Metformin Suppresses Abnormal Extracellular Matrix Remodeling in Adipose Tissue and Ameliorates Insulin Resistance in Obesity. Diabetes *65*, 2295-2310.
Luze, H., Hecker, A., Nischwitz, S.P., Schellnegger, M., Kohlhauser, M., Draschl, A., Müllegger, C., Kamolz, L.P., and Kotzbeck, P. (2022). Non-invasive cooling wear as an effective means of reducing subcutaneous adipose tissue mass: an in-vivo study. The Journal of international medical research *50*, 3000605221109391.
Lyle, R.E., Richon, V.M., and McGehee, R.E. (1998). TNFα Disrupts Mitotic Clonal Expansion and Regulation of Retinoblastoma Proteins p130 and p107 during 3T3-L1 Adipocyte Differentiation. Biochem Biophys Res Commun *247*, 373-378.
Maeda, N., Funahashi, T., Hibuse, T., Nagasawa, A., Kishida, K., Kuriyama, H., Nakamura, T., Kihara, S., Shimomura, I., and Matsuzawa, Y. (2004). Adaptation to fasting by glycerol transport through aquaporin 7 in adipose tissue. Proceedings of the National Academy of Sciences *101*, 17801-17806.
Magré, J., Delépine, M., Khallouf, E., Gedde-Dahl, T., Van Maldergem, L., Sobel, E., Papp, J., Meier, M., Mégarbané, A., Group, B.W.*, et al.* (2001). Identification of the gene altered in Berardinelli–Seip congenital lipodystrophy on chromosome 11q13. Nature Genetics *28*, 365-370.
Mahlapuu, M., Johansson, C., Lindgren, K., Hjälm, G., Barnes, B.R., Krook, A., Zierath, J.R., Andersson, L., and Marklund, S. (2004). Expression profiling of the γ-subunit isoforms of AMP-activated protein kinase suggests a major role for γ3 in white skeletal muscle. American Journal of Physiology-Endocrinology and Metabolism *286*, E194-E200.
Malone, J.I., and Hansen, B.C. (2019). Does obesity cause type 2 diabetes mellitus (T2DM)? Or is it the opposite? Pediatric Diabetes *20*, 5-9.

Mammucari, C., Milan, G., Romanello, V., Masiero, E., Rudolf, R., Del Piccolo, P., Burden, S.J., Di Lisi, R., Sandri, C., Zhao, J.*, et al.* (2007). FoxO3 Controls Autophagy in Skeletal Muscle In Vivo. Cell Metab *6*, 458-471.
Mancini, A., El Bounkari, O., Norrenbrock, A.F., Scherr, M., Schaefer, D., Eder, M., Banham, A.H., Pulford, K., Lyne, L., Whetton, A.D.*, et al.* (2007). FMIP controls the adipocyte lineage commitment of C2C12 cells by downmodulation of C/EBPalpha. Oncogene *26*, 1020-1027.
Mann, J.P., and Savage, D.B. (2019). What lipodystrophies teach us about the metabolic syndrome. J Clin Invest *129*, 4009-4021.
Marcelin, G., Ferreira, A., Liu, Y., Atlan, M., Aron-Wisnewsky, J., Pelloux, V., Botbol, Y., Ambrosini, M., Fradet, M., Rouault, C.*, et al.* (2017). A PDGFRα-Mediated Switch toward CD9high Adipocyte Progenitors Controls Obesity-Induced Adipose Tissue Fibrosis. Cell Metab *25*, 673-685.
Marin, T.L., Gongol, B., Martin, M., King, S.J., Smith, L., Johnson, D.A., Subramaniam, S., Chien, S., and Shyy, J.Y.J. (2015). Identification of AMP-activated protein kinase targets by a consensus sequence search of the proteome. BMC Systems Biology *9*, 13.
Marques, A.P., Cunha-Santos, J., Leal, H., Sousa-Ferreira, L., Pereira de Almeida, L., Cavadas, C., and Rosmaninho-Salgado, J. (2018). Dipeptidyl peptidase IV (DPP-IV) inhibition prevents fibrosis in adipose tissue of obese mice. Biochimica et Biophysica Acta (BBA) - General Subjects *1862*, 403-413.
Marsin, A.S., Bertrand, L., Rider, M.H., Deprez, J., Beauloye, C., Vincent, M.F., Van den Berghe, G., Carling, D., and Hue, L. (2000). Phosphorylation and activation of heart PFK-2 by AMPK has a role in the stimulation of glycolysis during ischaemia. Current biology : CB *10*, 1247-1255.
Martínez-Agustin, O., Hernández-Morante, J.J., Martínez-Plata, E., Sánchez de Medina, F., and Garaulet, M. (2010). Differences in AMPK expression between subcutaneous and visceral adipose tissue in morbid obesity. Regulatory Peptides *163*, 31-36.

Maurya, S.K., Bal, N.C., Sopariwala, D.H., Pant, M., Rowland, L.A., Shaikh, S.A., and Periasamy, M. (2015). Sarcolipin Is a Key Determinant of the Basal Metabolic Rate, and Its Overexpression Enhances Energy Expenditure and Resistance against Diet-induced Obesity. The Journal of biological chemistry *290*, 10840-10849.
Merrick, D., Sakers, A., Irgebay, Z., Okada, C., Calvert, C., Morley, M.P., Percec, I., and Seale, P. (2019). Identification of a mesenchymal progenitor cell hierarchy in adipose tissue. Science *364*.
Miki, H., Yamauchi, T., Suzuki, R., Komeda, K., Tsuchida, A., Kubota, N., Terauchi, Y., Kamon, J., Kaburagi, Y., Matsui, J.*, et al.* (2001). Essential Role of Insulin Receptor Substrate 1 (IRS-1) and IRS-2 in Adipocyte Differentiation. Molecular and Cellular Biology *21*, 2521-2532.
Min, S.Y., Desai, A., Yang, Z., Sharma, A., DeSouza, T., Genga, R.M.J., Kucukural, A., Lifshitz, L.M., Nielsen, S., Scheele, C.*, et al.* (2019). Diverse repertoire of human adipocyte subtypes develops from transcriptionally distinct mesenchymal progenitor cells. Proceedings of the National Academy of Sciences *116*, 17970.
Min, S.Y., Kady, J., Nam, M., Rojas-Rodriguez, R., Berkenwald, A., Kim, J.H., Noh, H.-L., Kim, J.K., Cooper, M.P., Fitzgibbons, T.*, et al.* (2016). Human 'brite/beige' adipocytes develop from capillary networks, and their implantation improves metabolic homeostasis in mice. Nature Medicine *22*, 312-318.
Mina, A.I., LeClair, R.A., LeClair, K.B., Cohen, D.E., Lantier, L., and Banks, A.S. (2018). CalR: A Web-Based Analysis Tool for Indirect Calorimetry Experiments. Cell Metab *28*, 656-666.e651.
Minokoshi, Y., Alquier, T., Furukawa, N., Kim, Y.-B., Lee, A., Xue, B., Mu, J., Foufelle, F., Ferré, P., Birnbaum, M.J.*, et al.* (2004). AMP-kinase regulates food intake by responding to hormonal and nutrient signals in the hypothalamus. Nature *428*, 569-574.
Minokoshi, Y., Kim, Y.B., Peroni, O.D., Fryer, L.G., Muller, C., Carling, D., and Kahn, B.B. (2002). Leptin stimulates fatty-acid oxidation by activating AMP-activated protein kinase. Nature *415*, 339-343.

Mishra, R., Cool, B.L., Laderoute, K.R., Foretz, M., Viollet, B., and Simonson, M.S. (2008). AMP-activated protein kinase inhibits transforming growth factor-beta-induced Smad3-dependent transcription and myofibroblast transdifferentiation. J Biol Chem *283*, 10461-10469.
Misra, A., Vikram, N.K., Gupta, R., Pandey, R.M., Wasir, J.S., and Gupta, V.P. (2006). Waist circumference cutoff points and action levels for Asian Indians for identification of abdominal obesity. Int J Obes *30*, 106-111.
Monteiro, C.A., Conde, W.L., Lu, B., and Popkin, B.M. (2004). Obesity and inequities in health in the developing world. Int J Obes *28*, 1181-1186.
Mortensen, B., Poulsen, P., Wegner, L., Stender-Petersen, K.L., Ribel-Madsen, R., Friedrichsen, M., Birk, J.B., Vaag, A., and Wojtaszewski, J.F.P. (2009). Genetic and metabolic effects on skeletal muscle AMPK in young and older twins. American Journal of Physiology-Endocrinology and Metabolism *297*, E956-E964.
Motoshima, H., Goldstein, B.J., Igata, M., and Araki, E. (2006). AMPK and cell proliferation – AMPK as a therapeutic target for atherosclerosis and cancer. J Physiol *574*, 63-71.
Mottillo, Emilio P., Desjardins, Eric M., Crane, Justin D., Smith, Brennan K., Green, Alex E., Ducommun, S., Henriksen, Tora I., Rebalka, Irena A., Razi, A., Sakamoto, K.*, et al.* (2016). Lack of Adipocyte AMPK Exacerbates Insulin Resistance and Hepatic Steatosis through Brown and Beige Adipose Tissue Function. Cell Metab *24*, 118-129.
Muller, S., Ader, I., Creff, J., Leménager, H., Achard, P., Casteilla, L., Sensebé, L., Carrière, A., and Deschaseaux, F. (2019). Human adipose stromal-vascular fraction self-organizes to form vascularized adipose tissue in 3D cultures. Scientific reports *9*, 7250.
Müller, S., Balaz, M., Stefanicka, P., Varga, L., Amri, E.-Z., Ukropec, J., Wollscheid, B., and Wolfrum, C. (2016). Proteomic Analysis of Human Brown Adipose Tissue Reveals Utilization of Coupled and Uncoupled Energy Expenditure Pathways. Scientific reports *6*, 30030-30030.

Mulligan, J.D., Gonzalez, A.A., Stewart, A.M., Carey, H.V., and Saupe, K.W. (2007). Upregulation of AMPK during cold exposure occurs via distinct mechanisms in brown and white adipose tissue of the mouse. J Physiol *580*, 677-684.
Munday, M.R., Campbell, D.G., Carling, D., and Hardie, D.G. (1988). Identification by amino acid sequencing of three major regulatory phosphorylation sites on rat acetyl-CoA carboxylase. European journal of biochemistry *175*, 331-338.
Münzberg, H., Laque, A., Yu, S., Rezai-Zadeh, K., and Berthoud, H.R. (2015). Appetite and body weight regulation after bariatric surgery. Obesity reviews : an official journal of the International Association for the Study of Obesity *16 Suppl 1*, 77-90.
Murano, I., Barbatelli, G., Parisani, V., Latini, C., Muzzonigro, G., Castellucci, M., and Cinti, S. (2008). Dead adipocytes, detected as crown-like structures, are prevalent in visceral fat depots of genetically obese mice. Journal of lipid research *49*, 1562-1568.
Murray, S., Tulloch, A., Gold, M.S., and Avena, N.M. (2014). Hormonal and neural mechanisms of food reward, eating behaviour and obesity. Nature Reviews Endocrinology *10*, 540-552.
Myers, R.W., Guan, H.-P., Ehrhart, J., Petrov, A., Prahalada, S., Tozzo, E., Yang, X., Kurtz, M.M., Trujillo, M., Gonzalez Trotter, D.*, et al.* (2017). Systemic pan-AMPK activator MK-8722 improves glucose homeostasis but induces cardiac hypertrophy. Science *357*, 507.
Nasrallah, C.M., and Horvath, T.L. (2014). Mitochondrial dynamics in the central regulation of metabolism. Nature Reviews Endocrinology *10*, 650-658.
NCD-RisC (2016). Trends in adult body-mass index in 200 countries from 1975 to 2014: a pooled analysis of 1698 population-based measurement studies with 19·2 million participants. Lancet (London, England) *387*, 1377-1396.
NCD-RisC (2017). Worldwide trends in body-mass index, underweight, overweight, and obesity from 1975 to 2016: a pooled analysis of 2416 population-based

measurement studies in 128·9 million children, adolescents, and adults. Lancet (London, England) *390*, 2627-2642.
Nechad, M., and Olson, L. (1983). Development of interscapular brown adipose tissue in the hamster. II - Differentiation of transplants in the anterior chamber of the eye: role of the sympathetic innervation. Biol Cell *48*, 167-174.
Nedergaard, J., Bengtsson, T., and Cannon, B. (2007). Unexpected evidence for active brown adipose tissue in adult humans. American Journal of Physiology-Endocrinology and Metabolism *293*, E444-E452.
Niesler, C.U., Myburgh, K.H., and Moore, F. (2007). The changing AMPK expression profile in differentiating mouse skeletal muscle myoblast cells helps confer increasing resistance to apoptosis. Experimental Physiology *92*, 207-217.
Nowack, J., Giroud, S., Arnold, W., and Ruf, T. (2017). Muscle Non-shivering Thermogenesis and Its Role in the Evolution of Endothermy. Frontiers in physiology *8*, 889-889.
Nuotio-Antar, A.M., Poungvarin, N., Li, M., Schupp, M., Mohammad, M., Gerard, S., Zou, F., and Chan, L. (2015). FABP4-Cre Mediated Expression of Constitutively Active ChREBP Protects Against Obesity, Fatty Liver, and Insulin Resistance. Endocrinology *156*, 4020-4032.
Nyman, E., Bartesaghi, S., Melin Rydfalk, R., Eng, S., Pollard, C., Gennemark, P., Peng, X.-R., and Cedersund, G. (2017). Systems biology reveals uncoupling beyond UCP1 in human white fat-derived beige adipocytes. npj Systems Biology and Applications *3*, 29.
O'Neill, H.M., Maarbjerg, S.J., Crane, J.D., Jeppesen, J., Jørgensen, S.B., Schertzer, J.D., Shyroka, O., Kiens, B., van Denderen, B.J., Tarnopolsky, M.A.*, et al.* (2011). AMP-activated protein kinase (AMPK) beta1beta2 muscle null mice reveal an essential role for AMPK in maintaining mitochondrial content and glucose uptake during exercise. Proceedings of the National Academy of Sciences of the United States of America *108*, 16092-16097.

O'Neill, H.M., Holloway, G.P., and Steinberg, G.R. (2013). AMPK regulation of fatty acid metabolism and mitochondrial biogenesis: Implications for obesity. Molecular and Cellular Endocrinology *366*, 135-151.
Oakhill, J.S., Chen, Z.-P., Scott, J.W., Steel, R., Castelli, L.A., Ling, N., Macaulay, S.L., and Kemp, B.E. (2010). β-Subunit myristoylation is the gatekeeper for initiating metabolic stress sensing by AMP-activated protein kinase (AMPK). Proceedings of the National Academy of Sciences of the United States of America *107*, 19237-19241.
Oakhill, J.S., Steel, R., Chen, Z.-P., Scott, J.W., Ling, N., Tam, S., and Kemp, B.E. (2011). AMPK Is a Direct Adenylate Charge-Regulated Protein Kinase. Science *332*, 1433.
Oguri, Y., Shinoda, K., Kim, H., Alba, D.L., Bolus, W.R., Wang, Q., Brown, Z., Pradhan, R.N., Tajima, K., Yoneshiro, T.*, et al.* (2020). CD81 Controls Beige Fat Progenitor Cell Growth and Energy Balance via FAK Signaling. Cell *182*, 563-577.e520.
Ohno, H., Shinoda, K., Ohyama, K., Sharp, L.Z., and Kajimura, S. (2013). EHMT1 controls brown adipose cell fate and thermogenesis through the PRDM16 complex. Nature *504*, 163-167.
Okla, M., Ha, J.-H., Temel, R.E., and Chung, S. (2015). BMP7 drives human adipogenic stem cells into metabolically active beige adipocytes. Lipids *50*, 111-120.
Olzmann, J.A., and Carvalho, P. (2019). Dynamics and functions of lipid droplets. Nature Reviews Molecular Cell Biology *20*, 137-155.
Oussaada, S.M., van Galen, K.A., Cooiman, M.I., Kleinendorst, L., Hazebroek, E.J., van Haelst, M.M., Ter Horst, K.W., and Serlie, M.J. (2019). The pathogenesis of obesity. Metabolism: clinical and experimental *92*, 26-36.
Pachón-Peña, G., and Bredella, M.A. (2022). Bone marrow adipose tissue in metabolic health. Trends in Endocrinology & Metabolism *33*, 401-408.
Palmer, B.F., and Clegg, D.J. (2015). The sexual dimorphism of obesity. Molecular and Cellular Endocrinology *402*, 113-119.

Park, B.O., Ahrends, R., and Teruel, M.N. (2012). Consecutive positive feedback loops create a bistable switch that controls preadipocyte-to-adipocyte conversion. Cell Rep *2*, 976-990.
Patel, Y.M., and Lane, M.D. (2000). Mitotic Clonal Expansion during Preadipocyte Differentiation: Calpain-mediated Turnover of p27 *. Journal of Biological Chemistry *275*, 17653-17660.
Penfold, L., Woods, A., Muckett, P., Nikitin, A.Y., Kent, T.R., Zhang, S., Graham, R., Pollard, A., and Carling, D. (2018). CAMKK2 Promotes Prostate Cancer Independently of AMPK via Increased Lipogenesis. Cancer research *78*, 6747-6761.
Perdikari, A., Kulenkampff, E., Rudigier, C., Neubauer, H., Luippold, G., Redemann, N., and Wolfrum, C. (2017). A high-throughput, image-based screen to identify kinases involved in brown adipocyte development. Science Signaling *10*, eaaf5357.
Petersen, K.F., Oral, E.A., Dufour, S., Befroy, D., Ariyan, C., Yu, C., Cline, G.W., DePaoli, A.M., Taylor, S.I., Gorden, P*., et al.* (2002). Leptin reverses insulin resistance and hepatic steatosis in patients with severe lipodystrophy. J Clin Invest *109*, 1345-1350.
Petrus, P., Lecoutre, S., Dollet, L., Wiel, C., Sulen, A., Gao, H., Tavira, B., Laurencikiene, J., Rooyackers, O., Checa, A*., et al.* (2020). Glutamine Links Obesity to Inflammation in Human White Adipose Tissue. Cell Metab *31*, 375-390.e311.
Phelan, S.M., Burgess, D.J., Yeazel, M.W., Hellerstedt, W.L., Griffin, J.M., and van Ryn, M. (2015). Impact of weight bias and stigma on quality of care and outcomes for patients with obesity. Obesity Reviews *16*, 319-326.
Phillips, A., and Clements, J.N. (2022). Clinical review of subcutaneous semaglutide for obesity. Journal of Clinical Pharmacy and Therapeutics *47*, 184-193.
Piché, M.-E., Poirier, P., Lemieux, I., and Després, J.-P. (2018). Overview of Epidemiology and Contribution of Obesity and Body Fat Distribution to Cardiovascular Disease: An Update. Progress in Cardiovascular Diseases *61*, 103-113.

Pigeyre, M., Yazdi, Fereshteh T., Kaur, Y., and Meyre, D. (2016). Recent progress in genetics, epigenetics and metagenomics unveils the pathophysiology of human obesity. Clinical Science *130*, 943-986.
Pini, M., Czibik, G., Sawaki, D., Mezdari, Z., Braud, L., Delmont, T., Mercedes, R., Martel, C., Buron, N., Marcelin, G.*, et al.* (2021). Adipose tissue senescence is mediated by increased ATP content after a short-term high-fat diet exposure. Aging cell *20*, e13421-e13421.
Polekhina, G., Gupta, A., van Denderen, B.J.W., Feil, S.C., Kemp, B.E., Stapleton, D., and Parker, M.W. (2005). Structural Basis for Glycogen Recognition by AMP-Activated Protein Kinase. Structure *13*, 1453-1462.
Pollard, A. (2017). Investigating the effect of chronic activation of AMP-activated protein kinase in vivo (Imperial College London), pp. 308.
Pollard, A.E., and Carling, D. (2020). Thermogenic adipocytes: lineage, function and therapeutic potential. Biochem J *477*, 2071-2093.
Pollard, A.E., Martins, L., Muckett, P.J., Khadayate, S., Bornot, A., Clausen, M., Admyre, T., Bjursell, M., Fiadeiro, R., Wilson, L.*, et al.* (2019). AMPK activation protects against diet induced obesity through Ucp1-independent thermogenesis in subcutaneous white adipose tissue. Nat Metab *1*, 340-349.
Porter, C., Herndon, David N., Chondronikola, M., Chao, T., Annamalai, P., Bhattarai, N., Saraf, M.K., Capek, K.D., Reidy, Paul T., Daquinag, Alexes C.*, et al.* (2016). Human and Mouse Brown Adipose Tissue Mitochondria Have Comparable UCP1 Function. Cell Metab *24*, 246-255.
Prevention, C.f.D.C.a. (2017). National Diabetes Statistics Report, 2017. Estimates of Diabetes and Its Burden in the United States, A.C.f.D.C.a. Prevention, ed.
Qi, R., Long, D., Wang, J., Wang, Q., Huang, X., Cao, C., Gao, G., and Huang, J. (2016). MicroRNA-199a Targets the Fatty Acid Transport Protein 1 Gene and Inhibits the Adipogenic Trans-Differentiation of C2C12 Myoblasts. Cellular physiology and biochemistry : international journal of experimental cellular physiology, biochemistry, and pharmacology *39*, 1087-1097.

Qi, Y., Sun, L., and Yang, H. (2017). Lipid droplet growth and adipocyte development: mechanistically distinct processes connected by phospholipids. Biochimica et biophysica acta Molecular and cell biology of lipids *1862*, 1273-1283.
Qiu, Z., Wei, Y., Chen, N., Jiang, M., Wu, J., and Liao, K. (2001). DNA Synthesis and Mitotic Clonal Expansion Is Not a Required Step for 3T3-L1 Preadipocyte Differentiation into Adipocytes*. Journal of Biological Chemistry *276*, 11988-11995.
Raajendiran, A., Krisp, C., Souza, D.P.D., Ooi, G., Burton, P.R., Taylor, R.A., Molloy, M.P., and Watt, M.J. (2021). Proteome analysis of human adipocytes identifies depot-specific heterogeneity at metabolic control points. American Journal of Physiology-Endocrinology and Metabolism *320*, E1068-E1084.
Raajendiran, A., Ooi, G., Bayliss, J., O'Brien, P.E., Schittenhelm, R.B., Clark, A.K., Taylor, R.A., Rodeheffer, M.S., Burton, P.R., and Watt, M.J. (2019). Identification of Metabolically Distinct Adipocyte Progenitor Cells in Human Adipose Tissues. Cell Rep *27*, 1528-1540 e1527.
Rahbani, J.F., Roesler, A., Hussain, M.F., Samborska, B., Dykstra, C.B., Tsai, L., Jedrychowski, M.P., Vergnes, L., Reue, K., Spiegelman, B.M.*, et al.* (2021). Creatine kinase B controls futile creatine cycling in thermogenic fat. Nature *590*, 480-485.
Rajakumari, S., Wu, J., Ishibashi, J., Lim, H.-W., Giang, A.-H., Won, K.-J., Reed, R.R., and Seale, P. (2013). EBF2 determines and maintains brown adipocyte identity. Cell Metab *17*, 562-574.
Rajamohan, F., Reyes, A.R., Frisbie, R.K., Hoth, L.R., Sahasrabudhe, P., Magyar, R., Landro, J.A., Withka, J.M., Caspers, N.L., Calabrese, M.F.*, et al.* (2016). Probing the enzyme kinetics, allosteric modulation and activation of α1- and α2-subunit-containing AMP-activated protein kinase (AMPK) heterotrimeric complexes by pharmacological and physiological activators. Biochem J *473*, 581-592.
Rennert, R.C., Januszyk, M., Sorkin, M., Rodrigues, M., Maan, Z.N., Duscher, D., Whittam, A.J., Kosaraju, R., Chung, M.T., Paik, K.*, et al.* (2016). Microfluidic single-cell transcriptional analysis rationally identifies novel surface marker profiles to enhance cell-based therapies. Nature Communications *7*, 11945.

Reusch Jane, E.B., Colton Lilliester, A., and Klemm Dwight, J. (2000). CREB Activation Induces Adipogenesis in 3T3-L1 Cells. Molecular and Cellular Biology *20*, 1008-1020.
Rippin, H.L., Hutchinson, J., Jewell, J., Breda, J.J., and Cade, J.E. (2019). Comparison of consumed portion sizes and on-pack serving sizes of UK energy dense foods. Appetite *134*, 193-203.
Robciuc, M.R., Kivelä, R., Williams, I.M., de Boer, J.F., van Dijk, T.H., Elamaa, H., Tigistu-Sahle, F., Molotkov, D., Leppänen, V.M., Käkelä, R.*, et al.* (2016). VEGFB/VEGFR1-Induced Expansion of Adipose Vasculature Counteracts Obesity and Related Metabolic Complications. Cell Metab *23*, 712-724.
Roberts, R., Hodson, L., Dennis, A.L., Neville, M.J., Humphreys, S.M., Harnden, K.E., Micklem, K.J., and Frayn, K.N. (2009). Markers of de novo lipogenesis in adipose tissue: associations with small adipocytes and insulin sensitivity in humans. Diabetologia *52*, 882-890.
Rochford, J.J. (2022). When Adipose Tissue Lets You Down: Understanding the Functions of Genes Disrupted in Lipodystrophy. Diabetes *71*, 589-598.
Rodeheffer, M.S., Birsoy, K., and Friedman, J.M. (2008). Identification of White Adipocyte Progenitor Cells In Vivo. Cell *135*, 240-249.
Roesler, A., and Kazak, L. (2020). UCP1-independent thermogenesis. Biochemical Journal *477*, 709-725.
Roh, H.C., Tsai, L.T.Y., Shao, M., Tenen, D., Shen, Y., Kumari, M., Lyubetskaya, A., Jacobs, C., Dawes, B., Gupta, R.K.*, et al.* (2018). Warming Induces Significant Reprogramming of Beige, but Not Brown, Adipocyte Cellular Identity. Cell Metab *27*, 1121-1137.e1125.
Rohde, K., Keller, M., la Cour Poulsen, L., Blüher, M., Kovacs, P., and Böttcher, Y. (2019). Genetics and epigenetics in obesity. Metabolism: clinical and experimental *92*, 37-50.
Rondini, E.A., and Granneman, J.G. (2020). Single cell approaches to address adipose tissue stromal cell heterogeneity. Biochemical Journal *477*, 583-600.

Rosen, E.D., Hsu, C.-H., Wang, X., Sakai, S., Freeman, M.W., Gonzalez, F.J., and Spiegelman, B.M. (2002). C/EBPalpha induces adipogenesis through PPARgamma: a unified pathway. Genes Dev *16*, 22-26.
Rosen, E.D., and Spiegelman, B.M. (2014). What we talk about when we talk about fat. Cell *156*, 20-44.
Rosenbaum, M., Hirsch, J., Gallagher, D.A., and Leibel, R.L. (2008). Long-term persistence of adaptive thermogenesis in subjects who have maintained a reduced body weight. The American Journal of Clinical Nutrition *88*, 906-912.
Rosenwald, M., Perdikari, A., Rülicke, T., and Wolfrum, C. (2013). Bi-directional interconversion of brite and white adipocytes. Nature cell biology *15*, 659-667.
Ross, F.A., Jensen, T.E., and Hardie, D.G. (2016). Differential regulation by AMP and ADP of AMPK complexes containing different γ subunit isoforms. Biochem J *473*, 189-199.
Rowland, L.A., Bal, N.C., Kozak, L.P., and Periasamy, M. (2015). Uncoupling Protein 1 and Sarcolipin Are Required to Maintain Optimal Thermogenesis, and Loss of Both Systems Compromises Survival of Mice under Cold Stress. The Journal of biological chemistry *290*, 12282-12289.
Rydén, M., Petrus, P., Andersson, D.P., Medina-Gómez, G., Escasany, E., Corrales Cordón, P., Dahlman, I., Kulyté, A., and Arner, P. (2019). Insulin action is severely impaired in adipocytes of apparently healthy overweight and obese subjects. Journal of Internal Medicine *285*, 578-588.
Sakoda, H., Ogihara, T., Anai, M., Fujishiro, M., Ono, H., Onishi, Y., Katagiri, H., Abe, M., Fukushima, Y., Shojima, N.*, et al.* (2002). Activation of AMPK is essential for AICAR-induced glucose uptake by skeletal muscle but not adipocytes. American Journal of Physiology-Endocrinology and Metabolism *282*, E1239-E1244.
Salo, V.T., Belevich, I., Li, S., Karhinen, L., Vihinen, H., Vigouroux, C., Magré, J., Thiele, C., Hölttä-Vuori, M., Jokitalo, E.*, et al.* (2016). Seipin regulates ER-lipid droplet contacts and cargo delivery. The EMBO journal *35*, 2699-2716.

Salo, V.T., Li, S., Vihinen, H., Hölttä-Vuori, M., Szkalisity, A., Horvath, P., Belevich, I., Peränen, J., Thiele, C., Somerharju, P.*, et al.* (2019). Seipin Facilitates Triglyceride Flow to Lipid Droplet and Counteracts Droplet Ripening via Endoplasmic Reticulum Contact. Developmental Cell *50*, 478-493.e479.
Sanchez-Gurmaches, J., and Guertin, D.A. (2014a). Adipocyte lineages: tracing back the origins of fat. Biochim Biophys Acta *1842*, 340-351.
Sanchez-Gurmaches, J., and Guertin, D.A. (2014b). Adipocytes arise from multiple lineages that are heterogeneously and dynamically distributed. Nature Communications *5*, 4099.
Sanchez-Gurmaches, J., Hung, C.-M., Sparks, C.A., Tang, Y., Li, H., and Guertin, D.A. (2012). PTEN loss in the Myf5 lineage redistributes body fat and reveals subsets of white adipocytes that arise from Myf5 precursors. Cell Metab *16*, 348-362.
Schneider, H., Schubert Kai, M., Blodow, S., Kreutz, C.-P., Erdogmus, S., Wiedenmann, M., Qiu, J., Fey, T., Ruth, P., Lubomirov Lubomir, T.*, et al.* (2015). AMPK Dilates Resistance Arteries via Activation of SERCA and BKCa Channels in Smooth Muscle. Hypertension *66*, 108-116.
Schoettl, T., Fischer, I.P., and Ussar, S. (2018). Heterogeneity of adipose tissue in development and metabolic function. Journal of Experimental Biology *221*, jeb162958.
Schuldiner, M., and Bohnert, M. (2017). A different kind of love – lipid droplet contact sites. Biochimica et Biophysica Acta (BBA) - Molecular and Cell Biology of Lipids *1862*, 1188-1196.
Schulz, T.J., Huang, P., Huang, T.L., Xue, R., McDougall, L.E., Townsend, K.L., Cypess, A.M., Mishina, Y., Gussoni, E., and Tseng, Y.-H. (2013). Brown-fat paucity due to impaired BMP signalling induces compensatory browning of white fat. Nature *495*, 379-383.
Schwalie, P.C., Dong, H., Zachara, M., Russeil, J., Alpern, D., Akchiche, N., Caprara, C., Sun, W., Schlaudraff, K.-U., Soldati, G.*, et al.* (2018a). A stromal cell population that inhibits adipogenesis in mammalian fat depots. Nature *559*, 103-108.

Schwalie, P.C., Dong, H., Zachara, M., Russeil, J., Alpern, D., Akchiche, N., Caprara, C., Sun, W., Schlaudraff, K.U., Soldati, G.*, et al.* (2018b). A stromal cell population that inhibits adipogenesis in mammalian fat depots. Nature *559*, 103-108.
Scott, John W., Ling, N., Issa, Samah M.A., Dite, Toby A., O'Brien, Matthew T., Chen, Z.-P., Galic, S., Langendorf, Christopher G., Steinberg, Gregory R., Kemp, Bruce E.*, et al.* (2014). Small Molecule Drug A-769662 and AMP Synergistically Activate Naive AMPK Independent of Upstream Kinase Signaling. Chemistry & Biology *21*, 619-627.
Seale, P., Bjork, B., Yang, W., Kajimura, S., Chin, S., Kuang, S., Scimè, A., Devarakonda, S., Conroe, H.M., Erdjument-Bromage, H.*, et al.* (2008). PRDM16 controls a brown fat/skeletal muscle switch. Nature *454*, 961.
Seale, P., Conroe, H.M., Estall, J., Kajimura, S., Frontini, A., Ishibashi, J., Cohen, P., Cinti, S., and Spiegelman, B.M. (2011). Prdm16 determines the thermogenic program of subcutaneous white adipose tissue in mice. J Clin Invest *121*, 96-105.
Seale, P., Kajimura, S., and Spiegelman, B.M. (2009). Transcriptional control of brown adipocyte development and physiological function--of mice and men. Genes Dev *23*, 788-797.
Seale, P., Kajimura, S., Yang, W., Chin, S., Rohas, L.M., Uldry, M., Tavernier, G., Langin, D., and Spiegelman, B.M. (2007). Transcriptional control of brown fat determination by PRDM16. Cell Metab *6*, 38-54.
Sebo, Z.L., and Rodeheffer, M.S. (2019). Assembling the adipose organ: adipocyte lineage segregation and adipogenesis <em>in vivo</em&gt. Development (Cambridge, England) *146*, dev172098.
Sera, Y., LaRue, A.C., Moussa, O., Mehrotra, M., Duncan, J.D., Williams, C.R., Nishimoto, E., Schulte, B.A., Watson, P.M., Watson, D.K.*, et al.* (2009). Hematopoietic stem cell origin of adipocytes. Exp Hematol *37*, 1108-1120.e11204.
Shabalina, Irina G., Petrovic, N., de Jong, Jasper M.A., Kalinovich, Anastasia V., Cannon, B., and Nedergaard, J. (2013). UCP1 in Brite/Beige Adipose Tissue Mitochondria Is Functionally Thermogenic. Cell Rep *5*, 1196-1203.

Shamsi, F., Piper, M., Ho, L.-L., Huang, T.L., Gupta, A., Streets, A., Lynes, M.D., and Tseng, Y.-H. (2021). Vascular smooth muscle-derived Trpv1+ progenitors are a source of cold-induced thermogenic adipocytes. Nature Metabolism.
Shao, M., Hepler, C., Zhang, Q., Shan, B., Vishvanath, L., Henry, G.H., Zhao, S., An, Y.A., Wu, Y., Strand, D.W*., et al.* (2021a). Pathologic HIF1α signaling drives adipose progenitor dysfunction in obesity. Cell Stem Cell.
Shao, M., Ishibashi, J., Kusminski, C.M., Wang, Q.A., Hepler, C., Vishvanath, L., MacPherson, K.A., Spurgin, S.B., Sun, K., Holland, W.L*., et al.* (2016). Zfp423 Maintains White Adipocyte Identity through Suppression of the Beige Cell Thermogenic Gene Program. Cell Metab *23*, 1167-1184.
Shao, M., Wang, Q.A., Song, A., Vishvanath, L., Busbuso, N.C., Scherer, P.E., and Gupta, R.K. (2019). Cellular Origins of Beige Fat Cells Revisited. Diabetes *68*, 1874.
Shao, M., Zhang, Q., Truong, A., Shan, B., Vishvanath, L., Li, L., Seale, P., and Gupta, R.K. (2021b). ZFP423 controls EBF2 coactivator recruitment and PPARγ occupancy to determine the thermogenic plasticity of adipocytes. Genes Dev.
Sharma, A., Huard, C., Vernochet, C., Ziemek, D., Knowlton, K.M., Tyminski, E., Paradis, T., Zhang, Y., Jones, J.E.C., von Schack, D*., et al.* (2014). Brown fat determination and development from muscle precursor cells by novel action of bone morphogenetic protein 6. PLoS One *9*, e92608-e92608.
Sharp, L.Z., Shinoda, K., Ohno, H., Scheel, D.W., Tomoda, E., Ruiz, L., Hu, H., Wang, L., Pavlova, Z., Gilsanz, V*., et al.* (2012). Human BAT possesses molecular signatures that resemble beige/brite cells. PLoS One *7*, e49452-e49452.
Shaw, R.J., Kosmatka, M., Bardeesy, N., Hurley, R.L., Witters, L.A., DePinho, R.A., and Cantley, L.C. (2004). The tumor suppressor LKB1 kinase directly activates AMP-activated kinase and regulates apoptosis in response to energy stress. Proceedings of the National Academy of Sciences of the United States of America *101*, 3329.
Shinoda, K., Luijten, I.H.N., Hasegawa, Y., Hong, H., Sonne, S.B., Kim, M., Xue, R., Chondronikola, M., Cypess, A.M., Tseng, Y.-H*., et al.* (2015). Genetic and functional

characterization of clonally derived adult human brown adipocytes. Nature medicine *21*, 389-394.
Shulman, G.I. (2014). Ectopic Fat in Insulin Resistance, Dyslipidemia, and Cardiometabolic Disease. New England Journal of Medicine *371*, 1131-1141.
Silva, F.J., Holt, D.J., Vargas, V., Yockman, J., Boudina, S., Atkinson, D., Grainger, D.W., Revelo, M.P., Sherman, W., Bull, D.A.*, et al.* (2014). Metabolically Active Human Brown Adipose Tissue Derived Stem Cells. Stem cells (Dayton, Ohio) *32*, 572-581.
Simha, V., Szczepaniak, L.S., Wagner, A.J., DePaoli, A.M., and Garg, A. (2003). Effect of Leptin Replacement on Intrahepatic and Intramyocellular Lipid Content in Patients With Generalized Lipodystrophy. Diabetes Care *26*, 30-35.
Singh, A.M., Zhang, L., Avery, J., Yin, A., Du, Y., Wang, H., Li, Z., Fu, H., Yin, H., and Dalton, S. (2020). Human beige adipocytes for drug discovery and cell therapy in metabolic diseases. Nature Communications *11*, 2758.
Sjöström, L., Narbro, K., Sjöström, C.D., Karason, K., Larsson, B., Wedel, H., Lystig, T., Sullivan, M., Bouchard, C., Carlsson, B.*, et al.* (2007). Effects of Bariatric Surgery on Mortality in Swedish Obese Subjects. New England Journal of Medicine *357*, 741-752.
Smith, B.K., Ford, R.J., Desjardins, E.M., Green, A.E., Hughes, M.C., Houde, V.P., Day, E.A., Marcinko, K., Crane, J.D., Mottillo, E.P.*, et al.* (2016). Salsalate (Salicylate) Uncouples Mitochondria, Improves Glucose Homeostasis, and Reduces Liver Lipids Independent of AMPK-β1. Diabetes *65*, 3352-3361.
Smith, U., Li, Q., Rydén, M., and Spalding, K.L. (2021). Cellular senescence and its role in white adipose tissue. Int J Obes *45*, 934-943.
Song, Z., Xiaoli, A.M., and Yang, F. (2018). Regulation and Metabolic Significance of De Novo Lipogenesis in Adipose Tissues. Nutrients *10*.
St-Onge, M.P. (2017). Sleep–obesity relation: underlying mechanisms and consequences for treatment. Obesity Reviews *18*, 34-39.

Stahl, A., Evans, J.G., Pattel, S., Hirsch, D., and Lodish, H.F. (2002). Insulin Causes Fatty Acid Transport Protein Translocation and Enhanced Fatty Acid Uptake in Adipocytes. Developmental Cell *2*, 477-488.
Stanford, K.I., Middelbeek, R.J.W., Townsend, K.L., An, D., Nygaard, E.B., Hitchcox, K.M., Markan, K.R., Nakano, K., Hirshman, M.F., Tseng, Y.-H.*, et al.* (2013). Brown adipose tissue regulates glucose homeostasis and insulin sensitivity. J Clin Invest *123*, 215-223.
Stefkovich, M., Traynor, S., Cheng, L., Merrick, D., and Seale, P. (2021). Dpp4+ interstitial progenitor cells contribute to basal and high fat diet-induced adipogenesis. Mol Metab *54*, 101357-101357.
Steinberg, G.R., and Carling, D. (2019). AMP-activated protein kinase: the current landscape for drug development. Nature Reviews Drug Discovery.
Steneberg, P., Lindahl, E., Dahl, U., Lidh, E., Straseviciene, J., Backlund, F., Kjellkvist, E., Berggren, E., Lundberg, I., Bergqvist, I.*, et al.* (2018). PAN-AMPK activator O304 improves glucose homeostasis and microvascular perfusion in mice and type 2 diabetes patients. JCI Insight *3*, e99114.
Stryjecki, C., Alyass, A., and Meyre, D. (2018). Ethnic and population differences in the genetic predisposition to human obesity. Obesity Reviews *19*, 62-80.
Styner, M., Sen, B., Xie, Z., Case, N., and Rubin, J. (2010). Indomethacin promotes adipogenesis of mesenchymal stem cells through a cyclooxygenase independent mechanism. J Cell Biochem *111*, 1042-1050.
Su, S., Guntur, A.R., Nguyen, D.C., Fakory, S.S., Doucette, C.C., Leech, C., Lotana, H., Kelley, M., Kohli, J., Martino, J.*, et al.* (2018). A Renewable Source of Human Beige Adipocytes for Development of Therapies to Treat Metabolic Syndrome. Cell Rep *25*, 3215-3228.e3219.
Sun, K., Tordjman, J., Clément, K., and Scherer, P.E. (2013a). Fibrosis and adipose tissue dysfunction. Cell Metab *18*, 470-477.

Sun, W., Dong, H., Balaz, M., Slyper, M., Drokhlyansky, E., Colleluori, G., Giordano, A., Kovanicova, Z., Stefanicka, P., Balazova, L.*, et al.* (2020). snRNA-seq reveals a subpopulation of adipocytes that regulates thermogenesis. Nature *587*, 98-102.
Sun, Y., Rahbani, J.F., Jedrychowski, M.P., Riley, C.L., Vidoni, S., Bogoslavski, D., Hu, B., Dumesic, P.A., Zeng, X., Wang, A.B.*, et al.* (2021). Mitochondrial TNAP controls thermogenesis by hydrolysis of phosphocreatine. Nature *593*, 580-585.
Sun, Z., Gong, J., Wu, H., Xu, W., Wu, L., Xu, D., Gao, J., Wu, J.-w., Yang, H., Yang, M.*, et al.* (2013b). Perilipin1 promotes unilocular lipid droplet formation through the activation of Fsp27 in adipocytes. Nature Communications *4*, 1594.
Sutherland, C.M., Hawley, S.A., McCartney, R.R., Leech, A., Stark, M.J.R., Schmidt, M.C., and Hardie, D.G. (2003). Elm1p Is One of Three Upstream Kinases for the Saccharomyces cerevisiae SNF1 Complex. Current Biology *13*, 1299-1305.
Swinburn, B.A., Sacks, G., Hall, K.D., McPherson, K., Finegood, D.T., Moodie, M.L., and Gortmaker, S.L. (2011). The global obesity pandemic: shaped by global drivers and local environments. The Lancet *378*, 804-814.
Sztalryd, C., and Brasaemle, D.L. (2017). The perilipin family of lipid droplet proteins: Gatekeepers of intracellular lipolysis. Biochimica et biophysica acta Molecular and cell biology of lipids *1862*, 1221-1232.
Tabuchi, C., and Sul, H.S. (2021). Signaling Pathways Regulating Thermogenesis. Front Endocrinol (Lausanne) *12*, 595020.
Tang, Q.-Q., Otto, T.C., and Lane, M.D. (2003a). CCAAT/enhancer-binding protein β is required for mitotic clonal expansion during adipogenesis. Proceedings of the National Academy of Sciences *100*, 850-855.
Tang, Q.-Q., Otto, T.C., and Lane, M.D. (2003b). Mitotic clonal expansion: A synchronous process required for adipogenesis. Proceedings of the National Academy of Sciences *100*, 44-49.
Tang, Q.Q., and Lane, M.D. (1999). Activation and centromeric localization of CCAAT/enhancer-binding proteins during the mitotic clonal expansion of adipocyte differentiation. Genes Dev *13*, 2231-2241.

Tang, Q.Q., and Lane, M.D. (2000). Role of C/EBP homologous protein (CHOP-10) in the programmed activation of CCAAT/enhancer-binding protein-beta during adipogenesis. Proceedings of the National Academy of Sciences of the United States of America *97*, 12446-12450.
Tang, W., Zeve, D., Suh, J.M., Bosnakovski, D., Kyba, M., Hammer, R.E., Tallquist, M.D., and Graff, J.M. (2008). White Fat Progenitor Cells Reside in the Adipose Vasculature. Science *322*, 583.
Tchoukalova, Y.D., Votruba, S.B., Tchkonia, T., Giorgadze, N., Kirkland, J.L., and Jensen, M.D. (2010). Regional differences in cellular mechanisms of adipose tissue gain with overfeeding. Proceedings of the National Academy of Sciences *107*, 18226.
Thivel, D., Brakonieki, K., Duche, P., Morio, B., Boirie, Y., and Laferrère, B. (2013). Surgical weight loss: impact on energy expenditure. Obes Surg *23*, 255-266.
Timmons, J.A., Wennmalm, K., Larsson, O., Walden, T.B., Lassmann, T., Petrovic, N., Hamilton, D.L., Gimeno, R.E., Wahlestedt, C., Baar, K.*, et al.* (2007). Myogenic gene expression signature establishes that brown and white adipocytes originate from distinct cell lineages. Proceedings of the National Academy of Sciences of the United States of America *104*, 4401-4406.
Torres-Fuentes, C., Schellekens, H., Dinan, T.G., and Cryan, J.F. (2017). The microbiota–gut–brain axis in obesity. The Lancet Gastroenterology & Hepatology *2*, 747-756.
Toyama, E.Q., Herzig, S., Courchet, J., Lewis, T.L., Jr., Losón, O.C., Hellberg, K., Young, N.P., Chen, H., Polleux, F., Chan, D.C.*, et al.* (2016). Metabolism. AMP-activated protein kinase mediates mitochondrial fission in response to energy stress. Science (New York, NY) *351*, 275-281.
Tran, K.-V., Gealekman, O., Frontini, A., Zingaretti, M.C., Morroni, M., Giordano, A., Smorlesi, A., Perugini, J., De Matteis, R., Sbarbati, A.*, et al.* (2012). The vascular endothelium of the adipose tissue gives rise to both white and brown fat cells. Cell Metab *15*, 222-229.

Trayhurn, P. (2014). Hypoxia and adipocyte physiology: implications for adipose tissue dysfunction in obesity. Annual review of nutrition *34*, 207-236.
Tseng, Y.-H., Kokkotou, E., Schulz, T.J., Huang, T.L., Winnay, J.N., Taniguchi, C.M., Tran, T.T., Suzuki, R., Espinoza, D.O., Yamamoto, Y.*, et al.* (2008). New role of bone morphogenetic protein 7 in brown adipogenesis and energy expenditure. Nature *454*, 1000-1004.
Tzameli, I., Fang, H., Ollero, M., Shi, H., Hamm, J.K., Kievit, P., Hollenberg, A.N., and Flier, J.S. (2004). Regulated production of a peroxisome proliferator-activated receptor-gamma ligand during an early phase of adipocyte differentiation in 3T3-L1 adipocytes. J Biol Chem *279*, 36093-36102.
Ukropec, J., Anunciado, R.P., Ravussin, Y., Hulver, M.W., and Kozak, L.P. (2006). UCP1-independent Thermogenesis in White Adipose Tissue of Cold-Acclimated Ucp1-/- Mice. J Biol Chem *281*, 31894-31908.
Um, J.-H., Park, S.-J., Kang, H., Yang, S., Foretz, M., McBurney, M.W., Kim, M.K., Viollet, B., and Chung, J.H. (2010). AMP-Activated Protein Kinase–Deficient Mice Are Resistant to the Metabolic Effects of Resveratrol. Diabetes *59*, 554.
Unamuno, X., Gómez-Ambrosi, J., Rodríguez, A., Becerril, S., Frühbeck, G., and Catalán, V. (2018). Adipokine dysregulation and adipose tissue inflammation in human obesity. European journal of clinical investigation *48*, e12997.
Valm, A.M., Cohen, S., Legant, W.R., Melunis, J., Hershberg, U., Wait, E., Cohen, A.R., Davidson, M.W., Betzig, E., and Lippincott-Schwartz, J. (2017). Applying systems-level spectral imaging and analysis to reveal the organelle interactome. Nature *546*, 162-167.
van Marken Lichtenbelt, W.D., Vanhommerig, J.W., Smulders, N.M., Drossaerts, J.M., Kemerink, G.J., Bouvy, N.D., Schrauwen, P., and Teule, G.J. (2009). Cold-activated brown adipose tissue in healthy men. N Engl J Med *360*, 1500-1508.
Vara-Ciruelos, D., Russell, F.M., and Hardie, D.G. The strange case of AMPK and cancer: Dr Jekyll or Mr Hyde?†. Open Biology *9*, 190099.

Varghese, M., Kimler, V.A., Ghazi, F.R., Rathore, G.K., Perkins, G.A., Ellisman, M.H., and Granneman, J.G. (2019). Adipocyte lipolysis affects Perilipin 5 and cristae organization at the cardiac lipid droplet-mitochondrial interface. Scientific reports *9*, 4734.
Verstraeten, V.L.R.M., Renes, J., Ramaekers, F.C.S., Kamps, M., Kuijpers, H.J., Verheyen, F., Wabitsch, M., Steijlen, P.M., van Steensel, M.A.M., and Broers, J.L.V. (2011). Reorganization of the nuclear lamina and cytoskeleton in adipogenesis. Histochemistry and Cell Biology *135*, 251-261.
Vertino, A.M., Taylor-Jones, J.M., Longo, K.A., Bearden, E.D., Lane, T.F., McGehee, R.E., Jr., MacDougald, O.A., and Peterson, C.A. (2005). Wnt10b deficiency promotes coexpression of myogenic and adipogenic programs in myoblasts. Mol Biol Cell *16*, 2039-2048.
Vijayakumar, A., Aryal, P., Wen, J., Syed, I., Vazirani, R.P., Moraes-Vieira, P.M., Camporez, J.P., Gallop, M.R., Perry, R.J., Peroni, O.D*., et al.* (2017). Absence of Carbohydrate Response Element Binding Protein in Adipocytes Causes Systemic Insulin Resistance and Impairs Glucose Transport. Cell Rep *21*, 1021-1035.
Vijgen, G.H.E.J., Sparks, L.M., Bouvy, N.D., Schaart, G., Hoeks, J., van Marken Lichtenbelt, W.D., and Schrauwen, P. (2013). Increased Oxygen Consumption in Human Adipose Tissue From the “Brown Adipose Tissue” Region. The Journal of Clinical Endocrinology & Metabolism *98*, E1230-E1234.
Villarroya, J., Cereijo, R., Gavaldà-Navarro, A., Peyrou, M., Giralt, M., and Villarroya, F. (2019). New insights into the secretory functions of brown adipose tissue. The Journal of endocrinology *243*, R19-r27.
Vimaleswaran, K.S., Li, S., Zhao, J.H., Luan, J.a., Bingham, S.A., Khaw, K.-T., Ekelund, U., Wareham, N.J., and Loos, R.J.F. (2009). Physical activity attenuates the body mass index–increasing influence of genetic variation in the FTO gene. The American Journal of Clinical Nutrition *90*, 425-428.

Vincent, E.E., Coelho, P.P., Blagih, J., Griss, T., Viollet, B., and Jones, R.G. (2015). Differential effects of AMPK agonists on cell growth and metabolism. Oncogene *34*, 3627-3639.
Vingtdeux, V., Chandakkar, P., Zhao, H., Davies, P., and Marambaud, P. (2011). Small-Molecule Activators of AMP-Activated Protein Kinase (AMPK), RSVA314 and RSVA405, Inhibit Adipogenesis. Molecular Medicine *17*, 1022-1030.
Virtanen, K.A., Lidell, M.E., Orava, J., Heglind, M., Westergren, R., Niemi, T., Taittonen, M., Laine, J., Savisto, N.-J., Enerbäck, S.*, et al.* (2009). Functional Brown Adipose Tissue in Healthy Adults. New England Journal of Medicine *360*, 1518-1525.
Vishvanath, L., MacPherson, K.A., Hepler, C., Wang, Q.A., Shao, M., Spurgin, S.B., Wang, M.Y., Kusminski, C.M., Morley, T.S., and Gupta, R.K. (2016). Pdgfrβ+ Mural Preadipocytes Contribute to Adipocyte Hyperplasia Induced by High-Fat-Diet Feeding and Prolonged Cold Exposure in Adult Mice. Cell Metab *23*, 350-359.
Wadden, T.A., Foster, G.D., Stunkard, A.J., and Conill, A.M. (1996). Effects of weight cycling on the resting energy expenditure and body composition of obese women. International Journal of Eating Disorders *19*, 5-12.
Wang, C., Liu, W., Nie, Y., Qaher, M., Horton, H.E., Yue, F., Asakura, A., and Kuang, S. (2017). Loss of MyoD Promotes Fate Transdifferentiation of Myoblasts Into Brown Adipocytes. EBioMedicine *16*, 212-223.
Wang, H., Becuwe, M., Housden, B.E., Chitraju, C., Porras, A.J., Graham, M.M., Liu, X.N., Thiam, A.R., Savage, D.B., Agarwal, A.K.*, et al.* (2016). Seipin is required for converting nascent to mature lipid droplets. Elife *5*, e16582.
Wang, H., Sreenivasan, U., Hu, H., Saladino, A., Polster, B.M., Lund, L.M., Gong, D.W., Stanley, W.C., and Sztalryd, C. (2011). Perilipin 5, a lipid droplet-associated protein, provides physical and metabolic linkage to mitochondria. Journal of lipid research *52*, 2159-2168.
Wang, H., Xu, P.-F., Li, J.-Y., Liu, X.-J., Wu, X.-Y., Xu, F., Xie, B.-C., Huang, X.-M., Zhou, Z.-H., Kayoumu, A.*, et al.* (2018). Adipose tissue transplantation ameliorates

lipodystrophy-associated metabolic disorders in seipin-deficient mice. American Journal of Physiology-Endocrinology and Metabolism *316*, E54-E62.
Wang, L., and Shan, T. (2021). Factors inducing transdifferentiation of myoblasts into adipocytes. J Cell Physiol *236*, 2276-2289.
Wang, Q.A., Tao, C., Gupta, R.K., and Scherer, P.E. (2013). Tracking adipogenesis during white adipose tissue development, expansion and regeneration. Nature Medicine *19*, 1338-1344.
Wang, S., Liang, X., Yang, Q., Fu, X., Rogers, C.J., Zhu, M., Rodgers, B.D., Jiang, Q., Dodson, M.V., and Du, M. (2015). Resveratrol induces brown-like adipocyte formation in white fat through activation of AMP-activated protein kinase (AMPK) α1. Int J Obes (Lond) *39*, 967-976.
Wang, W., Kissig, M., Rajakumari, S., Huang, L., Lim, H.-w., Won, K.-J., and Seale, P. (2014). Ebf2 is a selective marker of brown and beige adipogenic precursor cells. Proceedings of the National Academy of Sciences *111*, 14466.
Wang, Z.Q., Yu, Y., Zhang, X.H., Floyd, E.Z., and Cefalu, W.T. (2010). Human adenovirus 36 decreases fatty acid oxidation and increases de novo lipogenesis in primary cultured human skeletal muscle cells by promoting Cidec/FSP27 expression. Int J Obes *34*, 1355-1364.
Watt, Matthew J., and Steinberg, Gregory R. (2008). Regulation and function of triacylglycerol lipases in cellular metabolism. Biochemical Journal *414*, 313-325.
Wen, J.-P., Liu, C.-e., Hu, Y.-T., Chen, G., and Lin, L.-x. (2010). Globular adiponectin regulates energy homeostasis through AMP-activated protein kinase–acetyl-CoA carboxylase (AMPK/ACC) pathway in the hypothalamus. Molecular and Cellular Biochemistry *344*, 109-115.
Westcott, G.P., Emont, M.P., Li, J., Jacobs, C., Tsai, L., and Rosen, E.D. (2021). Mesothelial cells are not a source of adipocytes in mice. Cell Rep *36*, 109388.
White, J.D., Dewal, R.S., and Stanford, K.I. (2019). The beneficial effects of brown adipose tissue transplantation. Molecular Aspects of Medicine *68*, 74-81.

Whitehead, A., Krause, F.N., Moran, A., MacCannell, A.D.V., Scragg, J.L., McNally, B.D., Boateng, E., Murfitt, S.A., Virtue, S., Wright, J.*, et al.* (2021). Brown and beige adipose tissue regulate systemic metabolism through a metabolite interorgan signaling axis. Nature Communications *12*, 1905.
Whitfield, M.L., Sherlock, G., Saldanha, A.J., Murray, J.I., Ball, C.A., Alexander, K.E., Matese, J.C., Perou, C.M., Hurt, M.M., Brown, P.O.*, et al.* (2002). Identification of genes periodically expressed in the human cell cycle and their expression in tumors. Mol Biol Cell *13*, 1977-2000.
Whittle, A.J., Carobbio, S., Martins, L., Slawik, M., Hondares, E., Vázquez, M.J., Morgan, D., Csikasz, R.I., Gallego, R., Rodriguez-Cuenca, S.*, et al.* (2012). BMP8B increases brown adipose tissue thermogenesis through both central and peripheral actions. Cell *149*, 871-885.
Wilfling, F., Haas, J.T., Walther, T.C., and Jr, R.V.F. (2014). Lipid droplet biogenesis. Current opinion in cell biology *29*, 39-45.
Williamson, D.L., Butler, D.C., and Alway, S.E. (2009). AMPK inhibits myoblast differentiation through a PGC-1alpha-dependent mechanism. American journal of physiology Endocrinology and metabolism *297*, E304-E314.
Willows, R., Navaratnam, N., Lima, A., Read, J., and Carling, D. (2017a). Effect of different γ-subunit isoforms on the regulation of AMPK. Biochem J *474*, 1741-1754.
Willows, R., Sanders, M.J., Xiao, B., Patel, B.R., Martin, S.R., Read, J., Wilson, J.R., Hubbard, J., Gamblin, S.J., and Carling, D. (2017b). Phosphorylation of AMPK by upstream kinases is required for activity in mammalian cells. Biochem J *474*, 3059-3073.
Wilson, L., Pollard, A.E., Penfold, L., Muckett, P.J., Whilding, C., Bohlooly, Y.M., Wilson, P., and Carling, D. (2021). Chronic activation of AMP-activated protein kinase leads to early-onset polycystic kidney phenotype. Clinical science (London, England : 1979) *135*, 2393-2408.

Winder, W.W., and Hardie, D.G. (1996). Inactivation of acetyl-CoA carboxylase and activation of AMP-activated protein kinase in muscle during exercise. American Journal of Physiology-Endocrinology and Metabolism *270*, E299-E304.
Witte, N., Muenzner, M., Rietscher, J., Knauer, M., Heidenreich, S., Nuotio-Antar, A.M., Graef, F.A., Fedders, R., Tolkachov, A., Goehring, I.*, et al.* (2015). The Glucose Sensor ChREBP Links De Novo Lipogenesis to PPARγ Activity and Adipocyte Differentiation. Endocrinology *156*, 4008-4019.
Wolfgang, M.J., and Lane, M.D. (2006). The Role of Hypothalamic Malonyl-CoA in Energy Homeostasis. Journal of Biological Chemistry *281*, 37265-37269.
Woo Baidal, J.A., Locks, L.M., Cheng, E.R., Blake-Lamb, T.L., Perkins, M.E., and Taveras, E.M. (2016). Risk Factors for Childhood Obesity in the First 1,000 Days: A Systematic Review. American Journal of Preventive Medicine *50*, 761-779.
Woods, A., Dickerson, K., Heath, R., Hong, S.-P., Momcilovic, M., Johnstone, S.R., Carlson, M., and Carling, D. (2005). Ca2+/calmodulin-dependent protein kinase kinase-β acts upstream of AMP-activated protein kinase in mammalian cells. Cell Metab *2*, 21-33.
Woods, A., Johnstone, S.R., Dickerson, K., Leiper, F.C., Fryer, L.G.D., Neumann, D., Schlattner, U., Wallimann, T., Carlson, M., and Carling, D. (2003a). LKB1 Is the Upstream Kinase in the AMP-Activated Protein Kinase Cascade. Current Biology *13*, 2004-2008.
Woods, A., Vertommen, D., Neumann, D., Türk, R., Bayliss, J., Schlattner, U., Wallimann, T., Carling, D., and Rider, M.H. (2003b). Identification of Phosphorylation Sites in AMP-activated Protein Kinase (AMPK) for Upstream AMPK Kinases and Study of Their Roles by Site-directed Mutagenesis. Journal of Biological Chemistry *278*, 28434-28442.
Woods, A., Williams, J.R., Muckett, P.J., Mayer, F.V., Liljevald, M., Bohlooly-Y, M., and Carling, D. (2017). Liver-Specific Activation of AMPK Prevents Steatosis on a High-Fructose Diet. Cell Rep *18*, 3043-3051.

Wu, J., Boström, P., Sparks, L.M., Ye, L., Choi, J.H., Giang, A.-H., Khandekar, M., Virtanen, K.A., Nuutila, P., Schaart, G.*, et al.* (2012). Beige adipocytes are a distinct type of thermogenic fat cell in mouse and human. Cell *150*, 366-376.
Wu, L., Zhang, L., Li, B., Jiang, H., Duan, Y., Xie, Z., Shuai, L., Li, J., and Li, J. (2018). AMP-Activated Protein Kinase (AMPK) Regulates Energy Metabolism through Modulating Thermogenesis in Adipose Tissue. Frontiers in physiology *9*, 122-122.
Wu, N., Zheng, B., Shaywitz, A., Dagon, Y., Tower, C., Bellinger, G., Shen, C.H., Wen, J., Asara, J., McGraw, T.E.*, et al.* (2013). AMPK-dependent degradation of TXNIP upon energy stress leads to enhanced glucose uptake via GLUT1. Mol Cell *49*, 1167-1175.
Wu, X., Motoshima, H., Mahadev, K., Stalker, T.J., Scalia, R., and Goldstein, B.J. (2003). Involvement of AMP-Activated Protein Kinase in Glucose Uptake Stimulated by the Globular Domain of Adiponectin in Primary Rat Adipocytes. Diabetes *52*, 1355-1363.
Wu, Z., Rosen, E.D., Brun, R., Hauser, S., Adelmant, G., Troy, A.E., McKeon, C., Darlington, G.J., and Spiegelman, B.M. (1999). Cross-regulation of C/EBP alpha and PPAR gamma controls the transcriptional pathway of adipogenesis and insulin sensitivity. Mol Cell *3*, 151-158.
Xiao, B., Heath, R., Saiu, P., Leiper, F.C., Leone, P., Jing, C., Walker, P.A., Haire, L., Eccleston, J.F., Davis, C.T.*, et al.* (2007). Structural basis for AMP binding to mammalian AMP-activated protein kinase. Nature *449*, 496-500.
Xiao, B., Sanders, M.J., Carmena, D., Bright, N.J., Haire, L.F., Underwood, E., Patel, B.R., Heath, R.B., Walker, P.A., Hallen, S.*, et al.* (2013). Structural basis of AMPK regulation by small molecule activators. Nature Communications *4*, 3017.
Xiao, B., Sanders, M.J., Underwood, E., Heath, R., Mayer, F.V., Carmena, D., Jing, C., Walker, P.A., Eccleston, J.F., Haire, L.F.*, et al.* (2011). Structure of mammalian AMPK and its regulation by ADP. Nature *472*, 230-233.

Xu, B., Xing, A., and Li, S. (2022). The forgotten type 2 diabetes mellitus medicine: rosiglitazone. Diabetology International *13*, 49-65.
Xu, X.J., Apovian, C., Hess, D., Carmine, B., Saha, A., and Ruderman, N. (2015). Improved Insulin Sensitivity 3 Months After RYGB Surgery Is Associated With Increased Subcutaneous Adipose Tissue AMPK Activity and Decreased Oxidative Stress. Diabetes *64*, 3155-3159.
Xu, X.J., Gauthier, M.-S., Hess, D.T., Apovian, C.M., Cacicedo, J.M., Gokce, N., Farb, M., Valentine, R.J., and Ruderman, N.B. (2012). Insulin sensitive and resistant obesity in humans: AMPK activity, oxidative stress, and depot-specific changes in gene expression in adipose tissue. Journal of lipid research *53*, 792-801.
Yamauchi, T., Kamon, J., Minokoshi, Y., Ito, Y., Waki, H., Uchida, S., Yamashita, S., Noda, M., Kita, S., Ueki, K.*, et al.* (2002). Adiponectin stimulates glucose utilization and fatty-acid oxidation by activating AMP-activated protein kinase. Nature Medicine *8*, 1288-1295.
Yan, M., Audet-Walsh, É., Manteghi, S., Dufour, C.R., Walker, B., Baba, M., St-Pierre, J., Giguère, V., and Pause, A. (2016). Chronic AMPK activation via loss of FLCN induces functional beige adipose tissue through PGC-1α/ERRα. Genes Dev *30*, 1034-1046.
Yang, L., Jia, X., Fang, D., Cheng, Y., Zhai, Z., Deng, W., Du, B., Lu, T., Wang, L., Yang, C.*, et al.* (2022). Metformin Inhibits Lipid Droplets Fusion and Growth via Reduction in Cidec and Its Regulatory Factors in Rat Adipose-Derived Stem Cells. Int J Mol Sci *23*.
Yang, Q., Liang, X., Sun, X., Zhang, L., Fu, X., Rogers, C.J., Berim, A., Zhang, S., Wang, S., Wang, B.*, et al.* (2016a). AMPK/α-Ketoglutarate Axis Dynamically Mediates DNA Demethylation in the Prdm16 Promoter and Brown Adipogenesis. Cell Metab *24*, 542-554.
Yang, X., Mudgett, J., Bou-About, G., Champy, M.-F., Jacobs, H., Monassier, L., Pavlovic, G., Sorg, T., Herault, Y., Petit-Demoulière, B.*, et al.* (2016b). Physiological Expression of AMPKγ2RG Mutation Causes Wolff-Parkinson-White Syndrome and

Induces Kidney Injury in Mice. The Journal of biological chemistry *291*, 23428-23439.
Yavari, A., Stocker, C.J., Ghaffari, S., Wargent, E.T., Steeples, V., Czibik, G., Pinter, K., Bellahcene, M., Woods, A., Martínez de Morentin, P.B.*, et al.* (2016). Chronic Activation of γ2 AMPK Induces Obesity and Reduces β Cell Function. Cell Metab *23*, 821-836.
Yeh, W.C., Bierer, B.E., and McKnight, S.L. (1995). Rapamycin inhibits clonal expansion and adipogenic differentiation of 3T3-L1 cells. Proceedings of the National Academy of Sciences of the United States of America *92*, 11086-11090.
Yeow, K., Phillips, B., Dani, C., Cabane, C., Amri, E.Z., and Dérijard, B. (2001). Inhibition of myogenesis enables adipogenic trans-differentiation in the C2C12 myogenic cell line. FEBS letters *506*, 157-162.
Yin, W., Mu, J., and Birnbaum, M.J. (2003). Role of AMP-activated Protein Kinase in Cyclic AMP-dependent Lipolysis In 3T3-L1 Adipocytes. Journal of Biological Chemistry *278*, 43074-43080.
Yoneshiro, T., Aita, S., Matsushita, M., Kayahara, T., Kameya, T., Kawai, Y., Iwanaga, T., and Saito, M. (2013). Recruited brown adipose tissue as an antiobesity agent in humans. J Clin Invest *123*, 3404-3408.
Young, L.R., and Nestle, M. (2002). The contribution of expanding portion sizes to the US obesity epidemic. Am J Public Health *92*, 246-249.
Young, N.P., Kamireddy, A., Van Nostrand, J.L., Eichner, L.J., Shokhirev, M.N., Dayn, Y., and Shaw, R.J. (2016). AMPK governs lineage specification through Tfeb-dependent regulation of lysosomes. Genes Dev *30*, 535-552.
Young, P., Arch, J.R., and Ashwell, M. (1984). Brown adipose tissue in the parametrial fat pad of the mouse. FEBS letters *167*, 10-14.
Yu, W., Rohli, K.E., Yang, S., and Jia, P. (2021). Impact of obesity on COVID-19 patients. Journal of diabetes and its complications *35*, 107817.

Yuan, X., Hu, T., Zhao, H., Huang, Y., Ye, R., Lin, J., Zhang, C., Zhang, H., Wei, G., Zhou, H*., et al.* (2016). Brown adipose tissue transplantation ameliorates polycystic ovary syndrome. *113*, 2708-2713.
Zadra, G., Photopoulos, C., Tyekucheva, S., Heidari, P., Weng, Q.P., Fedele, G., Liu, H., Scaglia, N., Priolo, C., Sicinska, E*., et al.* (2014). A novel direct activator of AMPK inhibits prostate cancer growth by blocking lipogenesis. EMBO molecular medicine *6*, 519-538.
Zang, Y., Yu, L.F., Nan, F.J., Feng, L.Y., and Li, J. (2009). AMP-activated protein kinase is involved in neural stem cell growth suppression and cell cycle arrest by 5-aminoimidazole-4-carboxamide-1-beta-D-ribofuranoside and glucose deprivation by down-regulating phospho-retinoblastoma protein and cyclin D. J Biol Chem *284*, 6175-6184.
Zatterale, F., Longo, M., Naderi, J., Raciti, G.A., Desiderio, A., Miele, C., and Beguinot, F. (2020). Chronic Adipose Tissue Inflammation Linking Obesity to Insulin Resistance and Type 2 Diabetes. Frontiers in physiology *10*, 1607-1607.
Zechner, R., Madeo, F., and Kratky, D. (2017). Cytosolic lipolysis and lipophagy: two sides of the same coin. Nature Reviews Molecular Cell Biology *18*, 671-684.
Zhang, H.H., Huang, J., Düvel, K., Boback, B., Wu, S., Squillace, R.M., Wu, C.-L., and Manning, B.D. (2009). Insulin Stimulates Adipogenesis through the Akt-TSC2-mTORC1 Pathway. PLoS One *4*, e6189.
Zhang, J.-W., Tang, Q.-Q., Vinson, C., and Lane, M.D. (2004). Dominant-negative C/EBP disrupts mitotic clonal expansion and differentiation of 3T3-L1 preadipocytes. Proceedings of the National Academy of Sciences *101*, 43-47.
Zhang, T., Guan, X., Choi, U.L., Dong, Q., Lam, M.M.T., Zeng, J., Xiong, J., Wang, X., Poon, T.C.W., Zhang, H*., et al.* (2019a). Phosphorylation of TET2 by AMPK is indispensable in myogenic differentiation. Epigenetics & Chromatin *12*, 32.
Zhang, X., Heckmann, B.L., Xie, X., Saarinen, A.M., and Liu, J. (2014). Regulation of FSP27 protein stability by AMPK and HSC70. American Journal of Physiology-Endocrinology and Metabolism *307*, E1047-E1056.

Zhang, X., Yang, S., Chen, J., and Su, Z. (2019b). Unraveling the Regulation of Hepatic Gluconeogenesis. Front Endocrinol (Lausanne) *9*, 802.
Zhao, J., Brault, J.J., Schild, A., Cao, P., Sandri, M., Schiaffino, S., Lecker, S.H., and Goldberg, A.L. (2007). FoxO3 Coordinately Activates Protein Degradation by the Autophagic/Lysosomal and Proteasomal Pathways in Atrophying Muscle Cells. Cell Metab *6*, 472-483.
Zhao, J., Yang, Q., Zhang, L., Liang, X., Sun, X., Wang, B., Chen, Y., Zhu, M., and Du, M. (2017). AMPKα1 deficiency suppresses brown adipogenesis in favor of fibrogenesis during brown adipose tissue development. Biochem Biophys Res Commun *491*, 508-514.
Zhou, B., Lu, Y., Hajifathalian, K., Bentham, J., Di Cesare, M., Danaei, G., Bixby, H., Cowan, M.J., Ali, M.K., Taddei, C.*, et al.* (2016). Worldwide trends in diabetes since 1980: a pooled analysis of 751 population-based studies with 4·4 million participants. The Lancet *387*, 1513-1530.
Zhou, G., Myers, R., Li, Y., Chen, Y., Shen, X., Fenyk-Melody, J., Wu, M., Ventre, J., Doebber, T., Fujii, N.*, et al.* (2001). Role of AMP-activated protein kinase in mechanism of metformin action. J Clin Invest *108*, 1167-1174.
Zhou, Y., Wang, D., Zhu, Q., Gao, X., Yang, S., Xu, A., and Wu, D. (2009). Inhibitory Effects of A-769662, a Novel Activator of AMP-Activated Protein Kinase, on 3T3-L1 Adipogenesis. Biological and Pharmaceutical Bulletin *32*, 993-998.
Zhu, Z., Spicer, E.G., Gavini, C.K., Goudjo-Ako, A.J., Novak, C.M., and Shi, H. (2014). Enhanced sympathetic activity in mice with brown adipose tissue transplantation (transBATation). Physiology & Behavior *125*, 21-29.
Zoni, V., Khaddaj, R., Lukmantara, I., Shinoda, W., Yang, H., Schneiter, R., and Vanni, S. (2021). Seipin accumulates and traps diacylglycerols and triglycerides in its ring-like structure. Proceedings of the National Academy of Sciences *118*, e2017205118.